Appendicies

for

VISUAL CHANNEL DATA ANALYSIS FOR A SYNCHRONOUS METEOROLOGICAL SATELLITE

SSEC No.74.04.S1

A REPORT

from the space science and engineering center
the university of wisconsin-madison
madison, wisconsin

APPENDIX A

POWER SPECTRAL CALCULATIONS USING THE DISCRETE FOURIER TRANSFORM (DFT)

In this appendix we outline the procedure for determining the power spectral density using an approximation technique involving the Discrete Fourier Transform (DFT).

The Fourier Transform of a given function $y(x)$ is given by:

$$Y(\omega) = \int_{-\infty}^{\infty} y(x) e^{-j\omega x} dx \tag{A-1}$$

where x is spatial distance (or time) and ω is radian frequency measured in radians per spatial distance (or time). The energy content of $y(x)$ can be measured in either spatial distance or frequency and the equality of these two computations is given by Parseval's theorem (see, for example, Lathi, 1968, Ch. 2):

$$\int_{-\infty}^{\infty} |y(x)|^2 dx = \frac{1}{2\pi} \int_{-\infty}^{\infty} |Y(\omega)|^2 d\omega \tag{A-2}$$

Each integration in Eq. A-2 is in terms of energy so that the quantity $|Y(\omega)|^2$ is in terms of energy per unit of frequency ("energy spectral density").

Next, consider a function $z(x)$ of finite average power. The Fourier transform of a segment of $z(x)$ from -A to A is:

$$Z_A(\omega) = \int_{-A}^{A} z(x) e^{-j\omega x} dx \tag{A-3}$$

("box car")

In effect, we multiply the function $z(x)$ by a rectangular gating function, this is a function with value 1 from -A to +A and zero elsewhere, then we take the transform of the result. The energy

relations of Eq. A-2 become:

$$\int_{-A}^{A} |z(x)|^2 dx = \frac{1}{2\pi}\int_{-\infty}^{\infty} |Z_A(\omega)|^2 d\omega \ . \qquad \text{(A-4)}$$

Dividing both sides of Eq. A-4 by the interval and taking the limit as the interval becomes large, this smoothes out possible fluctuations from end effects, we obtain the following relation for the average power:

$$P_{avg} = \lim_{A\to\infty} \frac{1}{2A}\int_{-A}^{A} |z(x)|^2 dx = \frac{1}{2\pi}\lim_{A\to\infty}\frac{1}{2A}\int_{-\infty}^{\infty} |Z_A(\omega)|^2 d\omega \ . \qquad \text{(A-5)}$$

Provided that an interchange in operations is valid here*, the right side of Eq. A-5 can be rewritten as:

$$P_{avg} = \frac{1}{2\pi}\int_{-\infty}^{\infty}\left(\lim_{A\to\infty}\frac{1}{2A}|Z_A(\omega)|^2\right)d\omega \qquad \text{(A-6)}$$

The result of the integration is average power. Now the integrand in Eq. A-6 can be identified as the power spectral density (often referred to as power spectrum) of z(x) which we designate by $S_z(\omega)$:

$$S_z(\omega) = \lim_{A\to\infty}\frac{1}{2A}|Z_A(\omega)|^2 . \qquad \text{(A-7)}$$

The above reasoning can be extended to apply to random processes. Given a process {z(x)}, the power spectral density is defined as (Papoulis, 1965):

$$S_z(\omega) = \lim_{A\to\infty}\frac{1}{2A}\,E\left\{|Z_A(\omega)|^2\right\} \qquad \text{(A-8)}$$

---

*This discussion is heuristic and not intended to be exhaustive; it is sufficient for describing the operations performed in this report.

where $E\{\cdot\}$ designates an expected value operation over the ensemble. It is our purpose to estimate $S_z(\omega)$ as accurately as possible given a finite record length of discrete points. To do this, we use the Discrete Fourier Transform (DFT).

It is well known that the spectrum $Z_A(\omega)$ can be very closely approximated by the discrete version of Eq. A-3 (McGillem and Cooper, 1973):

$$Z(k\Omega) = \sum_{\ell=0}^{N-1} z(\ell \frac{2A}{N}) e^{-j(2\pi/N)\ell k} \qquad \Omega = 2\pi/2A. \tag{A-9}$$

We have divided the interval $(-A,A)$ into N equal segments and assigned $z(-A) = z(0 \frac{2A}{N})$ and $z(+A) = z(N \frac{2A}{N})$. To maintain equal areas we also require:

$$Z_A(\omega)\Big|_{\omega=k\Omega} = (2A)Z(k\Omega). \tag{A-10}$$

The values of the DFT are proportional to the sampled version of the true Fourier transform $Z_A(\omega)$ at the N sample points.

We approximate the expectation operation of the transform by averaging M adjacent samples of the spectrum:

$$E[|Z_A(\omega)|^2]\Big|_{\omega=k\Omega} = \frac{1}{M} \sum_{i=1}^{M} |Z_i(k\Omega)|^2 \tag{A-11}$$

The value of M is judiciously chosen in order that the M sample spectra represent adjacent samples which are indistinguishable as far as the aperture of the optics in the satellite is concerned. We further assume that the value of A is sufficiently large so that the limit in Eq. A-8 can be approximated. Then, for a fixed A, we have:

* there is not much room for this correction. What's wrong with "so that"?

$$S_z(\omega)\Big|_{\omega=k\Omega} = 2A\frac{1}{M}\sum_{i=1}^{M}|Z_i(k\Omega)|^2. \qquad \text{(A-12)}$$

Implicit in the use of the DFT is the assumption that the true spectrum is bandlimited. This assumption is sufficient to guarantee that the samples of z(x) fully represent the data. Hence, after the power spectrum has been computed, the results must be examined to verify the bandlimited criterion. This is discussed in Appendix B.

As noted earlier, the data has, in effect, been multiplied by a rectangular window function. Viewing these effects in the frequency domain, it is seen that the restriction of the data to a finite length tends to broaden the spectral estimate. This is a direct consequence of the finite record length. It is important, therefore, to obtain better frequency resolution in the spectral estimate than is eventually required. For a rectangular window, the theoretical frequency resolution obtainable is the inverse of the window length. The picture data we have used from Apollo VI is approximately 81 n. mi. per line, giving a maximum theoretical frequency resolution of 0.0124 cycles per n. mi. Actual frequency resolution is somewhat poorer than this as a result of windowing and smoothing.

Abrupt discontinuities in the data, arising from windowing the data with a rectangular function, may result in a high error variance in the spectral estimate. Results of these discontinuities can be suppressed to some extent by tapering the ends of the data window over the interval (-A, +A) rather than using the rectangular window described above. In fact, tapered windows are often employed instead of the rectangular ones (Otnes & Enochson, 1972). Choice of a good window can yield an improved dynamic range and lower error variance in the spectral estimate at the expense of a decrease in frequency resolution. An optimum window for all purposes does not exist, as a result

these trade-offs and the type of data to be handled.

We include the following examples to demonstrate several points. Since Eq. A-9 and subsequent computations are implemented on a digital computer, which must of necessity operate with finite word lengths to perform all of its functions, the first item of interest is the effect of round-off errors in the machine's arithmetic operations. The second point is the sensitivity of Eq. A-9 to monochromatic signals, that is, pure sine or cosine waves and the frequency resolution attainable. Finally, we are interested in the effects of different window functions both on pure sinusoidal and typically random signals.

In the accompanying figures we will always be plotting:

$$\log |Z(k\Omega)|^2 \qquad k = 0, 1, \ldots, N-1$$

where: (A-13)

$$Z(k\Omega) = \sum_{\ell=0}^{N-1} w(\ell\frac{2A}{N}) \ (\cos \frac{2\pi}{N} f\ell) e^{-j(2\pi/N)\ell k}$$

N-512.

There are four forms of the window function used here:

$$w_R(\ell \frac{2A}{N}) = 1 \qquad \text{Rectangular} \qquad \text{(A-14)}$$

$$w_{HN}(\ell \frac{2A}{N}) = 0.5(1 - \cos \frac{2\pi}{N} (\ell-1)) \qquad \text{Hanning} \qquad \text{(A-15)}$$

$$w_{HM}(\ell \frac{2A}{N}) = (0.54 - 0.46 \cos \frac{2\pi}{N} (\ell-1)) \qquad \text{Hamming} \qquad \text{(A-16)}$$

$$w_P(\ell \frac{2A}{N}) = \frac{1}{\pi}\left|\sin \pi\left[\frac{\ell-1-(N/2)}{N/2}\right]\right| + \left\{1 - \left|\frac{\ell-1-(N/2)}{N/2}\right|\right\} \cos \pi\left[\frac{\ell-1-(N/2)}{N/2}\right]$$

(Papoulis, 1973) (A-17)

We have selected eight purely sinusoidal test frequencies. Half ~~of them~~ represent functions which contain integer number of cycles in a sample of width 2A. ~~whereas~~ The remaining half have fractional numbers of cycles in the range sample width. Power spectral plots using these sinusoidal test frequencies are shown in Figure A-1. Because the plots are drawn to take advantage of the maximum dynamic range of the plotter, there is no uniform scaling among the ordinates of the figures. Furthermore, it must be emphasized that the ordinate axis represents the logarithm of the values. The maximum value of each figure occurs at the point(s) nearest the frequency of the input signal. However, the magnitude of sidelobes and their widths differ depending on the type of window function. It is also possible to observe the round-off noise generated by the operations in the computer. This is most easily seen in the graphs of signals with an integer number of cycles present.

From these graphs, it can be seen that the use of the Hanning, Hamming, and Papoulis window functions do suppress the effects of discontinuities at the ends of the records at the expense of frequency resolution. The Papoulis window was developed for processing random-type data (Papoulis, 1973) ~~and~~ It is not as well suited for purely sinusoidal signals as the other two windows. Because the sample lines of picture data appear quite random on a scan-by-scan basis, we have used the Papoulis window in the computation of spectral plots in this report. ~~The only exception to this is that the spectral plots in Appendix C which Appendix G have been computed using the rectangular window.~~

Spectral plots using a sample line from typical picture data and differing choice of window functions are shown in Figure A-2.

FIGURE A.1. POWER SPECTRAL PLOTS OF SELECTED SINUSOIDAL TEST FREQUENCIES

Notes:

1) A 512-point discrete Fourier transform was used and therefore all spectra are aliased about the 256 data point in the transforms.

2) The vertical scale is logarithmic and is adjusted to each plot.

3) The selected test frequency and the particular choice of data window is specified on each plot.

Cycles: 20.000
Window: Rectangular
Avg. Value: 0.00000
Date: 12/30/72-1

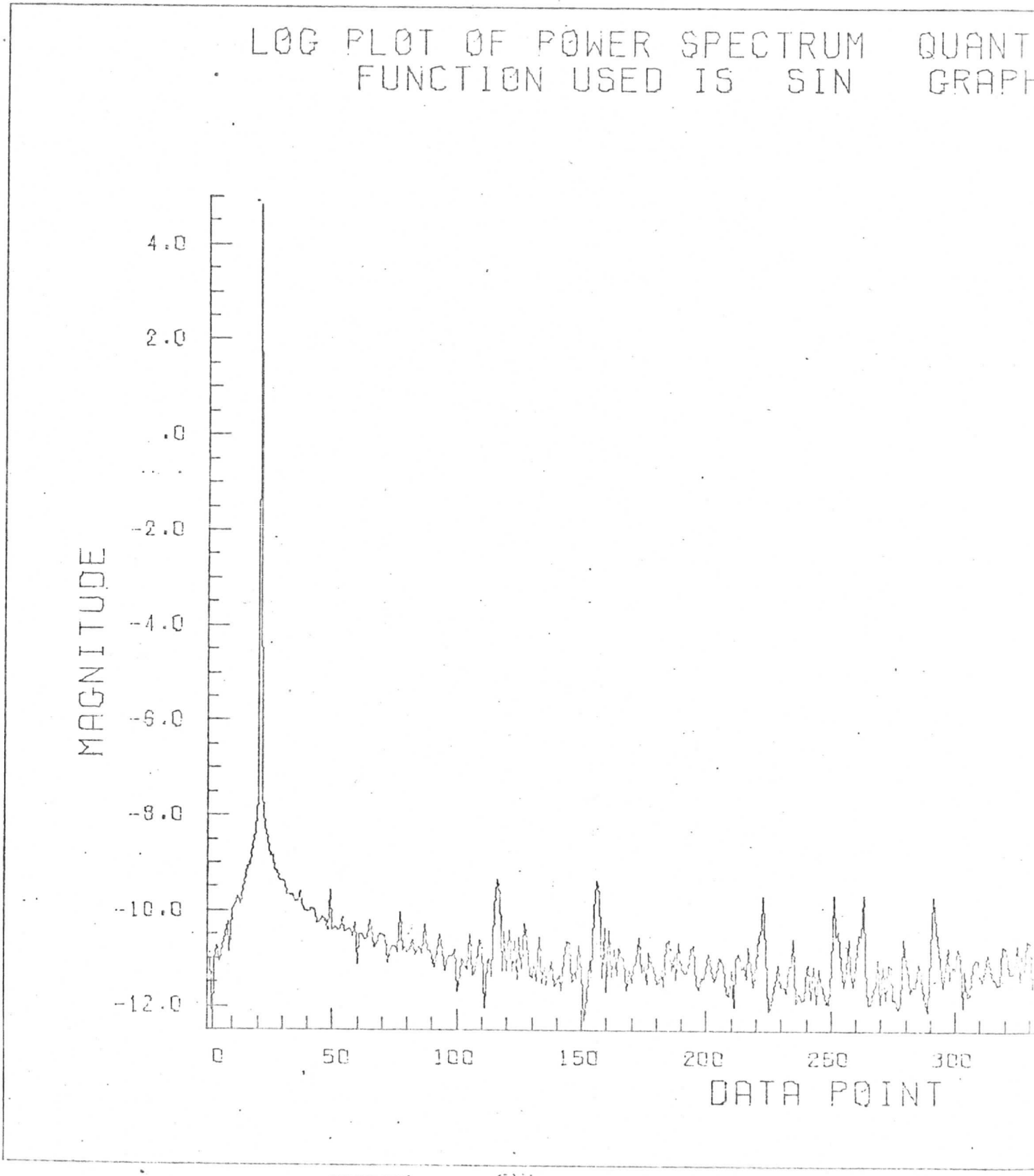

Cycles: 20.000
Window: Hanning
Avg. Value: 0.00000
Date: 12/30/72-2

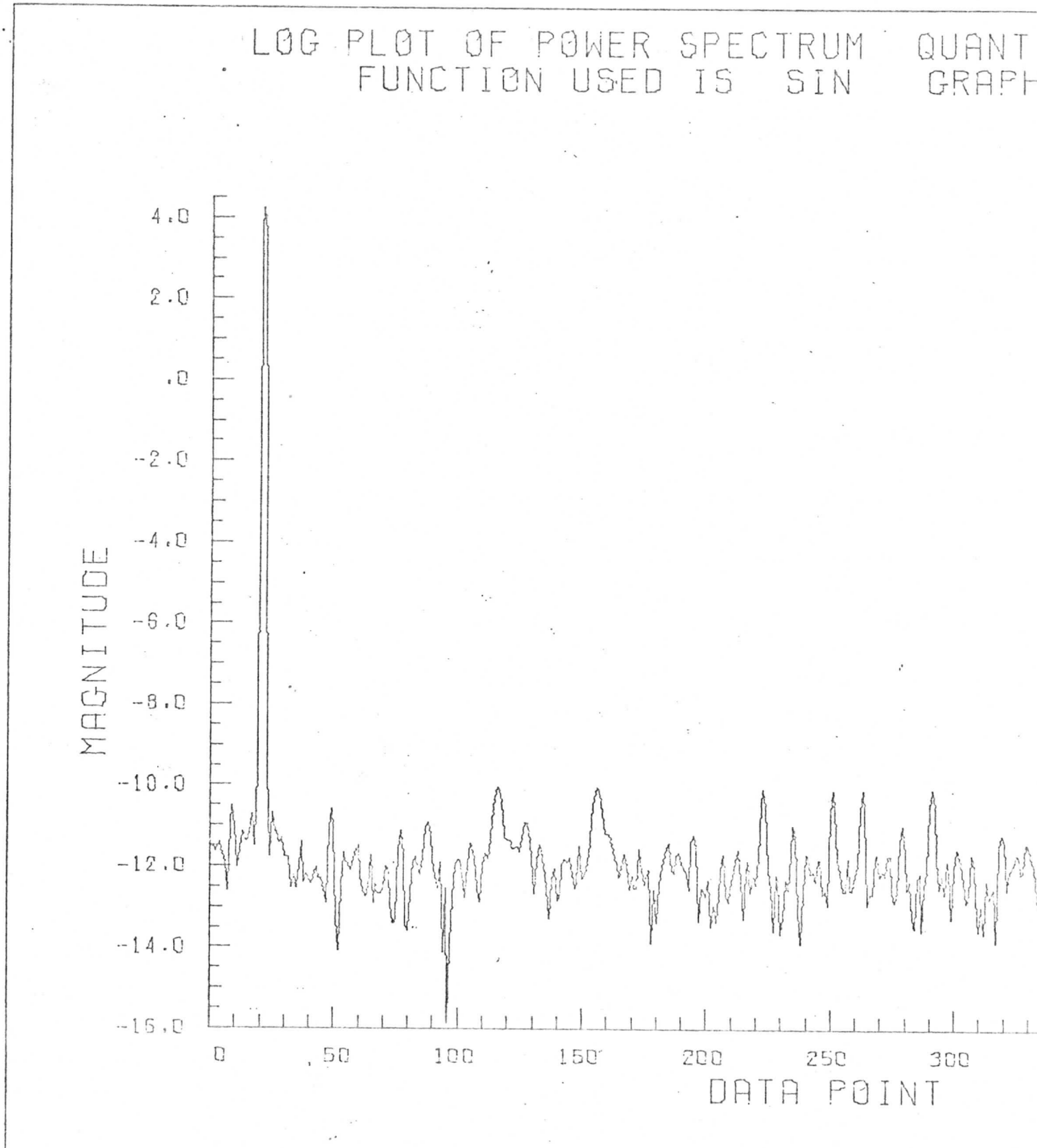

Cycles: 20.000
Window: Hamming
Avg. Value: 0.00000
Date: 12/30/72-3

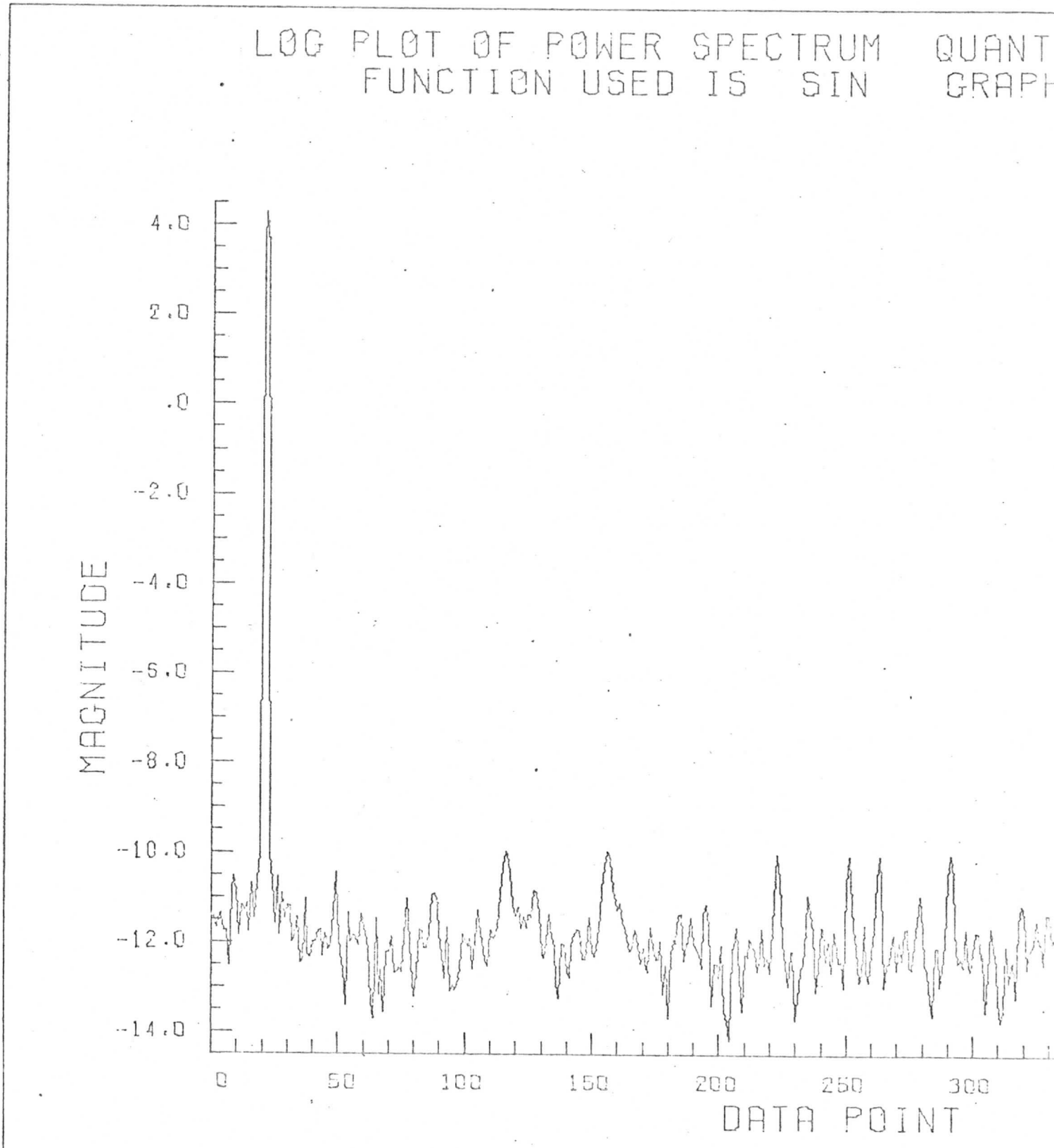

Cycles: 20.000
Window: Papoulis
Avg. Value: 0.0000
Date: 2/15/73-2

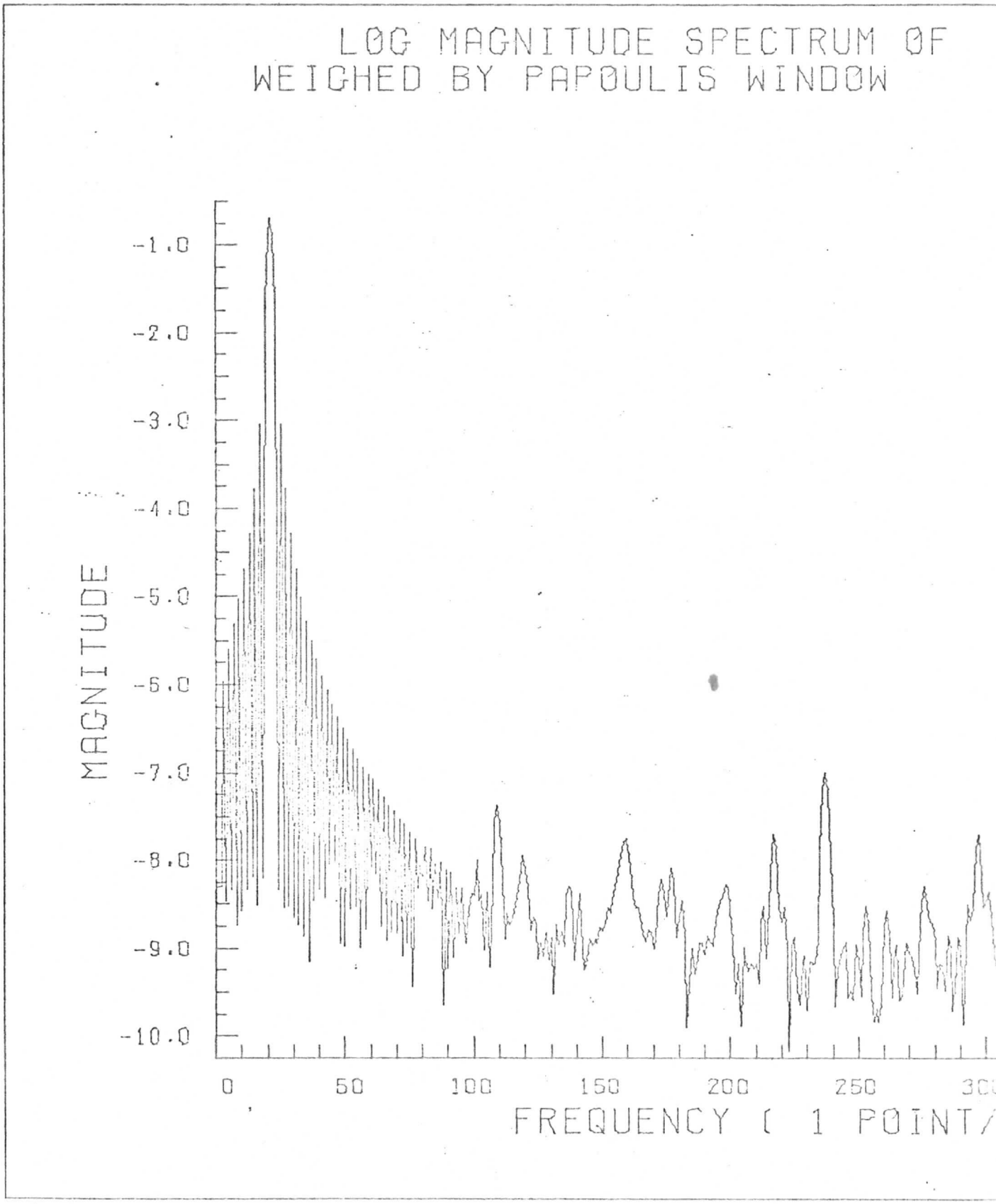

Cycles: 20.300
Window: Rectangular
Avg. Value: 0.00000
Date: 12/30/72-5

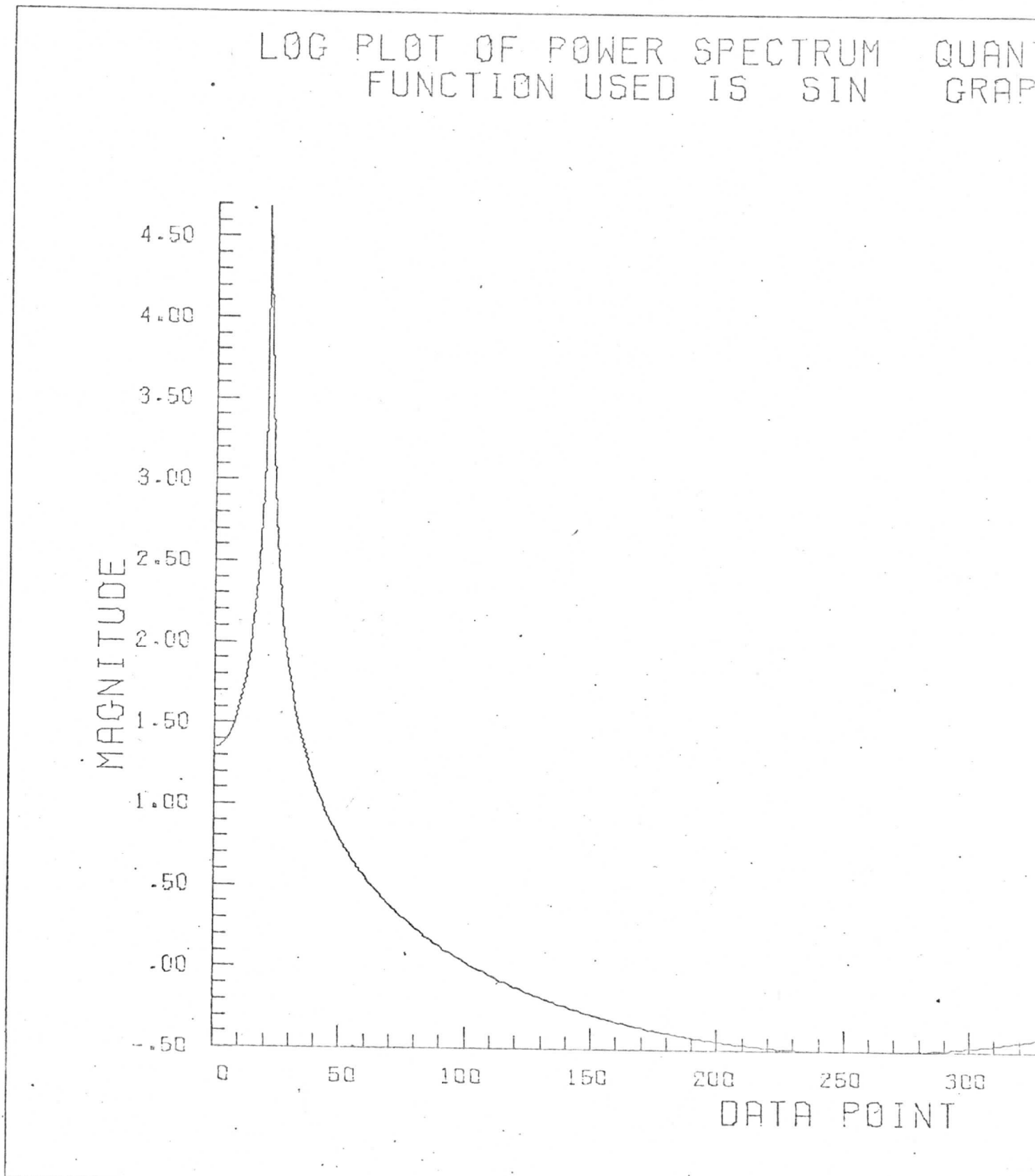

Cycles: 20.300
Window: Hanning
Avg. Value: 0.00000
Date: 12/30/72-6

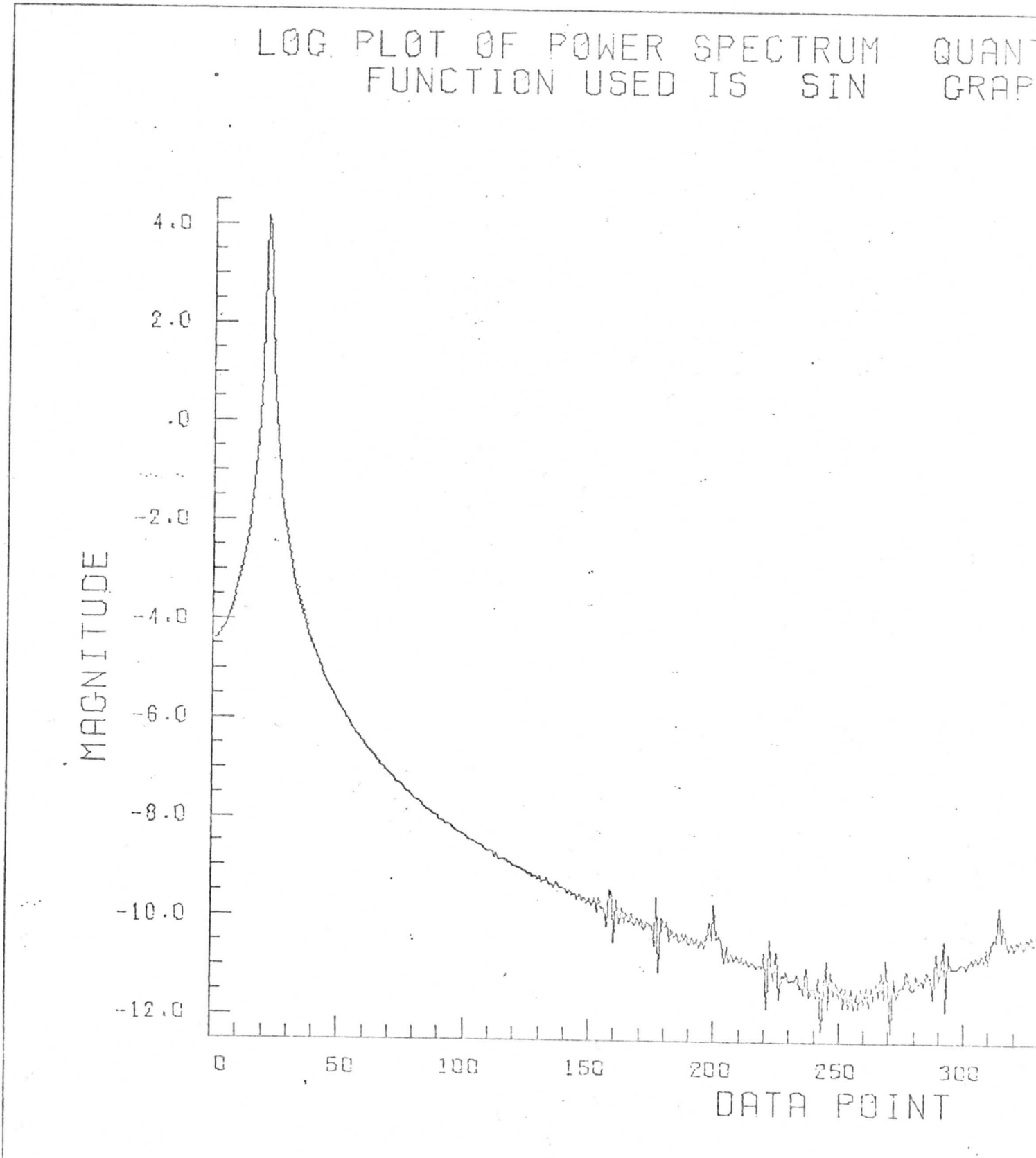

Cycles: 20.300
Window: Hamming
Avg. Value: 0.00000
Date: 12/30/72-7

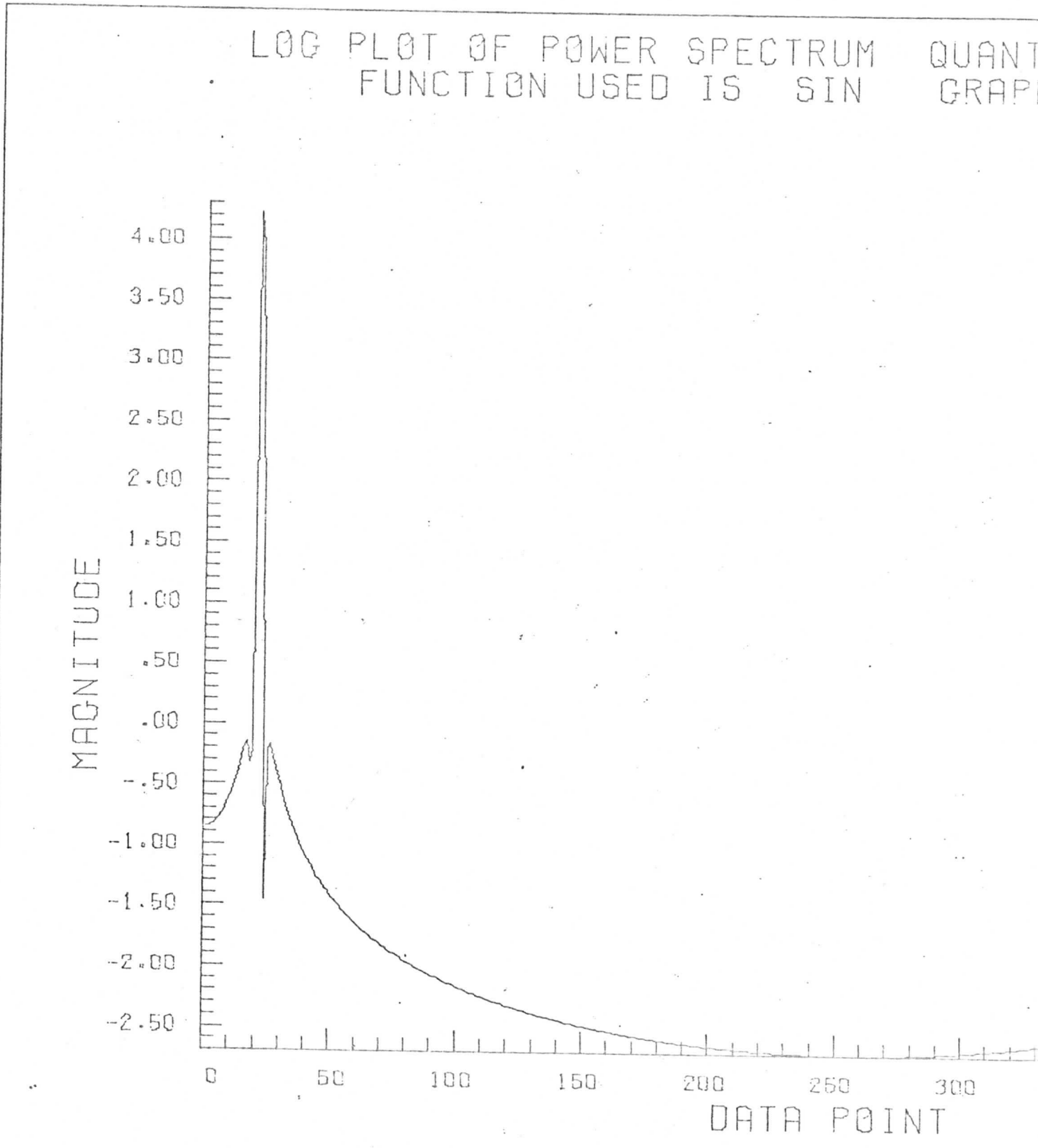

Cycles: 20.300
Window: Papoulis
Avg. Value: 0.0000
Date: 2/15/73-4

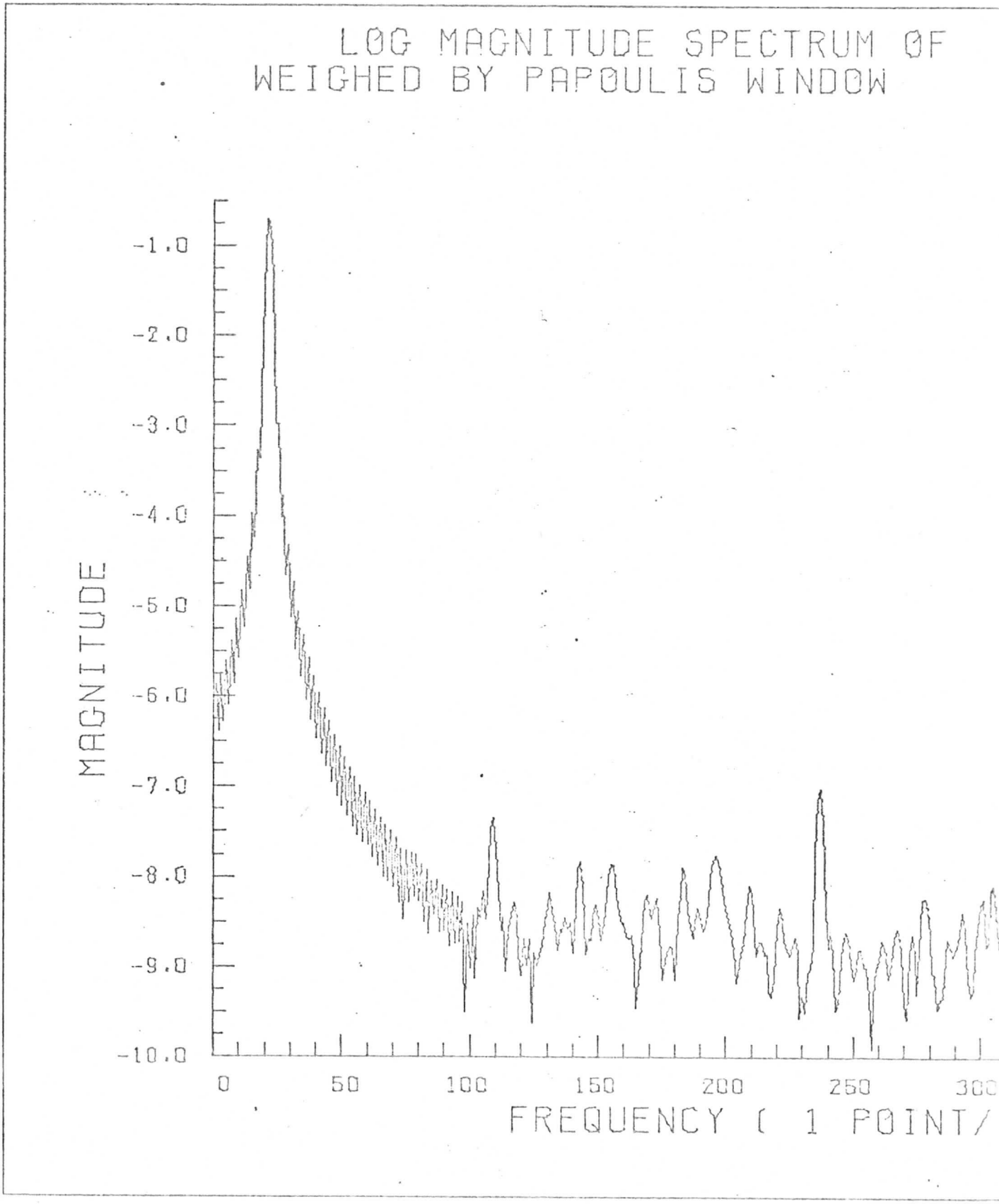

Cycles: 97.000
Window: Rectangular
Avg. Value: 0.01000
Date: 12/30/72-9

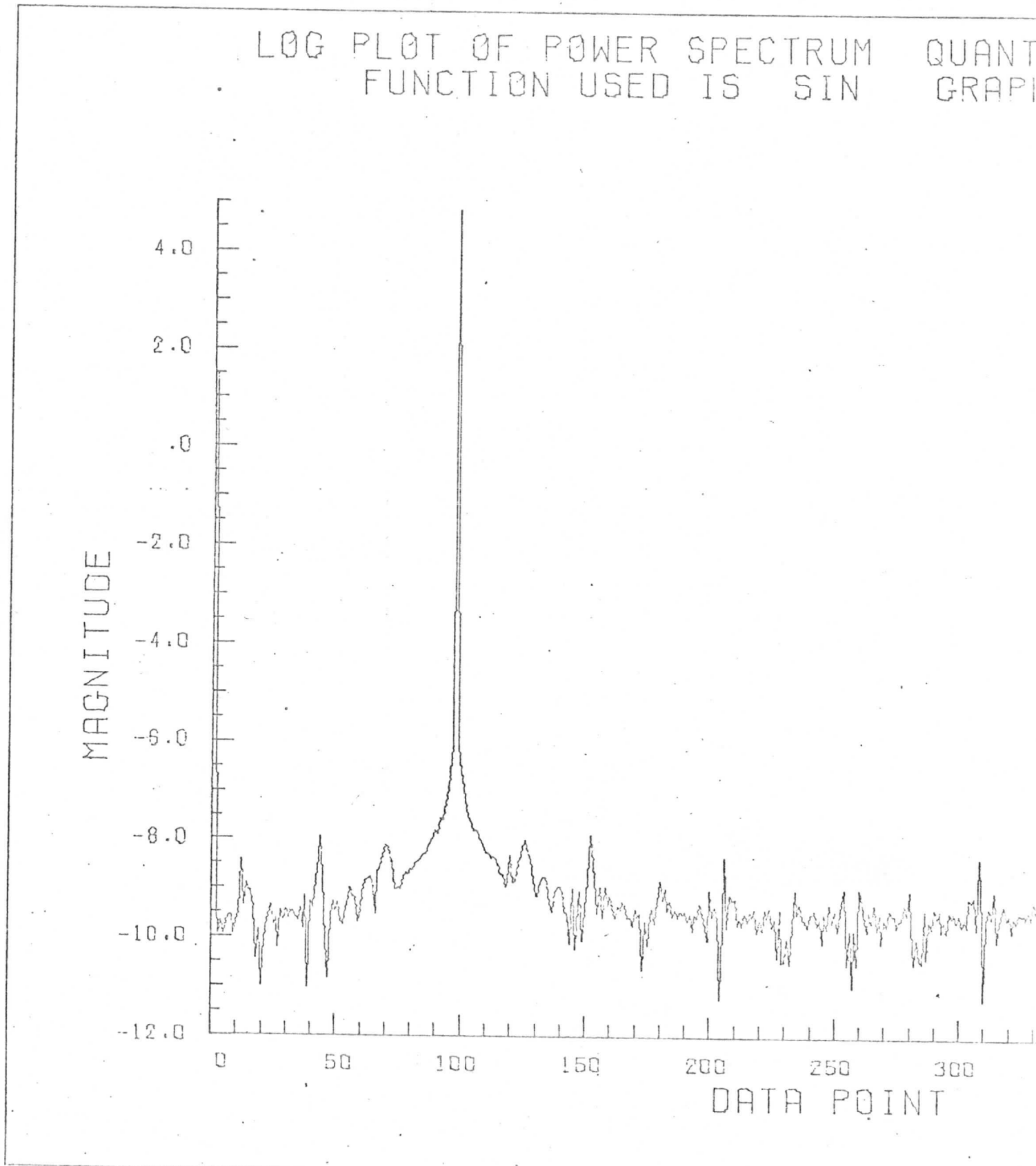

Cycles: 97.000
Window: Hanning
Avg. Value: 0.01000
Date: 12/30/72-10

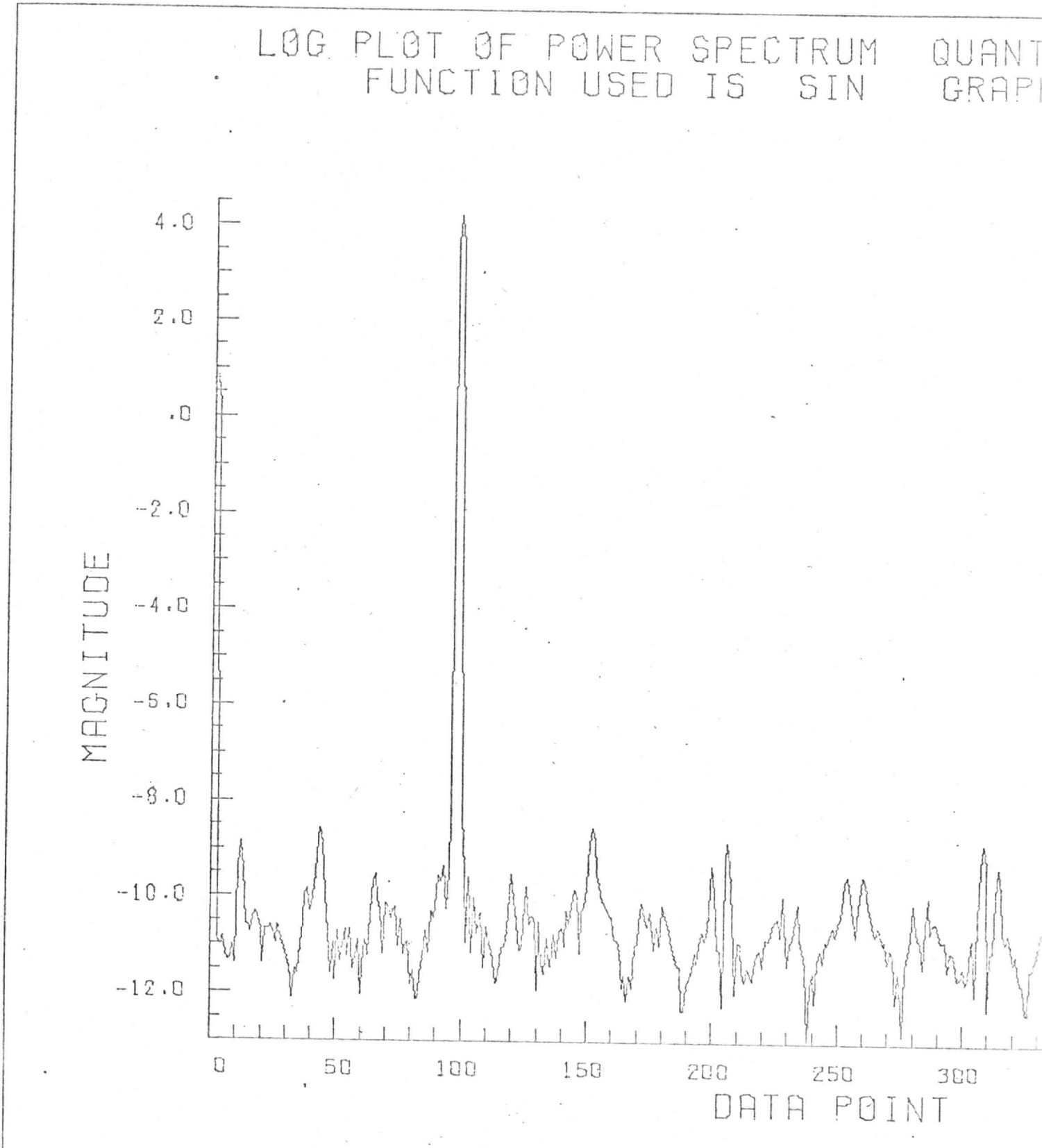

Cycles: 96.700
Window: Rectangular
Avg. Value: 0.01000
Date: 12/30/72-11

LØG PLØT ØF PØWER SPECTRUM QUAN
FUNCTION USED IS SIN GRA

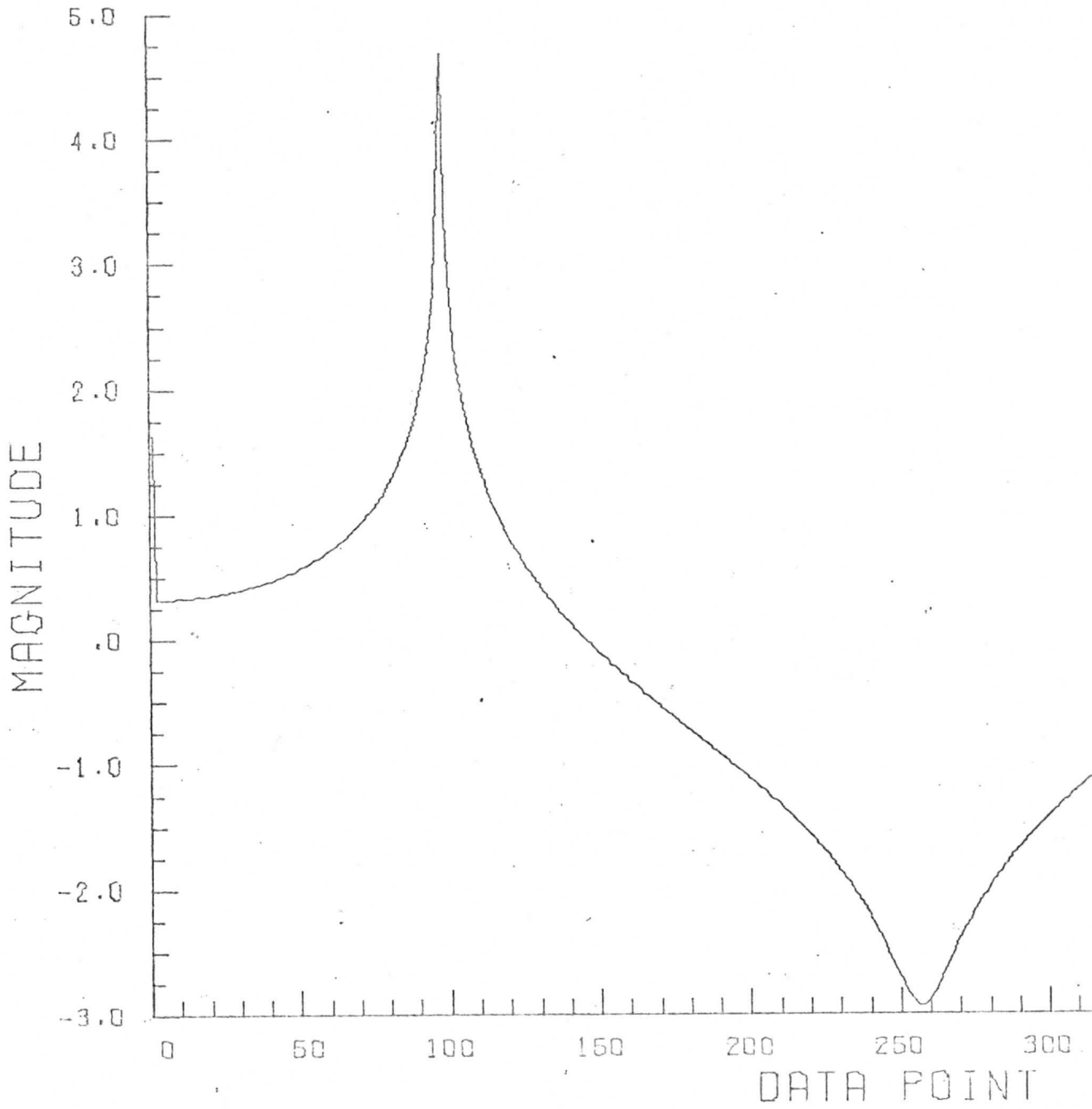

Cycles: 96.700
Window: Hanning
Avg. Value: 0.01000
Date: 12/30/72-12

LØG PLØT ØF POWER SPECTRUM QUAN
FUNCTION USED IS SIN GRA

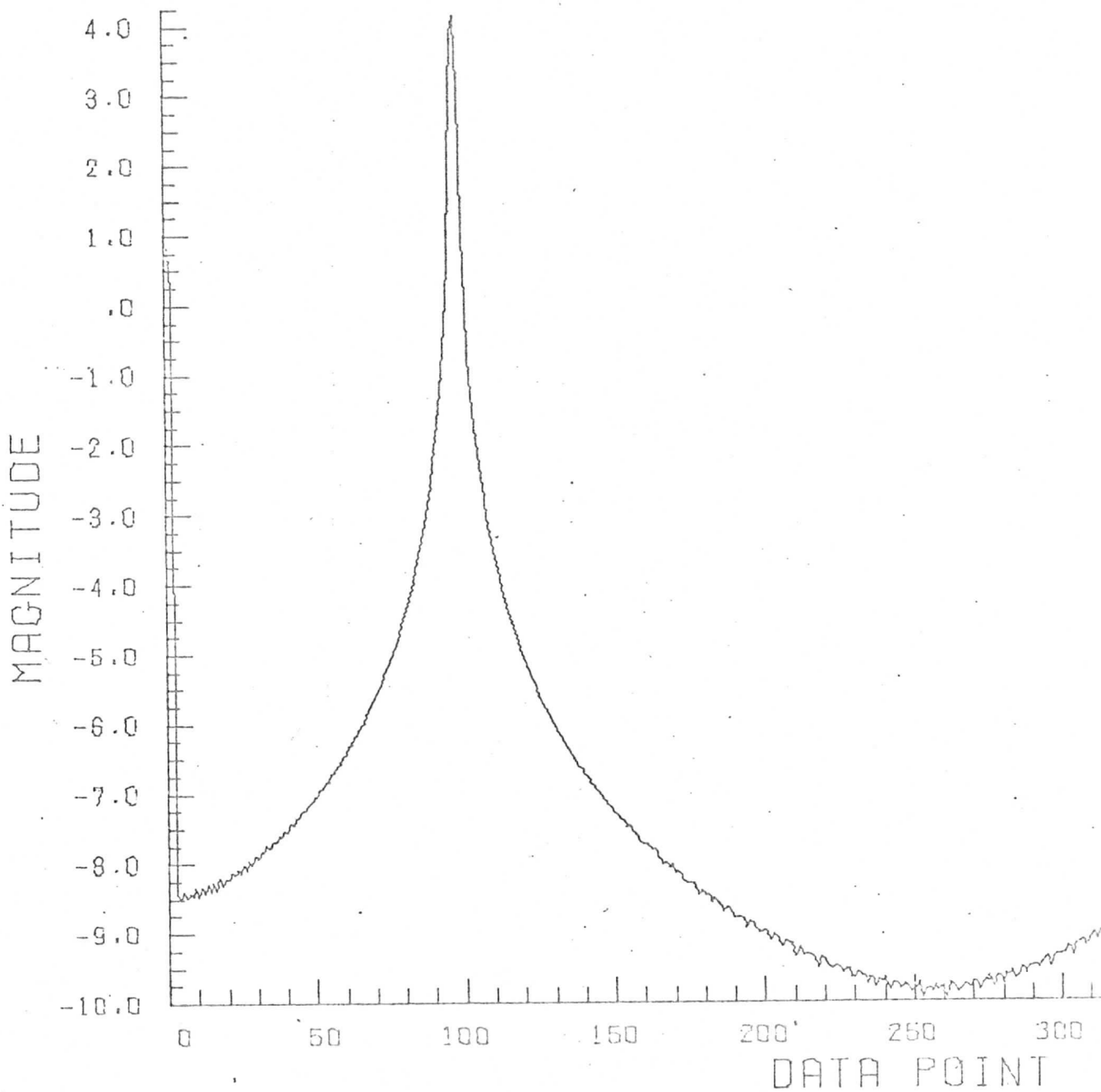

Cycles: 96.700
Window: Hamming
Avg. Value: 0.01000
Date: 12/30/72-13

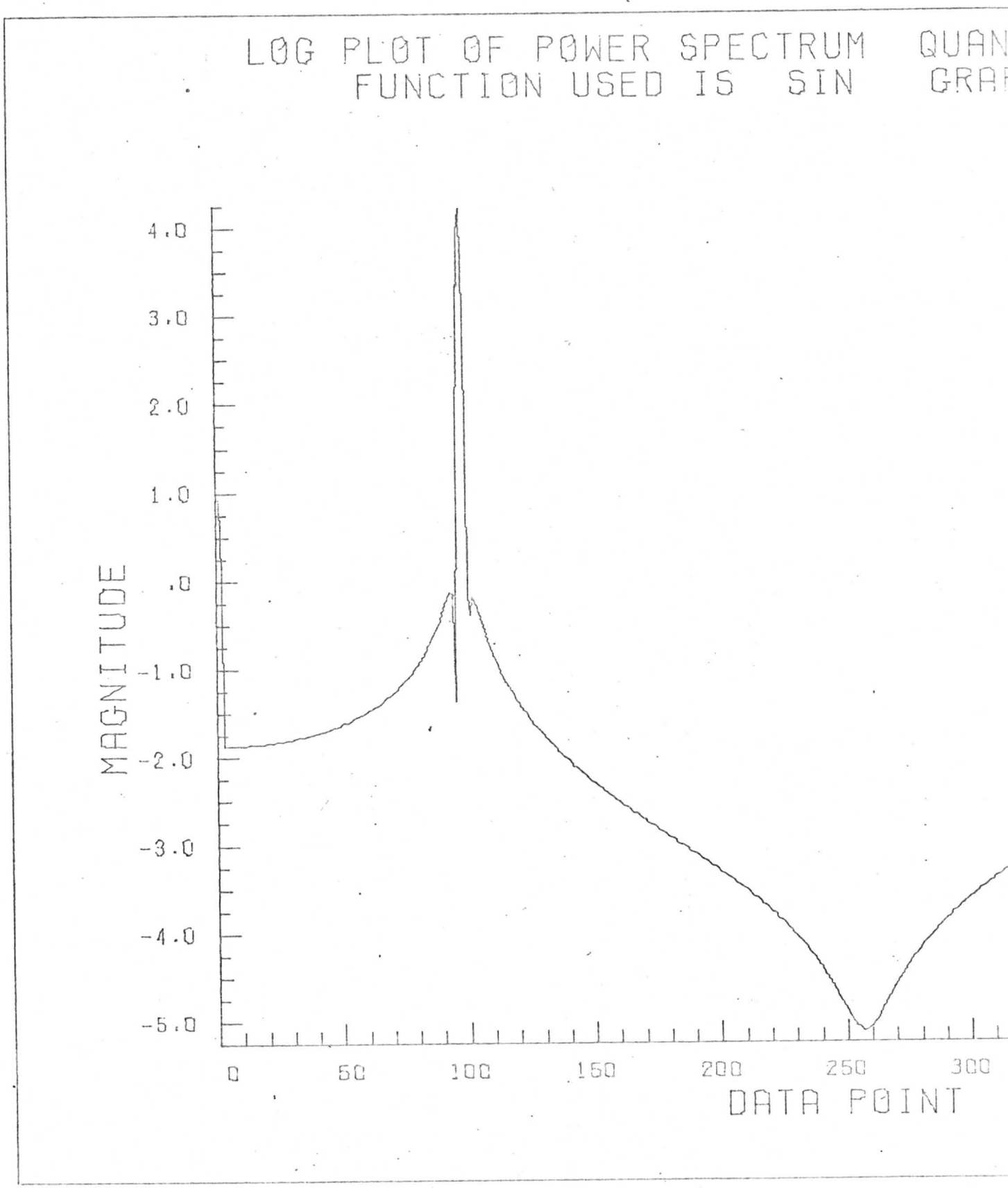

Cycles: 96.700
Window: Papoulis
Avg. Value: 0.0000
Date: 2/15/73-6

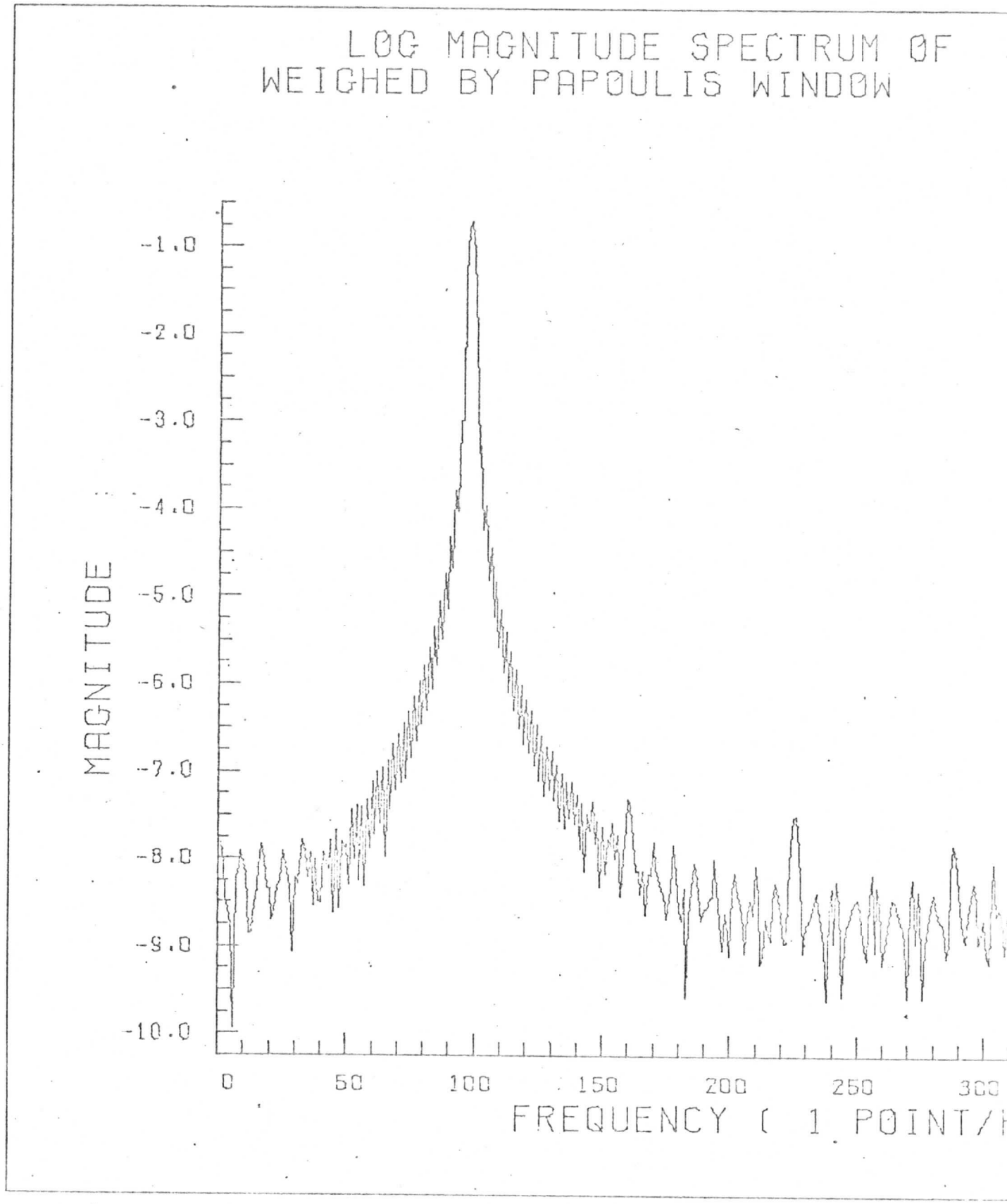

Cycles: 131.000
Window: Rectangular
Avg. Value: 0.10000
Date: 12/30/72-15

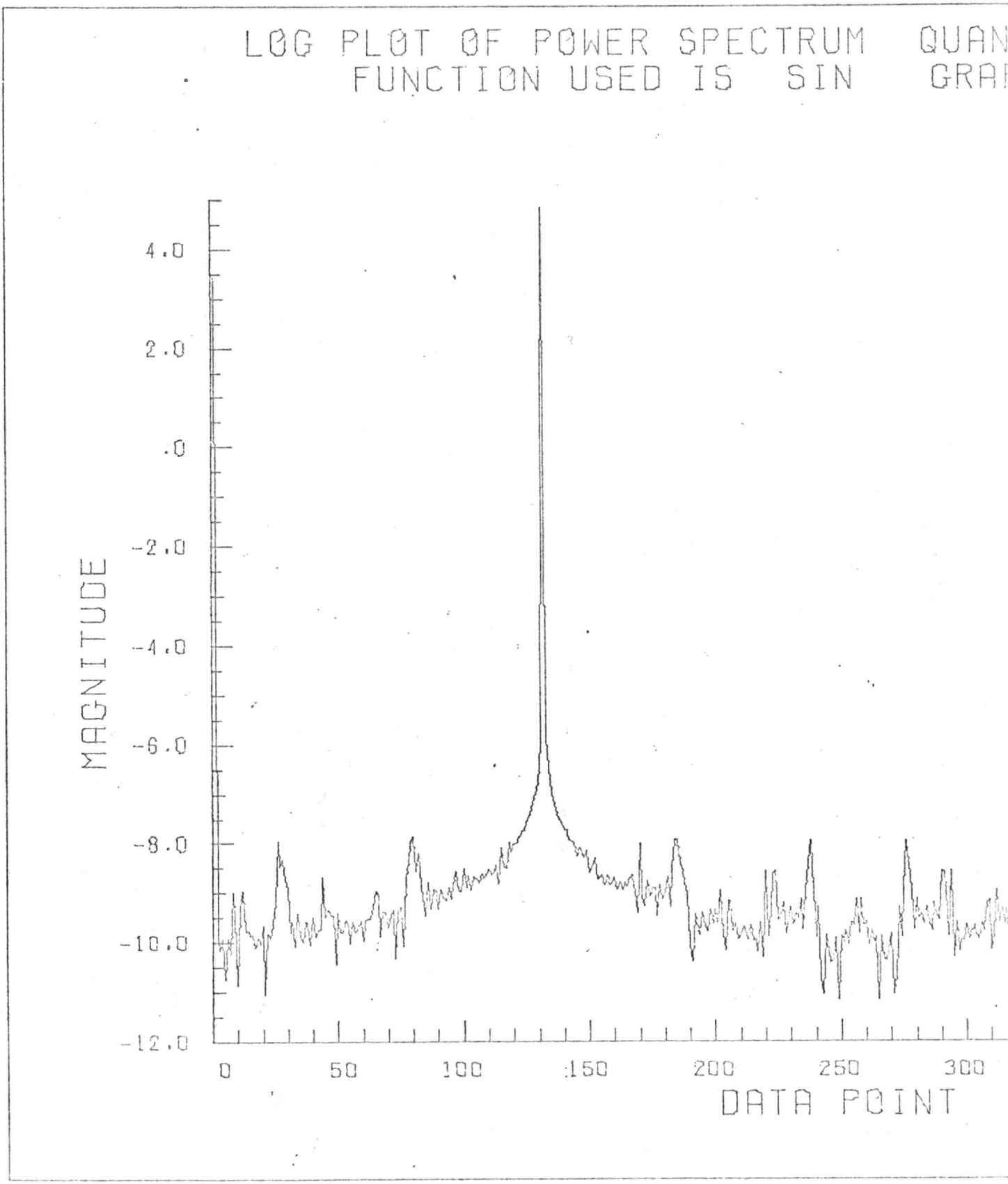

Cycles: 131.000
Window: Hanning
Avg. Value: 0.10000
Date: 12/30/72-16

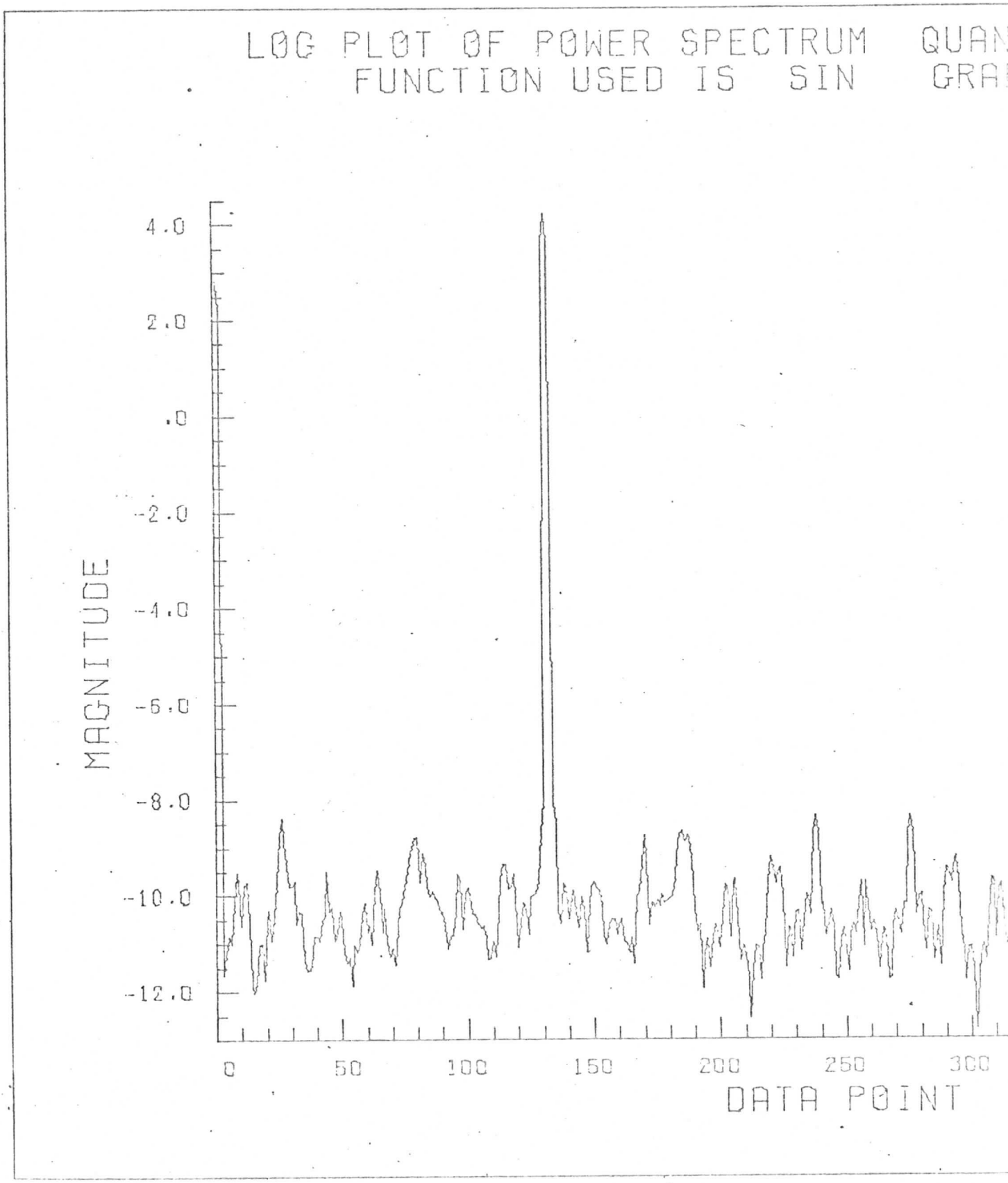

A-24

Cycles: 131.200
Window: Rectangular
Avg. Value: 0.10000
Date: 12/30/72-17

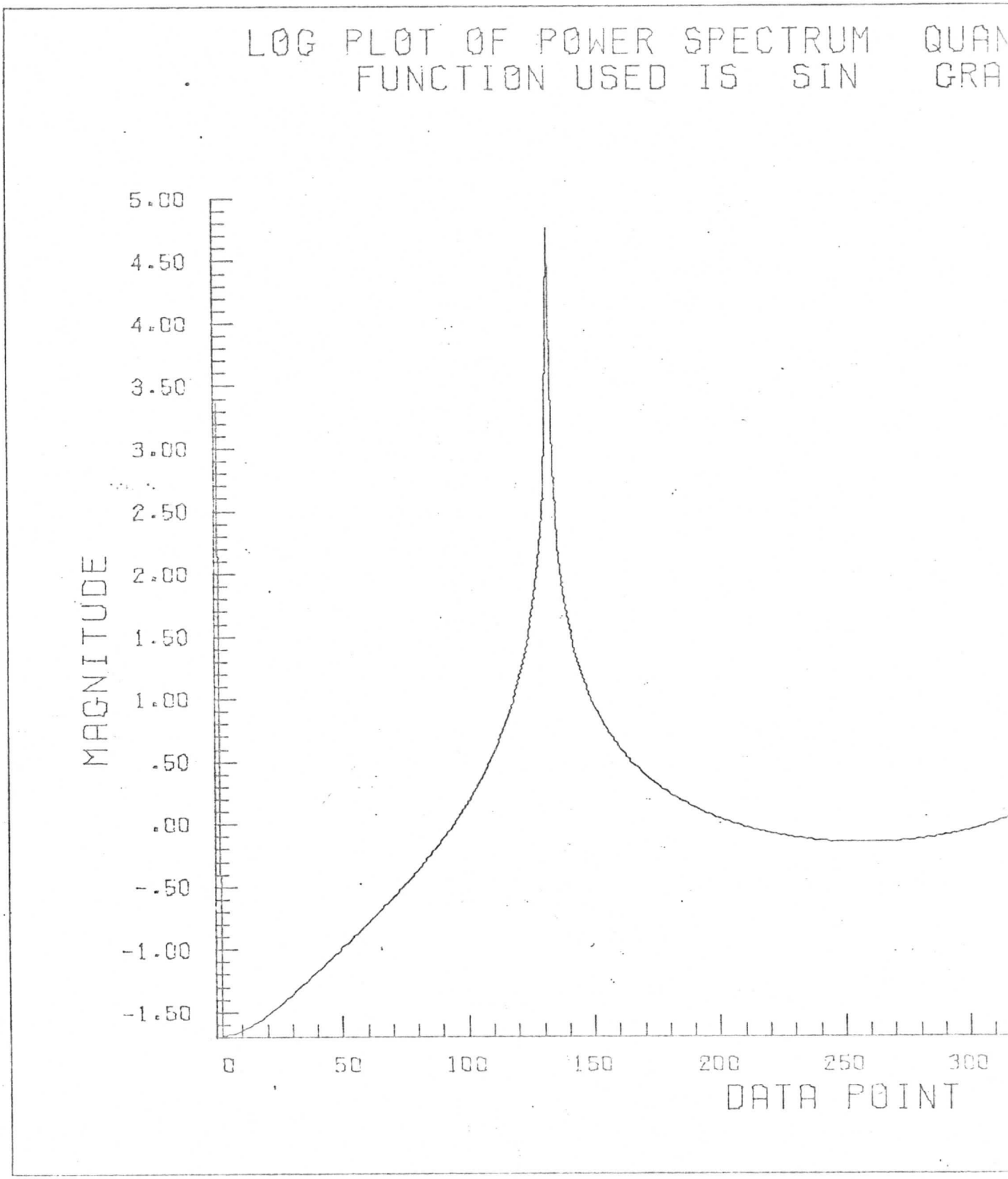

A-25

Cycles: 131.200
Window: Hanning
Avg. Value: 0.10000
Date: 12/30/72-18

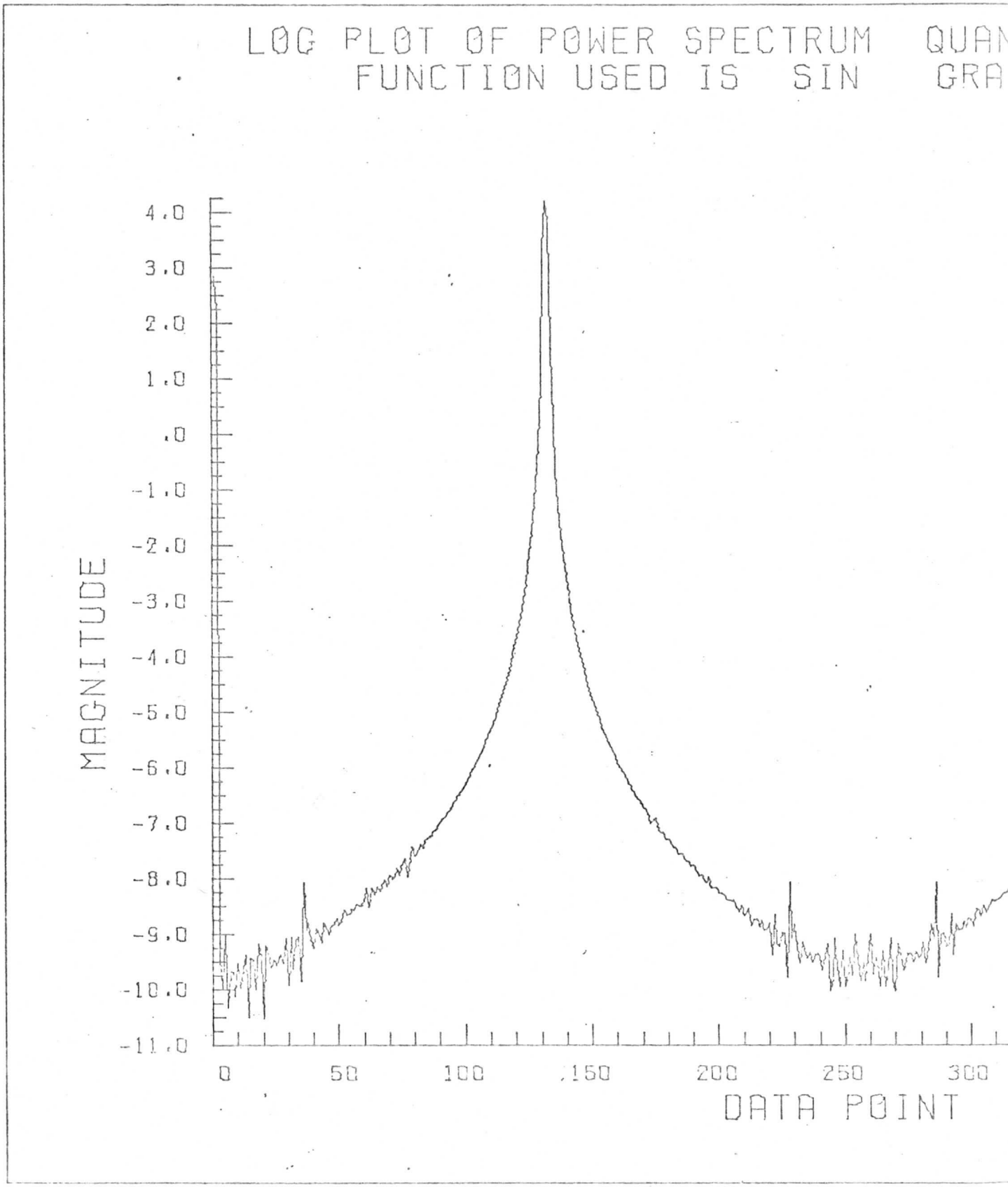

Cycles: 131.200
Window: Hamming
Avg. Value: 0.10000
Date: 12/30/72-19

LØG PLØT ØF PØWER SPECTRUM QUAN
FUNCTIØN USED IS SIN GRAF

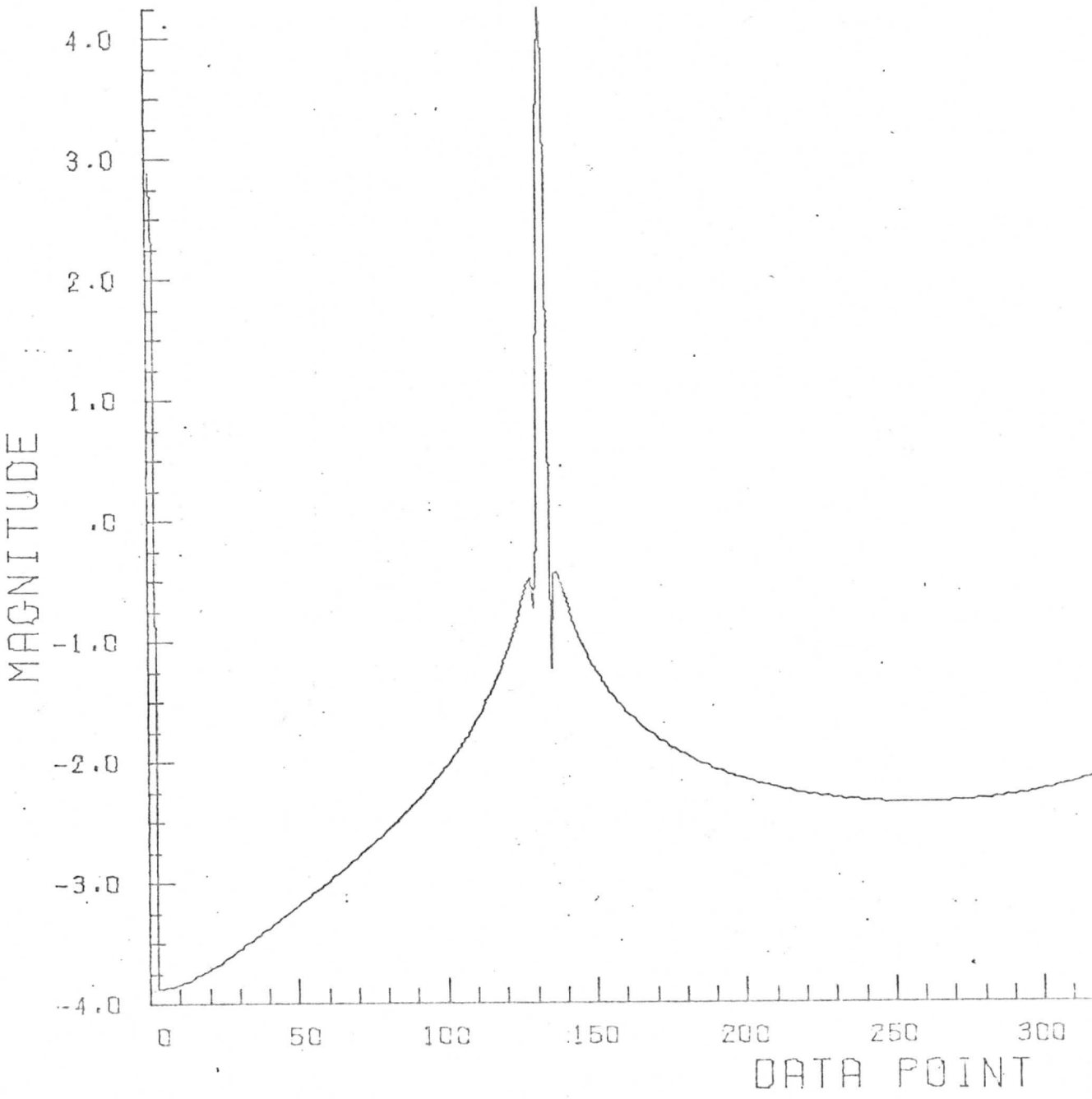

Cycles: 132.20
Window: Papoulis
Avg. Value: 0.0000
Date: 2/15/73-8

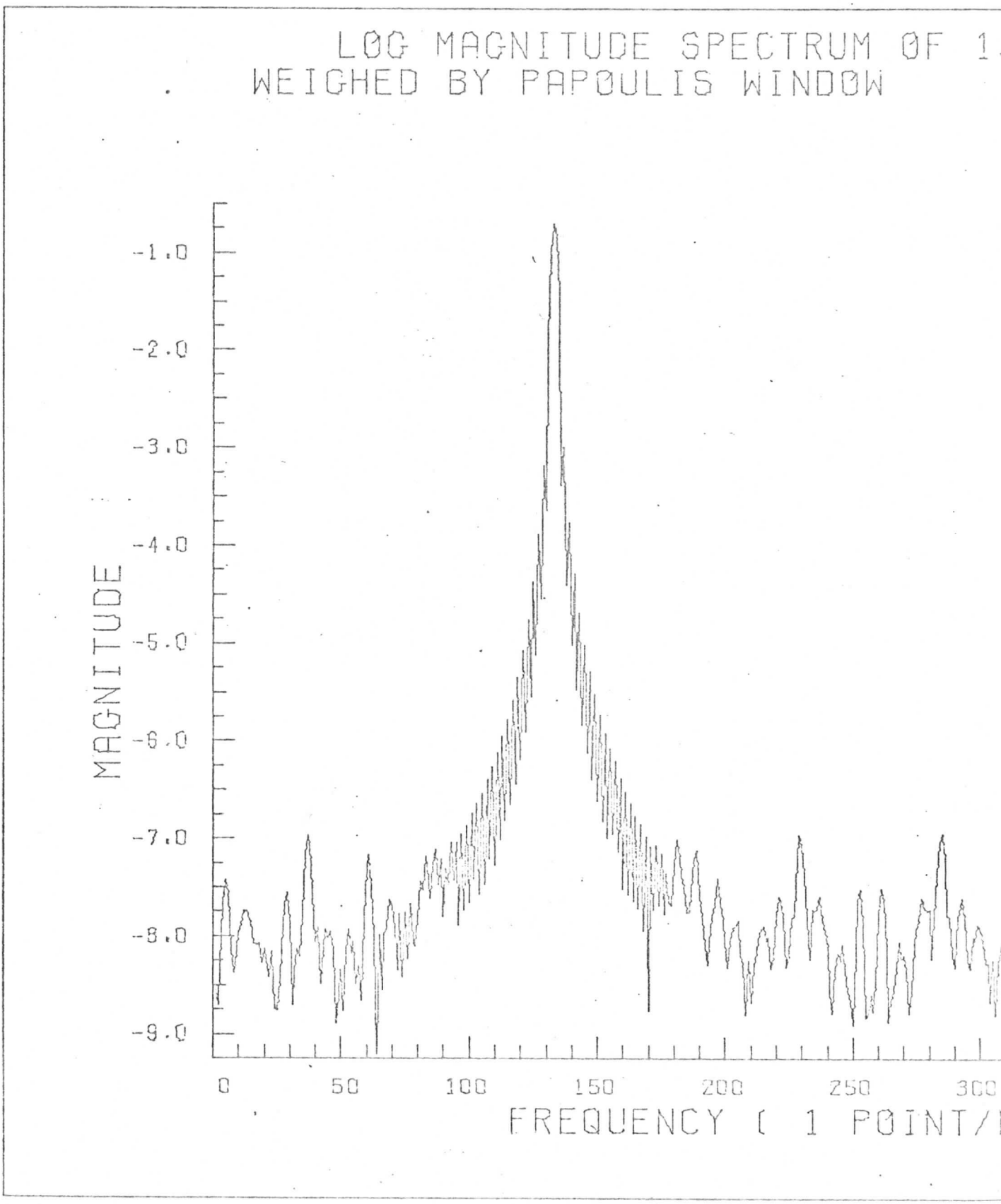

Cycles: 203.000
Window: Rectangular
Avg. Value: 0.50000
Date: 12/30/72-21

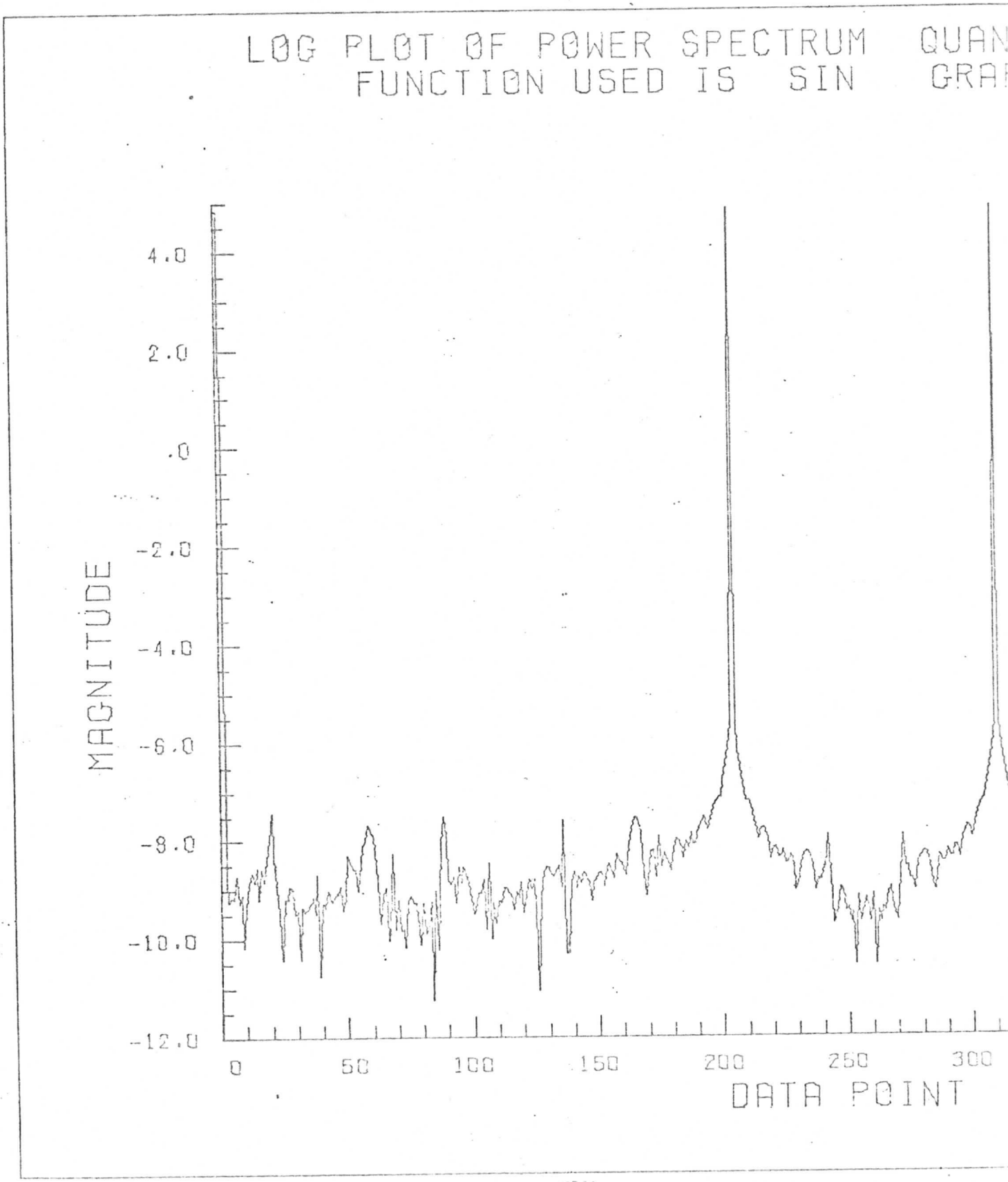

Cycles: 203.000
Window: Hanning
Avg. Value: 0.50000
Date: 12/30/72-22

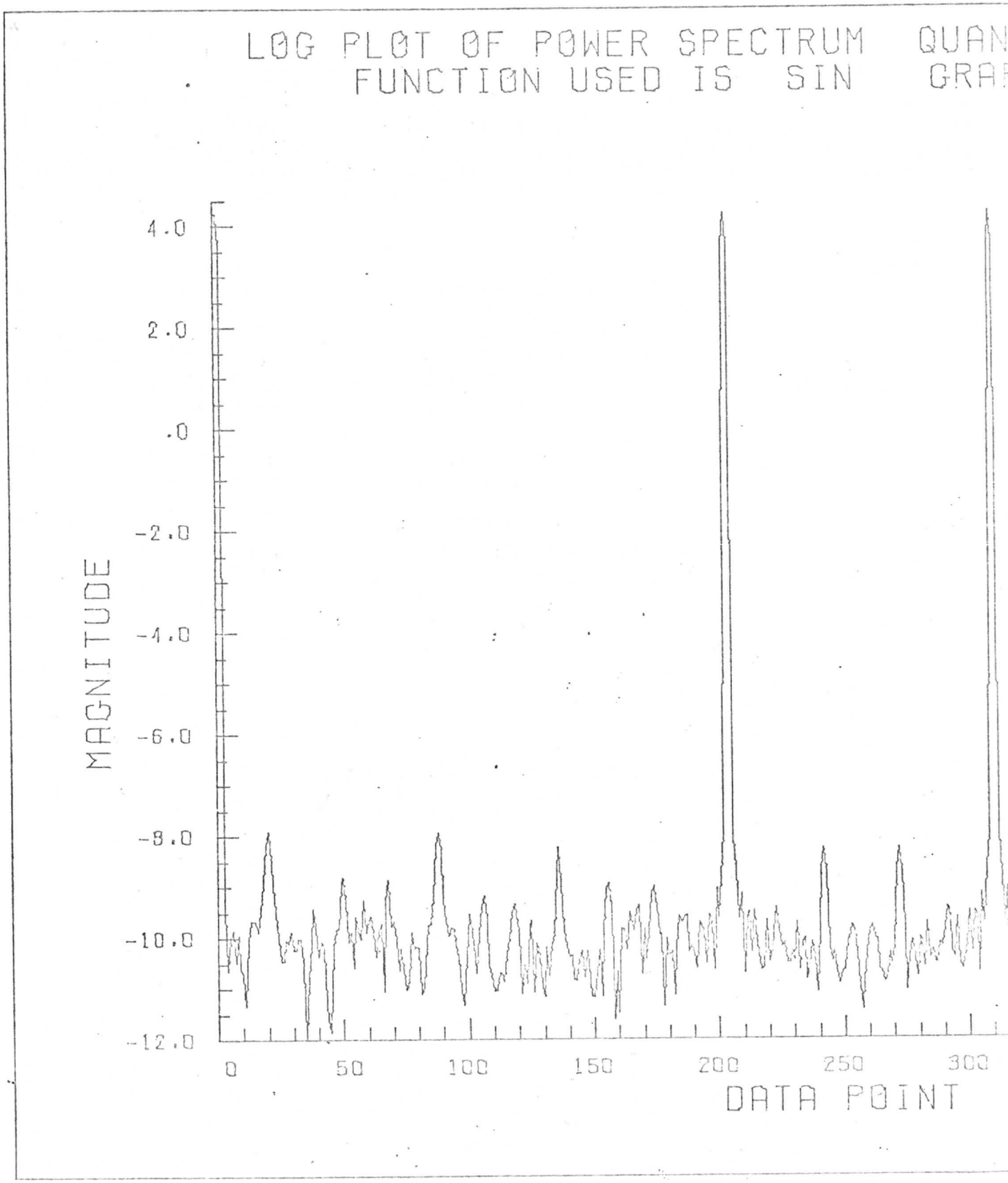

Cycles: 203.000
Window: Hamming
Avg. Value: 0.50000
Date: 12/30/72-23

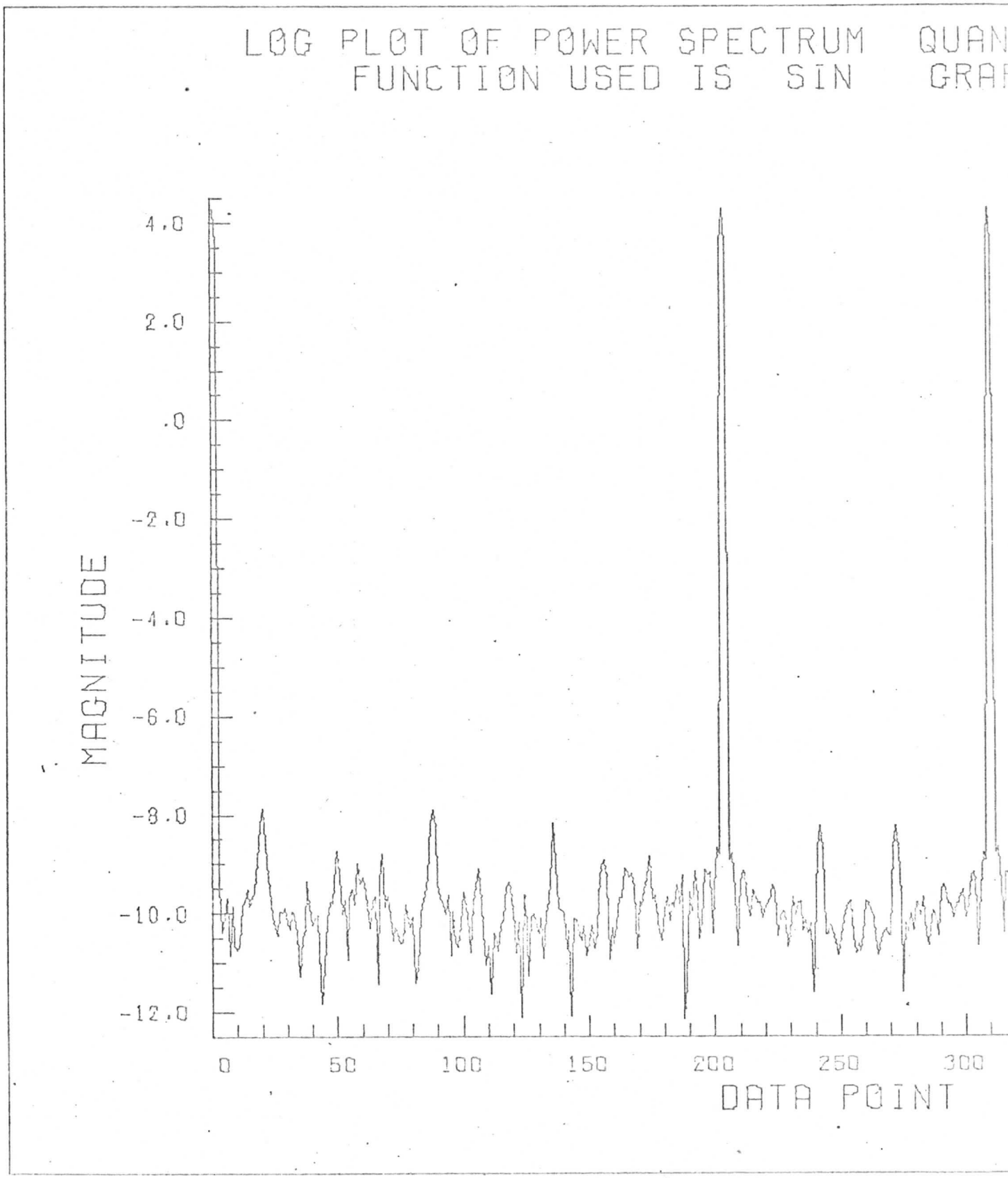

Cycles: 202.68
Window: Rectangular
Avg. Value: 0.00000
Date: 12/30/72-25

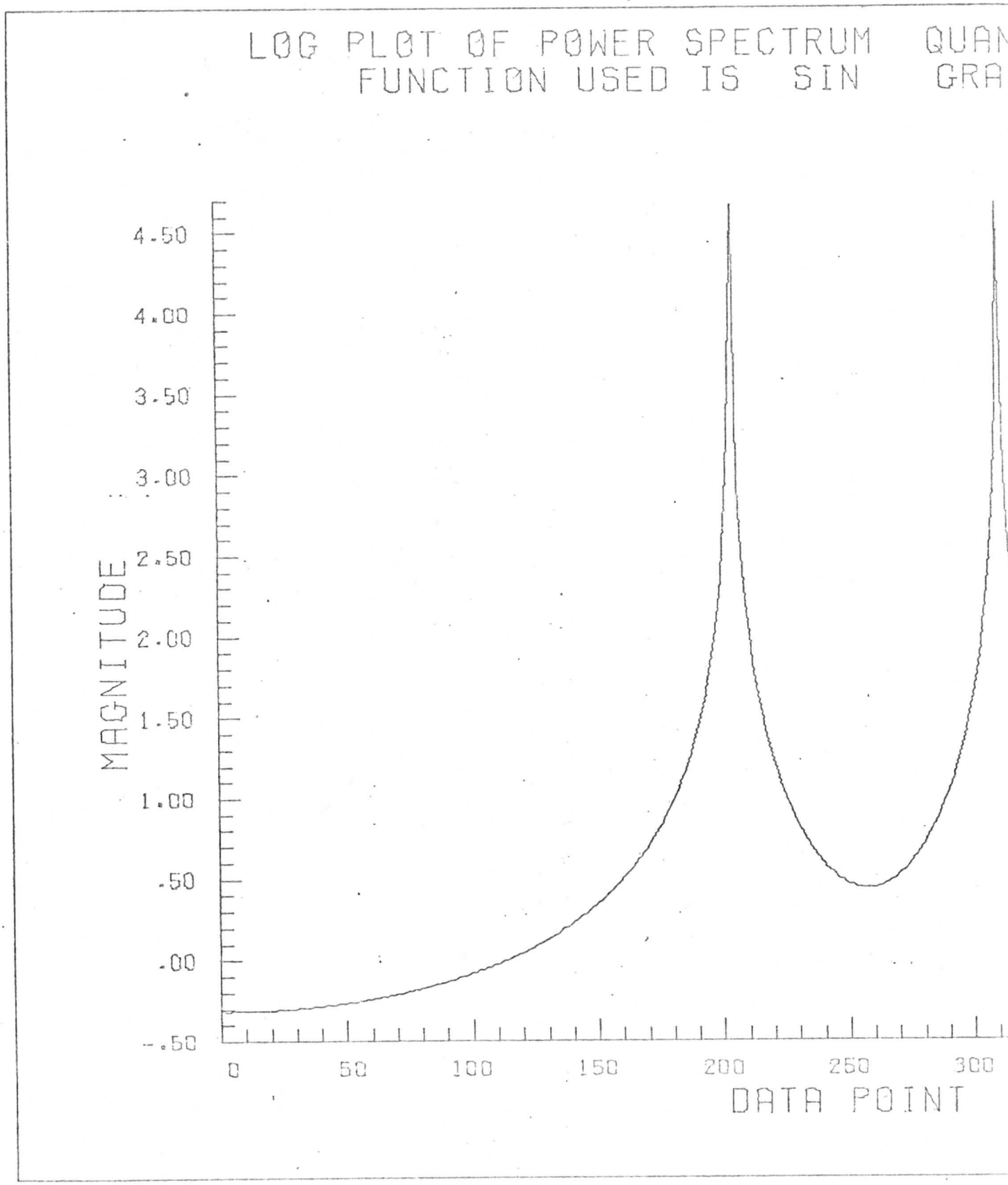

Cycles: 202.68
Window: Hanning
Avg. Value: 0.00000
Date: 12/30/72-26

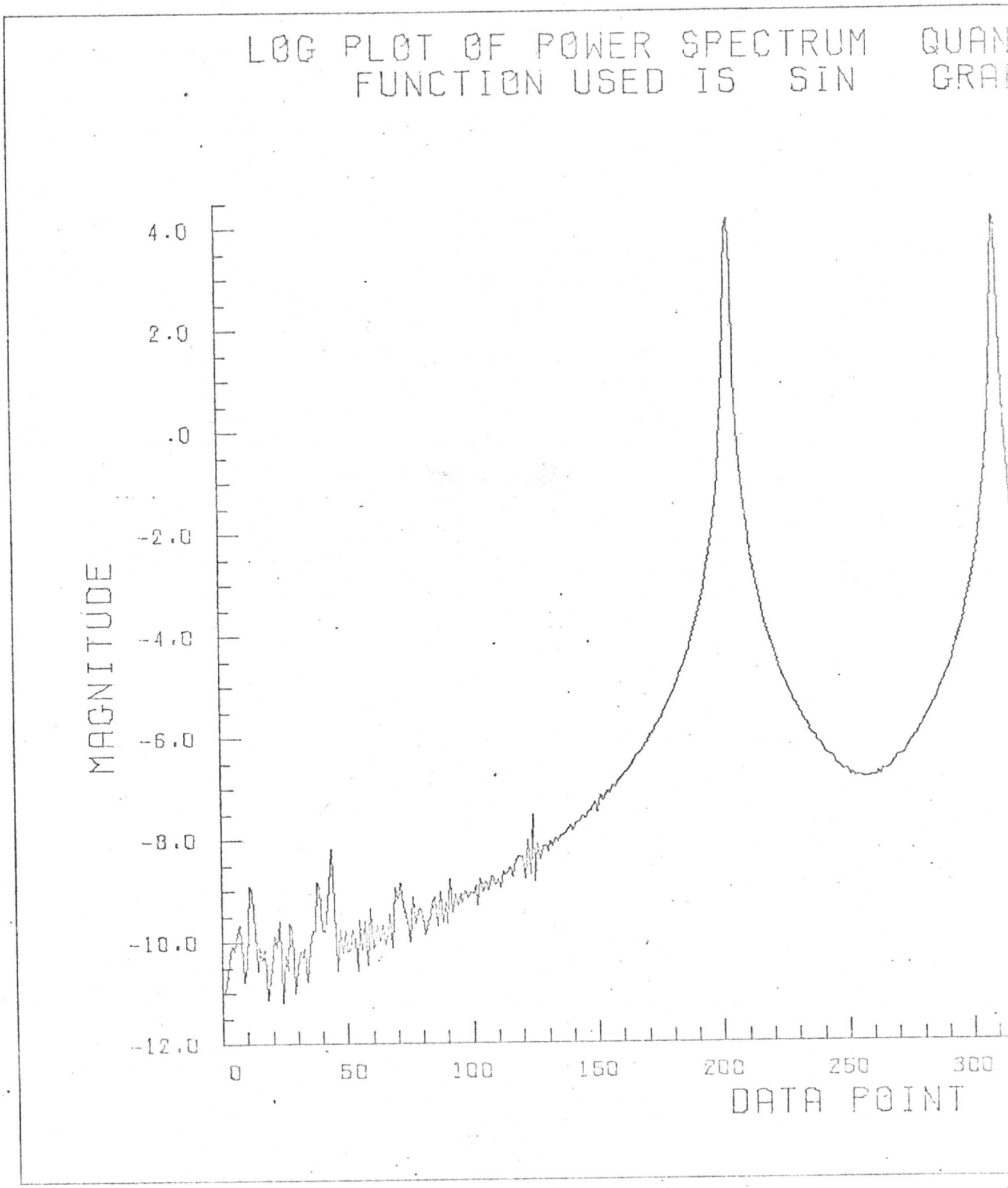

Cycles: 202.68
Window: Hamming
Avg. Value: 0.00000
Date: 12/30/72-27

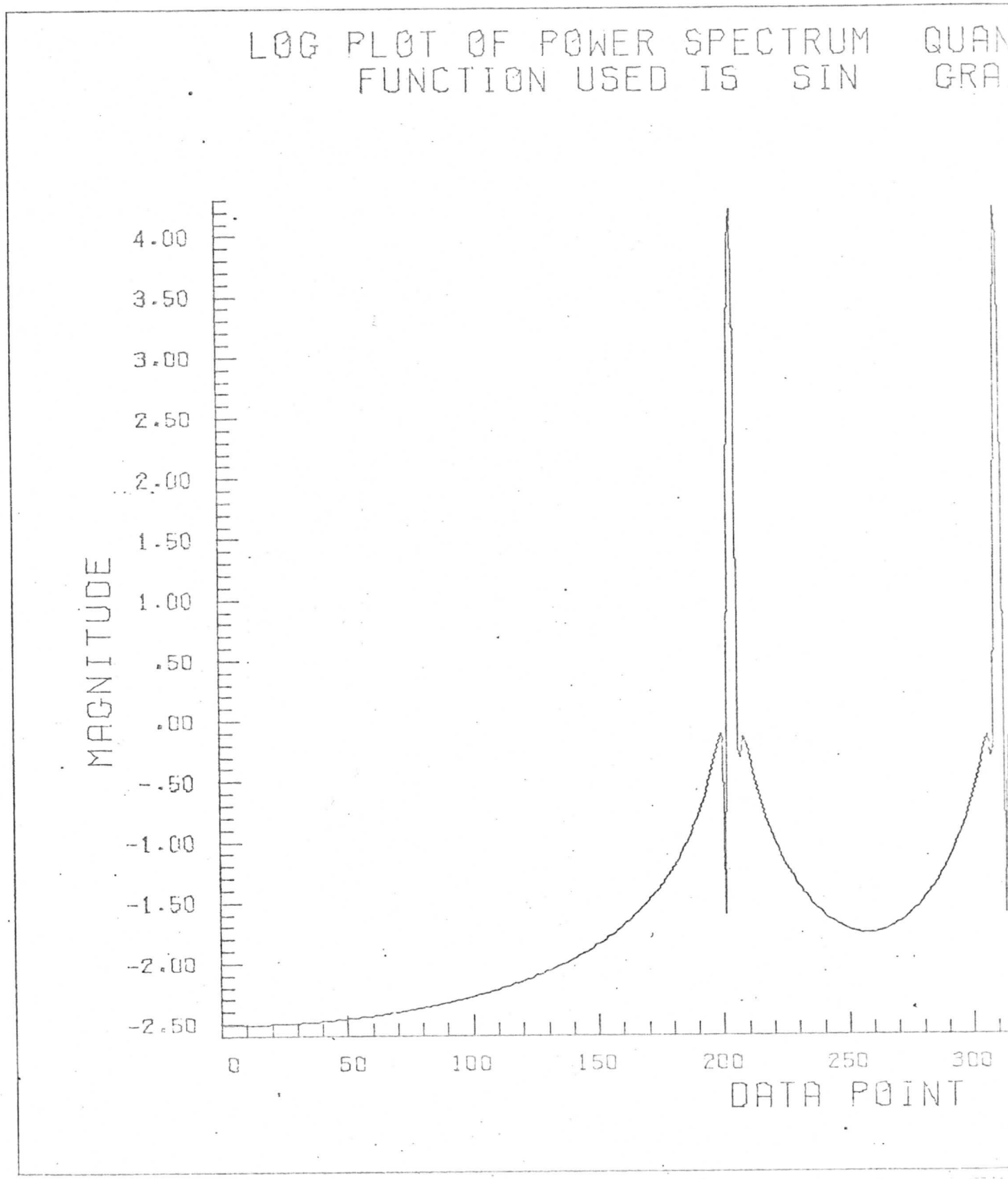

Cycles: 202.68
Window: Papoulis
Avg. Value: 0.0000
Date: 2/15/73-10

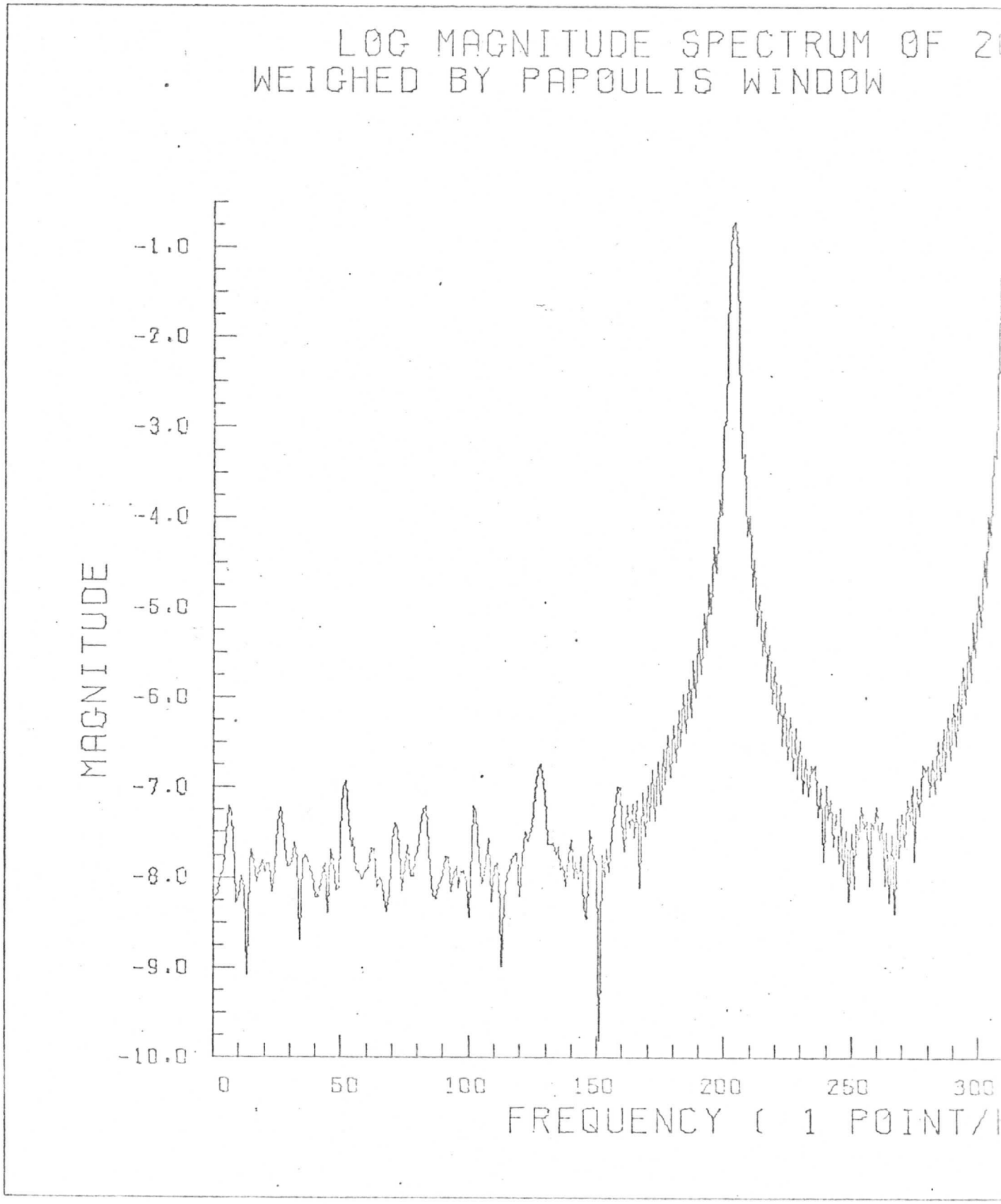

FIGURE A.2. POWER SPECTRAL PLOTS OF A SAMPLE LINE OF APOLLO VI PICTURE DATA

Notes:

1) A 512-point discrete Fourier transform was used and therefore all spectra are aliased about the 256 data point in the transforms.
2) The vertical scale is logarithmic ($S_{dB} = 10 \log_{10} S$).
3) The particular choice of data window is specified on each plot.

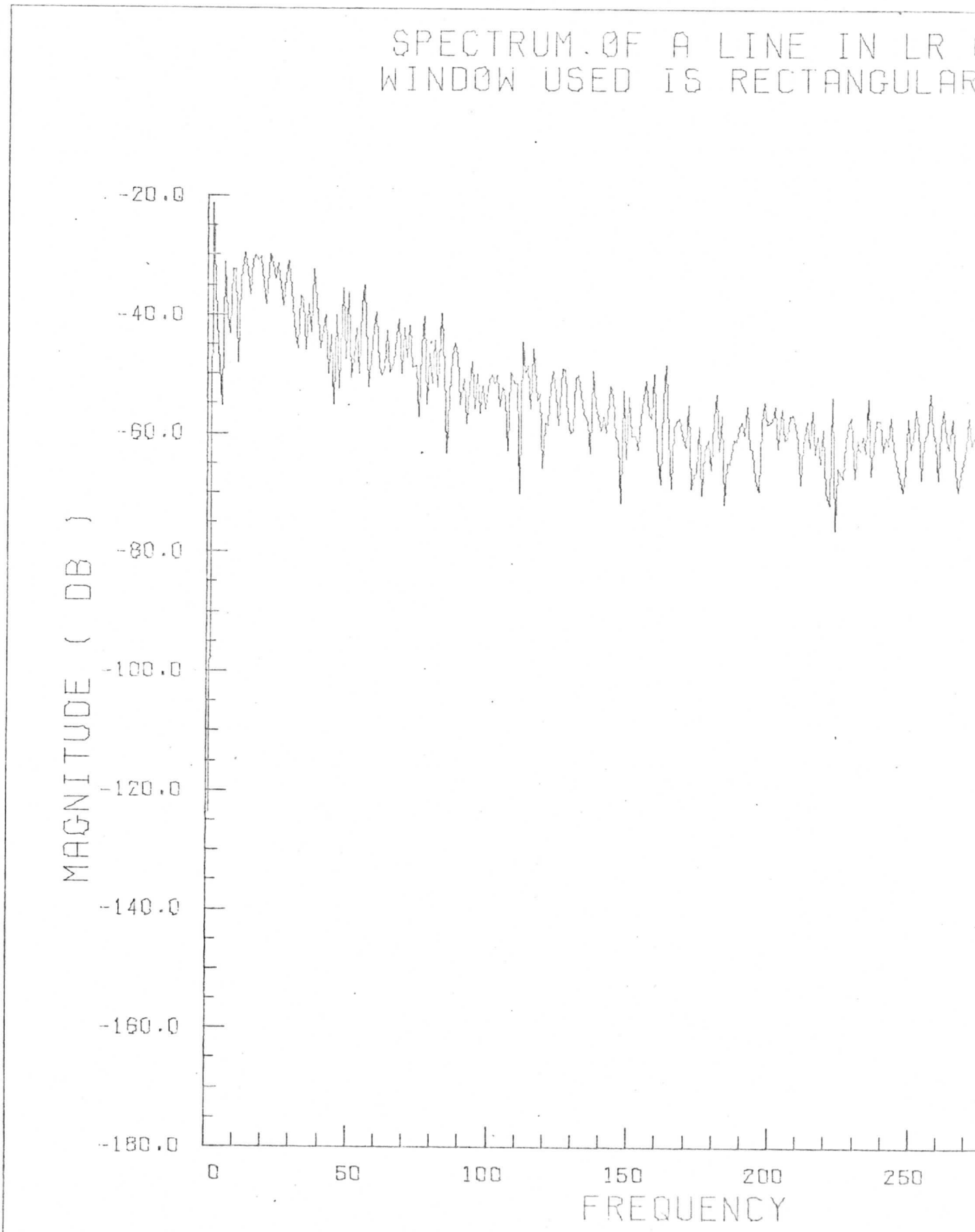
SPECTRUM.0F A LINE IN LR
WINDOW USED IS RECTANGULAR
-20.0
-40.0
-60.0
-80.0
-100.0
-120.0
-140.0
-160.0
-180.0
MAGNITUDE (DB)
0
50
100
150
200
250
FREQUENCY

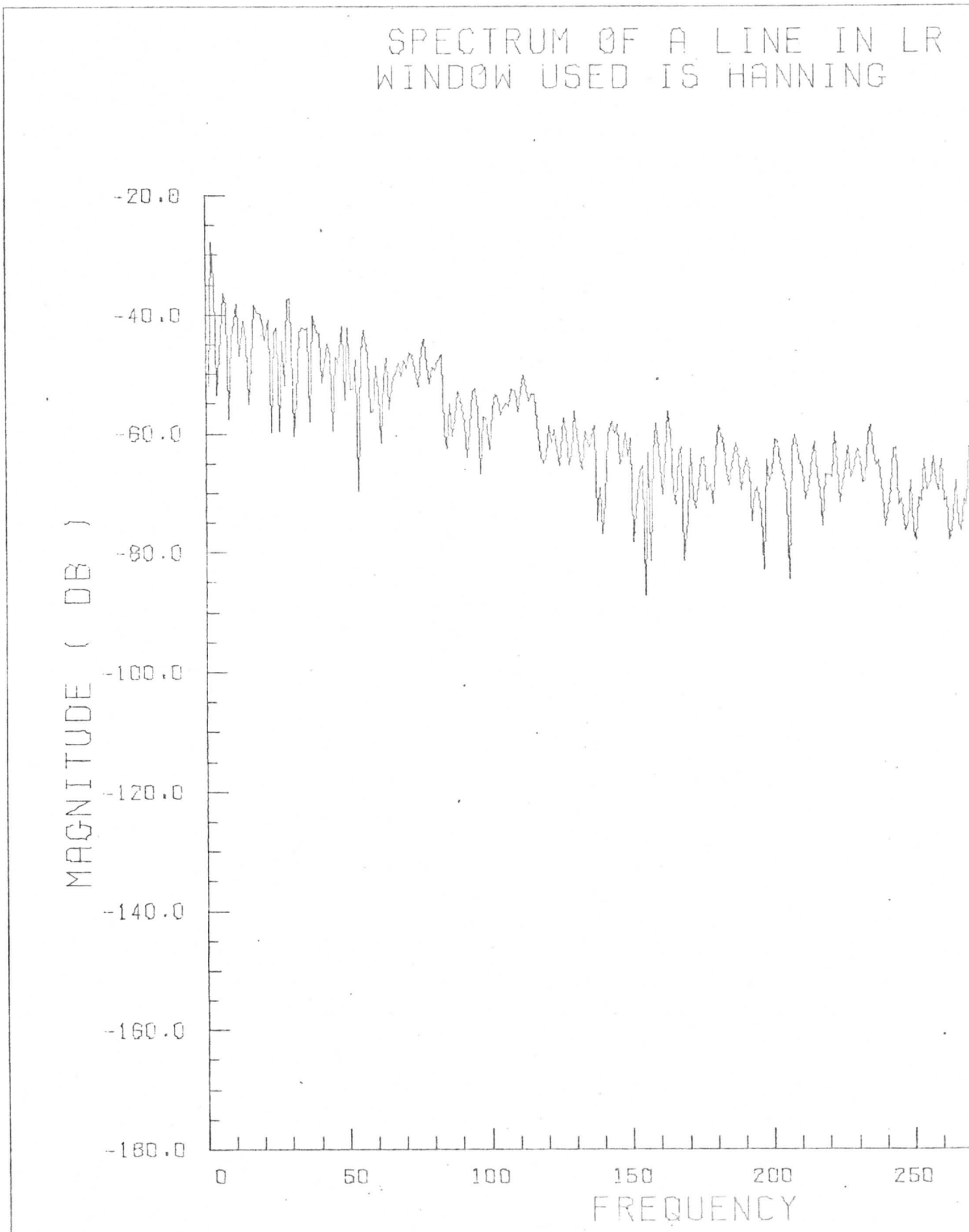
SPECTRUM OF A LINE IN LR
WINDOW USED IS HANNING
-20.0
-40.0
-60.0
-80.0
-100.0
-120.0
-140.0
-160.0
-180.0
MAGNITUDE (DB)
0
50
100
150
200
250
FREQUENCY

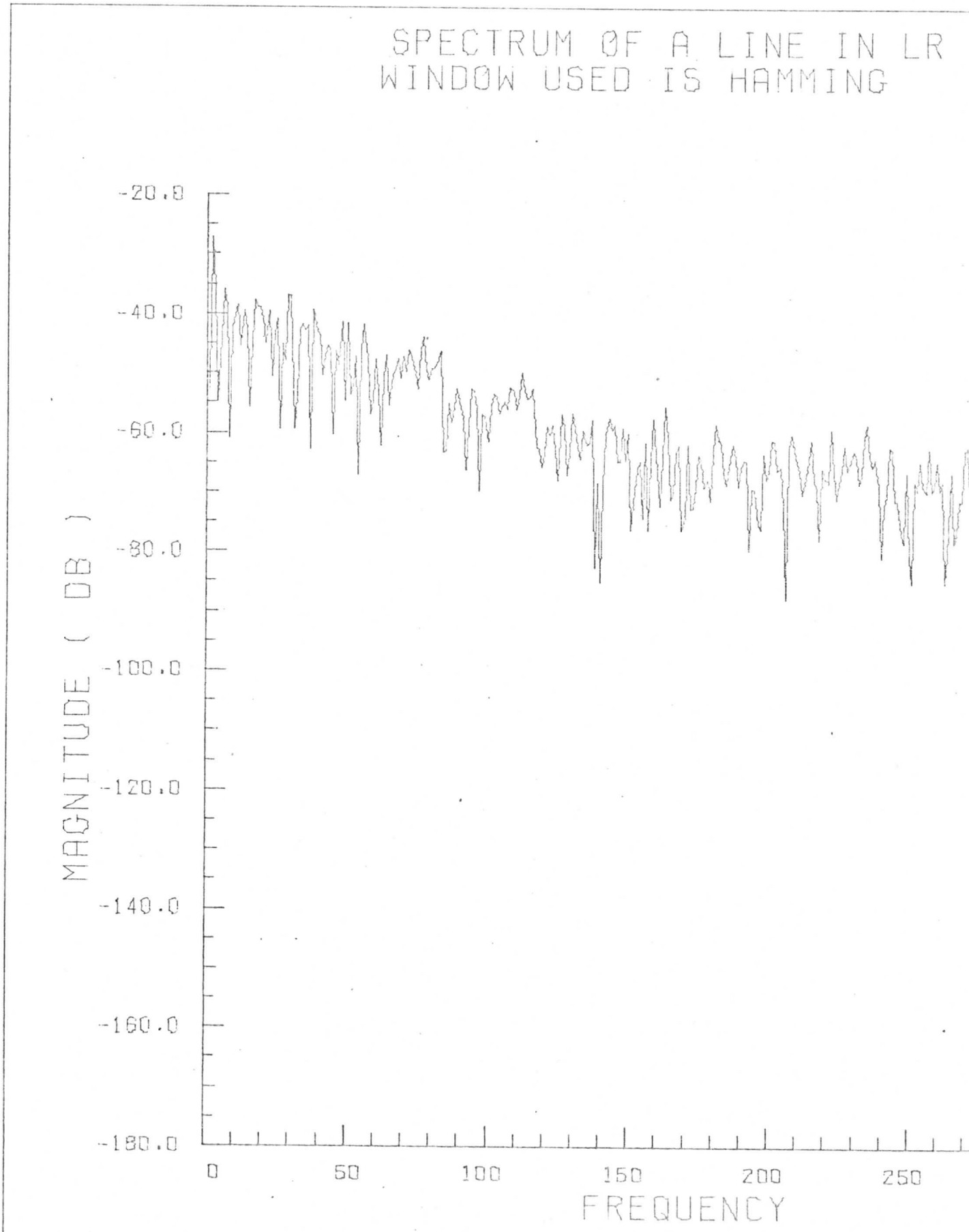
SPECTRUM OF A LINE IN LR
WINDOW USED IS HAMMING
-20.0
-40.0
-60.0
-80.0
-100.0
-120.0
-140.0
-160.0
-180.0
MAGNITUDE (DB)
0
50
100
150
200
250
FREQUENCY

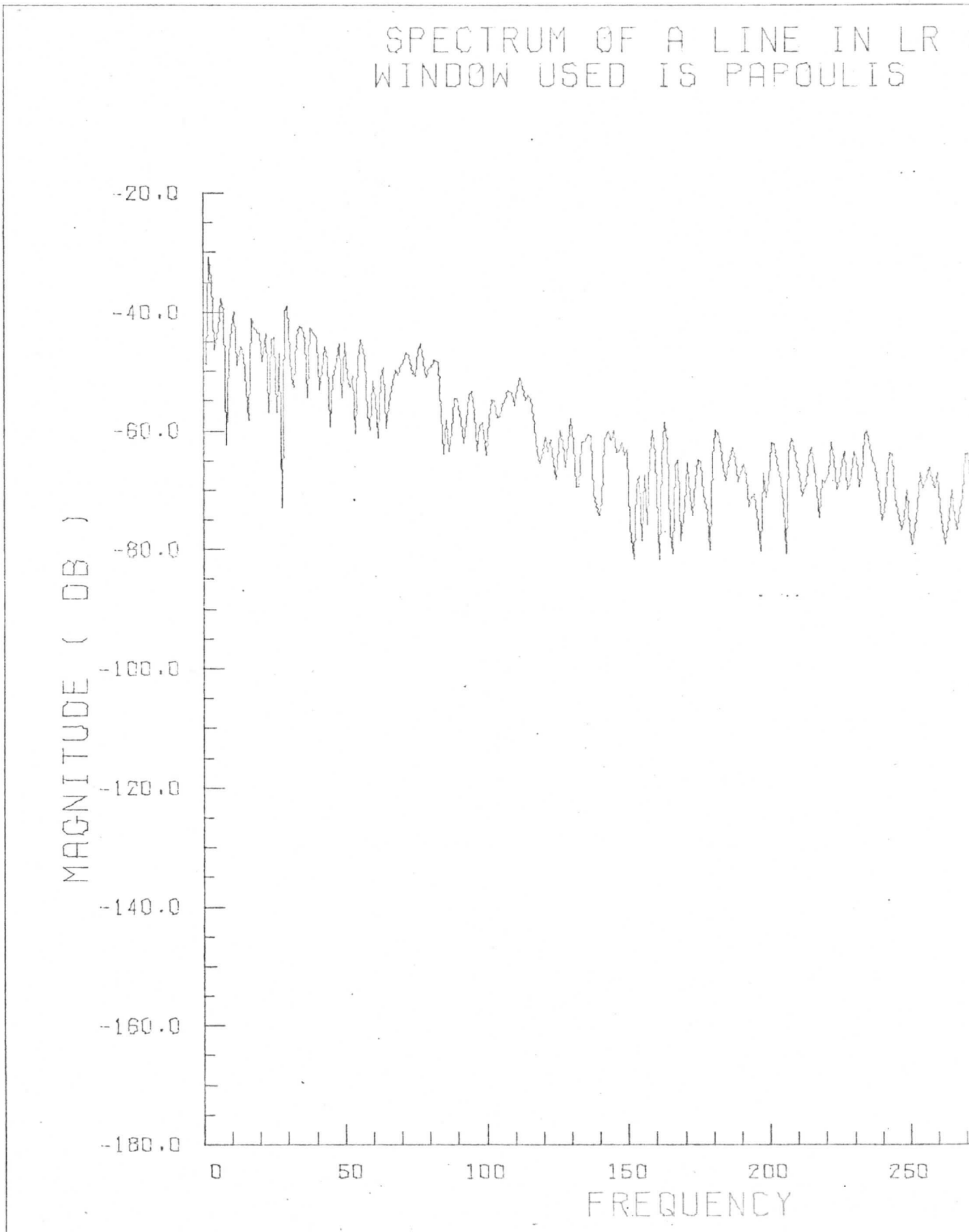
SPECTRUM OF A LINE IN LR
WINDOW USED IS PAPOULIS
-20.0
-40.0
-60.0
-80.0
-100.0
-120.0
-140.0
-160.0
-180.0
MAGNITUDE (DB)
0
50
100
150
200
250
FREQUENCY

APPENDIX B

OPTICAL SPECTRA AND DATA SAMPLING RESTRICTIONS

In analyzing continuous data using sampled values, it is necessary that the data be band-limited, or, if not, at least have spectral components at higher frequencies that are small compared to the frequencies of interest. If this is not the case, substantial aliasing (see Appendix D) may occur, destroying the accuracy of the desired data. Because the pictoral data of interest is not band-limited until one approaches the resolution limits of the film and camera, the question becomes how close should adjacent samples be to provide an acceptable margin at the frequencies of interest while at the same time keeping the samples independent and free from film irregularities. In order to help answer this question, we have obtained power spectra of selected portions of ten Apollo VI transparencies using the transparencies in an optical spectrum analyzer. Based on these results, we believe that independent samples taken at a rate of 20 samples/mm on 70 mm film is sufficient for our purposes. This appendix briefly describes this procedure.

The method of finding the two-dimensional Fourier transform of a modulated transparency is well-known (Goodman, 1968) and is illustrated in Figure B.1. The exposure of a film in the back focal plane of the lens produces a second transparency whose transmittance is proportional to the squared magnitude of the two-dimensional Fourier transform. Aside from a scaling constant, this is then the two-dimensional power spectrum (see Equation A.7) of the scene modulated on the first transparency.

The optical spectra shown here were made using the excellent optical facilities of Professor Howard J. Pincus at the Department of Geological

Figure B.1. Optical System Used to Generate Two-Dimensional Power Spectral Plots

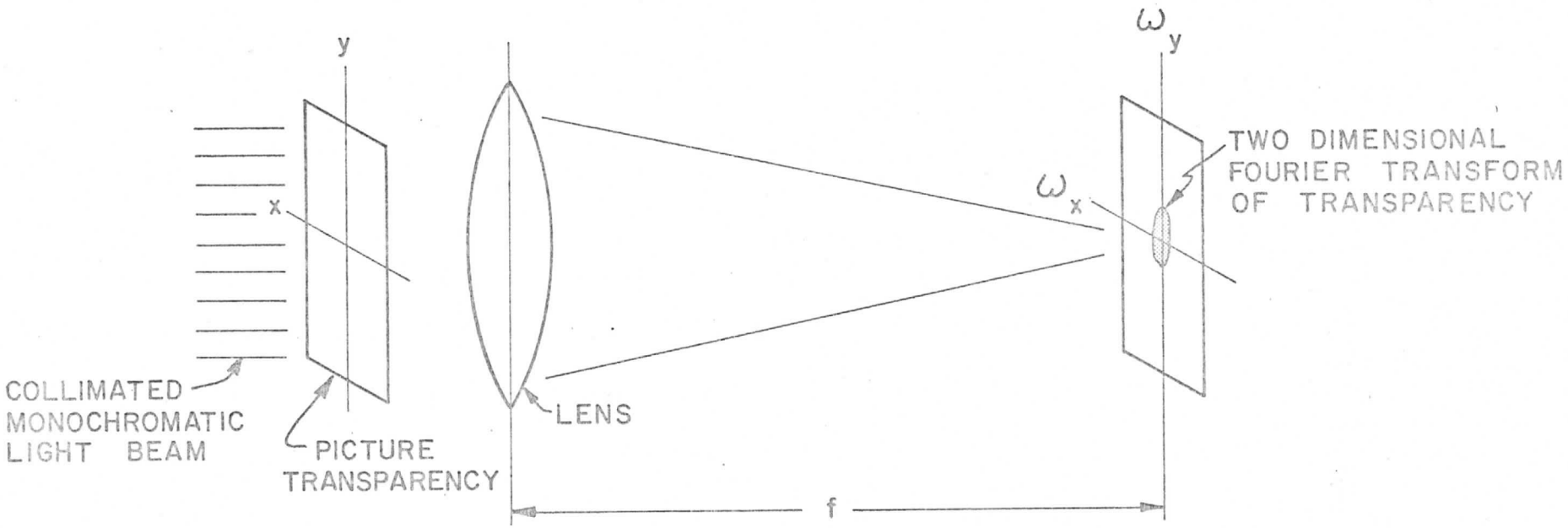
y
x
ω_y
ω_x
TWO DIMENSIONAL
FOURIER TRANSFORM
OF TRANSPARENCY
COLLIMATED
MONOCHROMATIC
LIGHT BEAM
PICTURE
TRANSPARENCY
LENS
f

Sciences, University of Wisconsin-Milwaukee. The picture transparencies used were 35 mm. (24 x 36 mm area) with the longer axis equal to the 57 mm width of the Apollo VI transparency on the 70 mm film. Both the 70 mm and the 35 mm black-and-while transparencies were copied from third-generation NASA color transparencies using Panatomic X high resolution film. The optical aperture was restricted to one-fourth the picture area. The corresponding two-dimensional power spectra for the designated quarter are shown in Figure B.2. A calibration grid with frequency spacings at multiples of 2.5 samples/mm is also shown.

In the plots of Figure B.2, the magnitude of the power spectra is in the intensity. Exposures were made at 1/4, 1/2, and 1 second and the prints shown are at the 1/2 second exposure time. Contours of miminum discernible exposure for the three exposure times are shown in Figure A.3 for four very different cases. The highest frequencies are less than 10 samples/mm, thus we feel that a sampling rate of 30/mm is adequate on 35 mm film for these pictures. Translated to the 70 mm format, this is equivalent to a sampling rate of 30 x 36/57 = 18.95/mm. We use an active area of 56 x 56 mm on the 70 mm film to allow a 1/2 mm margin and avoid edge effects. This is equivalent to 18.95 x 56 = 1061 samples per line. We have used 1024 samples per line throughout this report giving a data sampling frequency of 18.3 samples/mm.

The SMS sampling frequency is set at 500 kHz. The primary effects of aliasing in SMS then occur in the vicinity of 250 kHz, the half-sampling frequency. At the subsatellite point, this SMS sampling frequency corresponds to $\frac{500}{202} = 2.47$ cycles per n.mi. The spatial scaling for Apollo VI is about 81 n.mi. for the 57 mm frame width so that the equivalent SMS sampling frequency

on the 70 mm film is:

$$\frac{500}{202} = \frac{81}{57} = 3.52 \text{ cycles/mm.}$$

Thus, our Apollo VI data sampling frequency, compared to the SMS sampling frequency, is: 18.3/3.52 = 5.2, yielding a good margin.

Figure B.2. Optical Power Spectra of Selected Portions of Apollo VI Transparencies

Notes:

1) Scale factors and exposure held constant.

2) An equivalent aperture size 18 x 27 mm (referred to 70 mm film with an actual area of 57 x 57 mm) was used to restrict the scanning area. The position of this aperture is designated by quarters on the plots; e.g., ULQ refers to upper left quarter, etc.

3) Calibration grid generated using equally-spaced lines at 0.40 mm spacings in both dimensions.

4) Recorded on Panatomic X (35 mm) film at 1/2 second exposure.

5) Illumination supplied by He-Ne laser (λ = 6348A).

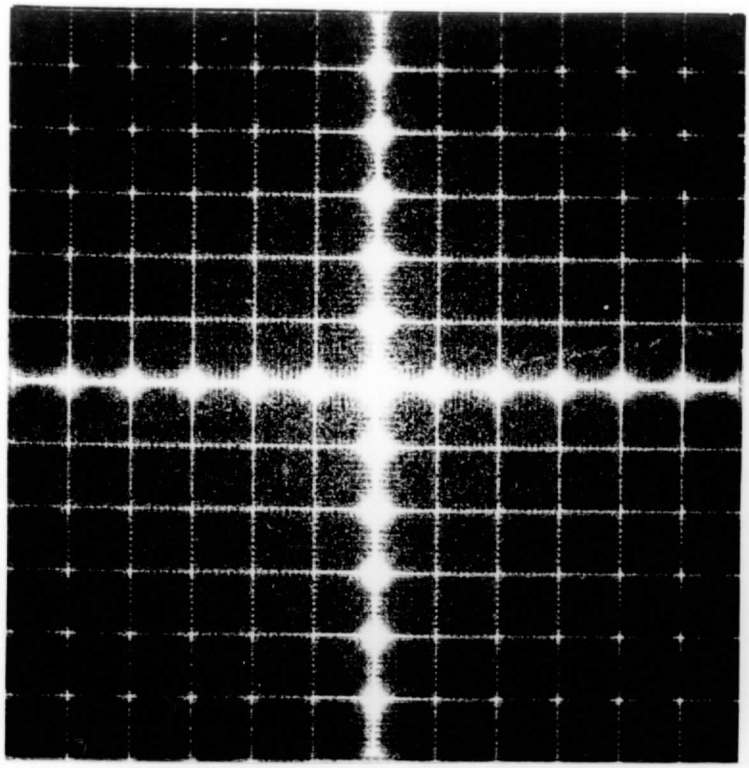

Calibration Pattern, 2.5 lines/mm.

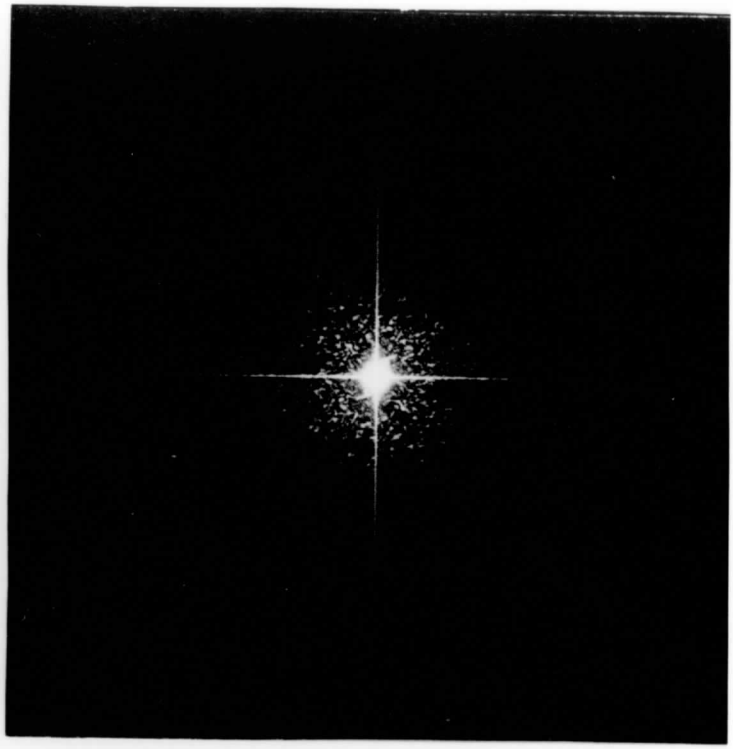

Apollo AS6-2-877 ULQ

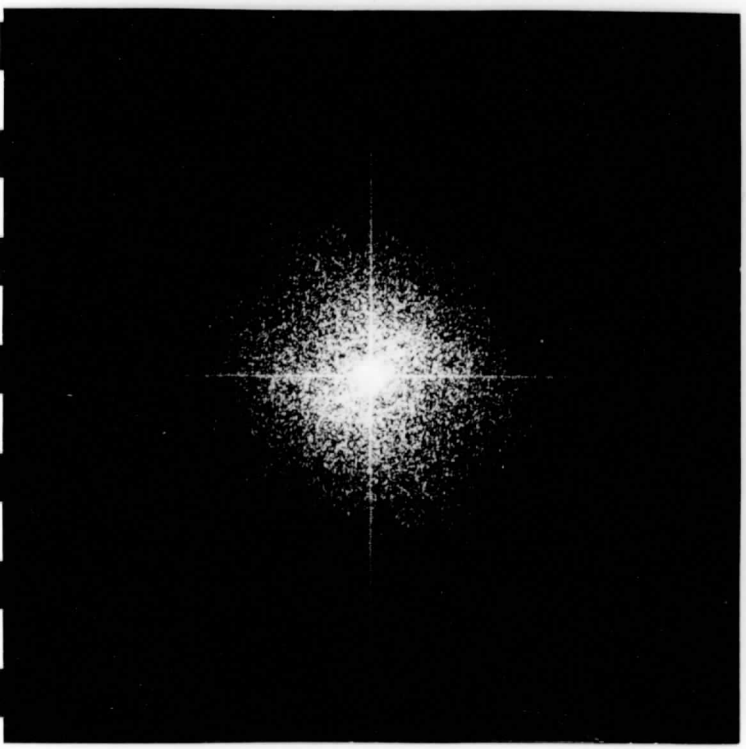

Apollo AS6-2-877 URQ

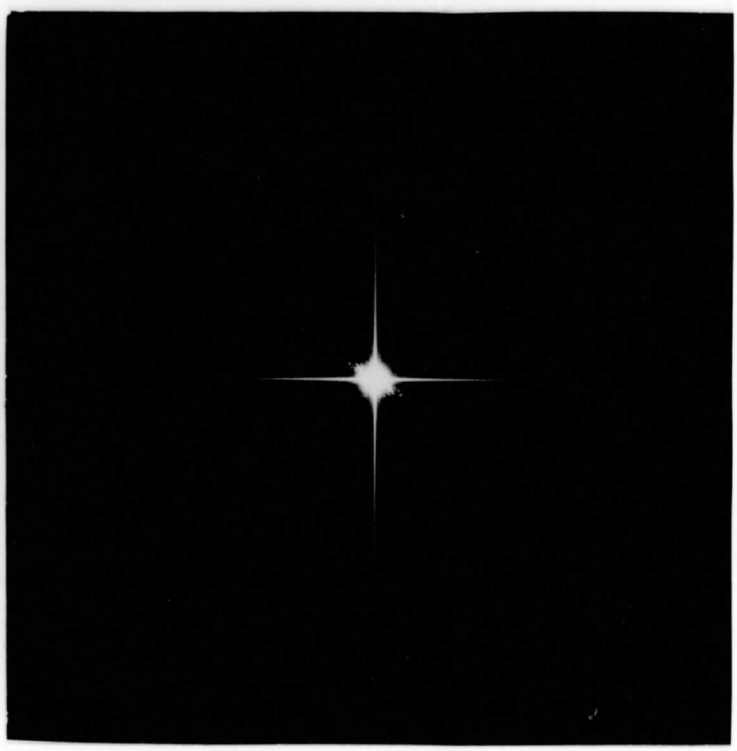

Apollo AS6-2-934 URQ

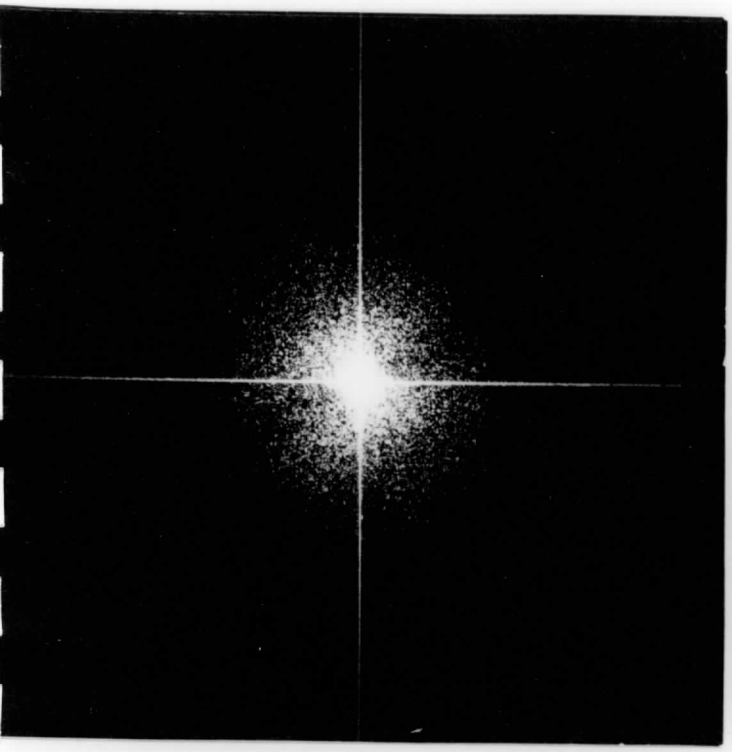

Apollo AS6-2-948 LLQ

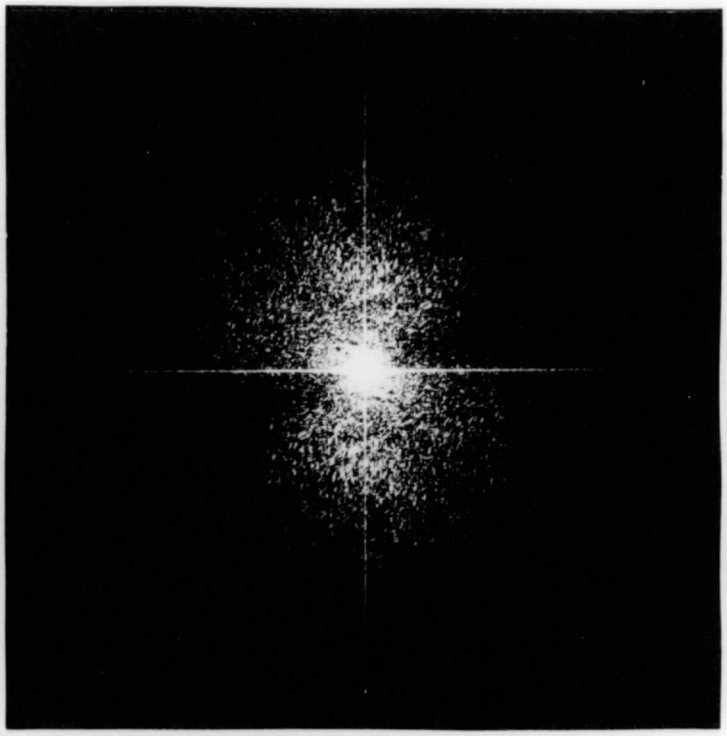

Apollo AS6-2-1064 URQ

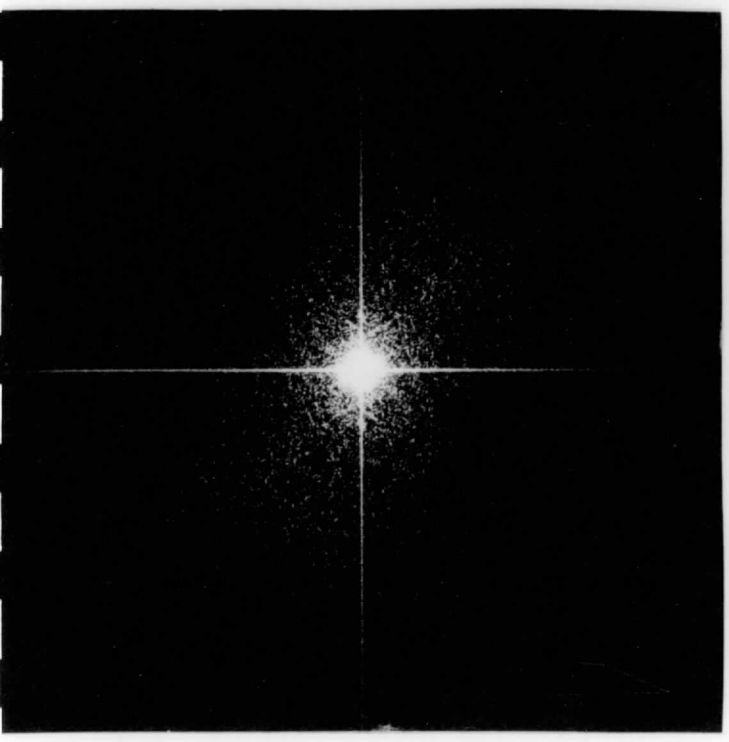

Apollo AS6-2-1429 LRQ

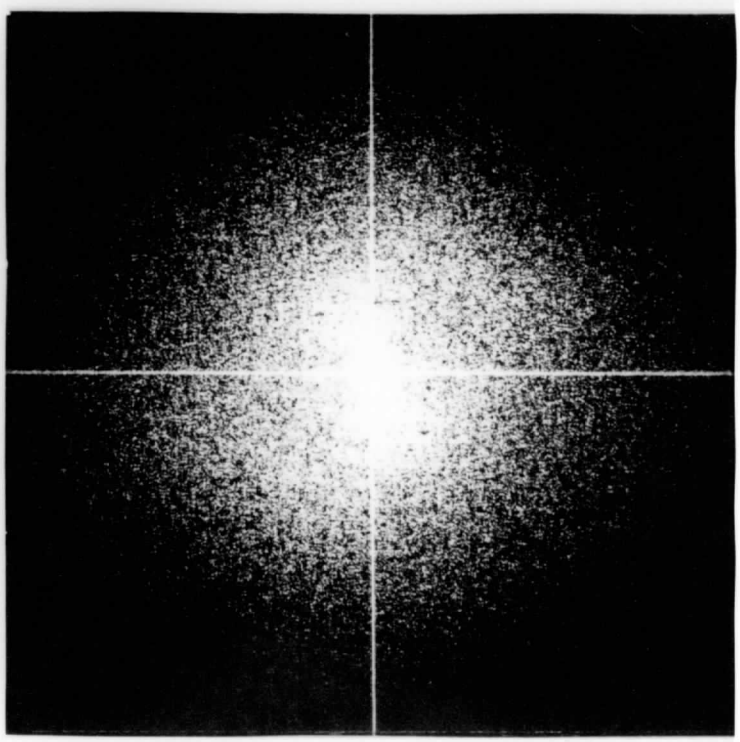

Apollo AS6-2-1430 Central

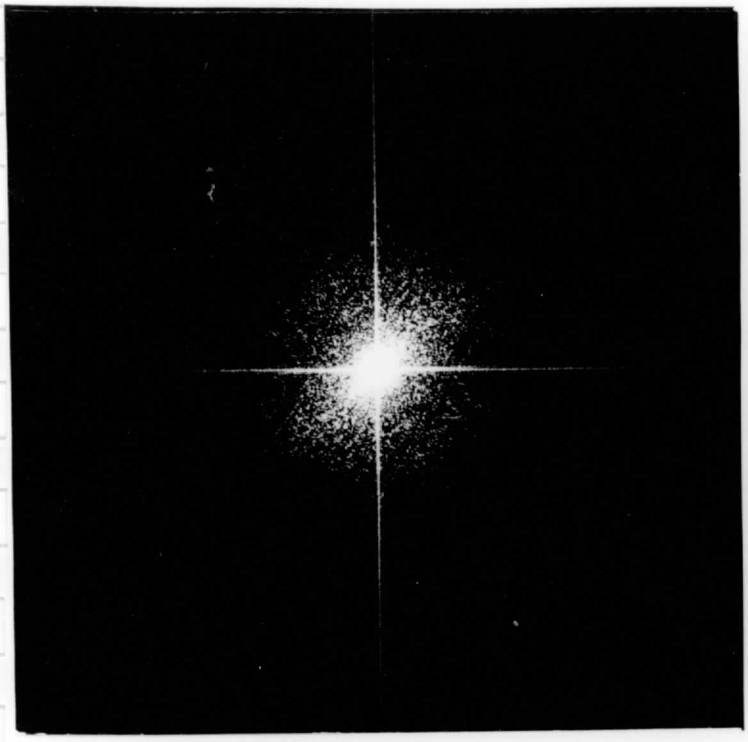

Apollo AS6-2-1467 LLQ

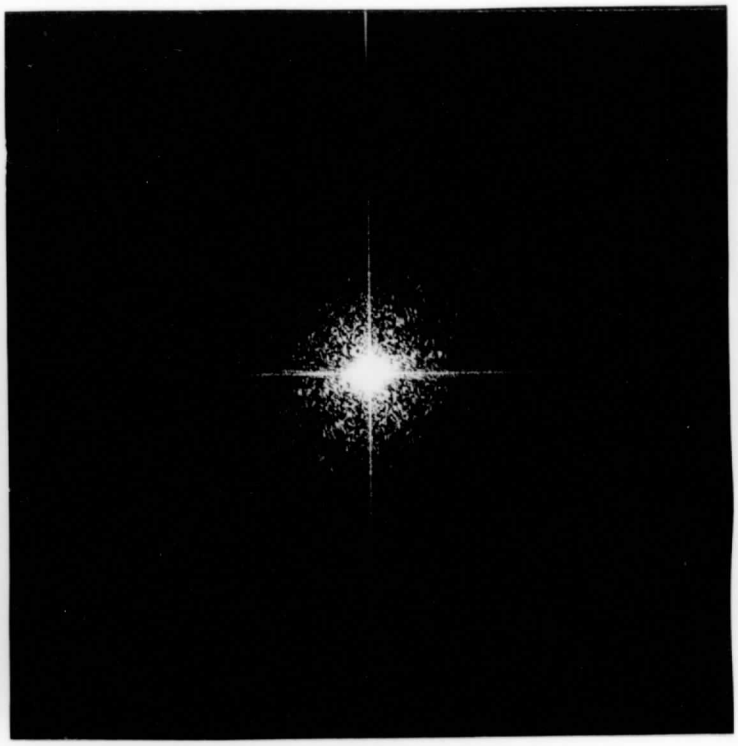

Apollo AS6-2-1468 LRQ

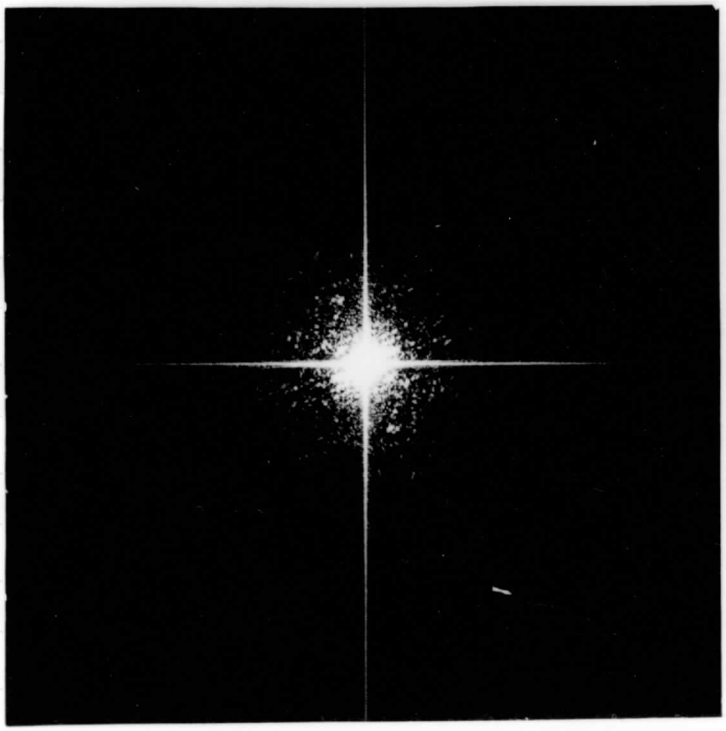

Apollo AS6-2-1469 LLQ

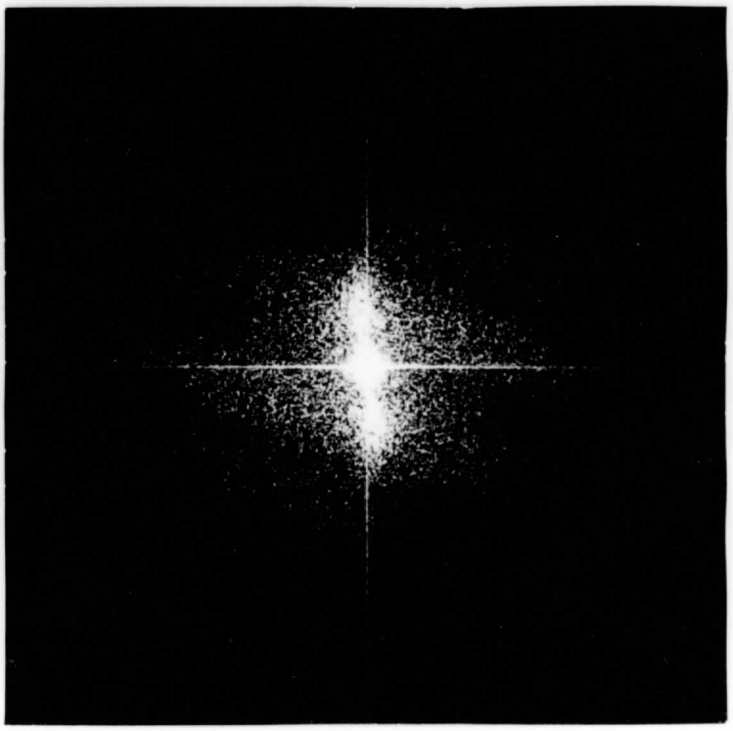

Apollo AS6-2-1484 Central

Figure B.3. Contours of Minimum Discernible Exposure in Four Selected Power Spectral Plots.

Notes:

1) Contours are for exposures of 1/4, 1/2, 1 second.
2) Circle for 10/mm on 35 mm film is shown.

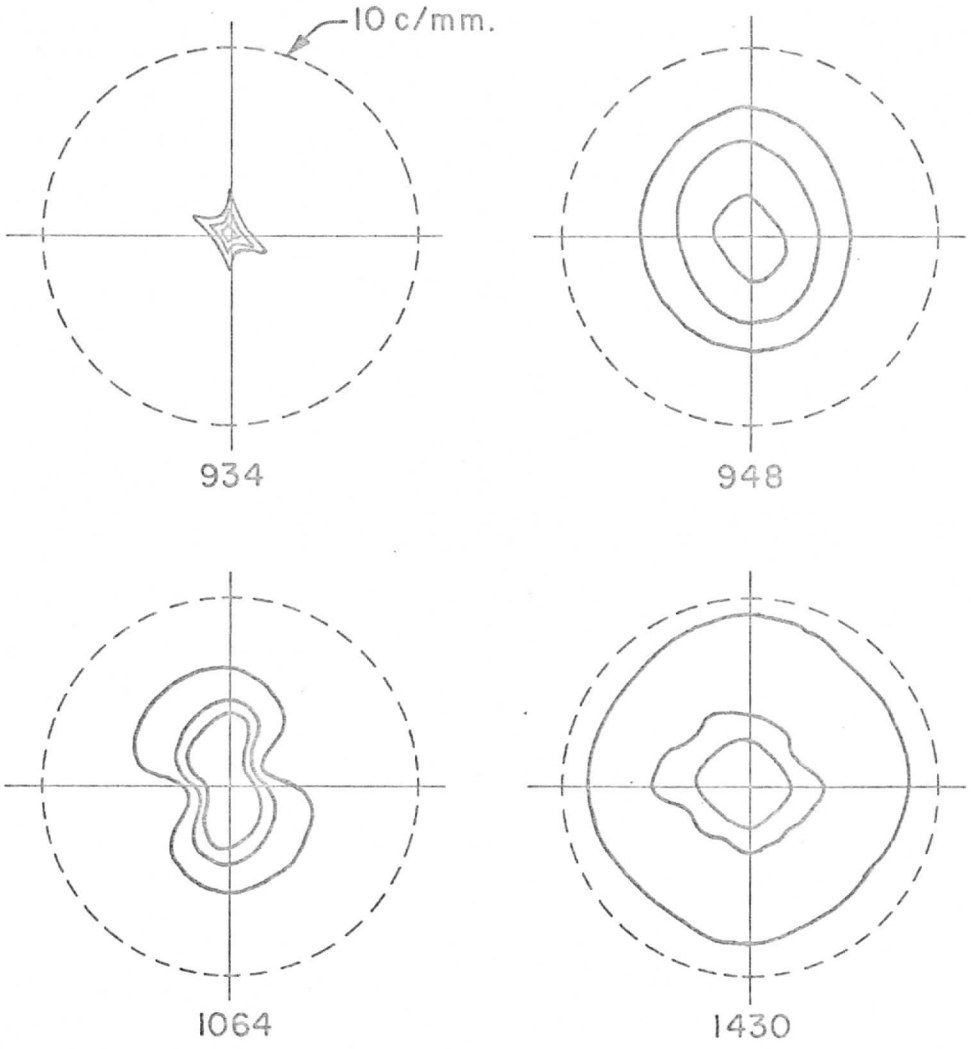
10 c/mm.
934
948
1064
1430

APPENDIX C

GEOMETRICAL SCALING AND DISTORTION EFFECTS

In this appendix, we develop the geometrical relations between the earth coordinates and the satellite coordinates and the rate of change (frequency) between them. The derivation is restricted to the case of a spin stabilized geostationary satellite.

The earth coordinate system is measured in terms of a longitude angle θ and a latitude angle ϕ. The satellite coordinate system is measured in terms of a spin scan angle β and a mirror tilt angle α. The VISSR channel measures a scene in terms of α, β, and this can be used to furnish an estimate of what the actual scene was in θ, ϕ. However, β is constant so that unequal amounts of time are spent in different parts of the hemisphere. This results in a nonuniform spatial resolution. The two items of interest here, then, are the coordinate mapping from α, β into ϕ, θ, and the frequency conversion factor from one system to the other.

C.1. Conversion of the Earth Coordinate System to the Satellite Coordinate System.

Let R be the distance between the centers of the earth and the satellite and r the radius of the earth, and let R_1 be the distance between the observed point on the surface of a spherical earth and the satellite. The geometry is shown in Figure C.1.

If P is a point on the surface of the earth of longitude and latitude angles θ and ϕ, and P' is its projection on the WE plane, then we can write:

FIGURE C.1. EARTH-SATELLITE GEOMETRY

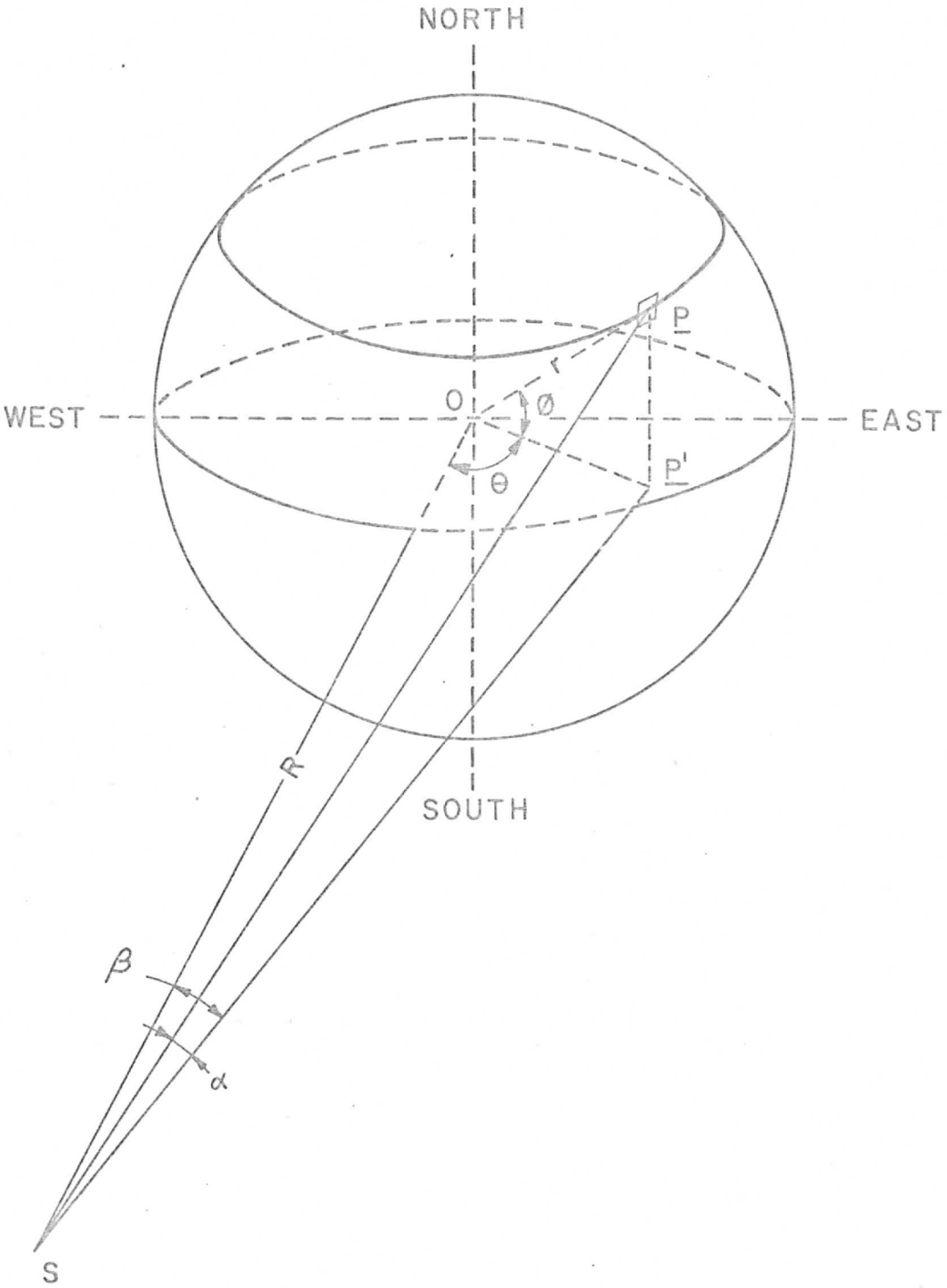
NORTH
WEST
EAST
SOUTH
O
P
P'
Ø
θ
R
β
α
S

$$OP = r \tag{C-1a}$$

$$PP' = r\sin\phi \tag{C-1b}$$

$$OP' = r\cos\phi \tag{C-1c}$$

From the geometry of the problem, we can express SP in terms of θ and ϕ (from $\Delta OSP'$):

$$\overline{SP'}^2 = r^2\cos^2\phi + R^2 - 2Rr\cos\phi\cos\theta \tag{C-2}$$

But since $\Delta SPP'$ is a right-angled triangle

$$\overline{SP}^2 = \overline{PP'}^2 + \overline{SP'}^2$$

$$= R^2 + r^2 - 2Rr\cos\phi\cos\theta \tag{C-3}$$

Also, because the angle between SP and its projection SP' is the tilting angle α, we can write:

$$\sin\alpha = \frac{r\sin\phi}{SP} \tag{C-4}$$

Substituting Equation C-3 into Equation C-4, we get:

$$\sin\alpha = \frac{r\sin\phi}{\sqrt{R^2 + r^2 - 2Rr\cos\phi\cos\theta}} \tag{C-5}$$

To find β in terms of θ and ϕ we consider $\Delta OSP'$, $\angle OSP'$ is equal to β because it is the projection of $\angle O'SP$ (which is also β) on the WE plane. It is obvious that:

$$\tan\beta = \frac{r\cos\phi\sin\theta}{R - r\cos\phi\cos\theta} \tag{C-6}$$

Thus, for any point on the surface of the earth with known longitude and latitude angles, we can determine the corresponding co-ordinates α and β of this point by using Equations C-5 and C-6.

A belief in reciprocity would encourage us to look for another couple of equations that would give the latitude and longitude of a point on the surface of the earth, knowing its coordinates α and β.

If we substitute Equations C-12 and C-13 in Equation C-10 we can express SP in terms of α and β:

$$SP = R_1 = R\cos\alpha\cos\beta - \sqrt{r^2 - R^2\sin^2\alpha - R^2\cos^2\alpha\sin^2\beta}$$

Also, we can write:

$$SP' = SP\cos\alpha$$

$$PP' = SP\sin\alpha$$

But we know that

$$PP' = r\sin\phi$$

Hence,

$$\sin\phi = \frac{R_1\sin\alpha}{r}$$

Considering $\Delta SOP'$ it can be easily found that:

$$\tan\theta = \frac{\overline{SP'}\sin\beta}{R - \overline{SP'}\cos\beta}$$

$$\tan\theta = \frac{R_1\cos\alpha\sin\beta}{R - R_1\cos\alpha\cos\beta}$$

C.2. Calculation of SMS Field of View and Frequency Scaling Conversion Factor

In this section, we show the conversion necessary to find the actual field of vision along the surface of the earth as viewed by the SMS. We will approximate the variation in the field of view, to be the same as the variation in the velocity as the satellite scans the surface of the earth (R. Parent). The item of interest is the relative scanning velocity factor at any point on the surface in terms of the co-ordinate system α and β defined at the satellite point, where α is the tilting angle, and β is the satellite scan angle (refer to Figure C-2). The problem is two-dimensional. However, it is not restricted to the plane passing through the center of the earth and perpendicular to the satellite spin axis, but to a plane that makes an angle α with the former plane.

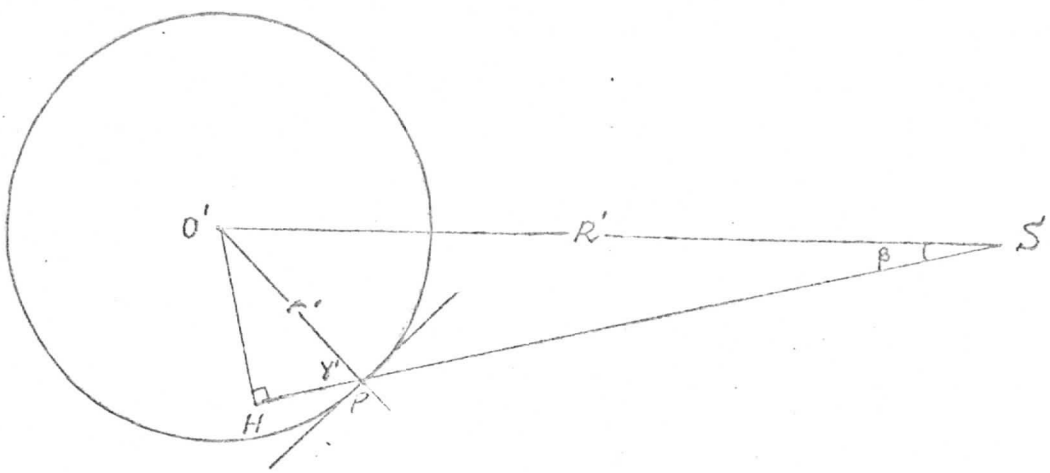

Figure C.2.

This plane intersects the earth in a circle of center $0'$. Let R' be the distance between $0'$ and the center of the satellite, r' the radius of the circle $0'$, Let and $0'H$ DE the projection of $0'$ on the line joining the observed point P on the surface of the earth and the satellite.

For a constant angular rate $\dot{\beta}$, the phase velocity along the earth's surface is:

$$v_p = v/\cos\gamma' \tag{C-7}$$

where v is the tangential velocity:

$$v = \dot{\beta}R_1. \tag{C-8}$$

The relative increase in the phase velocity v_p over that at the satellite subpoint, v_{p_0}, is then:

$$\Gamma = \frac{v_p}{v_{p_0}} = \frac{R_1}{(R-r)\cos\gamma'} \tag{C-9}$$

where

$$R_1 = R'\cos\beta - \sqrt{r'^2 - R'^2\sin^2\beta} \tag{C-10}$$

and

$$\cos\gamma' = \frac{\sqrt{r'^2 - R'^2\sin^2\beta}}{r'} \tag{C-11}$$

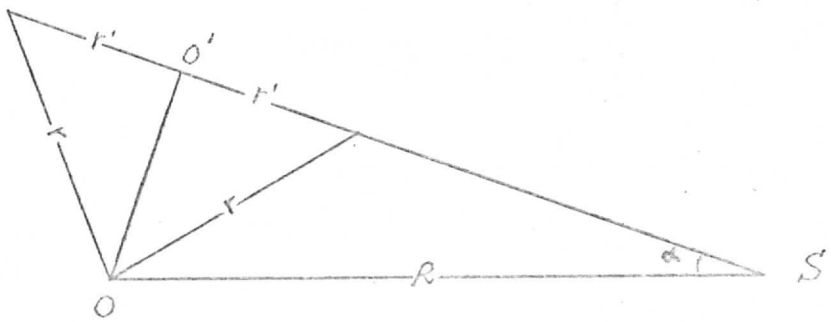

Figure C.3.

From the geometry of Figure C.3, we can express the parameters R' and r' in terms of R, r, and α, the tilting angle. We can write:

$$r' = \sqrt{r^2 - R^2\sin^2\alpha} \tag{C-12}$$

and

$$R' = R\cos\alpha \tag{C-13}$$

Substituting the values of r' and R' in Equations C-10 and C-11, the correction factor can be expressed as:

$$\Gamma = \frac{R\cos\alpha\cos\beta - \sqrt{r^2 - R^2\sin^2\alpha - R^2\cos^2\alpha\sin^2\beta}}{(R-r)\sqrt{\dfrac{r^2 - R^2\sin^2\alpha - R^2\cos^2\alpha\sin^2\beta}{r^2 - R^2\sin^2\alpha}}} \tag{C-14}$$

Using Equations C-5 and C-6 in C-14, we can find a frequency conversion factor giving the increase in surface scanning velocity as a function of θ, ϕ. This is shown in Figure 3.2. As noted, this graph also gives the relative increase in the field of view in the scan direction.

The apparent instantaneous frequency f_1 viewed from the satellite is proportional to the satellite spin rate ~~times~~ multiplied by the phase velocity correction factor Γ:

$$f_1 = f\,\dot{\beta}\,(R-r)\Gamma. \tag{C-15}$$

Because the satellite spin rate is a constant,

$$\dot{\beta} = 100 \text{ rpm} = 10.47 \text{ rad/sec.},$$

we can conveniently normalize everything to the satellite subpoint:

$$\dot{\beta}(R-r) = (10.47)(19,360) = 0.202 \text{ n.mi./}\mu\text{-sec.}$$

Thus the frequency conversion is:

$$f_1 = 0.202\ \Gamma f \qquad \text{(C-16)}$$

where:

f_1 = apparent instantaneous frequency in MHz

f = spatial frequency in cycles per nautical mile

Γ = phase velocity correction factor.

C.3. Geometrical Mapping From Satellite to Earth Coordinate System

The satellite measures coordinates in the α, β frame of reference. The scene is measured in the θ, ϕ frame of reference. The mapping between the two is quite linear for small angles from the subsatellite point, but may become quite nonlinear for larger angles. This mapping can be portrayed by tracing the locii of constant α and constant β in the θ, ϕ coordinate system.

From Equation C-6 we find the equation of the curves of constant β to be:

$$\phi = \cos^{-1}\left[\frac{\tan\beta}{\varepsilon(\cos\theta\tan\beta+\sin\theta)}\right] \qquad \text{(C-17)}$$

where $\varepsilon = r/R = 0.151$, and provided that:

$$\tan\beta \leq \frac{\sin\theta}{1-\varepsilon\cos\theta} \quad . \qquad \text{(C-18)}$$

Similarly, the equation of the curves of constant α is found from Equation C-5 to be:

$$\theta = \cos^{-1}\left[\frac{\varepsilon}{2\cos\phi}\left(1 + \frac{1}{\varepsilon^2} - \frac{\sin^2\phi}{\sin^2\alpha}\right)\right] \tag{C-19}$$

provided that:

$$\sin^2\alpha \leq \frac{\varepsilon^2\sin\phi}{(1+\varepsilon^2-2\varepsilon\cos\phi)} \; . \tag{C-20}$$

Curves of constant α and constant β are shown in Figure C.4.

FIGURE C.4. MAPPING FROM EARTH COORDINATES TO SATELLITE COORDINATES

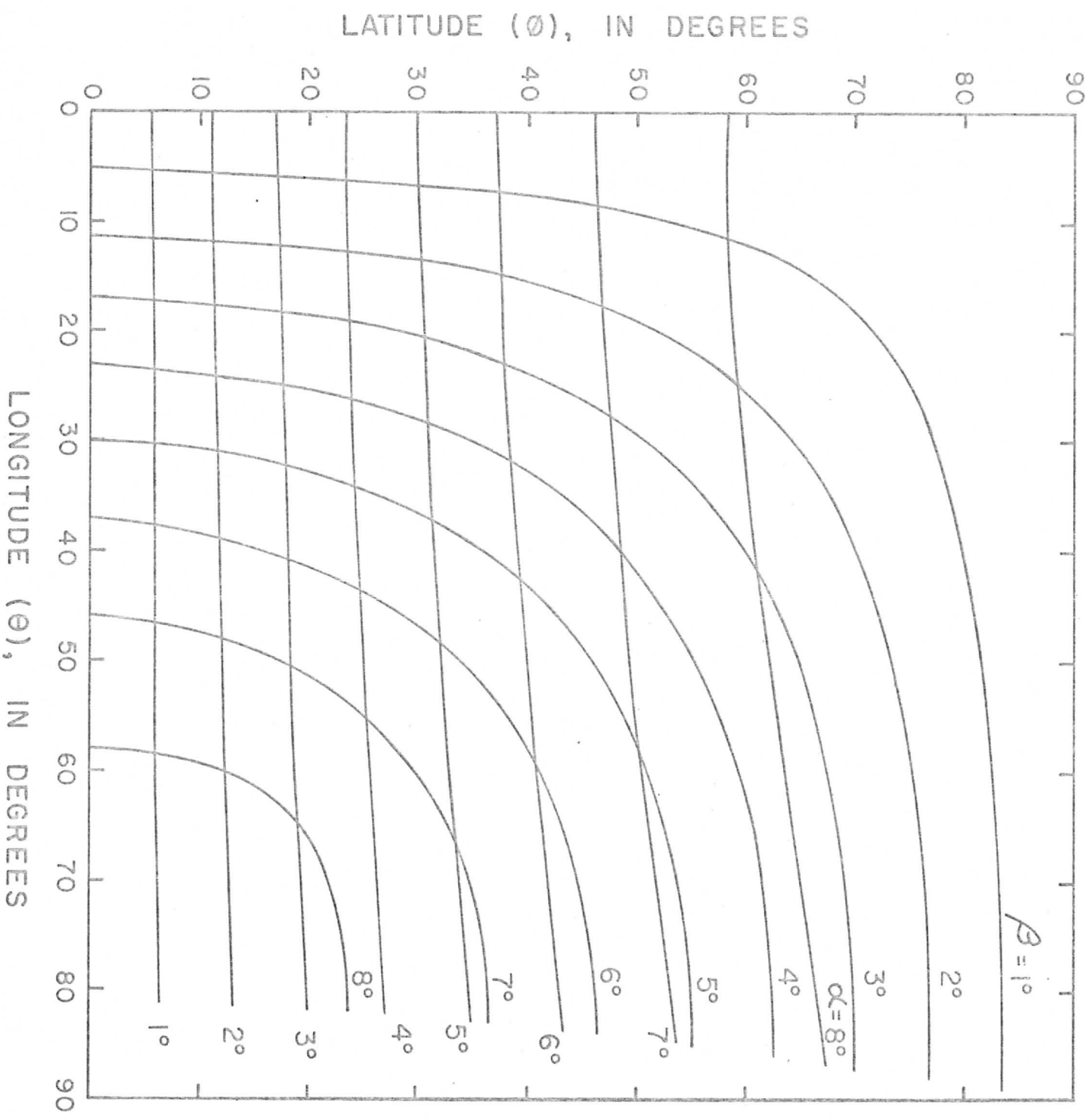
LATITUDE (Ø), IN DEGREES
0
10
20
30
40
50
60
70
80
90
LONGITUDE (Θ), IN DEGREES
0
10
20
30
40
50
60
70
80
90
β = 1°
2°
3°
α = 8°
4°
5°
6°
7°
8°
1°
2°
3°
4°
5°
6°
7°

Appendix D

A Measure of the Effective Bandwidth Due to Aliasing Errors

The purpose of this appendix is to motivate a measure of the effects of aliasing caused by under-sampling a signal. We begin by discussing the concept of sampling a deterministic signal. After the effects of aliasing ~~in this case~~ have been ~~illuminated~~ explained, we will extend the results to stochastic processes.

Suppose that we wish to sample a waveform f(t) every T seconds. The resulting sampled version $f_s(t)$ may be represented as:

$$f_s(t) = f(t)\ g(t) \tag{D-1}$$

The function g(t) is a periodic function with period T. For example, it could be a typical gate function, as is shown in figure D-1.

~~In order~~ To determine $F_s(\omega)$, the spectrum of $f_s(t)$, we expand g(t) in a Fourier series:

$$g(t) = \sum_{n=-\infty}^{+\infty} c_n\ e^{jn\omega_s t} \tag{D-2}$$

$$\text{where } c_n = \frac{1}{T}\int_0^T g(t)\ e^{-jn\omega_s t}\ dt$$

$$\text{and } \omega_s = \frac{2\pi}{T}\ .$$

From this series we readily obtain the Fourier transform of g(t):

$$G(\omega) = 2\pi \sum_{n=-\infty}^{+\infty} c_n\ \delta(\omega - n\omega_s)\ . \tag{D-3}$$

Because multiplication of two signals in the time domain corresponds to convolution in the frequency domain, we have:

$$F_s(\omega) = \frac{1}{2\pi}\ F(\omega) * G(\omega) \int_{-\infty}^{+\infty} F(y)\ G(y-\omega)\ dy\ . \tag{D-4}$$

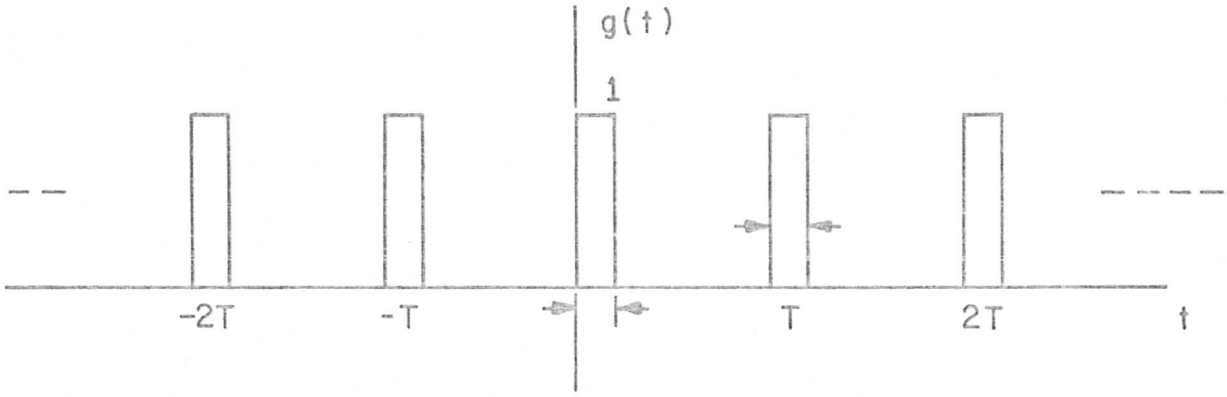

GATE FUNCTION
FIGURE D-1

Note that $F(\omega)$ is the transform of the waveform $f(t)$ before sampling. However, using the form of the transform of $g(t)$ and proceeding formally (which can be justified rigorously), we arrive at the following results

$$F_s(\omega) = \sum_{n=-\infty}^{+\infty} c_n \int_{y=-\infty}^{+\infty} F(y)\ \delta(y-\omega-n\omega_s)\ dy$$

$$= \sum_{n=-\infty}^{+\infty} c_n\ F(\omega+n\omega_s)\ . \qquad \text{(D-5)}$$

The function $F(\omega+n\omega_s)$ is just the original spectrum of $f(t)$ shifted to (or translated about) the frequency $n\omega_s$. Hence, the spectrum of the sampled waveform is a composite of shifted and weighted versions of the original spectrum. The weighting of each shifted version is determined by the line-spectrum of $g(t)$.

If the spectrum of $f(t)$ is strictly limited between the frequencies of $-\omega_s/2$ and $+\omega_s/2$, then the sum in equation (D-5) is trivial. This situation is depicted in figure D-2. However, in general, there can be a large number of terms in the series of equation (D-5) for each fixed ω. Anytime there is more than one term in this series we say that aliasing has occurred. The expression "fold-over" is sometimes frequently used because a copy of the original spectrum appears to be folded back or forward over other copies of the original spectrum. The relative weighting of the individual interfering, shifted version of the spectrum is determined by the nature of $g(t)$, which is equivalent to specifying the values of the Fourier coefficients. When all coefficients are unity, the sampler is called an impulse sampler; i.e.,

$$g(t) = \sum_{k=-\infty}^{+\infty} \delta(t-kT)\ .$$

Figure D-3 shows a situation in which the original spectrum is limited between the frequencies of $-\omega_s$ and $+\omega_s$. The cross-hatched areas indicate

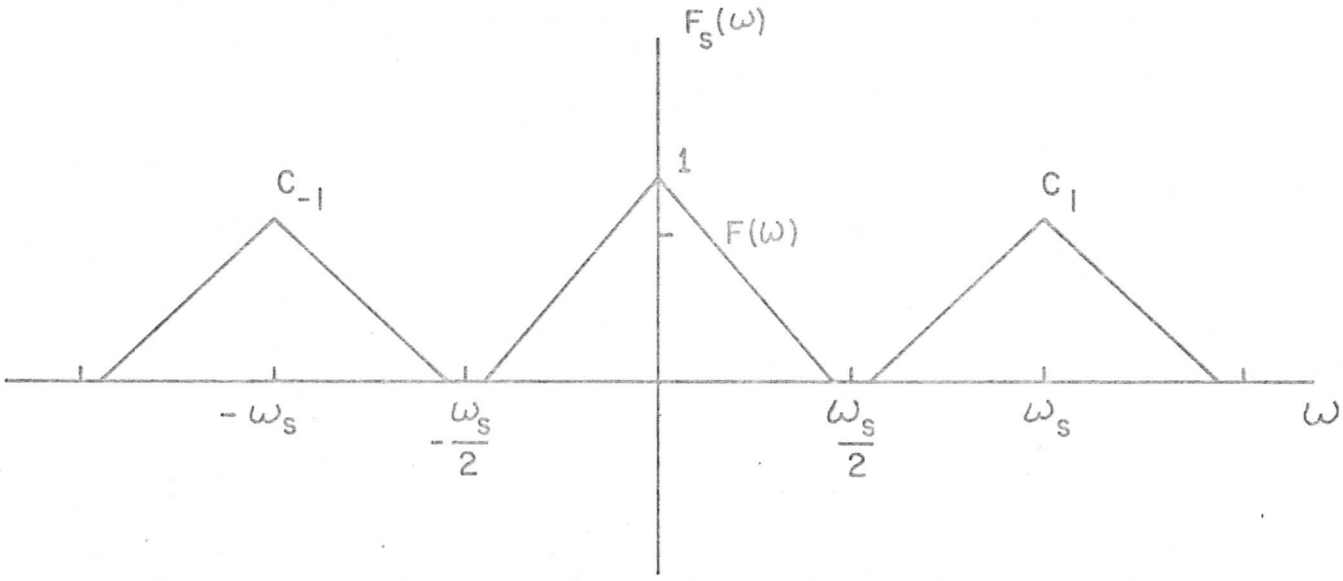

STRICTLY BANDLIMITED CASE
NO ALIASING
FIGURE D-2

frequencies which are distorted due to more than one term being present in the series of equation (D-5), ~~i.e.,~~ Thus, aliasing has occurred. This is the case in the SMS system and we now proceed to determine a measure of this distortion. We note that only the coefficients c_{-1} and c_{+1} affect the distortion included in the portion of the spectrum centered about zero.

As can be seen by consulting either Appendix A or (Papoulis, 1965), the effects of aliasing a stochastic process $\{y(t)\}$ are reflected in the aliasing of portions of its power-spectral density $S_y(\omega)$. In fact, in direct analogy with the previous development, ~~we have that~~ the power-spectral density of the sampled version of $y(t)$, $S_{ys}(\omega)$, is now given by

$$S_{ys}(\omega) = \sum_{n=-\infty}^{+\infty} |c_n|^2 \, S_y(\omega + n\omega_s) \quad . \tag{D-6}$$

Hence, all previous comments about band-limited signals apply to the case of band-limited processes. Since we may assume that $S_y(\omega)$ is bandlimited to the band from $-\omega_s$ to ω_s, we are concerned with an aliasing situation in which only the fold-over from adjacent bands of frequencies need be considered. A typical situation is depicted in figure (D-4). Since the sampling function $g(t)$ is real, we have a Hermitian symmetry among the coefficients; ~~i.e.,~~ $c_n = c_{-n}^*$.

We would like to choose some measure of the distortion ~~due~~ to aliasing. Thus, ~~Towards this~~ end we will first define an effective bandwidth of a stochastic process so that we can compare the effective bandwidth of original waveforms with that of the version which contains aliasing.

~~Suppose that~~ Consider that $S_z(\omega)$ is the power-spectral density of the process $\{Z(t)\}$. $S_z(\omega)$ is a real, even, nonnegative function of ω (Papoulis, 1965). If it were normalized, it would resemble a probability density function. Let $\tilde{S}_z(\omega)$ be this normalized function.

"even" in the sense of "not odd"

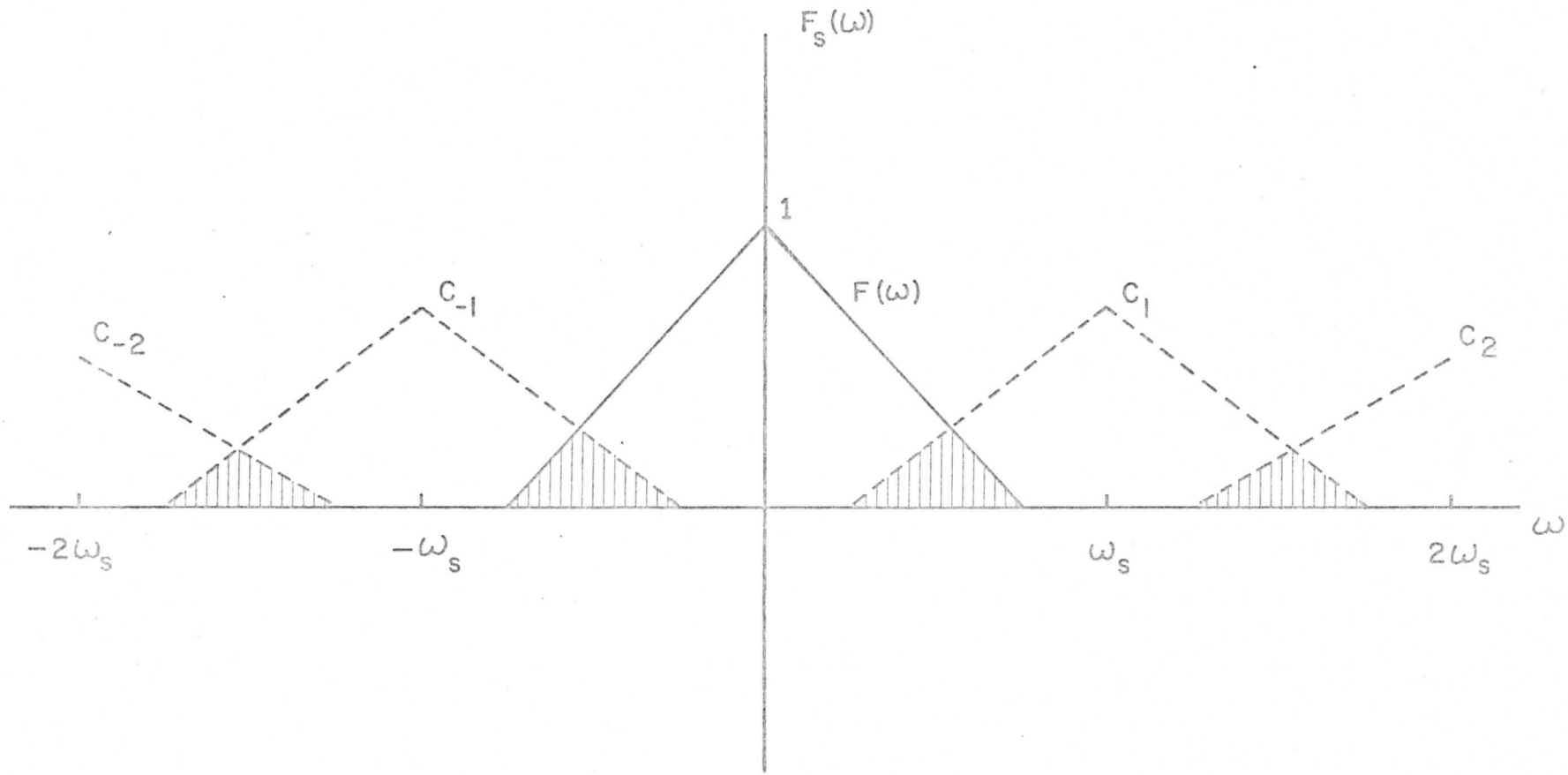

BANDLIMITED CASE
WITH ALIASING
FIGURE D-3

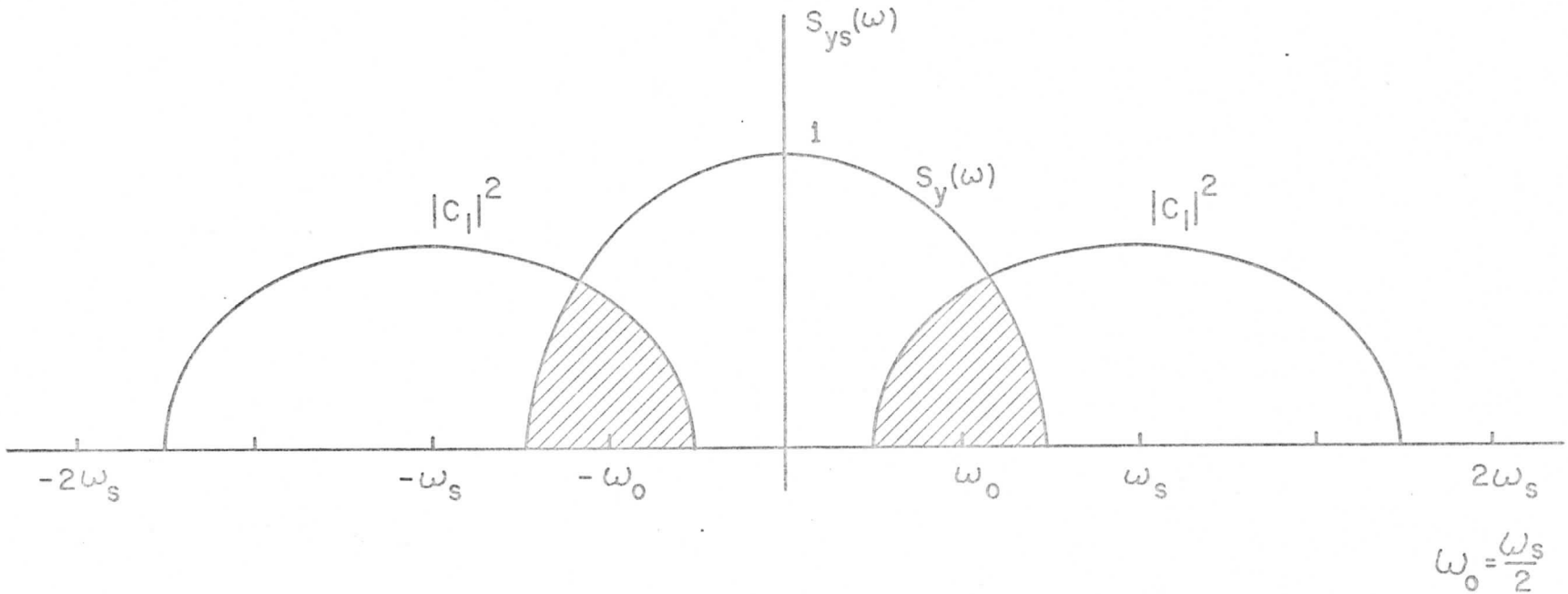

BANDLIMITED CASE FOR PROCESSES
WITH ALIASING
FIGURE D-4

$$\tilde{S}_z(\omega) = \frac{S_z(\omega)}{\int_{-\infty}^{+\infty} S_z(\omega)\, d\omega} \tag{D-7}$$

We will define the effective bandwidth of this process as the variance of $\tilde{S}_z(\omega)$ (sometimes called the radius of gyration.)

$$\gamma^2 = \int_{-\infty}^{+\infty} \omega^2 \tilde{S}_z(\omega)\, d\omega \tag{D-8}$$

Note that, since $S_z(\omega)$ is an even function of ω, i.e., $S_z(\omega) = S_z(-\omega)$, the equation does represents the second moment about the center of gravity (the variance). The use of the variance as a measure of the effective spread of ~~the range of~~ a variable is well-known and widely used in all branches of science and engineering.

There is an added bonus in using this definition; it is the uncertainty principle. This states that the variance γ^2 ~~times~~ a factor determined from the transform of $\sqrt{S_z(\omega)}$ must always be greater than $\pi/2$.

$$\gamma^2\, \alpha^2 \geq \pi/2 \tag{D-9}$$

$$\alpha^2 = \frac{\int_{-\infty}^{+\infty} \tau^2 \left|r(\tau)\right|^2 d\tau}{\int_{-\infty}^{+\infty} \left|r(\tau)\right|^2 d\tau} \tag{D-10}$$

$$r(\tau) = \frac{1}{2\pi} \int_{-\infty}^{+\infty} \sqrt{S_z(\omega)}\, e^{+j\omega\tau}\, d\omega \tag{D-11}$$

The quantity α^2 measures the spread of the inverse transform of $\sqrt{S_z(\omega)}$. Therefore, as we attempt to reduce the effective bandwidth of the process, the effective time-spread of its corresponding transform must increase so that inequaltiy (D-9) is fulfilled. Thus, there is a trade-off between the frequency-domain and the time-domain. For further discussion of this topic see the references (Brown, 1963), (Franks, 1969), and (Papoulis, 1962).

Suppose now that $S_y(\omega)$ represents the power-spectral density of the input to a sampler and that this spectrum is bandlimited to the range from $-\omega_s$ to $+\omega_s$. The effective bandwidth of the input is:

$$\gamma^2 = \frac{\int_0^{\omega_s} \omega^2 S_y(\omega)\, d\omega}{\int_0^{\omega_s} S_y(\omega)\, d\omega} \quad . \tag{D-12}$$

We have, of course, used the evenness of ω^2 and $S_y(\omega)$. If aliasing has been introduced by the sampler, the effective bandwidth of the center part of the spectrum depends on the way in which the folded part of the spectrum is added. A typical center lobe of an aliased spectrum is shown in figure D-4. We will define ϕ as the effective phase of the folded spectrum. A worst case is achieved when $\phi = \pi$. Then the effective bandwidth of the spectrum's corrupted center lobe is.

$$\beta^2 = \frac{\int_0^{\omega_0} \omega^2 [S_y(\omega) + |c_1|^2 \cos\phi\, S_y(\omega-\omega_s)]\, d\omega}{\int_0^{\omega_s} S_y(\omega)\, d\omega} \tag{D-13}$$

$$\text{where} \quad \omega_0 = \frac{\omega_s}{2}$$

This quantity measures the variance of the central part of the spectrum. If the effective phase of the aliasing is between $\pi/2$ and $3\pi/2$, the effective bandwidth as defined by β^2 is less than the original given by γ^2. The $|c_1|^2$ term results from the nature of the sampling waveform g(t). A worst case assumption is given by $|c_1|^2 \cos\phi = -1$. This is the case we will treat here.

Hence we will use:

$$\beta^2 = \frac{\int_0^{\omega_0} \omega^2 S_y(\omega)\, d\omega - \int_0^{\omega_0} (\omega-\omega_0)^2 S_y(\omega+\omega_0)\, d\omega}{\int_0^{2\omega_0} S_y(\omega)\, d\omega} \quad . \tag{D-14}$$

This is easily derived from equation (D-13) using the evenness of $S_y(\omega)$ and the definition of ω_0.

Since the input to the sampler is the output of the filter, we may relate $S_y(\omega)$ to the power-spectral density of the input $S_x(\omega)$ by the well-known formula (Papoulis, 1965):

$$S_y(\omega) = S_x(\omega)\, |H(j\omega)|^2 \quad . \tag{D-15}$$

Finally, since our picture data is in the form of a sampler and since the sampling rate for this data is clearly high enough, we may state the discrete versions of the expressions for the effective bandwidth. We use discrete frequency variables.

$$\gamma^2 = \frac{\sum_{k=1}^{2K} k^2 S_y(k)}{\sum_{k=1}^{2K} S_y(k)} \qquad \text{(D-16)}$$

K = half of the sampling frequency

$$\beta^2 = \frac{\sum_{k=1}^{K} k^2 S_y(k) - \sum_{k=1}^{K} (k-K)^2 S_y(k+K)}{\sum_{k=1}^{2K} S_y(k)} \qquad \text{(D-17)}$$

Helen — a number of spacers in the next appendices, are in red. Shapes may have to be retyped

APPENDIX E

A MODEL FOR THE PHOTOMULTIPLIER TUBE

The noise generated in a photomultiplier (p.m.) tube is studied, ~~and~~ A suitable model ~~of~~ for the p.m. tube ~~for the purpose of~~ suitable designing an optimum quantizer is also suggested.

In a p.m. tube, the photocathode emits electrons which are then accelerated and multiplied by a series of electrodes, These are known as "dynodes" ~~to which~~ and suitable voltages are applied to them. (Figures E-1 and E-2). The incident light intensity on the photocathode directly determines the photoemission current, ~~there being~~ because there is an excellent approximation ~~of~~ a linear relationship between the light intensity and the photo current over a wide range of light intensities.

We will now consider ~~The case where~~ light of a constant intensity is incident on the photocathode, in which ~~is considered~~. For constant voltages at the dynodes, we would expect that the current ~~which is~~ directly proportional to the light intensity will also be a constant quantity. Variation of the light intensity will produce corresponding variation in the current. Although it is said that the incident light is of constant intensity, this statement is not strictly true when viewed ~~one views this statement from a microscopic point of view~~ microscopically. When ~~one~~ we says that light of a particular intensity is incident on a photocathode, ~~one is~~ we refer~~ring~~ to the number of photons (packets or quanta of energy, each being equal to $h\nu$, ν - frequency of light) which strike the photocathode. The larger the number of photons ~~are~~, the larger the current ~~is~~. So by the term, "constant intensity", ~~one~~ we refers to the average number of photons. But the number of photons striking the photocathode is not a constant quantity, but it fluctuates about a quiescent quantity which is the "average" over a long period. This average is called ~~and is referred to as~~ "constant light intensity". Hence, there is a corresponding change in the

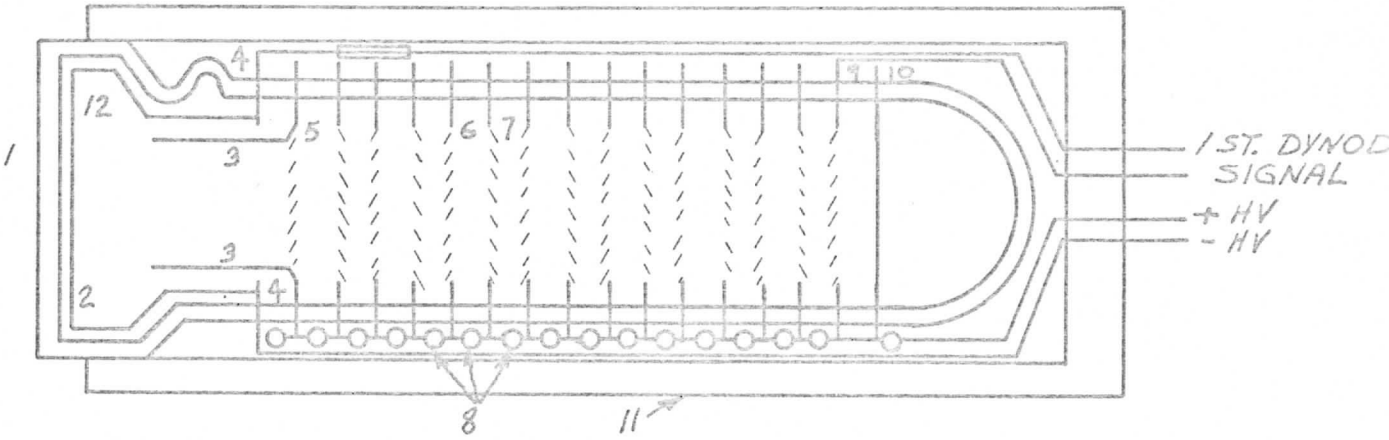

FIGURE E-1

1. FACE PLATE
2. SEMI-TRANSPARENT PHOTOCATHODE
3. FOCUSING ELECTRODE
4. CATHODE CONTACT
5. 1ST. DYNODE
6. FIELD SHAPING SCREEN
7. VENETIAN BLIND DYNODE
8. VOLTAGE DIVIDER
9. ANODE
10. LAST DYNODE
11. EPOXY FIBERGLASS SHELL
12. METAL COATING

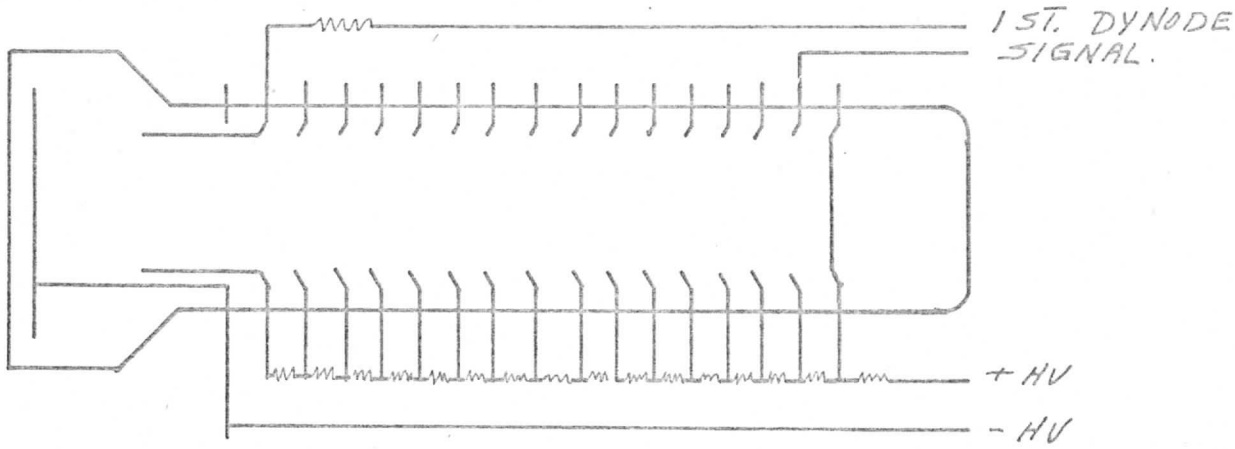

FIGURE E-2

number of photoelectrons emitted from the photocathode. ~~Thus,~~ The emission of electrons is actually random in form. More electrons are emitted at one instant, fewer the next, with the average number per unit time the same over a long period of time as that shown below in Figure E-3.

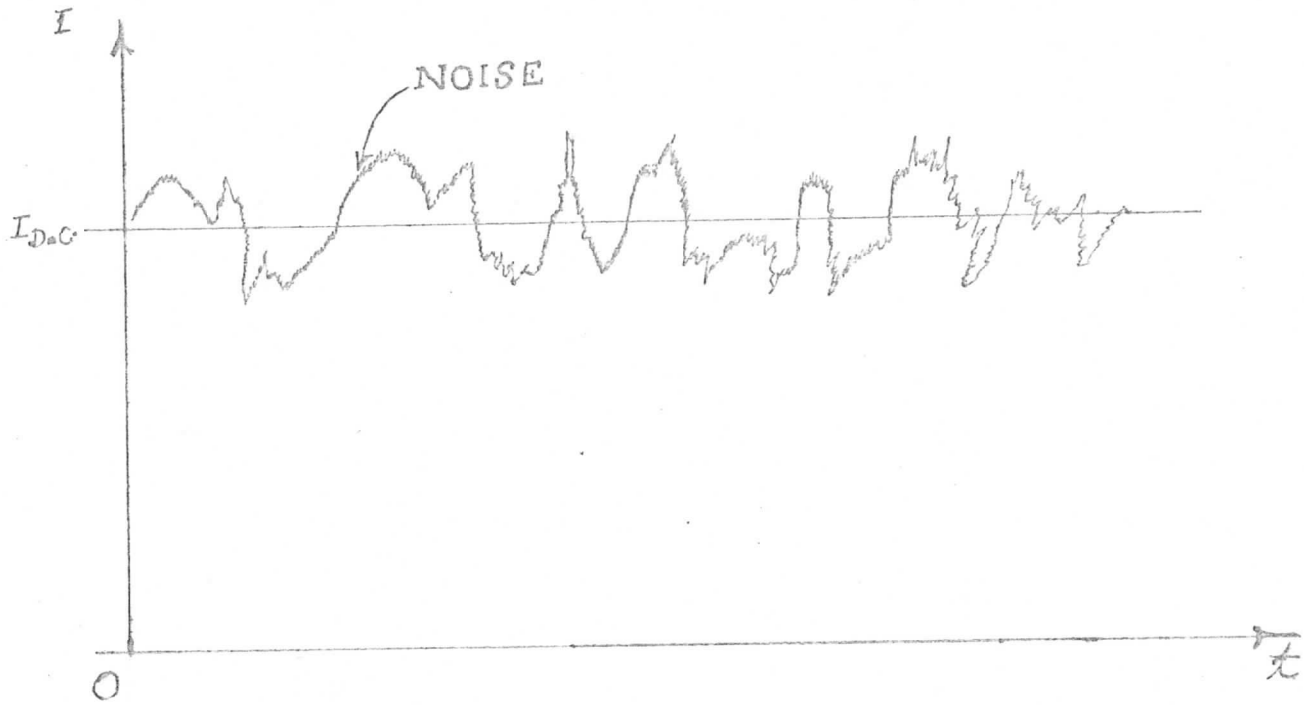

FIGURE E-3

The situation described above is exactly the same as that one that prevails in a vacuum diode operating in the temperature limited region at a fixed cathode temperature and a fixed data voltage. The one difference is that in the case of photoemission, the fluctuations in the current are due to fluctuations in the number of striking photons, with no heating of the cathode. Hence, the analysis carried out for the shot noise (Schwartz, 1959 and Davenport and Root, 1958), in a temperature limited diode is perfectly valid for the noise due to light intensity fluctuations. Hence (Schwartz, 1959),

$$\overline{i^2}_{noise} = (\text{r.m.s. noise}) = 2e\Delta f I_{D.C.} \qquad \text{(E-1)}$$

Δf = Noise equivalent bandwidth

$I_{D.C.}$ = Average photocurrent

But in an actual situation such as that in S.M.S. systems the light intensity incident on the photocathode is not a constant quantity, but varies with time, so the operating current changes continuously with time. At a given time, the current fluctuates about the average operating current I and so equation (E-1) can be used to describe the noise with $I_{D.C.}$ being in this case the average operating current. Intuitively it is obvious that as the light intensity and so, the operating point varies, the r.m.s. value of the noise also varies with the operating current.

Hence

$$\overline{i^2}_{noise} = 2e\Delta f I \qquad \text{(E-2)}$$

where I is the time varying photocurrent.

Let the stochastic process X(t) denote the current and N(t), the noise. Assuming that the photocurrent and the noise of the p.m. tube are members of

Why don't you put some of this line after "Eq 2" so there isn't so much empty space

ergodic process (Papoulis, 1965, Ch. 8) [illegible] ergodicity in the mean and the auto-correlation are assumed), we can write as

$$E[N^2] = 2e\Delta fX \tag{E-3}$$

Further, the time average of the noise can be assumed to be zero.

$$E(N) = 0 \tag{E-4}$$

Hence,

$$\sigma_N^2 = E(N^2) = \overline{N^2} = 2e\Delta fX$$

or

$$\sigma_N^2 = 2e\Delta fX \tag{E-5}$$

Thus, (E-5) gives the variance of the fluctuation noise at the output of the first stage of the p.m. tube (without considering secondary emission).

EXPRESSION FOR THE R.M.S. VALUE OF THE NOISE AT THE OUTPUT OF AN N-STAGE SECONDARY EMISSION MULTIPLIER PHOTO TUBE:

The p.m. tube shown in Figures E-1 and E-2 consists of a photocathode followed by n dynodes and an anode to form an N-stage secondary emission current multiplier. A simple sketch of the p.m. tube is shown (Figure E-4) as an aid in deriving the above mentioned expression. The current amplification due to secondary emission at a dynode is equal to "G" and it is assumed to be the same for each dynode.

$\overline{I}_{n0}$ refers to the r.m.s. value of the noise generated in the cathode. $\overline{I}_{n1}$ is the r.m.s. noise at the output of the first stage, including the effect of secondary emission from the first dynode. $\overline{I}_{ni}$ is the r.m.s. noise at the output of the ith stage, and so on. I is the average cathode current and I_0, the average output current.

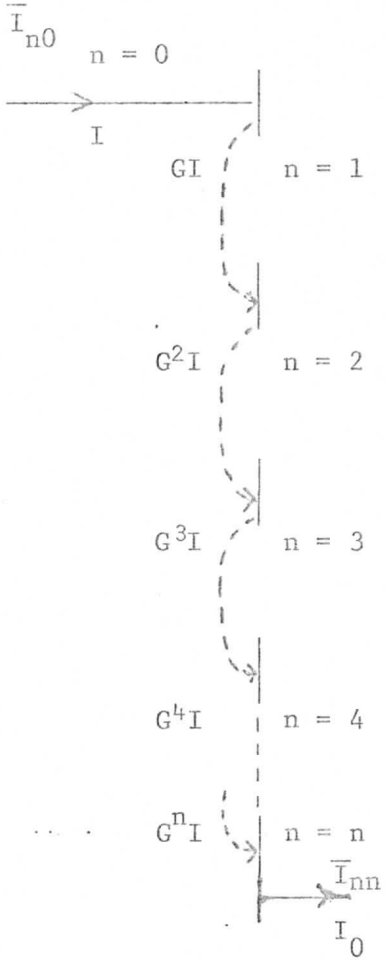

$$\overline{I^2_{n0}} = 2eI\Delta f$$

$$\overline{I^2_{n1}} = G^2\overline{I^2_{n0}} + 2e(GI)\Delta f = (G^2+G)2eI\Delta f$$
$$= G(G+1)\overline{I^2_{n0}}$$

$$\overline{I^2_{n2}} = G^2\overline{I^2_{n1}} + 2e(G^2I)\Delta f = \left(G^3(G+1)+G^2\right)2eI\Delta f$$
$$= G^2(G^2+G+1)\overline{I^2_{n0}}$$

$$\overline{I^2_{n3}} = G^2\overline{I^2_{n2}} + 2e(G^3I)\Delta f = \left[G^4(G^2+G+1)+G^3\right]2eI\Delta f$$
$$= G^3(G^3+G^2+G+1)\overline{I^2_{n0}}$$

$$\overline{I^2_{nn}} = G^n(G^n+G^{n-1}+G^{n-2}+ \ldots +G+1)2eI\Delta f$$
$$= \left[G^n \sum_{n=0}^{n} G^n\right] 2eI\Delta f$$

Figure E-4

$$\overline{I^2_{nn}} = 2eI\Delta f \cdot G^n \frac{(G^{n+}-1)}{G-1} \qquad \text{(E-6)}$$

$$I_0 = G^nI \qquad \text{(E-7)}$$

In the expression

$$\overline{I^2_{n1}} = G^2\overline{I^2_{n0}} + 2e(GI)\Delta f$$

the quantity $\left(G\sqrt{\overline{I^2_{n0}}}\right)^2$ is the mean square value of the fluctuation noise due to the incident current $G\sqrt{\overline{I^2_{n0}}}$. and The quantity $2e(GI)\Delta f$ is the mean-square value of the fluctuation noise about the average current GI due to the random emission from the first dynode.

From equation (E-6)

$$\overline{I_{nn}^2} = 2eI\Delta f G^n \frac{(G^{n+1}-1)}{G-1}$$

Since $G^{n+1} >> 1$, we can write the above as

$$\overline{I_{nn}^2} \simeq 2eI\Delta f \frac{G^{n+1}}{(G-1)} \qquad \text{(E-8)}$$

Thus, the mean-square value of the noise at the output of the p.m. tube is given by (E-8) and this noise fluctuates about $I_0 = G^n I$

PROBABILITY DENSITY FUNCTION OF THE NOISE AT THE OUTPUT OF THE P.M. TUBE

Recalling that the p.m. tube noise is shot-noise (Schwartz, 1959 and Davenport and Root, 1958), it can be expected that the total output current of the p.m. tube follows a normal probability density function. The total cathode current in the p.m. tube can be assumed to be the sum of a large number of independent and overlapping current pulses due to individual photons. Because of the random occurrence of these pulses, the total current fluctuates about a specific value, which is the effective average, over a very long period. The total current, ~~being~~ is the sum of a large number of independent random variables (current pulses), It can be expected to follow a normal density, in view of the central limit theorem (Papoulis, 1965, Ch. 8), under certain broad conditions. Experimental results totally support this conclusion.

Hence, the probability density function of the total current is given by,

$$f_{I_{Total}}(i_{Total}) = \frac{1}{\sqrt{2\pi}\,\sigma_{i_T}} \exp\left[-\frac{(i_T-I)^2}{2\sigma_{i_T}^2}\right] \qquad \text{(E-9)}$$

where I is the average current, σ_{i_T}, the standard deviation of the total current and I_T, a random variable.

Now the noise I_n (again a random variable) is given by

$$I_n = I_T - I \tag{E-10}$$

The conditional probability density function of the noise, assuming the signal, is given by,

$$f_{I_n}(i_n|_{I=i}) = f_{I_T}(i_n+I)$$

$$f_{I_n}(i_n|_{I=i}) = \frac{1}{\sqrt{2\pi}\,\sigma_{i_T}} \exp\left[-\frac{i_n^2}{2\sigma_{i_T}^2}\right] \tag{E-11}$$

because $\sigma_{i_T} = \sigma_{i_n}$

or

$$f_{n'}(n'|_{X=x}) = \frac{1}{\sqrt{2\pi}\,\sigma_{N'}} \exp\left[-\frac{n'^2}{2\sigma_{N'}^2}\right] \tag{E-12}$$

where $\sigma_{N'}^2 = 2e\Delta f X$ with X corresponding to the variable operating current I. Thus, it may be observed that the variance of the noise is proportional to the operating current X.

Equation (E-12) gives the conditional probability density function of the noise at the output of the first stage of the p.m. tube, without considering secondary emission from the first dynode. It is a simple matter to deduce that, because the system is linear (Papoulis, 1965, Ch. 12), the conditional probability density function of the noise at the output of the p.m. tube is also normal with zero mean, however, the variance given by equation (E-8) where $\overline{I_{nn}^2}$ is the variance of the noise.

Thus, the output of the p.m. tube can be written as

$$Y = G^n X + N$$

where N is normal with the variance given by ε_N

It may be worthwhile to mention that an increase in the gain of the first dynode (for example, $G_1 = 2G_2 = 2G_3 = \ldots 2G_n = 2G$) over those of the rest can be shown to result in a small improvement of the peak-to-peak signal to r.m.s. noise current.

So far, only the noise due to the fluctuations in the number of incident photons, or equivalently, in the intensity of the incident light has been considered. However, there are other factors which contribute noise. Figure (E-5) (Amos and Wang, 1969) shows a "model" of the p.m. tube including the other components:

2. It is inevitable that extraneous and undesirable light from the background of the p.m. tube is incident on the photocathode. This, then, contributes to another noise component. Again, the noise due to background intensity fluctuations obeys the shot-noise (Schwartz, 1959 and Davenport and Root, 1958), the mean-square value given by

$$\overline{I_{nb}^2} = 2e\Delta f I_b \frac{G^{2n+1}}{G-1} \qquad \text{(E-14)}$$

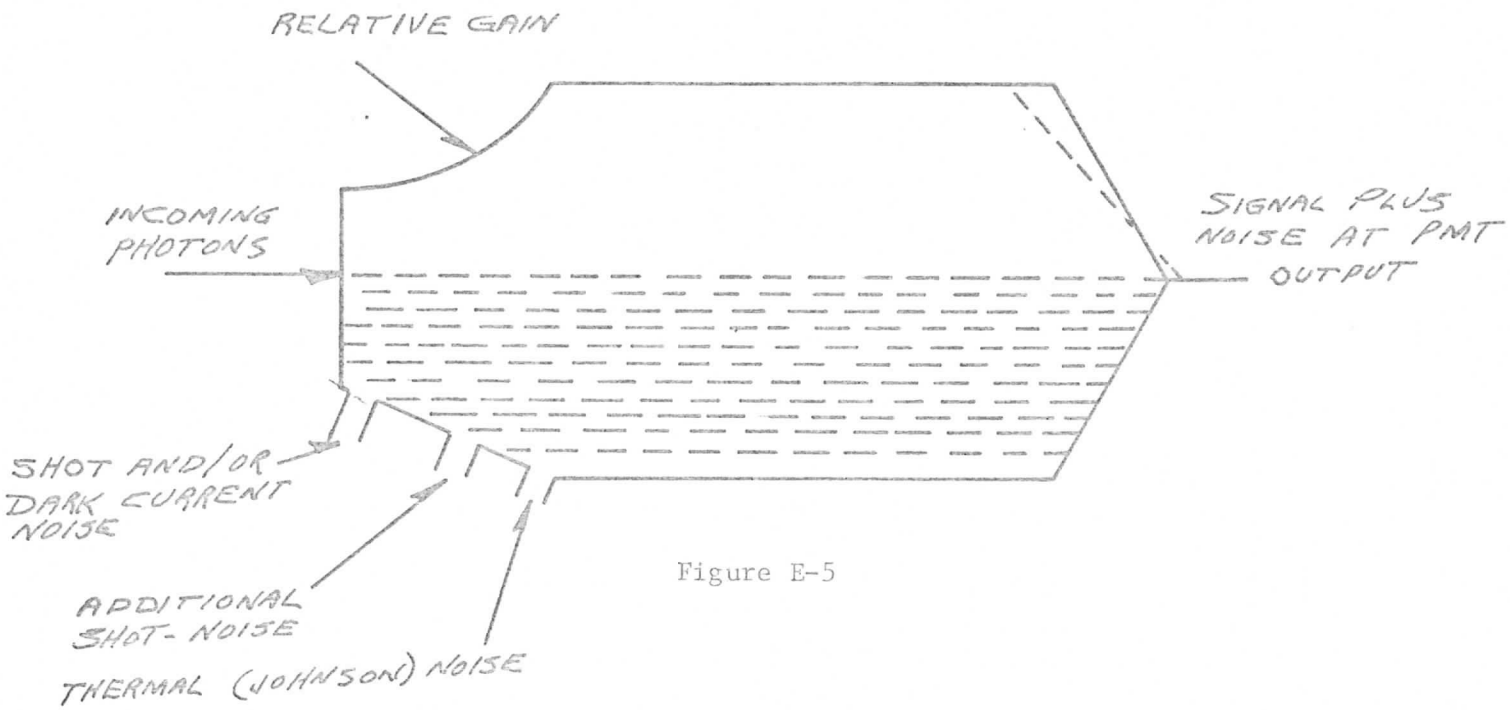

Figure E-5

A SHOT-NOISE DUE TO SIGNAL CURRENT = $\alpha(2e\Delta f I)^{1/2}$

SHOT NOISE DUE TO BACKROUND = $B(2e\Delta f I_B)^{1/2}$

SHOT NOISE DUE TO DARK CURRENT = $\alpha(2e\Delta f I_D)^{1/2}$

B SHOT NOISE DUE TO AMPLIFICATION = $\gamma(2e\Delta f I_n)^{1/2}$

C JOHNSON OR THERMAL NOISE DUE THERMAL AGITATION = $\delta\left(\frac{4kT\Delta f}{R_{eq}}\right)^{1/2}$

$$\alpha = \frac{G^{2n+1}}{G-1}$$

where I_b is the "average background" photocurrent about which the noise fluctuates. Because of the origin of this noise, this is very difficult to account for and so will be omitted.

2) Dark current (Amos and Wang, 1969): Another noise component in a p.m. tube is due to what is known as the "dark current". When a p.m. tube is operated in complete darkness, electrons are still emitted from the photocathode due to agencies other than incident light. The resulting "dark current" is amplified by the multiplier system and sets a limit to the lowest intensity of light that can be detected directly. With most photocathodes, thermionic emission appears to be responsible for the largest component of the dark current. At ambient temperatures, the thermal dark current I_t obeys Richardson's law approximately as

$$I_t = 1.20 \times 10^2 T^2 \exp\left[\frac{-1.16\times10^4}{T}\,\phi_t\right] \text{amp. cm}^{-2} \qquad \text{(E-15)}$$

where T is the absolute temperature in K and ϕ_t is the thermal work function for the cathode material. It is clear from Equation (E-15) that cooling the photocathode will have the effect of reducing the thermal component of the dark current. For all normal cathodes except the $AgOC_s$(s-1) type, it is found that the thermal component of the dark current may be virtually eliminated by cooling to -40°C. and no significant improvement is obtained by cooling to lower temperatures, below this. But the photocathode of the S.M.S. p.m. tube is not cooled to such low temperatures.

Again the mean-square value of the short-noise due to dark current (principally thermionic emission current) is given by

$$\overline{I_{nd}^2} \simeq 2e\Delta f I_t \cdot \frac{G^{2n+1}}{G-1} \qquad \text{(E-16)}$$

The final model for the p.m. tube is shown below.

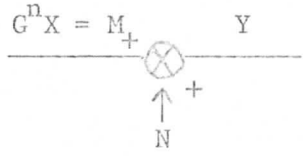

$$f_N\left(n \Big/ _{M=m}\right) = \frac{1}{\sqrt{2\pi\sigma_n^2}} \exp\left[-\frac{n^2}{2\sigma_n^2}\right]$$

$$\sigma_n^2 = 2e\Delta f \frac{G^{2n+1}}{G-1} x$$

$$\sigma_n^2 = 2e\Delta f \frac{G^{n+1}}{G-1} M$$

Figure E-6

Finally, the term "pulse height distribution" (Bay and Prapp, 1964) used in connection with p.m. tubes needs some explanation. In a multiplier phototube, each photoelectron undergoes cascade amplification within the tube and arrives at the anode as a pulse of many (say 10^{16}) electrons. If all the photoelectrons were multiplied equally, they would contribute to the signal current equally. In actual practice, however, the amount of multiplication is very different from one photoelectron to another, so that the stream of pulses at the anode includes a very broad range of amplitudes. Some contribute ~~as much as~~ ten times as much as the ~~to the photo current as~~ do others. Since the pulses are not of equal size, it is evident that the SNR of a multiplier phototube will be lower when used in combination with an ordinary current measuring system which introduces measurement noise, than when used in a system that counts only the pulses with equal weight regardless of their sizes. This is the fundamental difference between pulse counting techniques and current measuring techniques.

APPENDIX F

Optimum Quantizer

We develop the necessary conditions for the parameters of a quantizer to be optimum on the basis of overall mean-square error. It is not clear what criterion was used in the design of the present SMS quantizer. The performance of the present quantizer is equivalent to optimally quantizing the noise from the photomultiplier tube, which is only statistically dependent on the VISSR data. Our results, while not complete through the actual numerical solution of the equations, indicate that the design is not as simple as the reasoning which produced the present quantizer would suggest. An adjunct of the development of the necessary equations is that the quantizer parameters are sensitive to the statistical distribution of the input data.

A simple block diagram of the S.M.S. system (one visible channel) is shown below:

Figure F-1

The optical signal at the input to the PMT is converted to electrical signal by the PMT at its output. During this process, a noise is also added to the signal. The principal component of this noise is due to the signal itself, and for a given signal, it has a normal conditional probability density function, with a zero mean and a variance proportional to the signal itself. It is now assumed that any other noise generated after the PMT output up to the input to the quantizer is very small compared to the noise due to the signal, and so will be omitted in the following analysis. So, for the purpose of designing an optimum quantizer such that the mean-square error between the output of the quantizer and the signal is minimum, the following model is assumed.

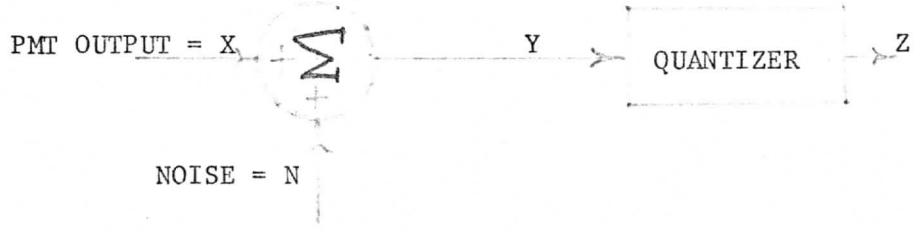

Figure F-2

The PMT output signal is equal to the PMT input signal multiplied by the PMT total gain.

As mentioned before, the criterion or performance index, which is minimized while choosing the quantizer levels, is the mean-square error between Z and X, and is defined by:

$$\overline{\varepsilon^2} \triangleq E\left[(Z-X)^2\right] = E\left\{E\left((Z-X)^2 \mid N=n\right)\right\} \qquad \text{(F-1)}$$

The following notations are adopted throughout this appendix:

1) Capital letters indicate random variables.

2) Small letters indicate the variables assumed by the random variables.

3) $f_X(x)$ represents the probability density function of X.

4) $f_N(n|X=x)$ represents the conditional probability density function of N, given X=x.

5) E( ) denotes the expected value of a random variable.

6) $f_{XN}(x,n)$ denotes the joint probability density function of X and N.

If we denote the quantizer thresholds by the set of real numbers, $\{y_i\}_{i=1}^{k+1}$, and the corresponding output levels by the set $\{z_i\}_{i=1}^{k}$, we may proceed to develop the necessary equations for these quantities to yield a minimum mean-square error.

$$E\left\{(Z-X)^2|N=n\right\} = \int_{x=0}^{b} (z-x)^2 f_X(x|N=n)\,dx \qquad \text{(F-2)}$$

$$= \sum_{i=1}^{k} \int_{x_i}^{x_{i+1}} (z_i-x)^2 f_X(x|N=n)\,dx$$

$$= \sum_{i=1}^{k} \int_{y_i-n}^{y_{i+1}-n} (z_i-x)^2 f_X(x|N=n)\,dx$$

The above equations imply that, for a fixed noise n, there is a one-to-one mapping between the x_i's, and the y_i's, and so the z_i's. Otherwise, for a given X=x, there is no unique Y=y because of the addition of noise.

The overall mean-square error is given by:

$$\overline{\varepsilon^2} = \int_{n=-\infty}^{\infty} \left\{ \sum_{i=1}^{k} \int_{y_i-n}^{y_{i+1}-n} (z_i-x)^2 f_{XN}(x,n)\,dx \right\} dn \qquad \text{(F-3)}$$

To minimize the mean-square error, a necessary set of conditions are is

$$\frac{\partial(\overline{\varepsilon^2})}{\partial y_j} = 0 \qquad \text{(F-4)}$$

and

$$\frac{\partial(\overline{\varepsilon^2})}{\partial z_j} = 0 \quad \text{for } j = 1, 2, 3, \ldots, k \tag{F-4}$$

The first set of these equations yields:

$$\int_{n=-\infty}^{\infty} \left[(y_j - n - z_{j-1})^2 - (y_j - n - z_j)^2 \right] f_{XN}(y_j - n, n)\, dn = 0 \tag{F-5}$$

$j = 2, 3, \ldots k$

(For $j=1$, $y_1 = 0$ because x_1 is assumed to be zero ~~and so also~~ as is the corresponding noise. Further, $f_{XN}(0,n) =$ Zero.)

Similarly, setting $\frac{\partial(\overline{\varepsilon^2})}{\partial z_j}$ equal to zero,

$$\frac{\partial(\overline{\varepsilon^2})}{\partial z_j} = \int_{n=-\infty}^{\infty} \left[\int_{y_j - n}^{y_{j+1} - n} (z_j - x)\, f_{XN}(x,n)\, dx \right] dn = 0 \tag{F-6}$$

$j = 1, 2, 3 \ldots k$

Up to this point, the treatment has been ~~very~~ general and without the assumption of any particular joint probability density $f_{XN}(x,n)$. To illustrate the procedure for obtaining the levels of an optimum quantizer, let it be assumed that X has a uniform distribution.

$$f_X(x) = \begin{cases} \frac{1}{b} & 0 < x \leq b \\ 0 & \text{elsewhere} \end{cases} \tag{F-7}$$

Equation (F-5) can be written as:

$$\int_{n=-\infty}^{\infty} \left[z_{j-1} + z_j - 2(y_j - n) \right] f_{XN}(y_j - n, n)\, dn = 0 \tag{F-8}$$

$j = 2, 3, \ldots k$

The "noise" due to the signal has a conditional probability density function (p·d·f). (See Appendix E.)

$$f_N(n|X=x) = \frac{1}{\sqrt{2\pi}\sqrt{\delta x}} \cdot \exp(-n^2|2\delta x)$$

where (F-9)

$$E[N|X=x] = 0; \quad \sigma^2_{N|X=x} = E[N^2|X=x] = \delta x,$$

δ is a known constant.

We can

As a check on the equation (F-8) we note that if it is assumed that the noise is very small, i.e., the fluctuations about any signal level are very small, then

$$y_j - n \simeq y_j .$$

In this case, the factor, $[z_{j-1} + z_j - 2(y_j-n)] \simeq (z_{j-1} + z_j - 2y_j)$ can be taken outside the integral over n as follows:

$$(z_{j-1} + z_j - 2y_j) \int_{\substack{\text{over a} \\ \text{small} \\ \text{range of n}}} f_{XN}(y_j,n)\, dn \simeq 0$$

yielding

$$y_j \simeq \frac{z_{j-1}+z_j}{2} \quad \text{in agreement with (Max, 1962).}$$

Equation (F-8) can be rewritten, using (F-9) and (F-7), as:

$$\int_{n=-\infty}^{\infty} [z_{j-1} + z_j - 2(y_j-n)] \left\{ \frac{1}{b} \frac{\exp[-n^2|2\delta(y_j-n)]}{\sqrt{2\pi\delta}\sqrt{y_j-n}} \right\} dn = 0 \qquad \text{(F-10)}$$

$$j = 2, 3, \ldots k$$

By using Bayes Rule (Papoulis, 1965) we have

$$f_{XN}(y_j-n,n) = f_X(y_j-n)\, f_N(n|X=y_j-n) \qquad \text{(F-11)}$$

Thus the random variable X takes values between 0 and b. And the argument of f_X (....) takes values between 0 and b, and in the expression, $x=y_j-n$, n

can only vary so that x is between 0 and b.

So: $n = y_j - b$ (corresponding to x = b)
negative maximum

(F-12)

$n = y_j$ (corresponding to x = 0)
positive maximum

Substituting these results in equation (F-10) and performing a change of variables, we have that part of a set of necessary conditions is given by:

$$\int_{m=0}^{b} (z_{j-1} + z_j - 2m) \exp\left(-\frac{m}{2\delta} - \frac{y_j^2}{2\delta m}\right) \frac{dm}{\sqrt{m}} = 0 \qquad \text{(F-13)}$$

$j = 2, 3, \ldots k.$

After some straightforward but tedious manipulations which involve the use of standard integral tables, we finally arrive at one set of necessary equations.

$$z_{j-1} + z_j = \delta \left\{ \frac{2}{\sqrt{\pi}} \frac{\exp\left(-\frac{(y_j - b)^2}{2\delta b}\right)}{\operatorname{erfc}\left(\frac{y_j - b}{\sqrt{\delta b}}\right)} \left[\frac{y_j - b}{\sqrt{2\delta b}}\right] + 2 + \frac{2y_j}{\delta} \right\} \qquad \text{(F-14)}$$

$j = 2, 3, \ldots k$

Here where the complimentary error function x is defined by:

$$\operatorname{erfc}(x) = \frac{1}{2} - \int_0^x \frac{1}{\sqrt{2\pi}} \exp\left(\frac{-\alpha^2}{2}\right) d\alpha$$

Now the second set of equations become, from equation (F-6):

$$\frac{\partial(\overline{\varepsilon^2})}{\partial z_j} = \int_{n=-\infty}^{\infty} \left[\int_{y_j - n}^{y_{j+1} - n} (z_j - x) \exp\left(-n^2 / 2\delta x\right) \frac{dx}{\sqrt{x}} \right] dn = 0 \qquad \text{(F-15)}$$

$j = 1, 2, \ldots k$

This may be rewritten as

$$\int_{n=-\infty}^{+\infty} (I'' - z_j I') \, dn = 0 \qquad j = 1, 2, \ldots k \tag{F-16}$$

where

$$I' = \int_{y_j - n}^{y_{j+1} - n} \exp\left\{\frac{-n^2}{2\delta x}\right\} \frac{dx}{\sqrt{x}} \tag{F-17}$$

$$I'' = \int_{y_j - n}^{y_{j+1} - n} \sqrt{x} \exp\left\{\frac{-n^2}{2\delta x}\right\} dx \tag{F-18}$$

Since I' and I" involve "error" functions with arguments as function of n, the above integral can be evaluated only by doing a numerical double integration, with the limits of the inner integral, a function of n. To avoid this difficulty and to arrive at an analytical expression relating the z_j's, y_j's and the y_{j+1}'s, the following approximations are made over the interval $[y_j - n, y_{j+1} - n]$.

For low levels of x, the function $\exp\left(\frac{-n^2}{2\delta x}\right)$ varies or increases somewhat faster than it does at higher levels. At higher levels, it varies ~~very~~ slowly, as it approaches 1 asymptotically.

The function $\frac{1}{\sqrt{x}}$ decreases faster at low levels (quite fast for very small values of x) than it does at higher levels. At higher levels, it varies slowly, as it asymptotically approaches zero.

Hence, over the range $(y_j - n, y_{j+1} - n)$, the function $\exp\left(-\frac{n^2}{2\delta x}\right)$ increases, $\frac{1}{\sqrt{x}}$ decreases, and ~~so~~ the product $\frac{1}{\sqrt{x}} \exp\left(\frac{-n^2}{2\delta x}\right)$ is smoothed by these changes. ~~Further,~~ only at very low levels are their variations significant.

Next, we consider the product $\sqrt{x} \exp\left(-\frac{n^2}{2\delta x}\right)$. Both $\sqrt{x}$ and $\exp\left(-\frac{n^2}{2\delta x}\right)$ ~~are~~ increasing over the indicated range. $\sqrt{x}$ increases faster than $\exp\left(-\frac{n^2}{2\delta x}\right)$. But $\sqrt{x}$ itself increases ~~only~~ slowly over the whole range of x ~~and~~.

so its variation over an interval $\left[y_j-n,\ y_{j+1}-n\right]$ will be relatively small. So the product $\sqrt{x}\exp\left(-\frac{n^2}{2\delta x}\right)$ can be expected to vary only slightly over any range $\left[y_j-n,\ y_{j+1}-n\right]$.

Hence, for both the functions, $\sqrt{x}\exp(-n^2/2\delta x)$ and $\frac{1}{\sqrt{x}}\exp(-n^2/2\delta x)$, we can approximate in the integral with

$$x \simeq \frac{y_j-n + y_{j+1}-n}{2} \qquad \text{(mean value)} \qquad \text{(F-19)}$$

Hence,

$$\frac{\partial(\overline{\varepsilon}_j^2)}{\partial Z_j} \simeq \int_{n=-\infty}^{\infty}\left[\frac{\left(y_{j+1}+y_j-2n\right)}{2} - z_j\right]\frac{1}{b\sqrt{2\pi\delta}}\ \exp\frac{\left[\frac{-n^2}{2\delta\left(\frac{y_j+y_{j+1}-2n}{2}\right)}\right]}{\sqrt{\frac{y_j+y_{j+1}-2n}{2}}}\left(y_{j+1}-y_j\right)dn$$

$$= 0 \qquad \text{(F-20)}$$

$$j = 1, 2, 3, \ldots k$$

Using the fact that the thresholds are distinct and performing extensive manipulations, equation (F-20) can be reduced to:

$$\exp\left\{-\frac{\left(\frac{y_j+y_{j+1}}{2}-b\right)^2}{2\delta b}\ \frac{\left(\frac{y_j+y_{j+1}}{2}-b\right)}{\sqrt{2\delta b}}\right\} + (1 + 2\sqrt{cd}\ \sqrt{\pi}\ \operatorname{erfc}\left\{\frac{\frac{y_j+y_{j+1}}{2}-b}{\sqrt{\delta b}}\right\}$$

$$\simeq \sqrt{c^3}\frac{Z_j}{\sqrt{c}}\ 2\sqrt{\pi}\ \operatorname{erfc}\left\{\frac{\frac{y_j+y_{j+1}}{2}-b}{\sqrt{\delta b}}\right\} \qquad \text{(F-21)}$$

where $c = \frac{1}{2\delta}$ and $d = \left(\frac{y_j+y_{j+1}}{2}\right)^2\Big|2\delta$

Finally solving for the output levels of the quantizer

$$Z_j \simeq \delta\left\{\frac{\frac{1}{\sqrt{\pi}}\exp\left[-\frac{\left(\frac{y_j+y_{j+1}}{2}-b\right)^2}{2\delta b}\right]\ \frac{\left(\frac{y_j+y_{j+1}}{2}-b\right)}{\sqrt{2\delta b}}}{\operatorname{erfc}\left\{\frac{\frac{y_j+y_{j+1}}{2}-b}{\sqrt{\delta b}}\right\}} + 1 + \frac{y_j+y_{j+1}}{2\delta}\right\} \qquad \text{(F-22)}$$

$$j = 1, 2, \ldots k$$

This set of equations, coupled with those in equations (F-14), represents the necessary conditions for selecting the threshold levels $\{y_j\}$ and the output levels $\{z_j\}$.

We will briefly outline a numerical technique for solving for the unknown levels. Assume that $y_1=0$. Then one item in equations (F-22) relates z_1 and y_2, and likewise, one of the equations (F-14) relates z_1, z_2, and y_2.

So if we can pick some z_1, we can generate y_2 from (F-22), and using this y_2, we can find z_2 from (F-14). Thus, we can, step by step, find all the y_i's and the z_i's.

One procedure will be to pick z_1 first, generate all the z_i's and y_i's, and then calculate the mean-square error. Then the value of z_1 may be changed and again the corresponding m·s· error can be found out. If this is greater than the previous one, then another z_1 on the other side of the original z_1 may be tried and the m·s· error can be computed again. This iterative procedure is repeated till we get a set of y_i's and z_i's corresponding to the minimum mean-square error.

However, to use this approach, we must compute the mean-square error. This is given by:

$$\overline{\varepsilon^2} = \int_{n=-\infty}^{n=\infty} \left[\sum_{j=1}^{k} \int_{y_j-n}^{y_{j+1}-n} (x-z_j)^2 \frac{1}{b\sqrt{2\pi\delta}} \exp\left(\frac{-n^2}{2\delta x}\right) \frac{dx}{\sqrt{x}} \right] dn \qquad \text{(F-23)}$$

Employing the same approximations which lead to equation (F-19), we may arrive at the following complicated expression for $\overline{\varepsilon^2}$.

$$\overline{\varepsilon^2} \simeq \sum_{j=1}^{k}\left(y_{j+1}-y_j\right)\left[Z_j^2\exp(-2\sqrt{cd})\operatorname{erfc}\left(\frac{\frac{y_j+y_{j+1}}{2}-b}{\sqrt{\delta b}}\right)\cdot\frac{2\sqrt{\pi}}{\sqrt{c}}\right.$$

$$-2z_j\frac{\exp(-2\sqrt{cd})}{\sqrt{c^3}}\cdot\left\{\exp\left[-\left(\frac{\frac{y_j+y_{j+1}}{2}-b}{2\delta b}\right)^2\right]\left[\frac{\frac{y_j+y_{j+1}}{2}-b}{\sqrt{2\delta b}}\right]\right.$$

$$\left.+(1+2\sqrt{cd})\sqrt{\pi}\operatorname{erfc}\frac{\left(\frac{y_j+y_{j+1}}{2}-b\right)}{\sqrt{\delta b}}\right\}$$

$$+\frac{\exp(-2\sqrt{cd})}{\sqrt{c^5}}\left\{\exp\left[-\left(\frac{\frac{y_j+y_{j+1}}{2}-b}{2\delta b}\right)^2\right]\cdot\left[\left(\frac{\frac{y_j+y_{j+1}}{2}-b}{2\delta b}\right)^2\right]^{3/2}\right.$$

$$+3\exp\left[-\left(\frac{\frac{y_j+y_{j+1}}{2}-b}{2\delta b}\right)^2\right]\left(\frac{\frac{y_j+y_{j+1}}{2}-b}{2\delta b}\right)\cdot\left[\frac{1}{2}+\left(\frac{y_j+y_{j+1}}{2}\cdot\frac{1}{2\delta}\right)\right]$$

$$+\sqrt{\pi}\operatorname{erfc}\left[\frac{\left(\frac{y_j+y_{j+1}}{2}-b\right)}{\sqrt{\delta b}}\right]\left[\frac{3}{2}+3\left(\frac{y_j+y_{j+1}}{2}\cdot\frac{1}{2\delta}\right)\right.$$

$$\left.\left.+2\cdot\left(\frac{\frac{y_j+y_{j+1}}{2}}{4\delta^2}\right)^2\right\}\right] \qquad \text{(F-24)}$$

where for each j, $2\sqrt{cd}=\dfrac{y_j+y_{j+1}}{2\delta}$.

The procedure described previously can be used to get the quantizer levels corresponding to the minimum mean-square error.

Similarly, other probability density functions, such as Rayleigh, normal, can be assumed for $f_X(x)$ and the quantizer levels are again obtained by using the above procedure. It may be difficult to evaluate equation (F-3) and (F-5). In such cases, numerical integration may be employed. Also, the sensitivity of the quantizer levels to different probability density functions may be studied. The merit of this procedure lies in the fact that a chosen performance index (mean-square error) is minimized while obtaining the quantizer levels and thresholds.

APPENDIX G

AUTOCORRELATION PLOTS

The autocorrelation function is the inverse Fourier transform of the power spectral density. It is useful in some data analysis using second-order statistics and is included for reference here. Essentially what was done ~~is to take~~ we took the inverse Fourier transform of the power spectra presented in Chapter 2. For convenience, the plots are normalized so that: $R(0) = 1$.

FIGURE G.1. PLOTS OF THE NORMALIZED

AUTOCORRELATION OF SELECTED PORTIONS OF APOLLO VI PHOTOGRAPHS

Apollo AS6-2-877
Lines: 200-204
Elements: 10-521

AVERAGE AUTOCORRELATION
GRAPH PLOT NO. 03

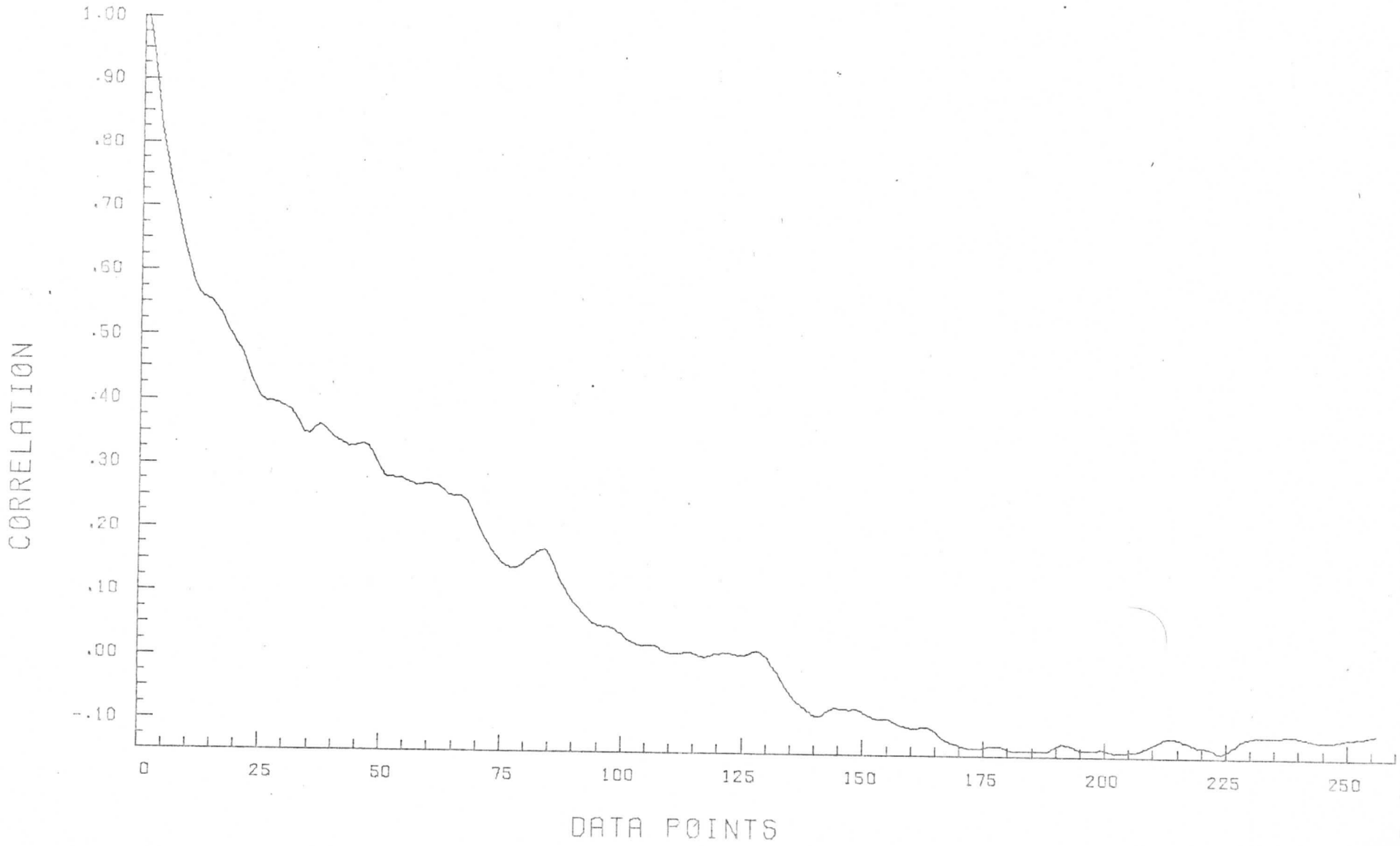

Apollo AS6-2-877
Lines: 200-204
Elements: 510-1021

AVERAGE AUTOCORRELATION
GRAPH PLOT NO. 06

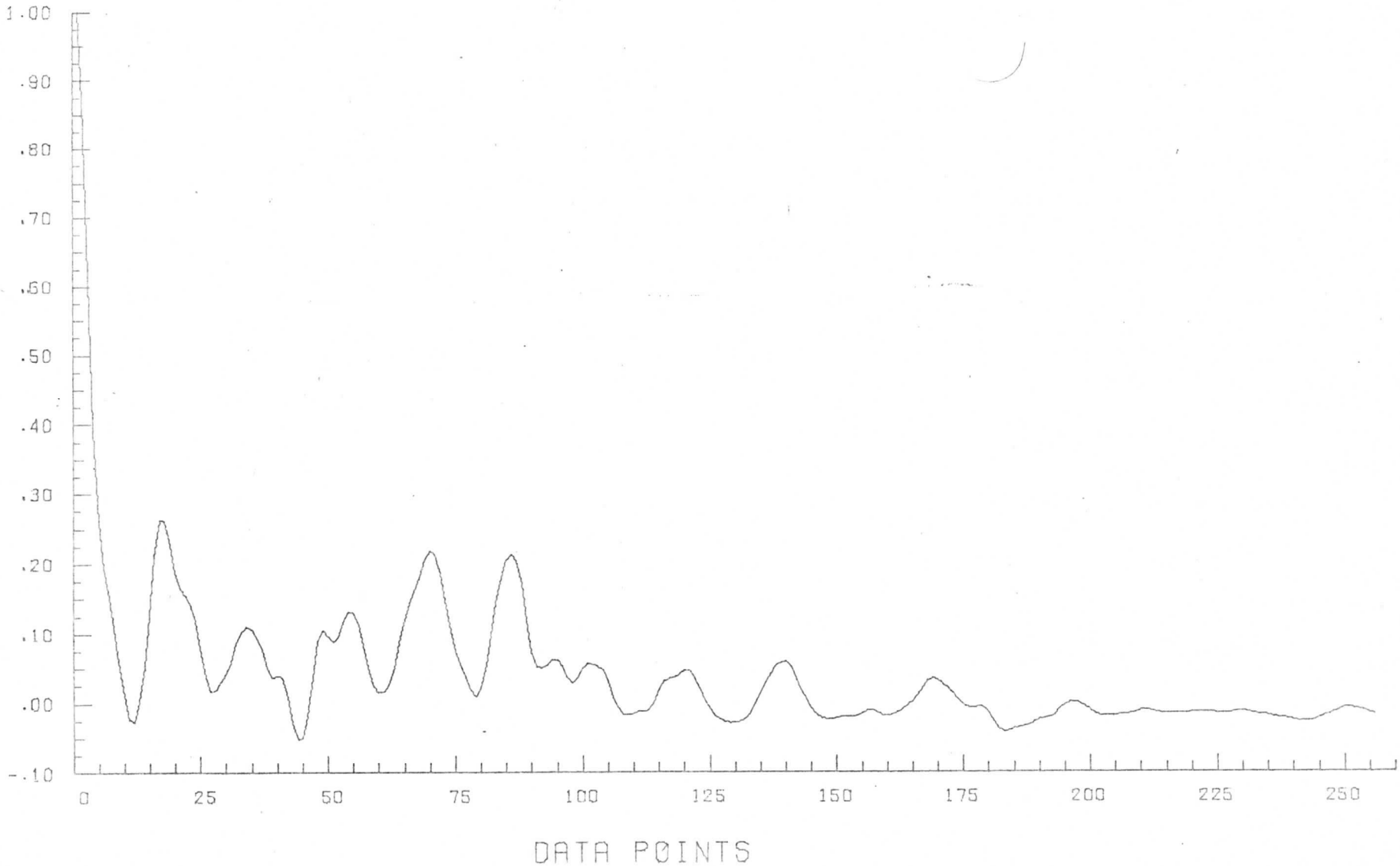

Apollo AS6-2-877
Lines: 850-854
Elements: 510-1021

AVERAGE AUTOCORRELATION
GRAPH PLOT NO. 09

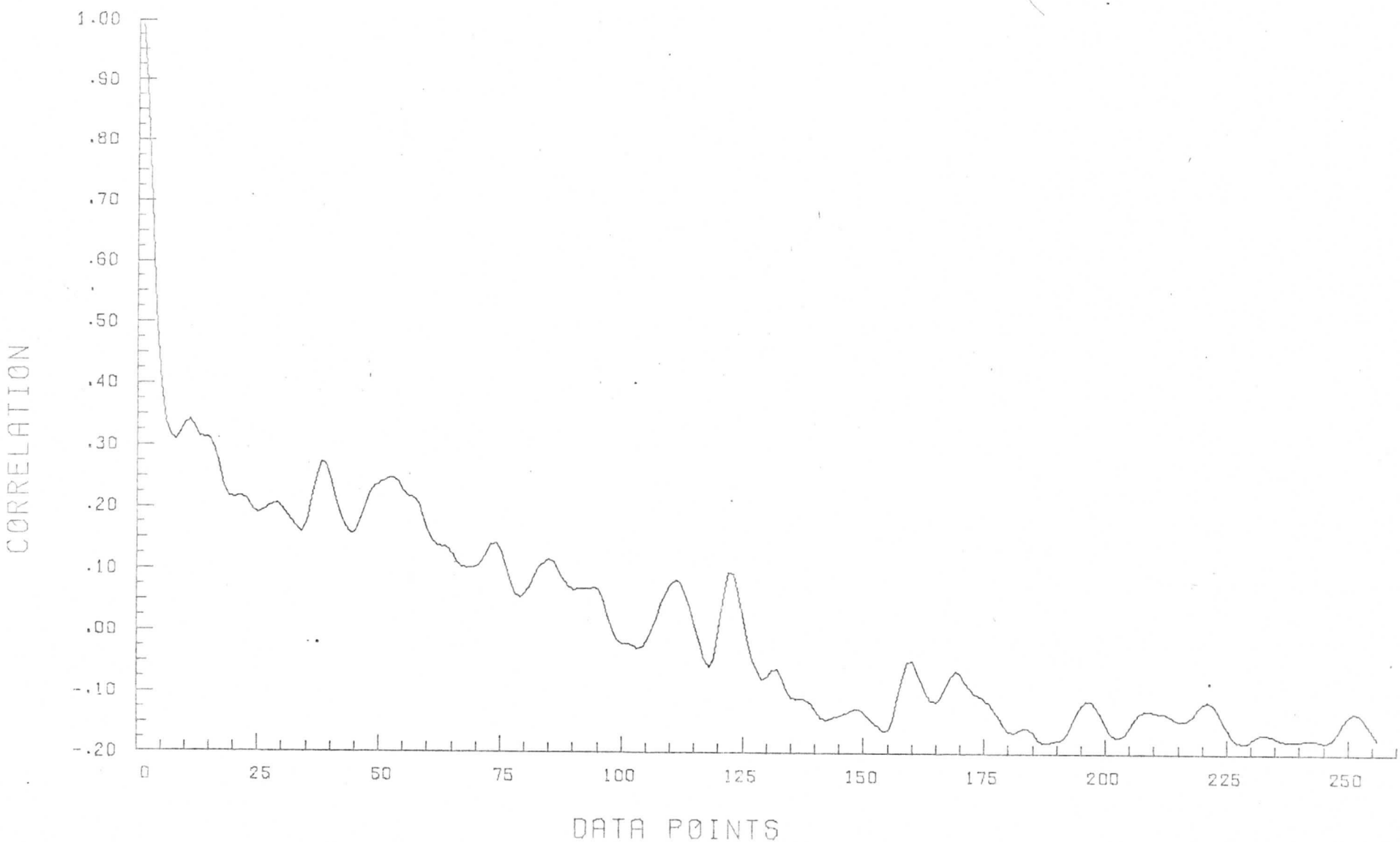

Apollo AS6-2-934
Lines: 100-104
Elements: 510-1021

AVERAGE AUTOCORRELATION
GRAPH PLOT NO. 12

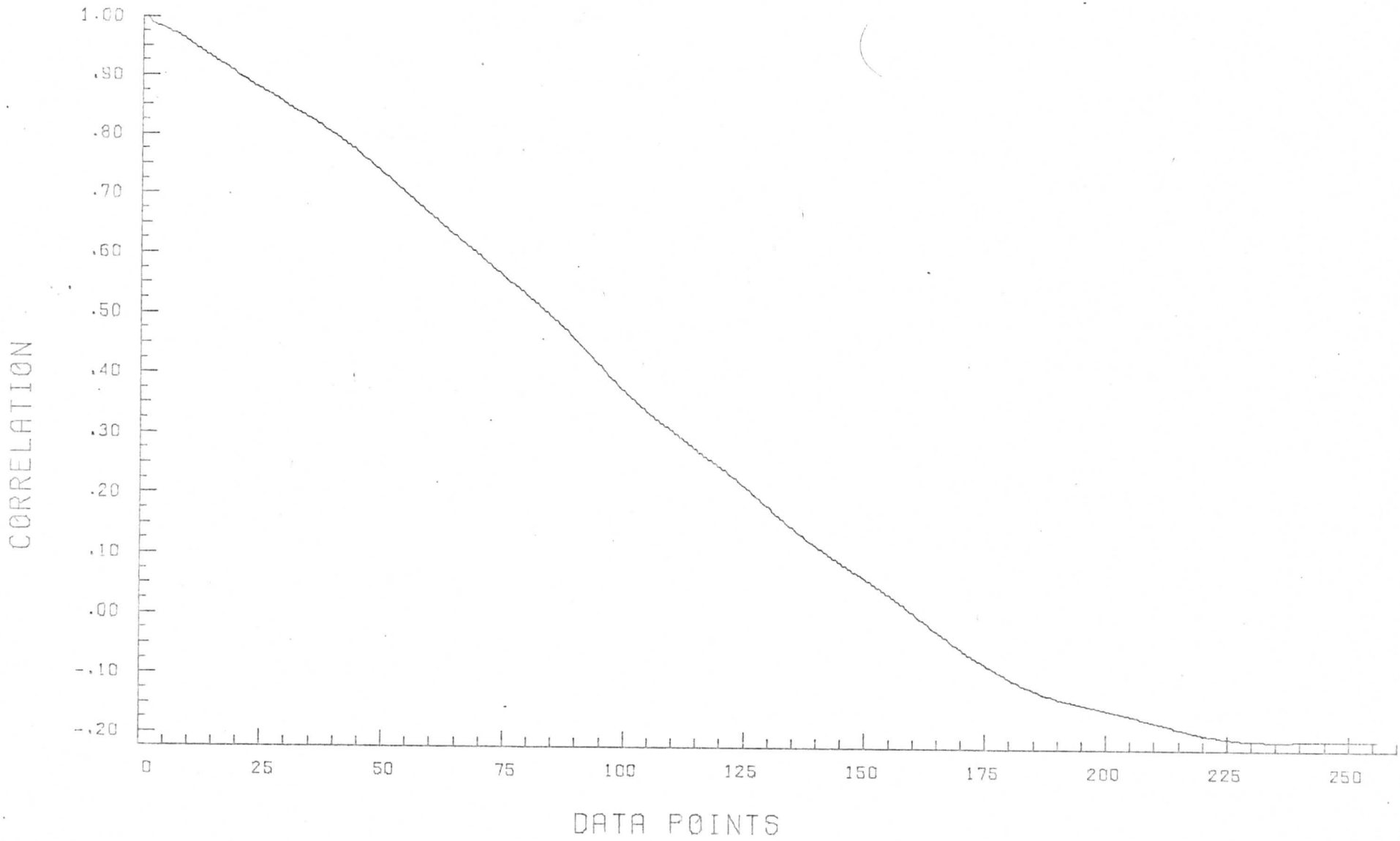

Apollo AS6-2-934
Lines: 250-254
Elements: 510-1021

AVERAGE AUTOCORRELATION
GRAPH PLOT NO. 15

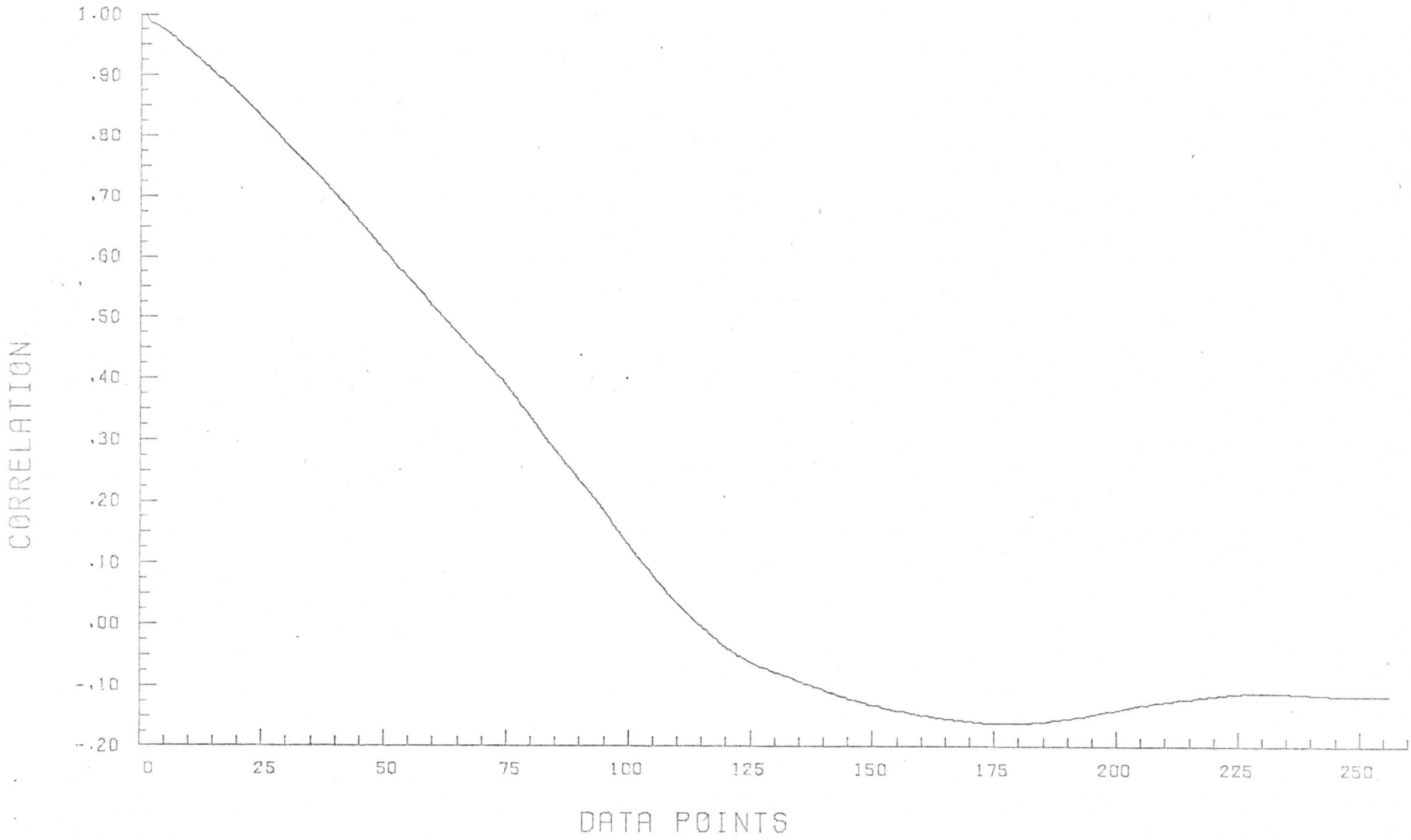

Apollo AS6-2-948
Lines: 800-804
Elements: 10-521

AVERAGE AUTOCORRELATION
GRAPH PLOT NO. 18

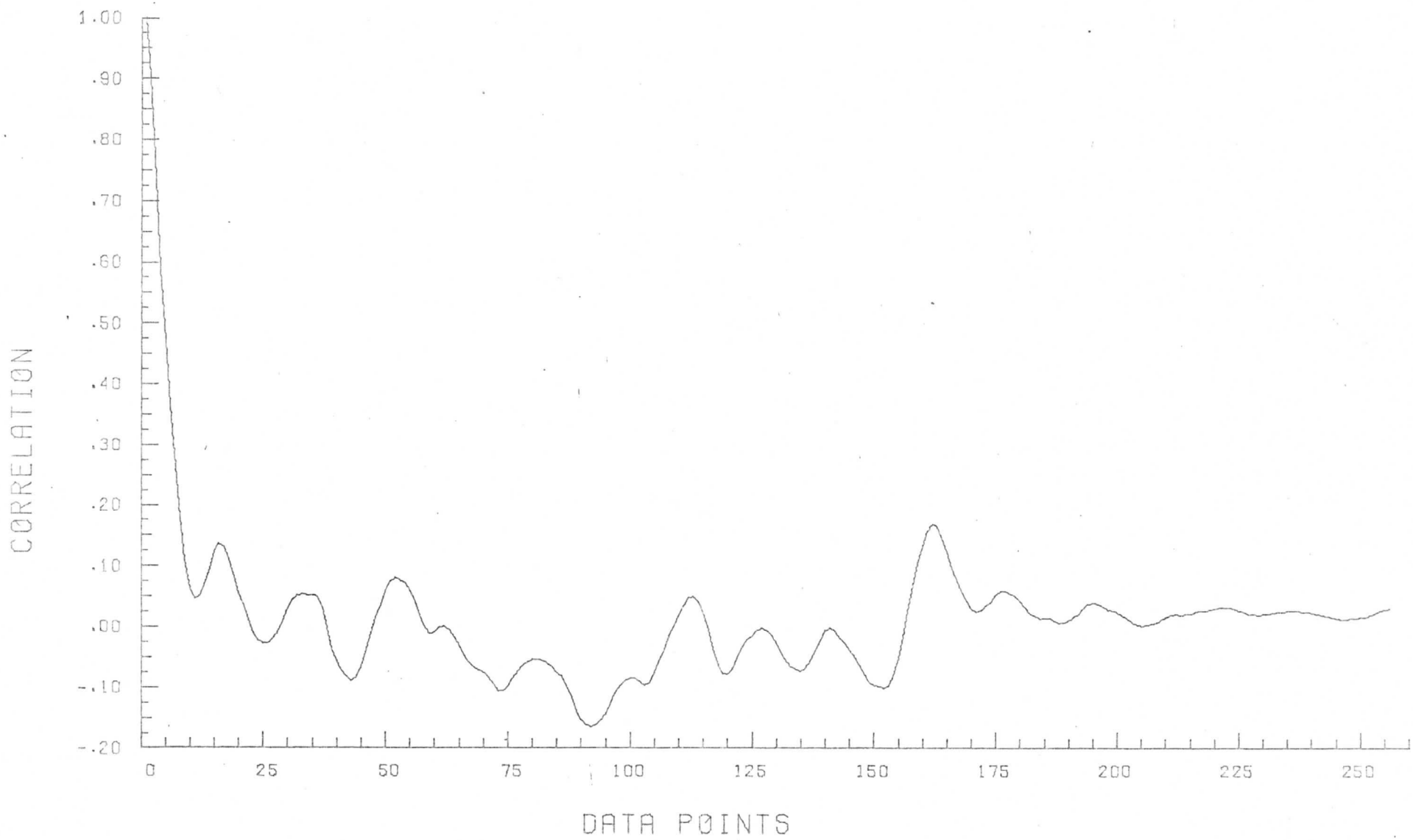

Apollo AS6-2-1064
Lines: 130-134
Elements: 510-1021

AVERAGE AUTOCORRELATION
GRAPH PLOT NO. 21

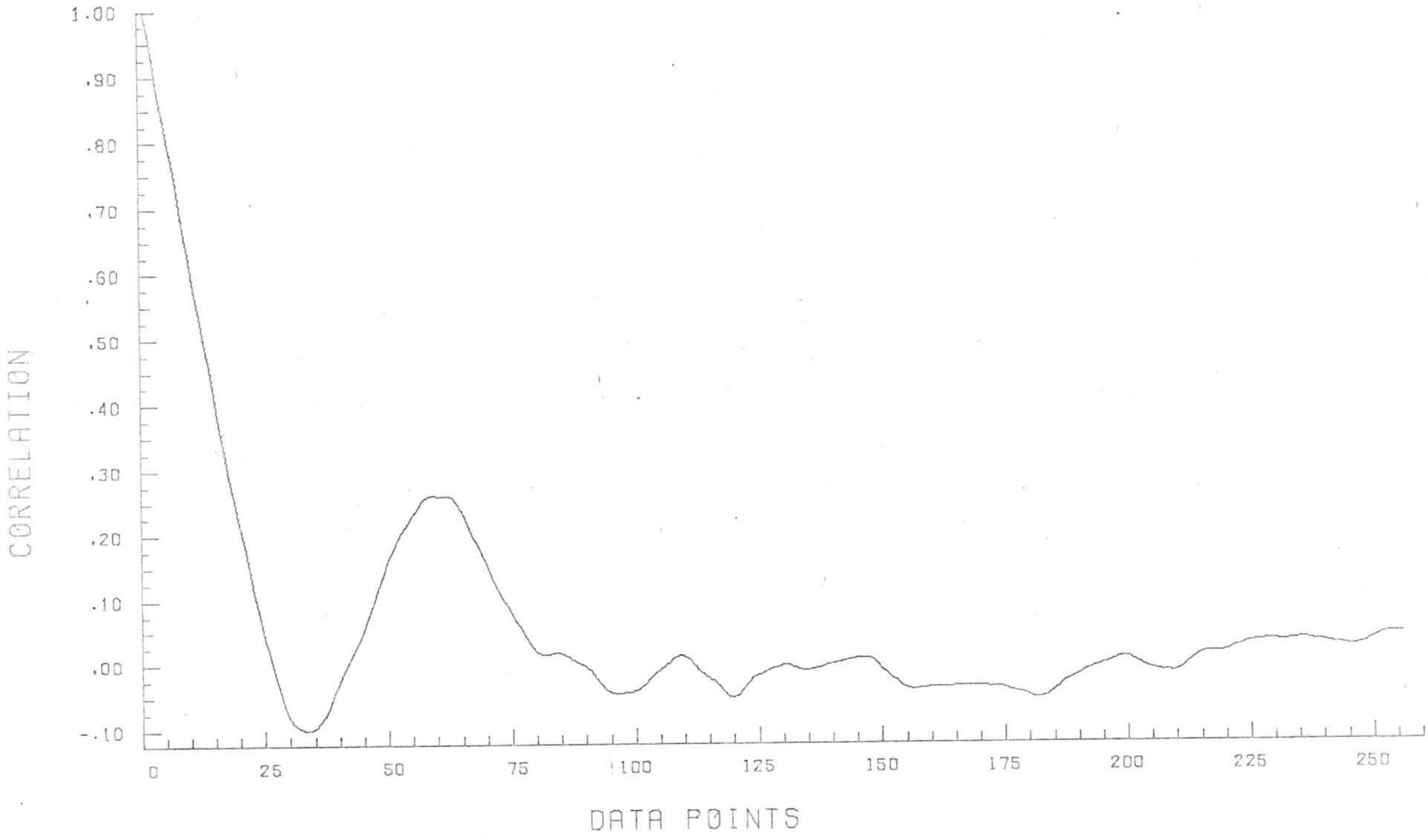

Apollo AS6-2-1429
Lines: 250-254
Elements: 510-1021

AVERAGE AUTOCORRELATION
GRAPH PLOT NO. 24

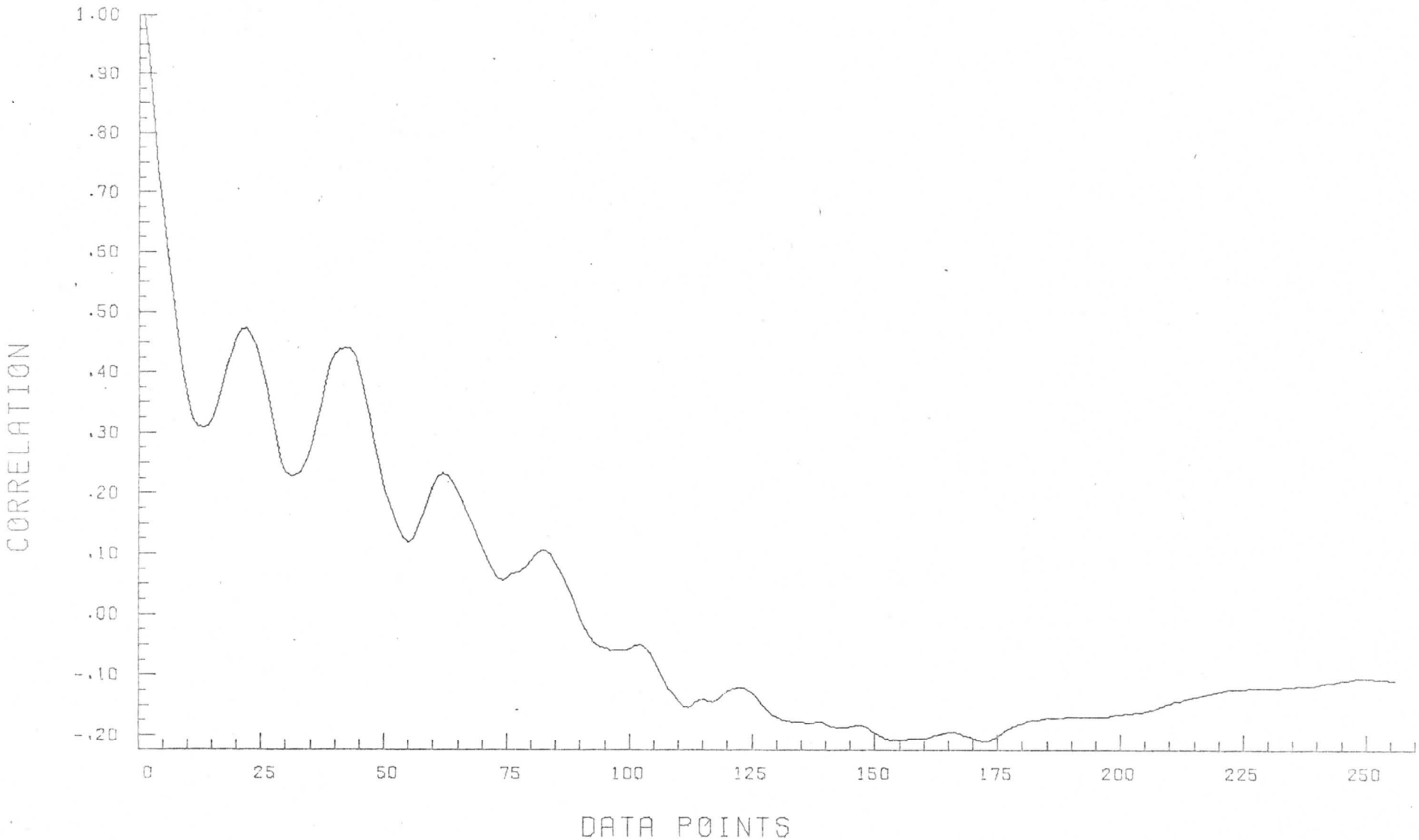

Apollo AS6-2-1429
Lines: 700-704
Elements: 510-1021

AVERAGE AUTOCORRELATION
GRAPH PLOT NO. 27

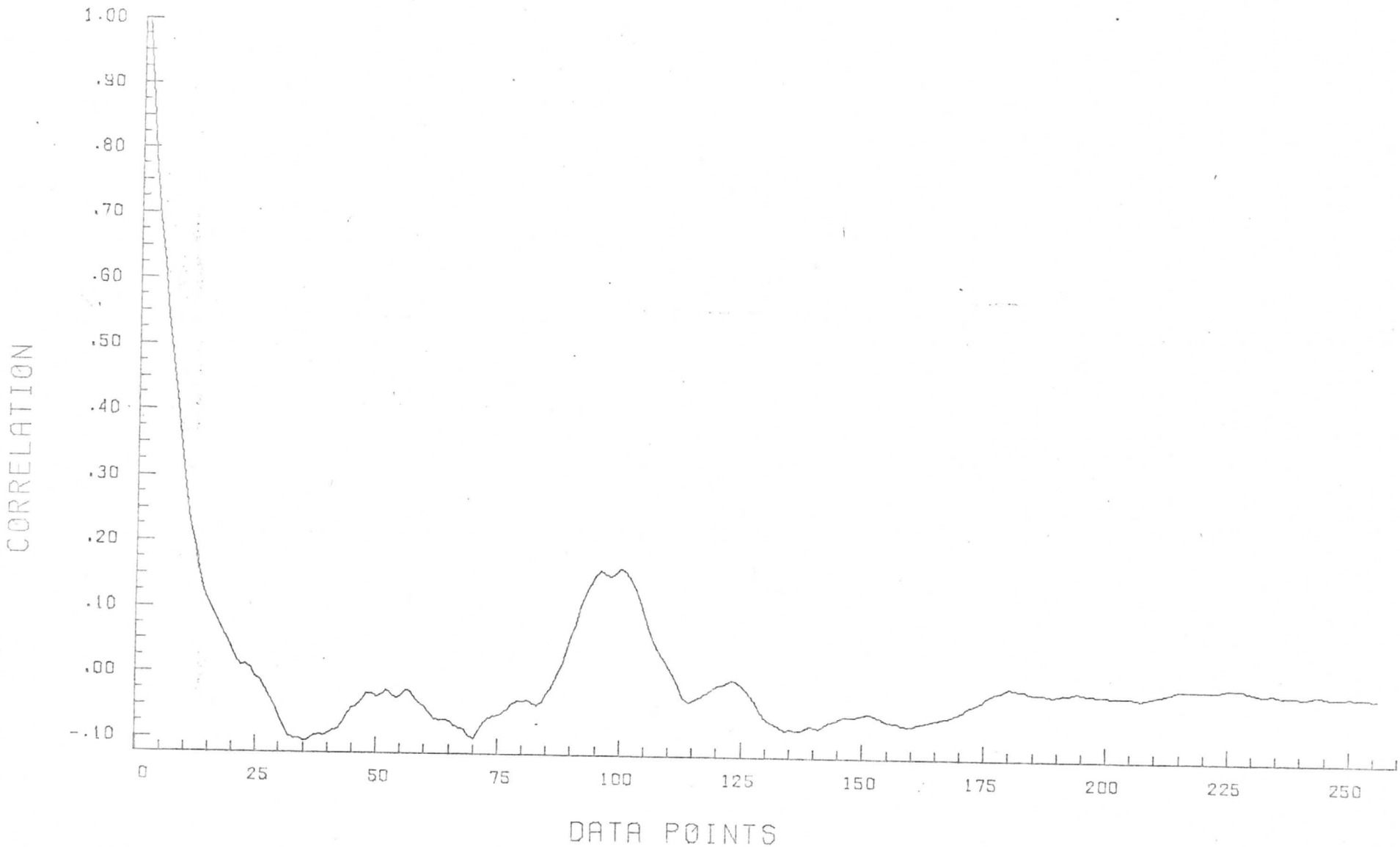

Apollo AS6-2-1430
Lines: 500-504
Elements: 260-771

AVERAGE AUTOCORRELATION
GRAPH PLOT NO. 30

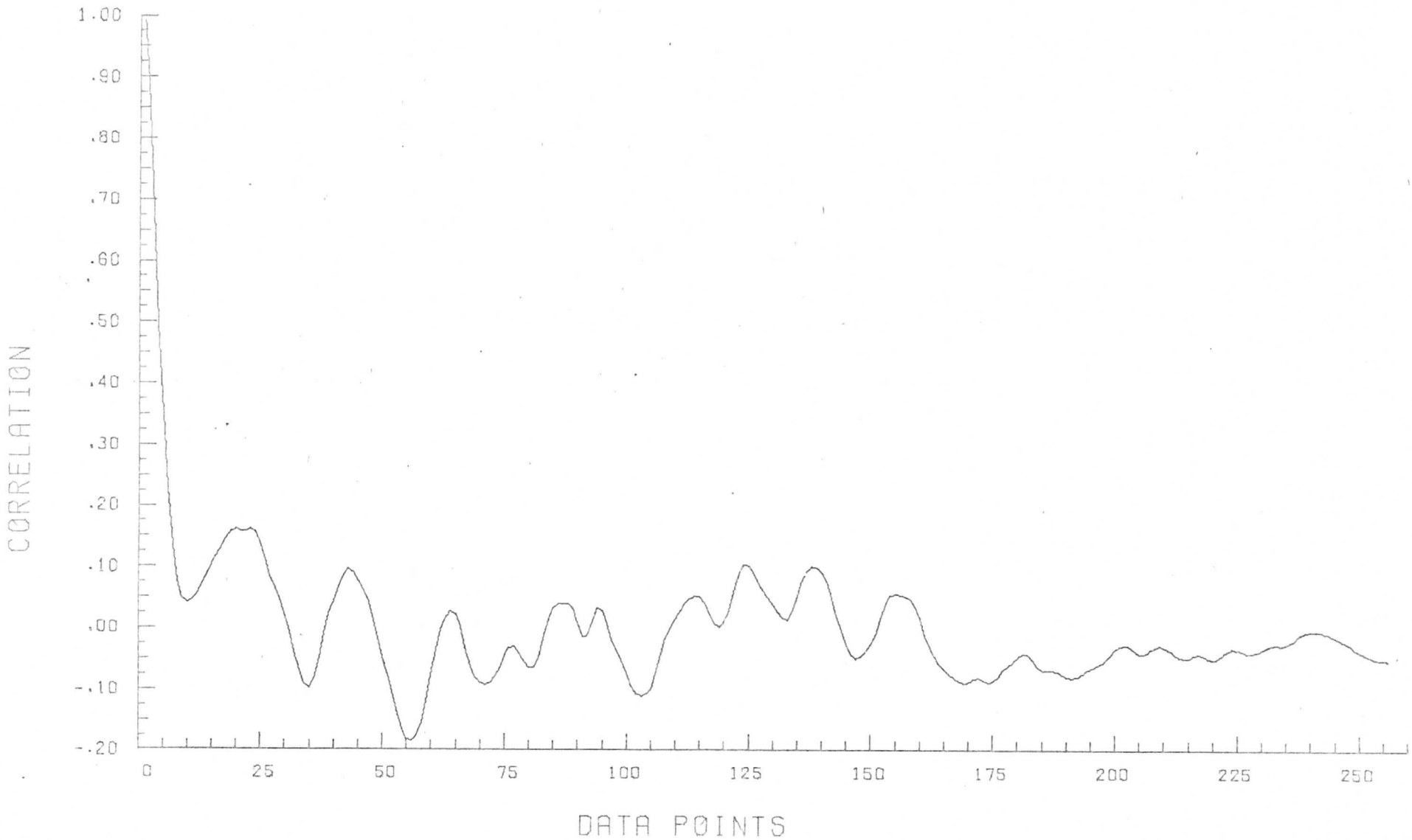

Apollo AS6-2-1467
Lines: 800-804
Elements: 10-521

AVERAGE AUTOCORRELATION
GRAPH PLOT NO. 33

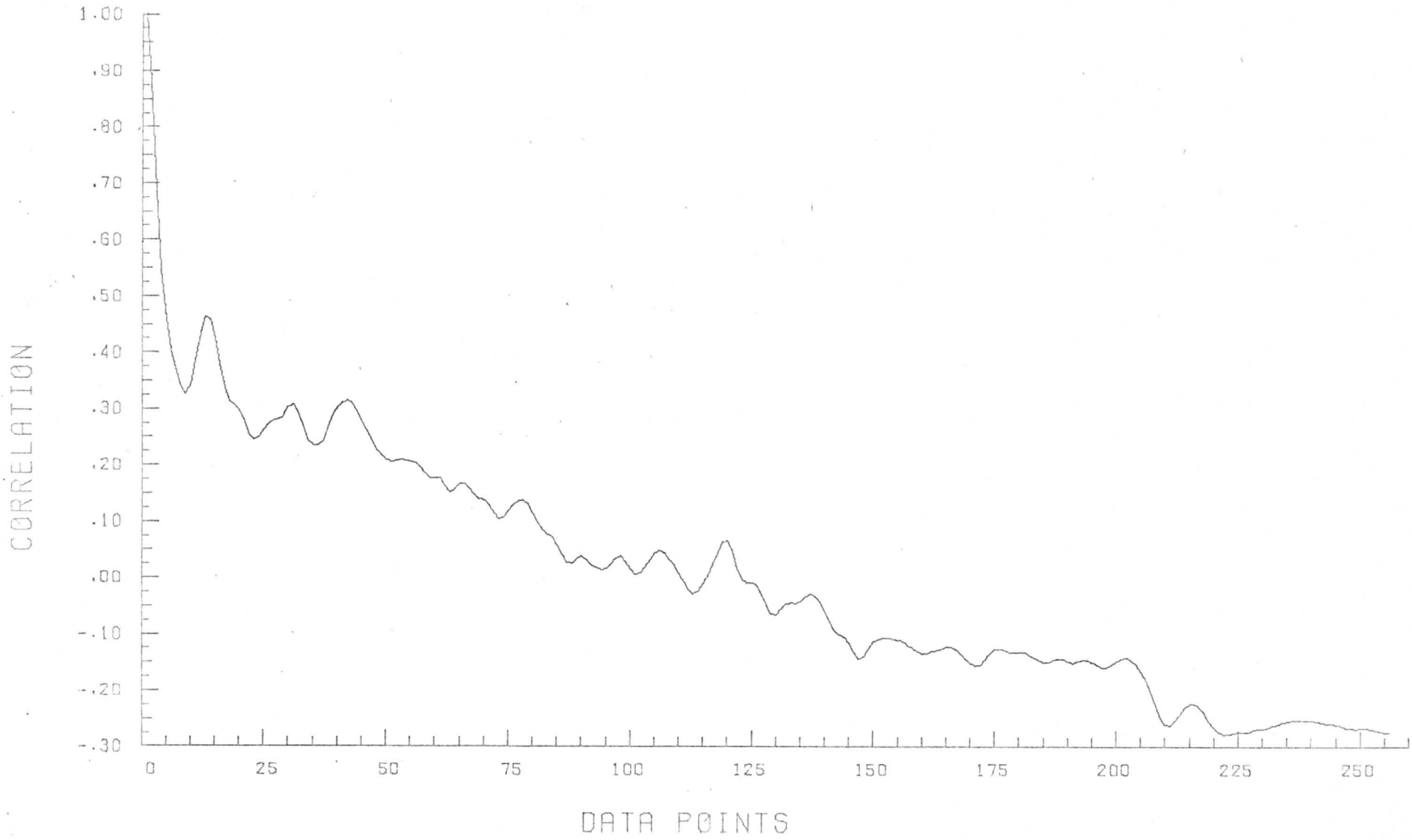

Apollo AS6-2-1468
Lines: 650-654
Elements: 510-1021

AVERAGE AUTOCORRELATION
GRAPH PLOT NO. 36

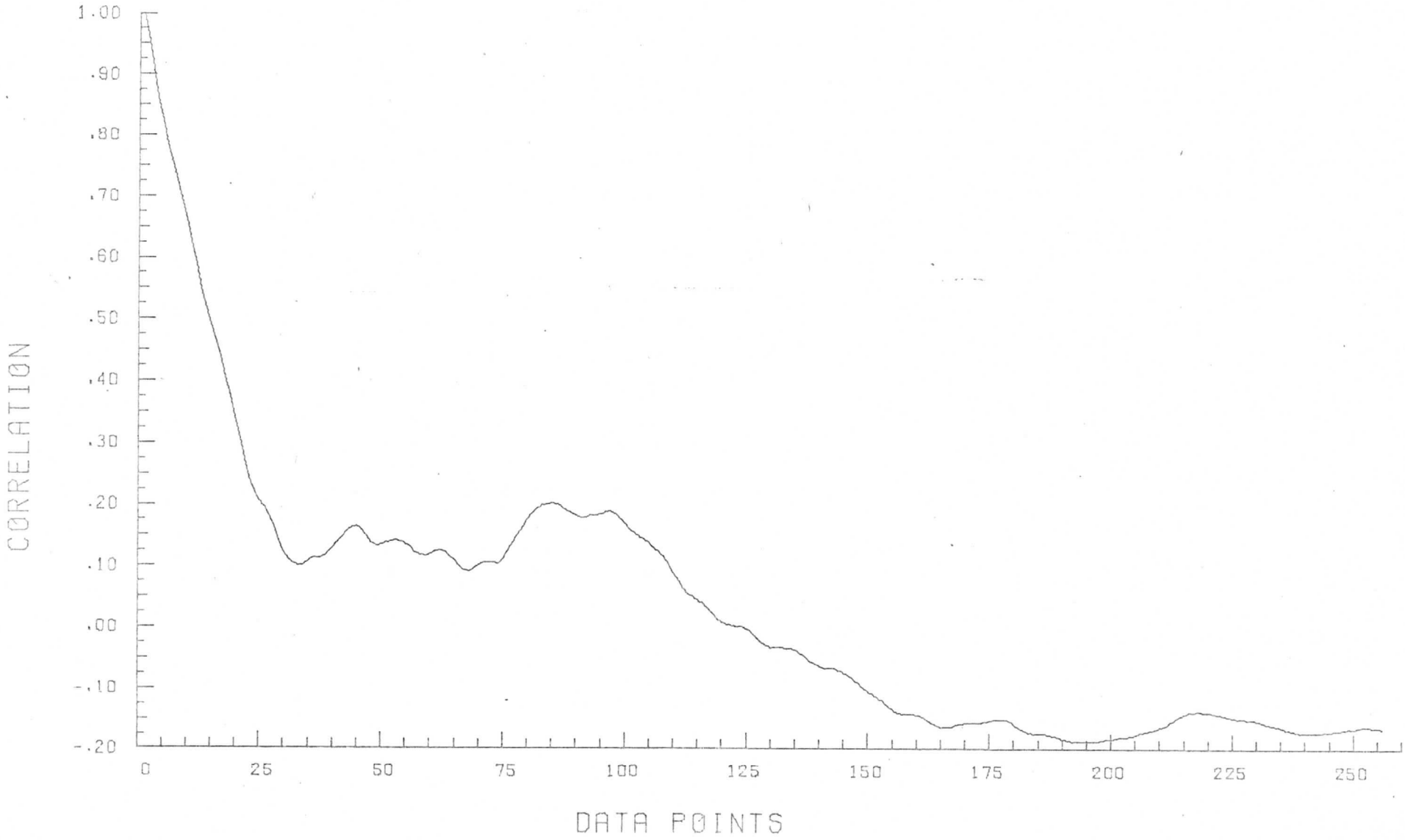

Apollo AS6-2-1468
Lines: 850-854
Elements: 10-521

AVERAGE AUTOCORRELATION
GRAPH PLOT NO. 39

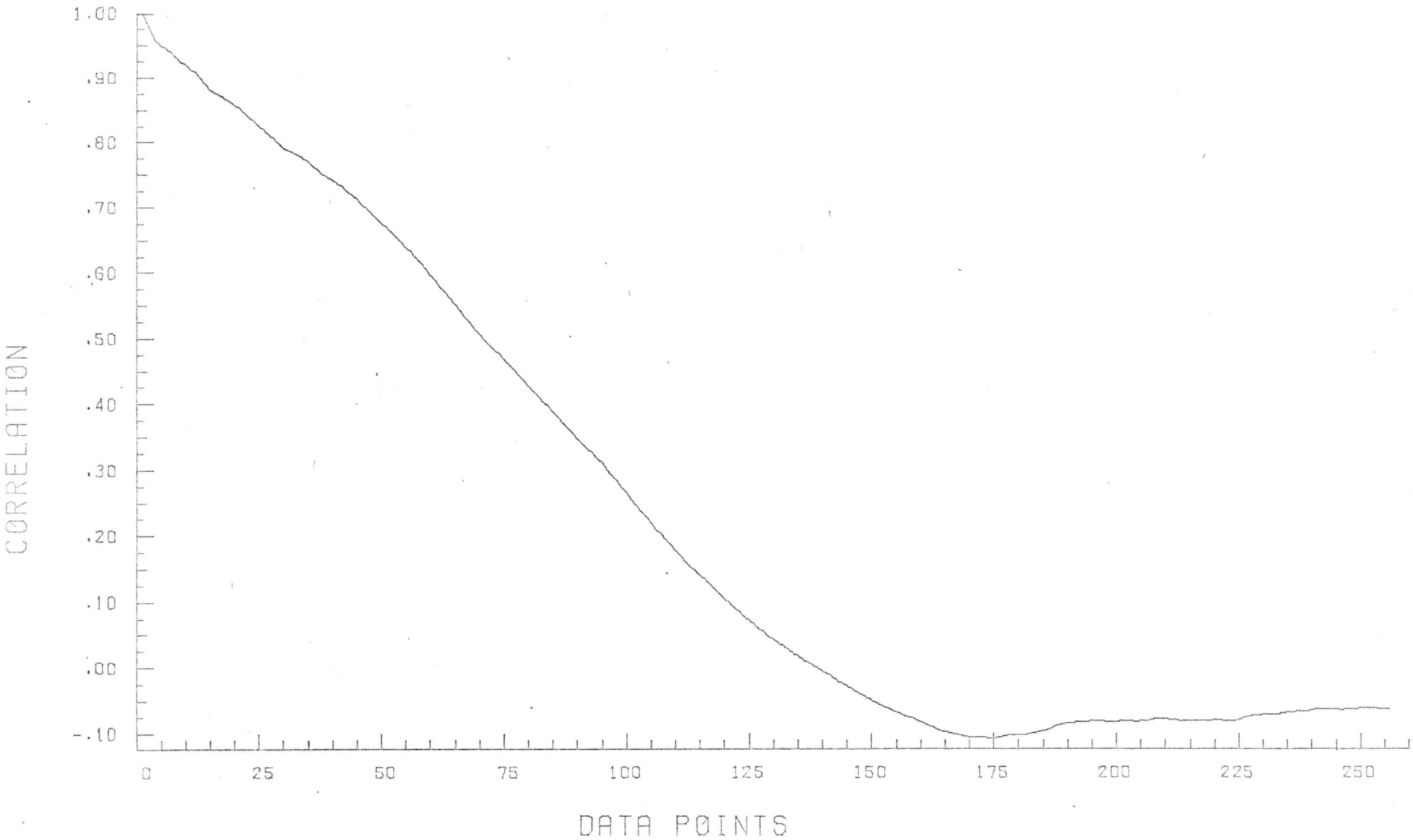

Apollo AS6-2-1469
Lines: 100-104
Elements: 510-1021

AVERAGE AUTOCORRELATION
GRAPH PLOT NO. 42

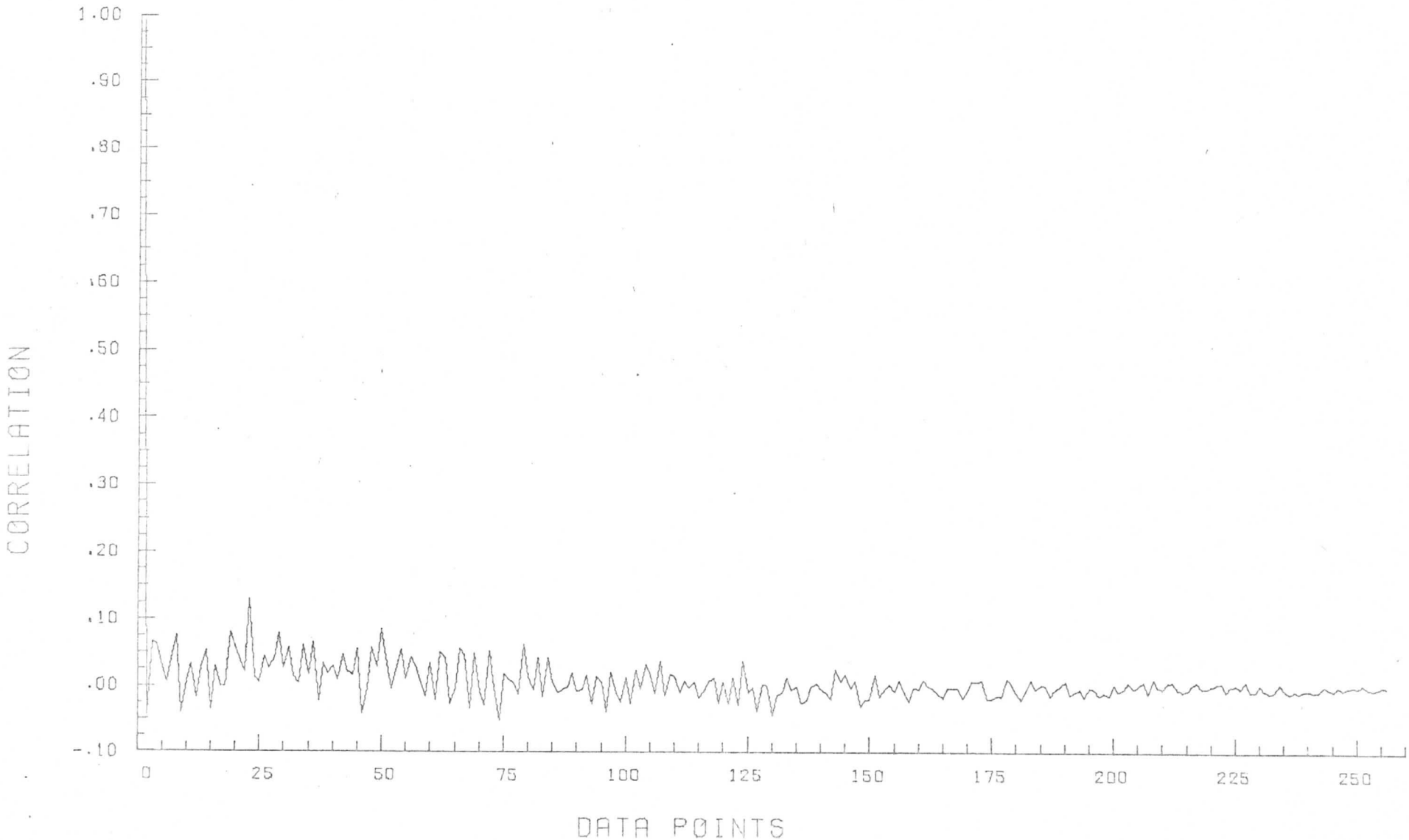

Apollo AS6-2-1469
Lines: 760-764
Elements: 10-521

AVERAGE AUTOCORRELATION
GRAPH PLOT NO. 45

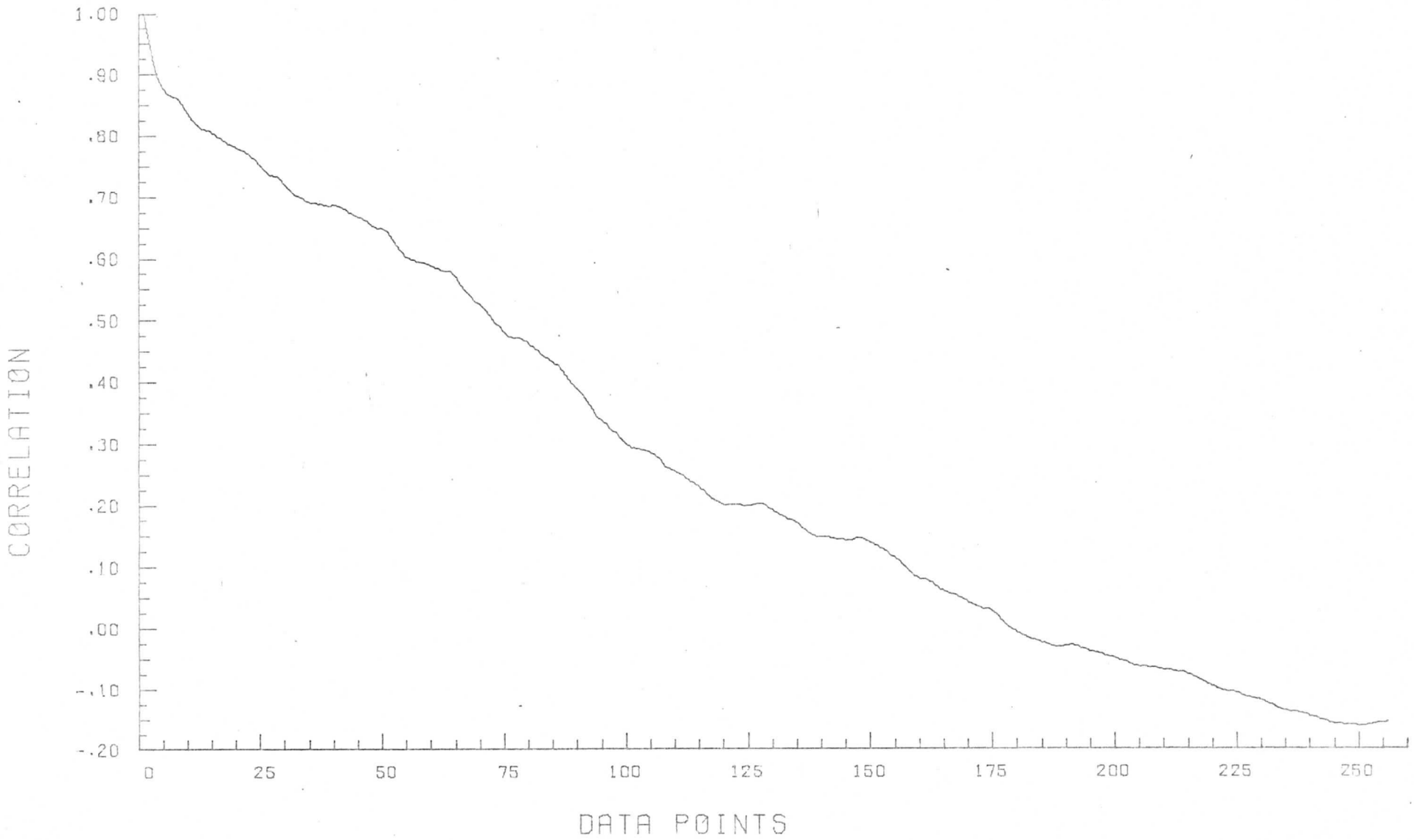

Apollo AS6-2-1469
Lines: 760-764
Elements: 510-1021

AVERAGE AUTOCORRELATION
GRAPH PLOT NO. 48

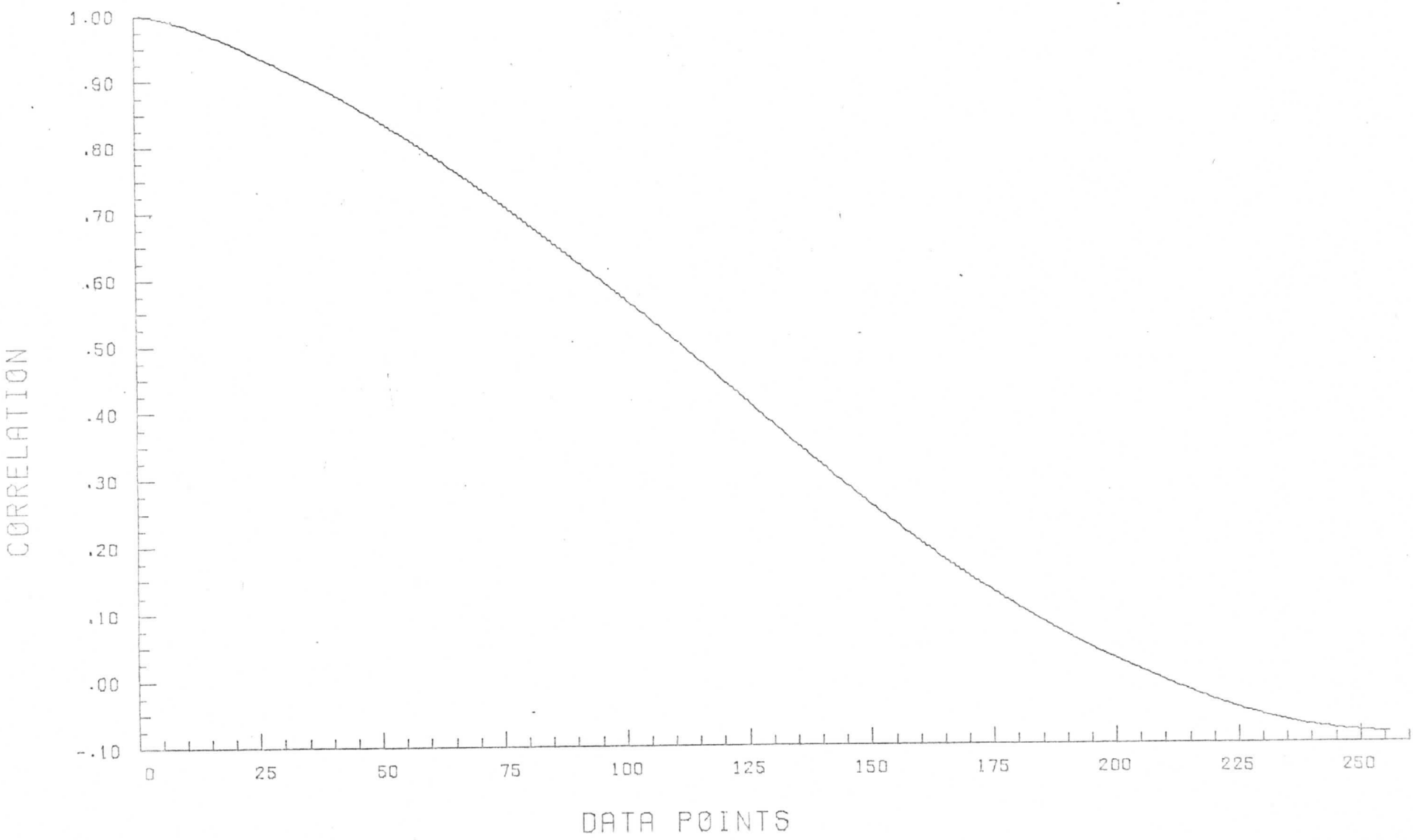

Apollo AS6-2-1484 (horiz.)
Lines: 350-354
Elements: 510-1021

AVERAGE AUTOCORRELATION
GRAPH PLOT NO. 51

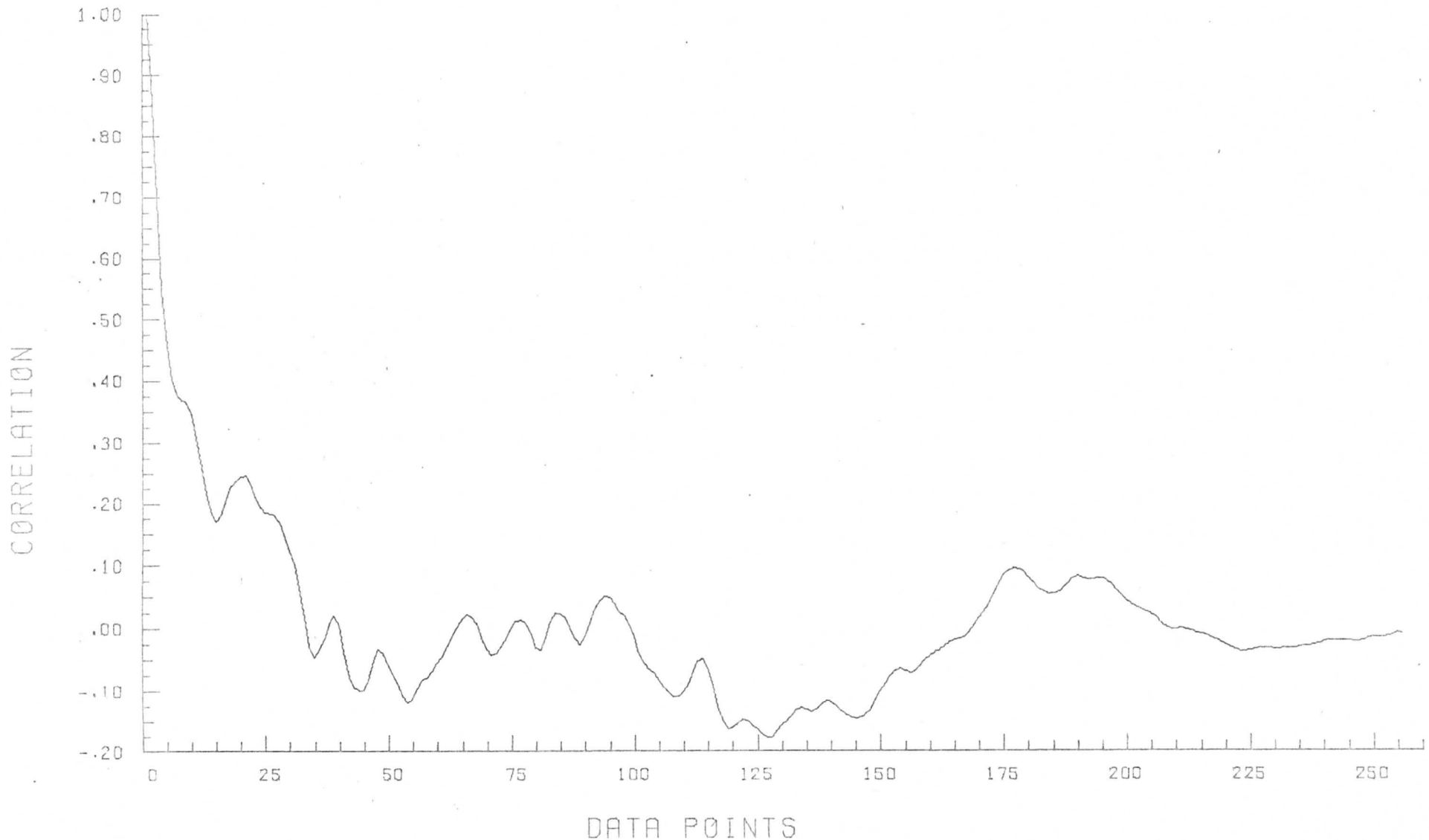

Apollo AS6-2-1484 (horiz.)
Lines: 350-354
Elements: 260-771

AVERAGE AUTOCORRELATION
GRAPH PLOT NO. 54

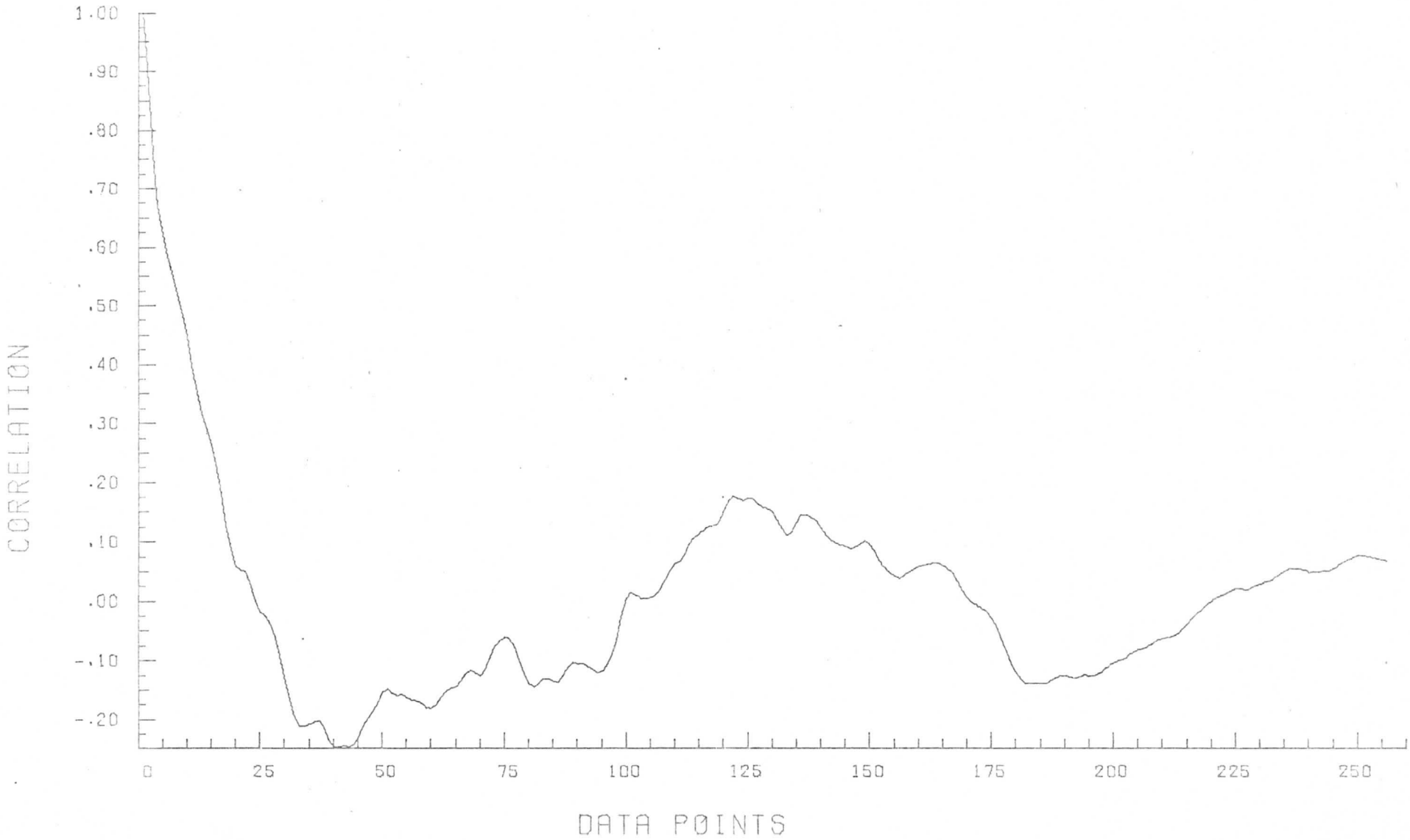

Apollo AS6-2-1484 (vert.)
Lines: 100-104
Elements: 260-771

AVERAGE AUTOCORRELATION
GRAPH PLOT NO. 57

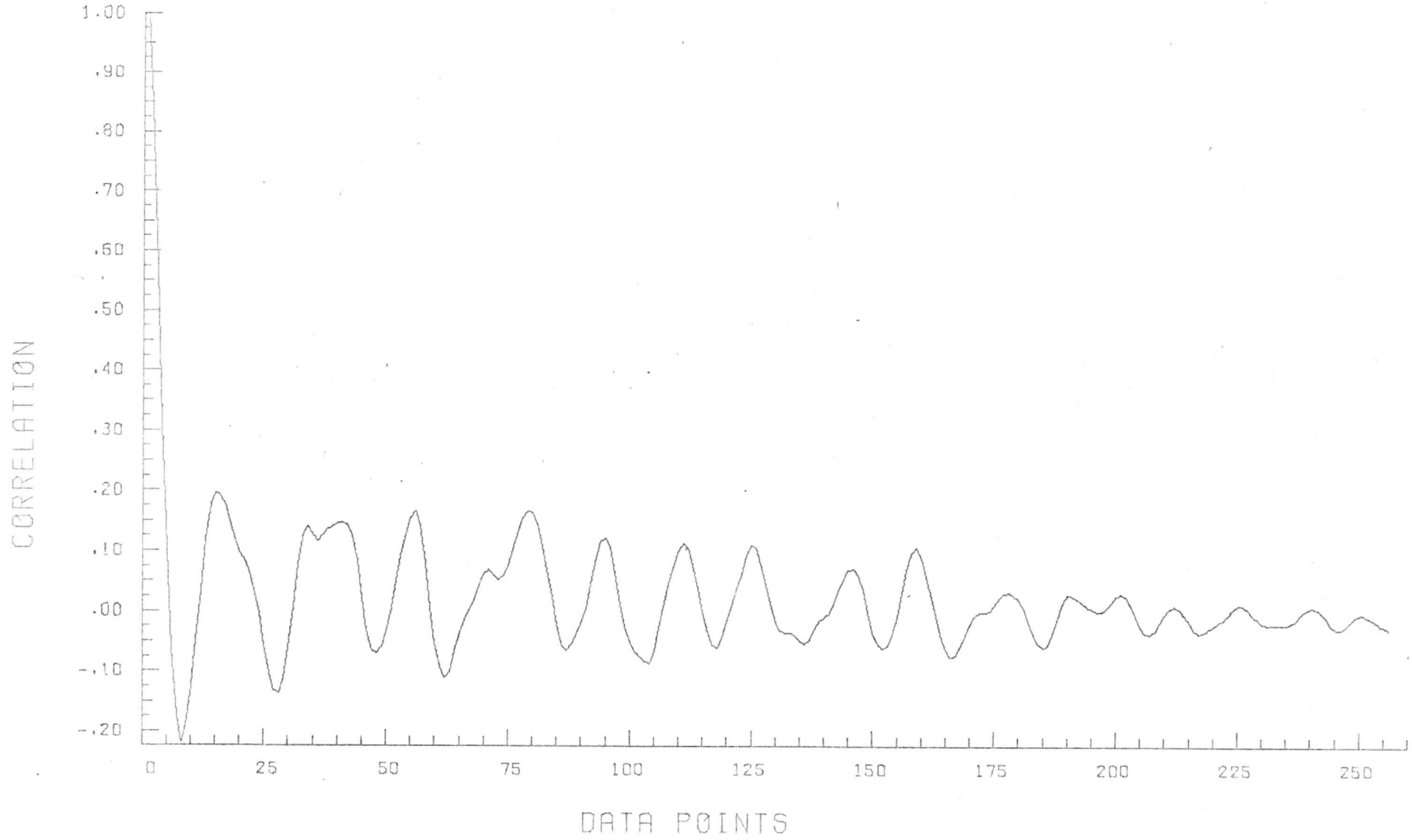

Delete Appendix H

APPENDIX H

UNSMOOTH POWER SPECTRAL PLOTS

The plots shown were generated using a 512-point FFT routine in the UNIVAC 1108 with a rectangular data window and no data smoothing. The average value was also removed.

The computer-generated plots follow the same order: (1) the (logarithimic) power spectral plot of the first sample line; (2) the autocorrelation function of the first sample line; (3) the (logarithimic) power spectral plot of the fifth sample line; (4) the log of the average power spectrum of five consecutive lines; (5) the average autocorreclation function of five consecutive lines. Averaging over five lines decreases the spectral randomness in the measurement and is essentially averaging over a scan of 5 x .079 = 0.395 n.mi. in width.

FIGURE H.1. UNSMOOTHED POWER SPECTRAL

PLOTS OF APOLLO VI PHOTOGRAPHS

Apollo 56-2-877, (rect.)
Locator: Tape 17, File 1
Records: 860 - 864 Date: 2/1/73
Elements: 510 - 1021
Plot: Log Power Spectrum, First Line

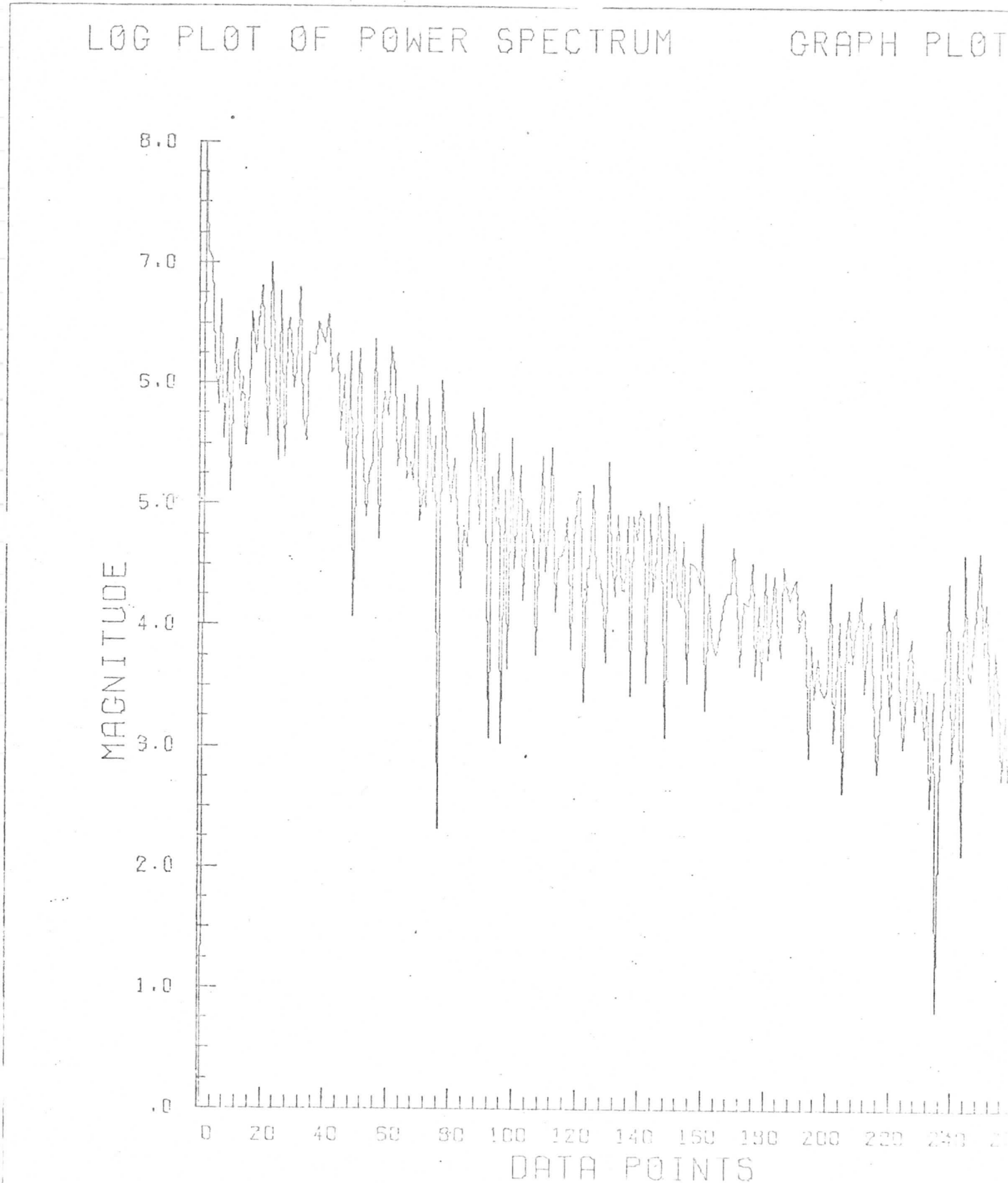

Apollo 56-2-877, (rect.)
Locator: Tape 17, File 1
Records: 860 - 864 Date: 2/1/73
Elements: 510 - 1021
Plot: Autocorrelation, First Line

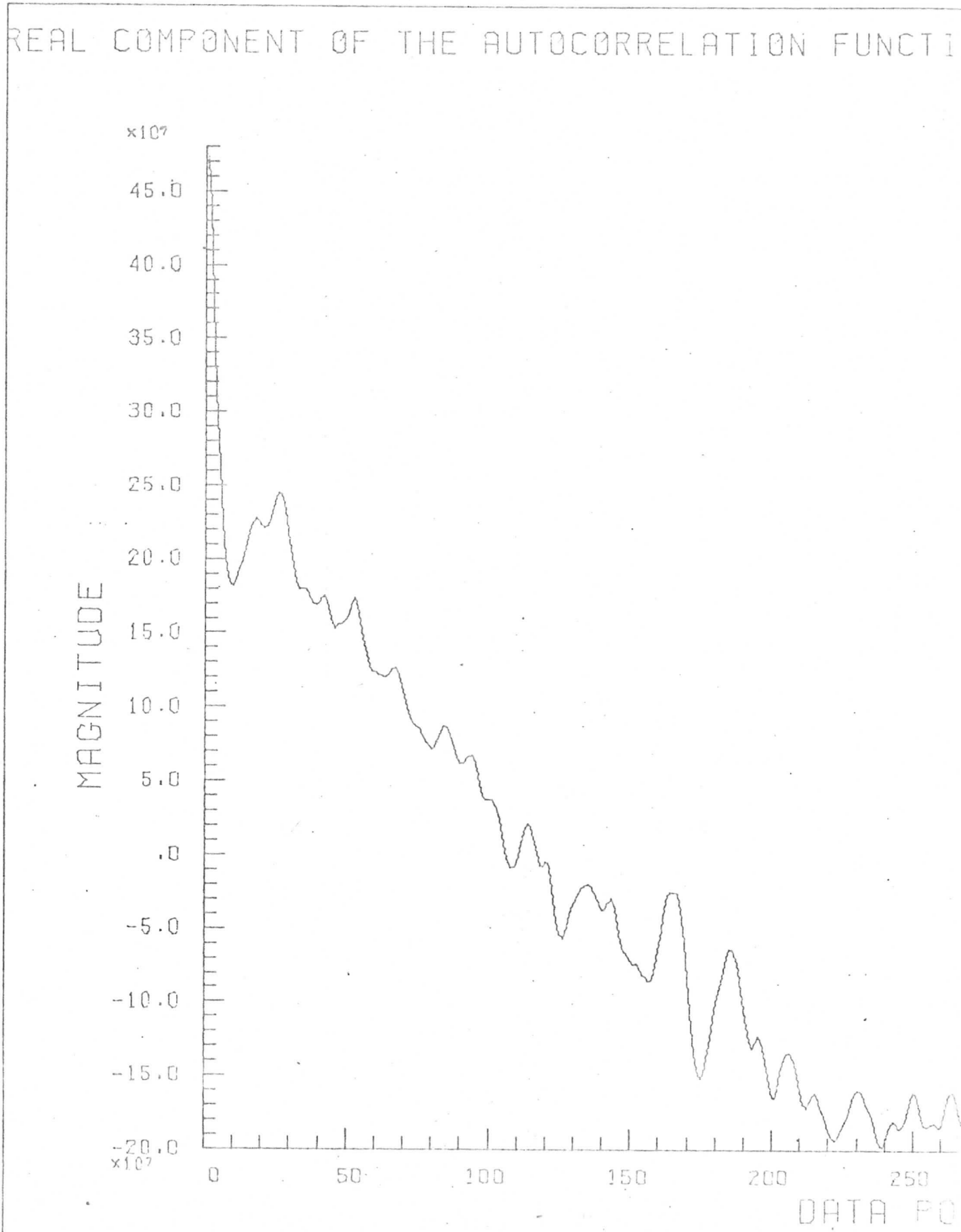

Apollo 56-2-877, (rect.)
Locator: Tape 17, File 1
Records 860 - 864 Date: 2/1/73
Elements: 510 - 1021
Plot: Log Power Spectrum, Fifth Line

H-5

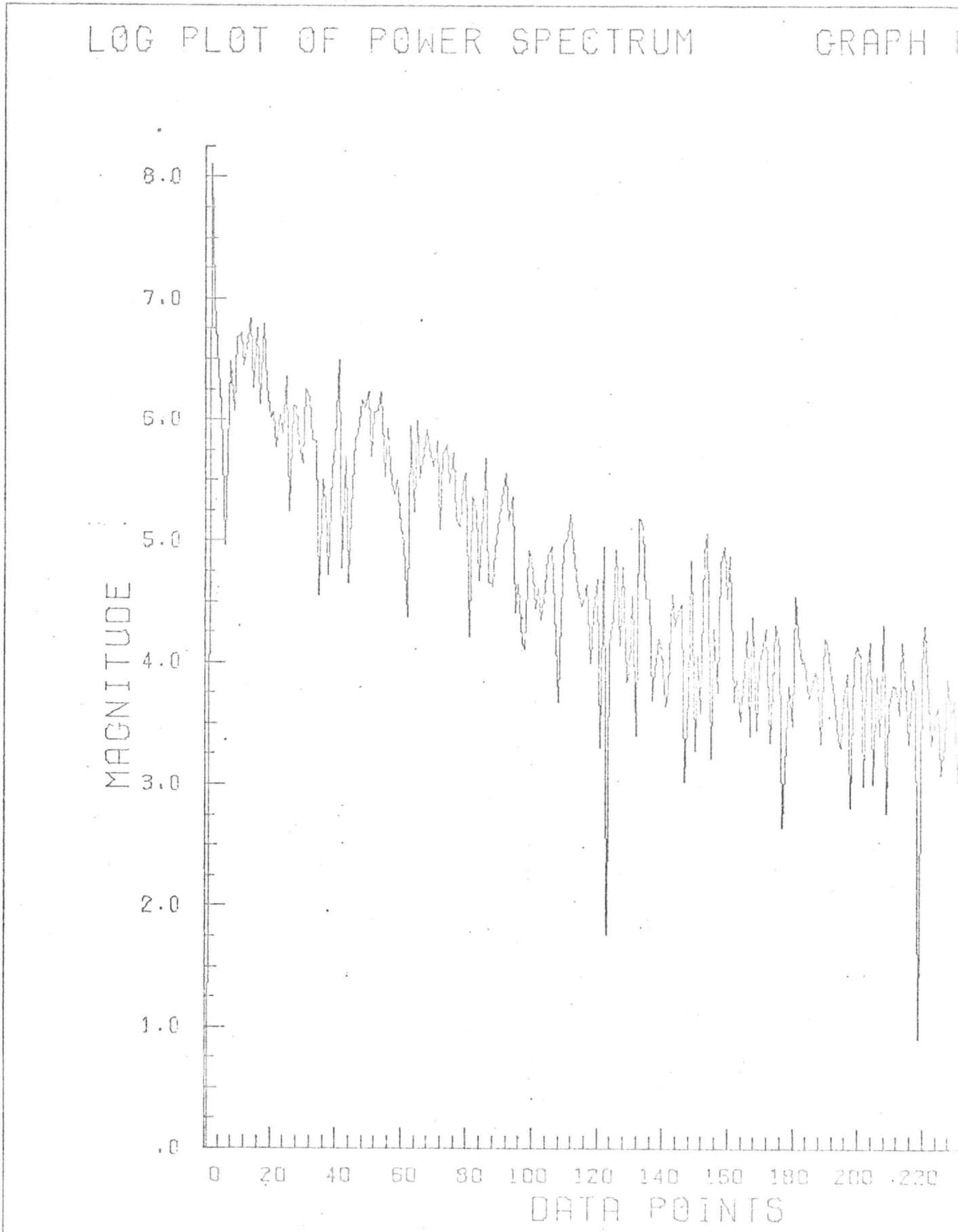

Apollo 56-2-877, (rect.)
Locator: Tape 17, File 1
Records: 860 - 864 Date: 2/1/73
Elements: 510 - 1021
Plot: Log Avg. Power Spectrum

H-6

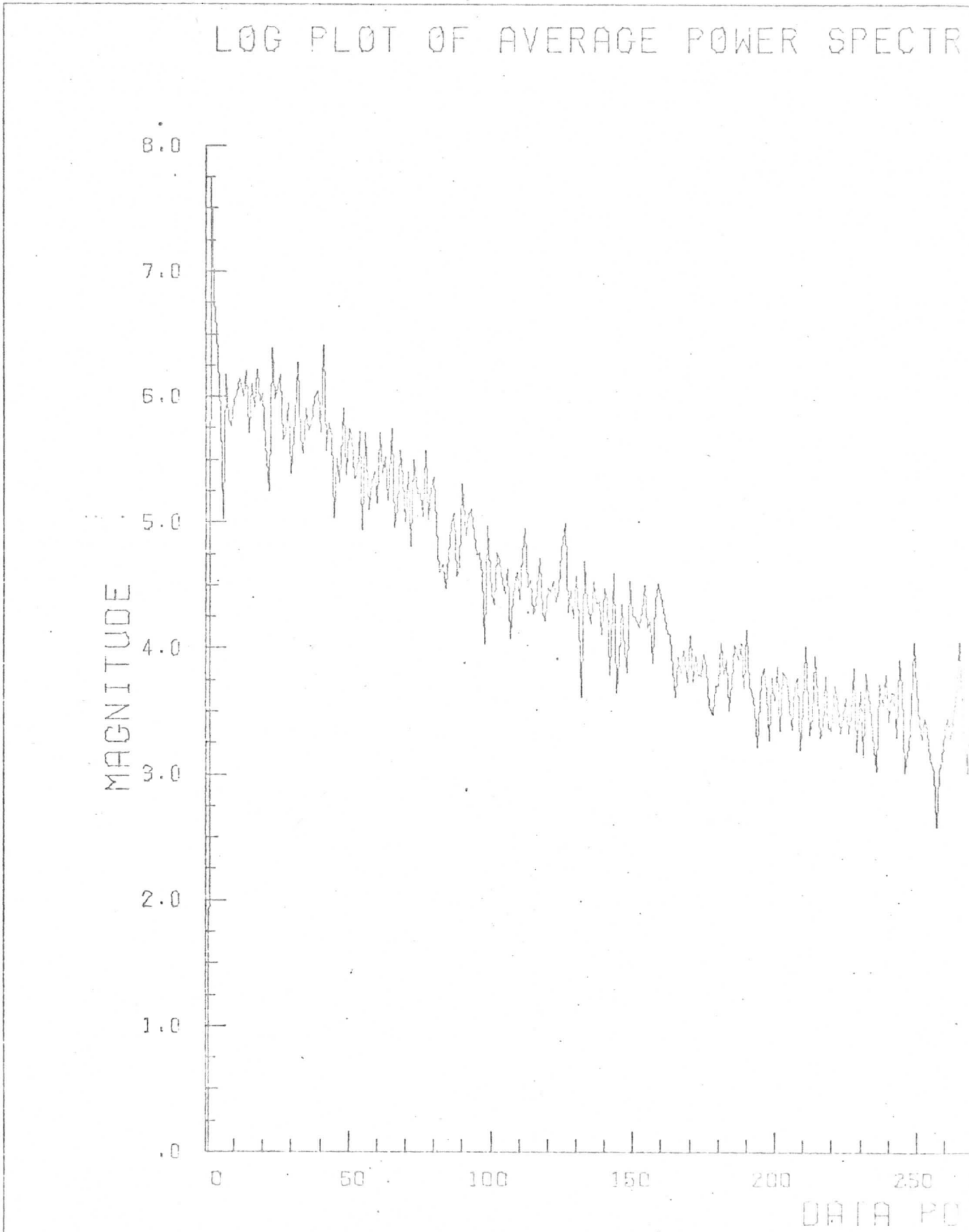

Apollo 56-2-877, (rect.)
Locator: Tape 17, File 1
Records: 860 - 864 Date: 2/1/73
Elements: 510 - 1021
Plot: Avg. Autocorrelation

H-7

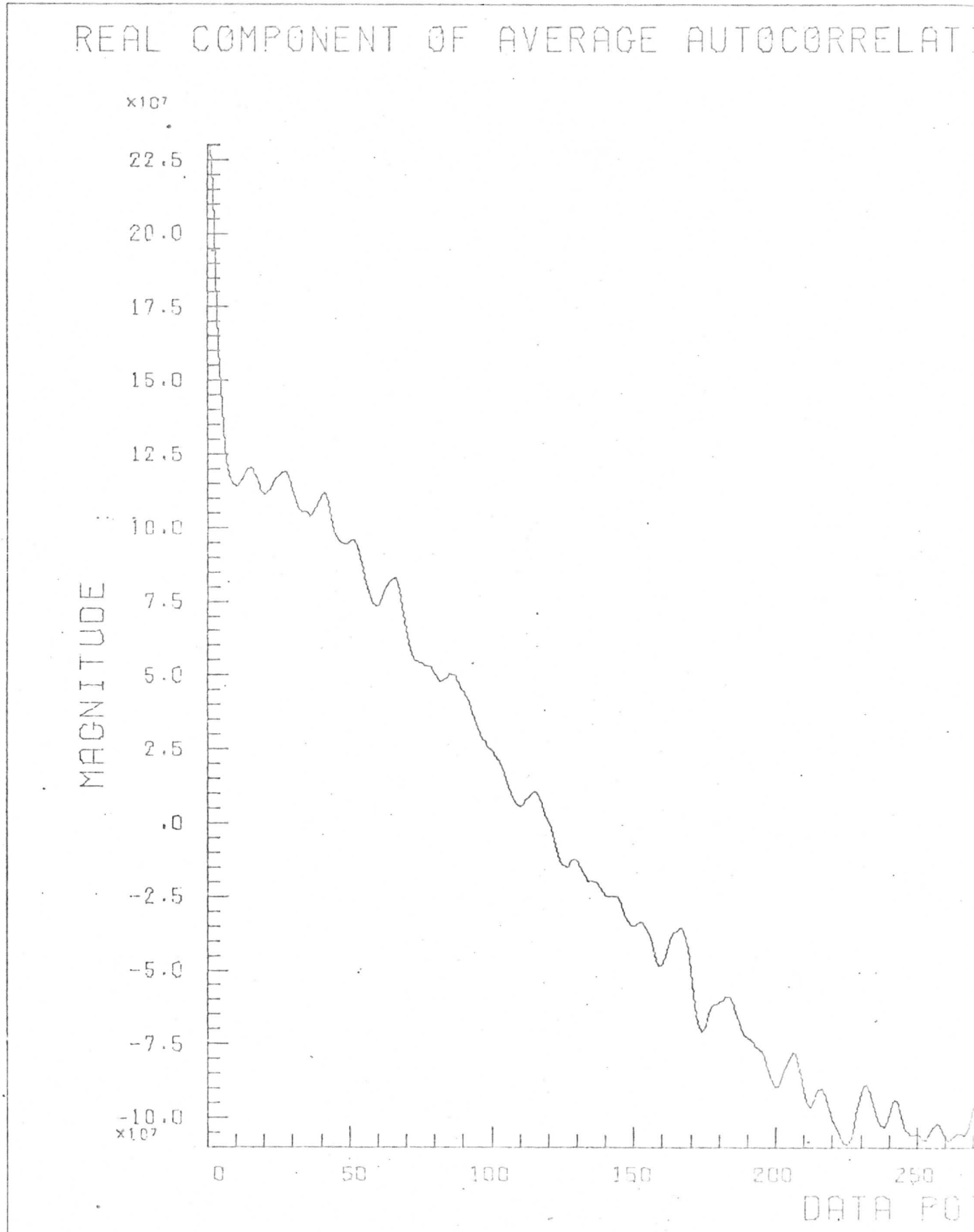

Apollo 56-2-934, (rect.)
Locator: Tape 17, File 2
Records: 100 - 104 Date: 2/1/73
Elements: 510 - 1021
Plot: Log Power Spectrum, First Line

H-8

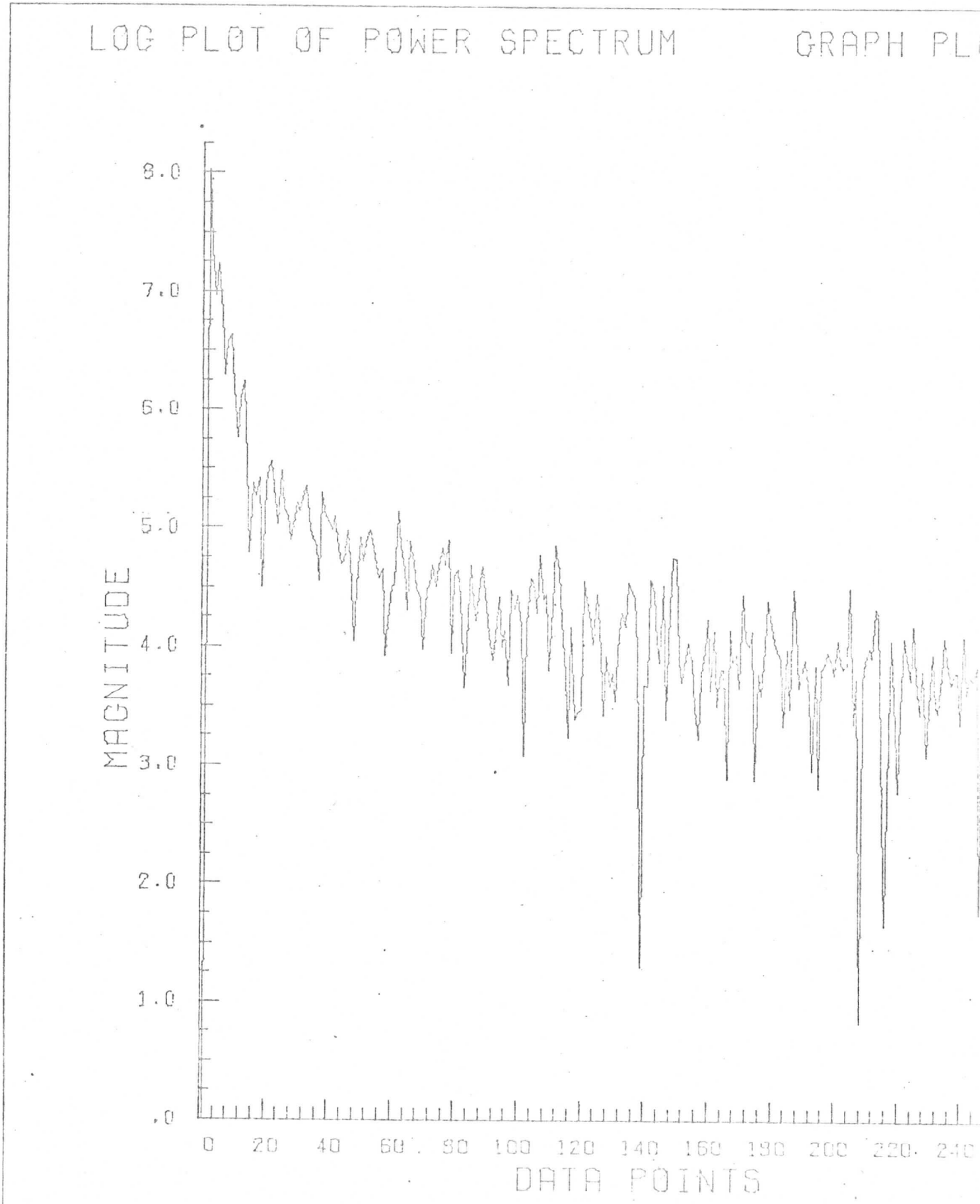

$$\dot{\beta}(R-r) = (10.47)(19,360) = 0.202 \text{ n.mi./}\mu\text{-sec.}$$

Thus the frequency conversion is:

$$f_1 = 0.202\ \Gamma f \qquad \text{(C-16)}$$

where:

f_1 = apparent instantaneous frequency in MHz

f = spatial frequency in cycles per nautical mile

Γ = phase velocity correction factor.

C.3. Geometrical Mapping From Satellite to Earth Coordinate System

The satellite measures coordinates in the α, β frame of reference. The scene is measured in the θ, ϕ frame of reference. The mapping between the two is quite linear for small angles from the subsatellite point, but may become quite nonlinear for larger angles. This mapping can be portrayed by tracing the locii of constant α and constant β in the θ, ϕ coordinate system.

From Equation C-6 we find the equation of the curves of constant β to be:

$$\phi = \cos^{-1}\left[\frac{\tan\beta}{\varepsilon(\cos\theta\tan\beta+\sin\theta)}\right] \qquad \text{(C-17)}$$

where $\varepsilon = r/R = 0.151$, and provided that:

$$\tan\beta \leq \frac{\sin\theta}{1-\varepsilon\cos\theta} \quad . \qquad \text{(C-18)}$$

Similarly, the equation of the curves of constant α is found from Equation C-5 to be:

$$\theta = \cos^{-1}\left[\frac{\varepsilon}{2\cos\phi}\left(1 + \frac{1}{\varepsilon^2} - \frac{\sin^2\phi}{\sin^2\alpha}\right)\right] \tag{C-19}$$

provided that:

$$\sin^2\alpha \leq \frac{\varepsilon^2\sin\phi}{(1+\varepsilon^2-2\varepsilon\cos\phi)} \; . \tag{C-20}$$

Curves of constant α and constant β are shown in Figure C.4.

FIGURE C.4. MAPPING FROM EARTH COORDINATES TO SATELLITE COORDINATES

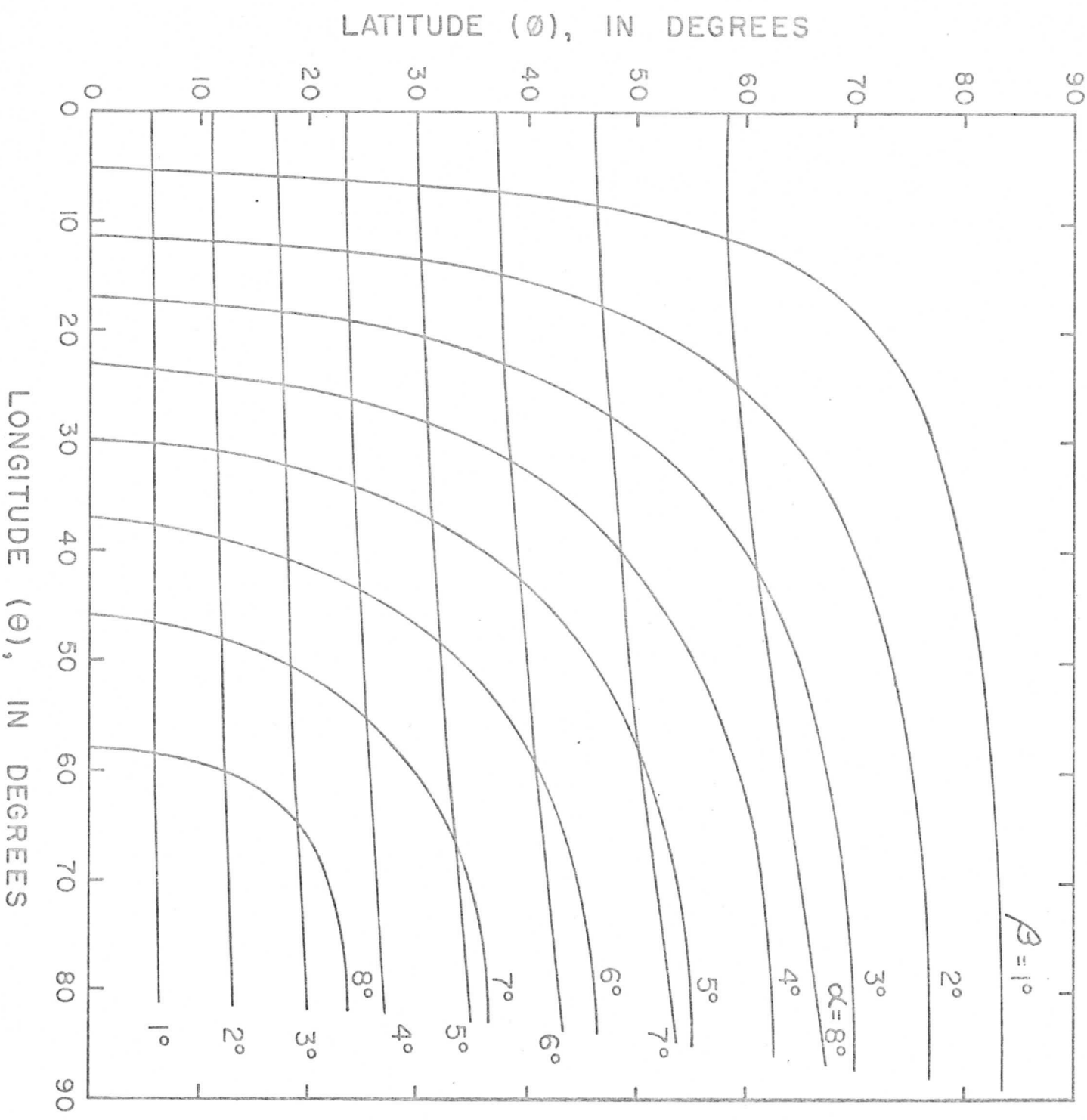
LATITUDE (Ø), IN DEGREES
0
10
20
30
40
50
60
70
80
90
LONGITUDE (Θ), IN DEGREES
0
10
20
30
40
50
60
70
80
90
β = 1°
2°
3°
α = 8°
4°
5°
6°
7°
8°
1°
2°
3°
4°
5°
6°
7°

Appendix D

A Measure of the Effective Bandwidth Due to Aliasing Errors

The purpose of this appendix is to motivate a measure of the effects of aliasing caused by under-sampling a signal. We begin by discussing the concept of sampling a deterministic signal. After the effects of aliasing ~~in this case~~ have been ~~illuminated~~ explained, we will extend the results to stochastic processes.

Suppose that we wish to sample a waveform f(t) every T seconds. The resulting sampled version $f_s(t)$ may be represented as:

$$f_s(t) = f(t)\ g(t) \tag{D-1}$$

The function g(t) is a periodic function with period T. For example, it could be a typical gate function, as is shown in figure D-1.

~~In order~~ To determine $F_s(\omega)$, the spectrum of $f_s(t)$, we expand g(t) in a Fourier series:

$$g(t) = \sum_{n=-\infty}^{+\infty} c_n\ e^{jn\omega_s t} \tag{D-2}$$

$$\text{where } c_n = \frac{1}{T}\int_0^T g(t)\ e^{-jn\omega_s t}\ dt$$

$$\text{and } \omega_s = \frac{2\pi}{T}\ .$$

From this series we readily obtain the Fourier transform of g(t):

$$G(\omega) = 2\pi \sum_{n=-\infty}^{+\infty} c_n\ \delta(\omega - n\omega_s)\ . \tag{D-3}$$

Because multiplication of two signals in the time domain corresponds to convolution in the frequency domain, we have:

$$F_s(\omega) = \frac{1}{2\pi}\ F(\omega) * G(\omega) \int_{-\infty}^{+\infty} F(y)\ G(y-\omega)\ dy\ . \tag{D-4}$$

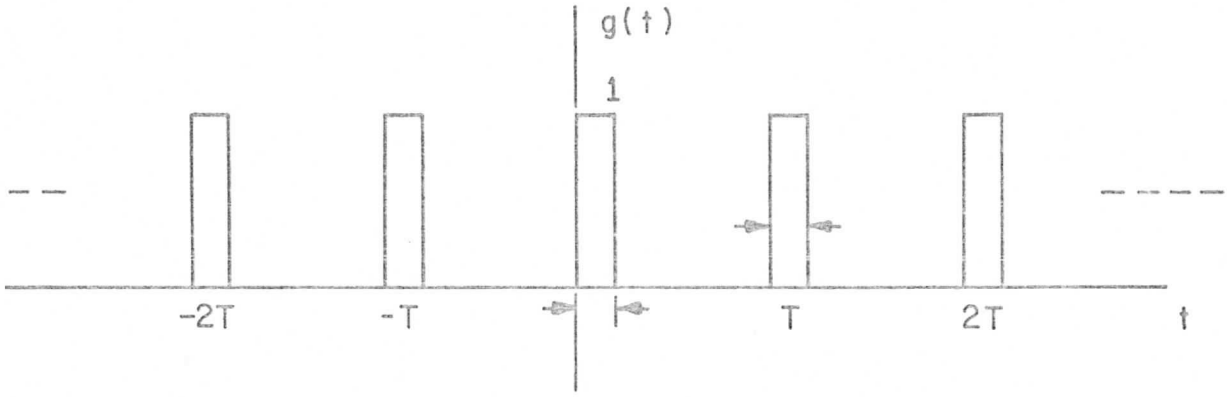

GATE FUNCTION
FIGURE D-1

Note that $F(\omega)$ is the transform of the waveform $f(t)$ before sampling. However, using the form of the transform of $g(t)$ and proceeding formally (which can be justified rigorously), we arrive at the following results

$$F_s(\omega) = \sum_{n=-\infty}^{+\infty} c_n \int_{y=-\infty}^{+\infty} F(y)\ \delta(y-\omega-n\omega_s)\ dy$$

$$= \sum_{n=-\infty}^{+\infty} c_n\ F(\omega+n\omega_s)\ . \qquad \text{(D-5)}$$

The function $F(\omega+n\omega_s)$ is just the original spectrum of $f(t)$ shifted to (or translated about) the frequency $n\omega_s$. Hence, the spectrum of the sampled waveform is a composite of shifted and weighted versions of the original spectrum. The weighting of each shifted version is determined by the line-spectrum of $g(t)$.

If the spectrum of $f(t)$ is strictly limited between the frequencies of $-\omega_s/2$ and $+\omega_s/2$, then the sum in equation (D-5) is trivial. This situation is depicted in figure D-2. However, in general, there can be a large number of terms in the series of equation (D-5) for each fixed ω. Anytime there is more than one term in this series we say that aliasing has occurred. The expression "fold-over" is sometimes frequently used because a copy of the original spectrum appears to be folded back or forward over other copies of the original spectrum. The relative weighting of the individual interfering, shifted version of the spectrum is determined by the nature of $g(t)$, which is equivalent to specifying the values of the Fourier coefficients. When all coefficients are unity, the sampler is called an impulse sampler; i.e.,

$$g(t) = \sum_{k=-\infty}^{+\infty} \delta(t-kT)\ .$$

Figure D-3 shows a situation in which the original spectrum is limited between the frequencies of $-\omega_s$ and $+\omega_s$. The cross-hatched areas indicate

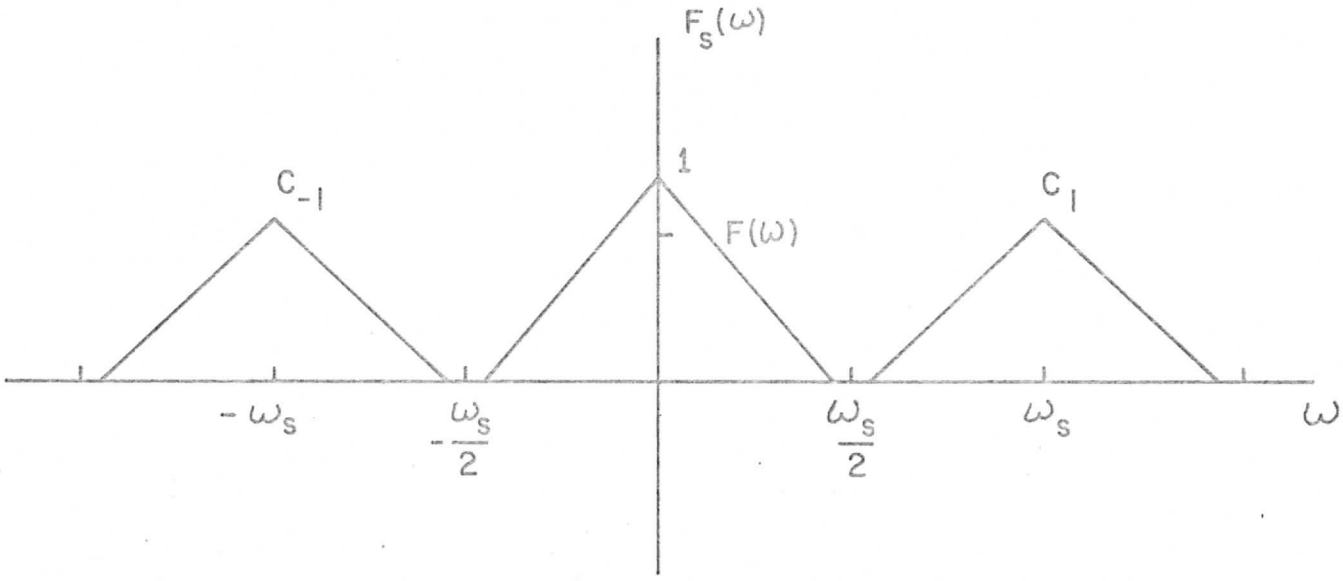

STRICTLY BANDLIMITED CASE
NO ALIASING
FIGURE D-2

frequencies which are distorted due to more than one term being present in the series of equation (D-5), ~~i.e.,~~ Thus, aliasing has occurred. This is the case in the SMS system and we now proceed to determine a measure of this distortion. We note that only the coefficients c_{-1} and c_{+1} affect the distortion included in the portion of the spectrum centered about zero.

As can be seen by consulting either Appendix A or (Papoulis, 1965), the effects of aliasing a stochastic process $\{y(t)\}$ are reflected in the aliasing of portions of its power-spectral density $S_y(\omega)$. In fact, in direct analogy with the previous development, ~~we have that~~ the power-spectral density of the sampled version of $y(t)$, $S_{ys}(\omega)$, is now given by

$$S_{ys}(\omega) = \sum_{n=-\infty}^{+\infty} |c_n|^2 \, S_y(\omega + n\omega_s) \quad . \tag{D-6}$$

Hence, all previous comments about band-limited signals apply to the case of band-limited processes. Since we may assume that $S_y(\omega)$ is bandlimited to the band from $-\omega_s$ to ω_s, we are concerned with an aliasing situation in which only the fold-over from adjacent bands of frequencies need be considered. A typical situation is depicted in figure (D-4). Since the sampling function $g(t)$ is real, we have a Hermitian symmetry among the coefficients; ~~i.e.,~~ $c_n = c_{-n}^*$.

We would like to choose some measure of the distortion ~~due~~ to aliasing. Thus, ~~Towards this~~ end we will first define an effective bandwidth of a stochastic process so that we can compare the effective bandwidth of original waveforms with that of the version which contains aliasing.

~~Suppose that~~ Consider that $S_z(\omega)$ is the power-spectral density of the process $\{Z(t)\}$. $S_z(\omega)$ is a real, even, nonnegative function of ω (Papoulis, 1965). If it were normalized, it would resemble a probability density function. Let $\tilde{S}_z(\omega)$ be this normalized function.

"even" in the sense of "not odd"

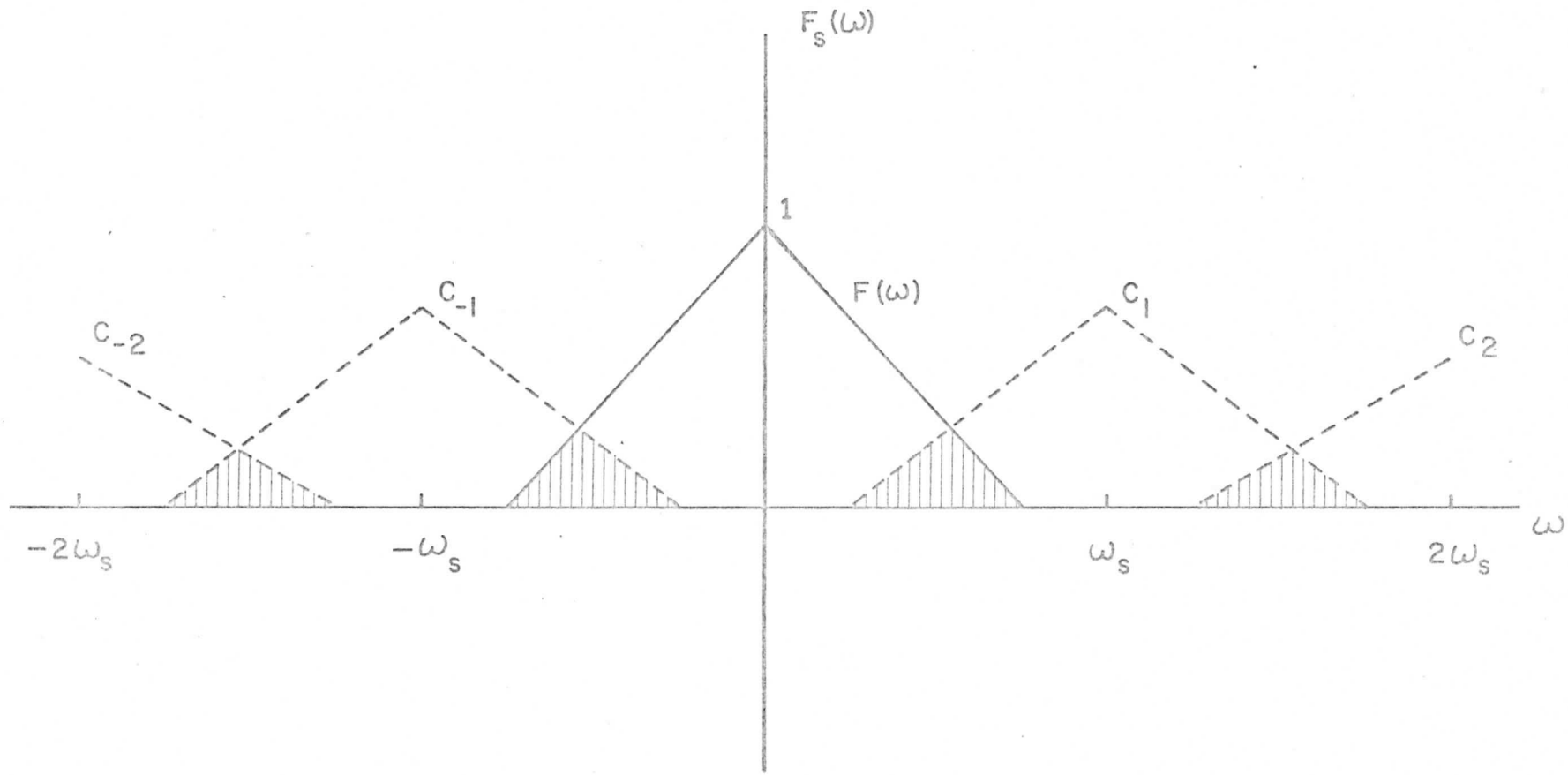

BANDLIMITED CASE
WITH ALIASING
FIGURE D-3

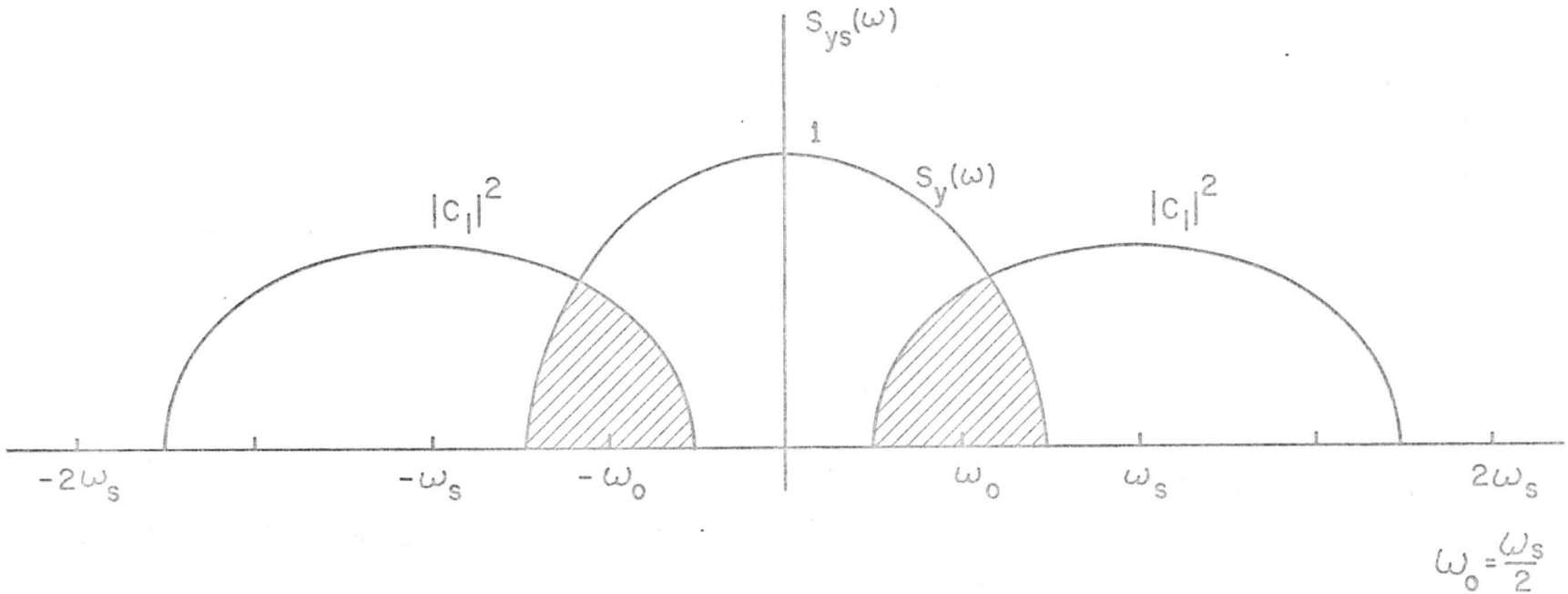

BANDLIMITED CASE FOR PROCESSES
WITH ALIASING
FIGURE D-4

$$\tilde{S}_z(\omega) = \frac{S_z(\omega)}{\int_{-\infty}^{+\infty} S_z(\omega)\, d\omega} \tag{D-7}$$

We will define the effective bandwidth of this process as the variance of $\tilde{S}_z(\omega)$ (sometimes called the radius of gyration.)

$$\gamma^2 = \int_{-\infty}^{+\infty} \omega^2 \tilde{S}_z(\omega)\, d\omega \tag{D-8}$$

Note that, since $S_z(\omega)$ is an even function of ω, i.e., $S_z(\omega) = S_z(-\omega)$, the equation does represents the second moment about the center of gravity (the variance). The use of the variance as a measure of the effective spread of ~~the range of~~ a variable is well-known and widely used in all branches of science and engineering.

There is an added bonus in using this definition; it is the uncertainty principle. This states that the variance γ^2 ~~times~~ a factor determined from the transform of $\sqrt{S_z(\omega)}$ must always be greater than $\pi/2$.

$$\gamma^2\, \alpha^2 \geq \pi/2 \tag{D-9}$$

$$\alpha^2 = \frac{\int_{-\infty}^{+\infty} \tau^2 \left|r(\tau)\right|^2 d\tau}{\int_{-\infty}^{+\infty} \left|r(\tau)\right|^2 d\tau} \tag{D-10}$$

$$r(\tau) = \frac{1}{2\pi} \int_{-\infty}^{+\infty} \sqrt{S_z(\omega)}\, e^{+j\omega\tau}\, d\omega \tag{D-11}$$

The quantity α^2 measures the spread of the inverse transform of $\sqrt{S_z(\omega)}$. Therefore, as we attempt to reduce the effective bandwidth of the process, the effective time-spread of its corresponding transform must increase so that inequaltiy (D-9) is fulfilled. Thus, there is a trade-off between the frequency-domain and the time-domain. For further discussion of this topic see the references (Brown, 1963), (Franks, 1969), and (Papoulis, 1962).

Suppose now that $S_y(\omega)$ represents the power-spectral density of the input to a sampler and that this spectrum is bandlimited to the range from $-\omega_s$ to $+\omega_s$. The effective bandwidth of the input is:

$$\gamma^2 = \frac{\int_0^{\omega_s} \omega^2 S_y(\omega)\, d\omega}{\int_0^{\omega_s} S_y(\omega)\, d\omega} \quad . \tag{D-12}$$

We have, of course, used the evenness of ω^2 and $S_y(\omega)$. If aliasing has been introduced by the sampler, the effective bandwidth of the center part of the spectrum depends on the way in which the folded part of the spectrum is added. A typical center lobe of an aliased spectrum is shown in figure D-4. We will define ϕ as the effective phase of the folded spectrum. A worst case is achieved when $\phi = \pi$. Then the effective bandwidth of the spectrum's corrupted center lobe is.

$$\beta^2 = \frac{\int_0^{\omega_0} \omega^2 [S_y(\omega) + |c_1|^2 \cos\phi\, S_y(\omega-\omega_s)]\, d\omega}{\int_0^{\omega_s} S_y(\omega)\, d\omega} \tag{D-13}$$

$$\text{where} \quad \omega_0 = \frac{\omega_s}{2}$$

This quantity measures the variance of the central part of the spectrum. If the effective phase of the aliasing is between $\pi/2$ and $3\pi/2$, the effective bandwidth as defined by β^2 is less than the original given by γ^2. The $|c_1|^2$ term results from the nature of the sampling waveform g(t). A worst case assumption is given by $|c_1|^2 \cos\phi = -1$. This is the case we will treat here.

Hence we will use:

$$\beta^2 = \frac{\int_0^{\omega_0} \omega^2 S_y(\omega)\, d\omega - \int_0^{\omega_0} (\omega-\omega_0)^2 S_y(\omega+\omega_0)\, d\omega}{\int_0^{2\omega_0} S_y(\omega)\, d\omega} \quad . \tag{D-14}$$

This is easily derived from equation (D-13) using the evenness of $S_y(\omega)$ and the definition of ω_0.

Since the input to the sampler is the output of the filter, we may relate $S_y(\omega)$ to the power-spectral density of the input $S_x(\omega)$ by the well-known formula (Papoulis, 1965):

$$S_y(\omega) = S_x(\omega)\, |H(j\omega)|^2 \quad . \tag{D-15}$$

Finally, since our picture data is in the form of a sampler and since the sampling rate for this data is clearly high enough, we may state the discrete versions of the expressions for the effective bandwidth. We use discrete frequency variables.

$$\gamma^2 = \frac{\sum_{k=1}^{2K} k^2 S_y(k)}{\sum_{k=1}^{2K} S_y(k)} \qquad \text{(D-16)}$$

K = half of the sampling frequency

$$\beta^2 = \frac{\sum_{k=1}^{K} k^2 S_y(k) - \sum_{k=1}^{K} (k-K)^2 S_y(k+K)}{\sum_{k=1}^{2K} S_y(k)} \qquad \text{(D-17)}$$

Helen — a number of spacers in the next appendices, are in red. Shapes may have to be retyped

APPENDIX E

A MODEL FOR THE PHOTOMULTIPLIER TUBE

The noise generated in a photomultiplier (p.m.) tube is studied, ~~and~~ A suitable model ~~of~~ for the p.m. tube ~~for the purpose of~~ suitable designing an optimum quantizer is also suggested.

In a p.m. tube, the photocathode emits electrons which are then accelerated and multiplied by a series of electrodes, These are known as "dynodes" ~~to which~~ and suitable voltages are applied to them. (Figures E-1 and E-2). The incident light intensity on the photocathode directly determines the photoemission current, ~~there being~~ because there is an excellent approximation ~~of~~ a linear relationship between the light intensity and the photo current over a wide range of light intensities.

We will now consider ~~The case where~~ light of a constant intensity is incident on the photocathode, in which ~~is considered~~. For constant voltages at the dynodes, we would expect that the current ~~which is~~ directly proportional to the light intensity will also be a constant quantity. Variation of the light intensity will produce corresponding variation in the current. Although it is said that the incident light is of constant intensity, this statement is not strictly true when viewed ~~one views this statement from a microscopic point of view~~ microscopically. When ~~one~~ we says that light of a particular intensity is incident on a photocathode, ~~one is~~ we refer~~ring~~ to the number of photons (packets or quanta of energy, each being equal to $h\nu$, ν - frequency of light) which strike the photocathode. The larger the number of photons ~~are~~, the larger the current ~~is~~. So by the term, "constant intensity", ~~one~~ we refers to the average number of photons. But the number of photons striking the photocathode is not a constant quantity, but it fluctuates about a quiescent quantity which is the "average" over a long period. This average is called ~~and is referred to as~~ "constant light intensity". Hence, there is a corresponding change in the

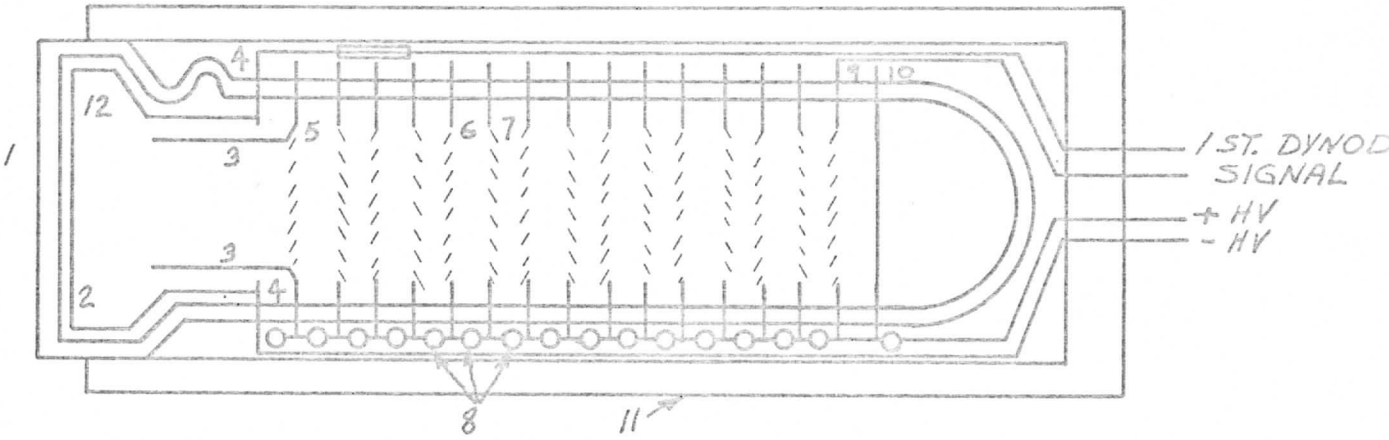

FIGURE E-1

1. FACE PLATE
2. SEMI-TRANSPARENT PHOTOCATHODE
3. FOCUSING ELECTRODE
4. CATHODE CONTACT
5. 1ST. DYNODE
6. FIELD SHAPING SCREEN
7. VENETIAN BLIND DYNODE
8. VOLTAGE DIVIDER
9. ANODE
10. LAST DYNODE
11. EPOXY FIBERGLASS SHELL
12. METAL COATING

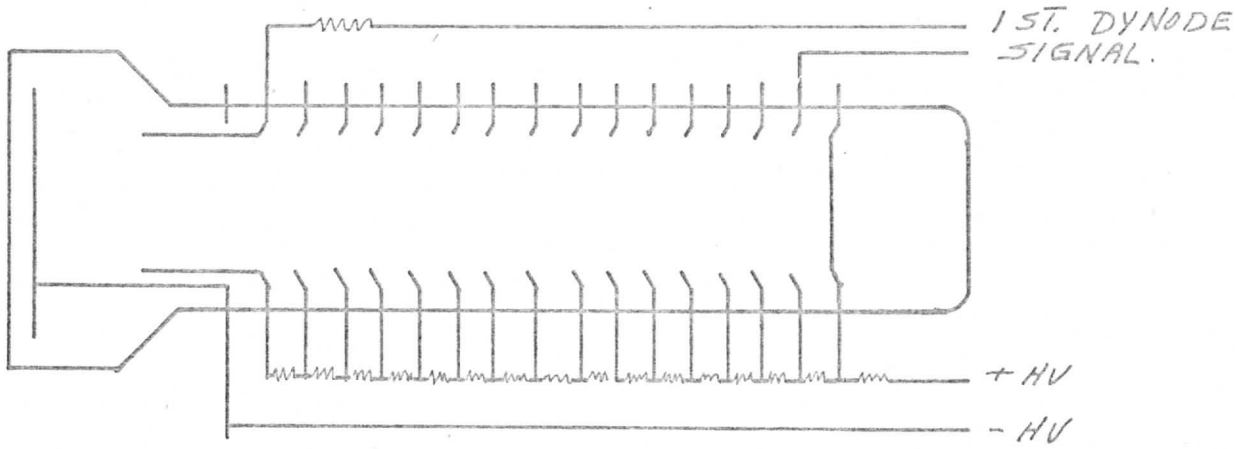

FIGURE E-2

number of photoelectrons emitted from the photocathode. ~~Thus,~~ The emission of electrons is actually random in form. More electrons are emitted at one instant, fewer the next, with the average number per unit time the same over a long period of time as that shown below in Figure E-3.

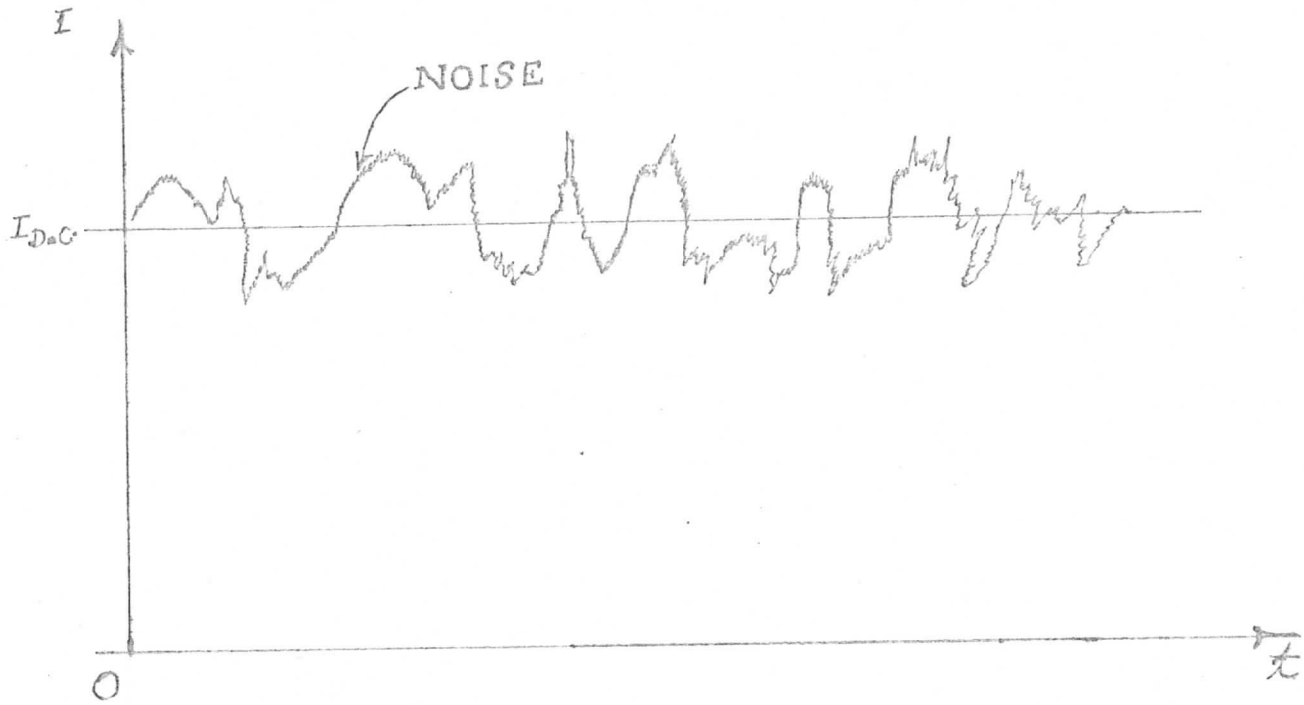

FIGURE E-3

The situation described above is exactly the same as that one that prevails in a vacuum diode operating in the temperature limited region at a fixed cathode temperature and a fixed data voltage. The one difference is that in the case of photoemission, the fluctuations in the current are due to fluctuations in the number of striking photons, with no heating of the cathode. Hence, the analysis carried out for the shot noise (Schwartz, 1959 and Davenport and Root, 1958) in a temperature limited diode is perfectly valid for the noise due to light intensity fluctuations. Hence (Schwartz, 1959),

$$\overline{i^2}_{noise} = \text{(r.m.s. noise)} = 2e\Delta f I_{D.C.} \qquad \text{(E-1)}$$

Δf = Noise equivalent bandwidth

$I_{D.C.}$ = Average photocurrent

But in an actual situation such as that in S.M.S. systems the light intensity incident on the photocathode is not a constant quantity but varies with time, so the operating current changes continuously with time. At a given time, the current fluctuates about the average operating current I and so equation (E-1) can be used to describe the noise with $I_{D.C.}$ being in this case the average operating current. Intuitively it is obvious that as the light intensity and so the operating point varies, the r.m.s. value of the noise also varies with the operating current.

Hence

$$\overline{i^2}_{noise} = 2e\Delta f I \qquad \text{(E-2)}$$

where I is the time varying photocurrent.

Let the stochastic process X(t) denote the current and N(t), the noise. Assuming that the photocurrent and the noise of the p.m. tube are members of

ergodic process (Papoulis, 1965, Ch. 8) [illegible] ergodicity in the mean and the auto-correlation are assumed), we can write as

$$E[N^2] = 2e\Delta fX \tag{E-3}$$

Further, the time average of the noise can be assumed to be zero.

$$E(N) = 0 \tag{E-4}$$

Hence,

$$\sigma_N^2 = E(N^2) = \overline{N^2} = 2e\Delta fX$$

or

$$\sigma_N^2 = 2e\Delta fX \tag{E-5}$$

Thus, (E-5) gives the variance of the fluctuation noise at the output of the first stage of the p.m. tube (without considering secondary emission).

EXPRESSION FOR THE R.M.S. VALUE OF THE NOISE AT THE OUTPUT OF AN N-STAGE SECONDARY EMISSION MULTIPLIER PHOTO TUBE:

The p.m. tube shown in Figures E-1 and E-2 consists of a photocathode followed by n dynodes and an anode to form an N-stage secondary emission current multiplier. A simple sketch of the p.m. tube is shown (Figure E-4) as an aid in deriving the above mentioned expression. The current amplification due to secondary emission at a dynode is equal to "G" and it is assumed to be the same for each dynode.

$\overline{I}_{n0}$ refers to the r.m.s. value of the noise generated in the cathode. $\overline{I}_{n1}$ is the r.m.s. noise at the output of the first stage, including the effect of secondary emission from the first dynode. $\overline{I}_{ni}$ is the r.m.s. noise at the output of the ith stage, and so on. I is the average cathode current and I_0, the average output current.

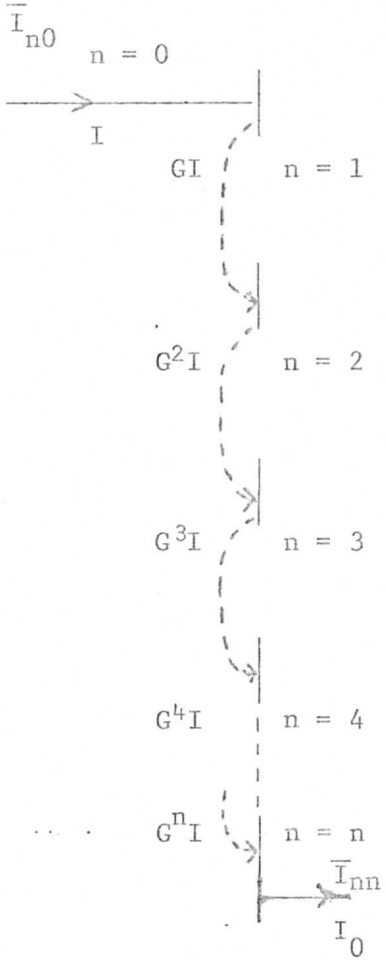

$$\overline{I^2_{n0}} = 2eI\Delta f$$

$$\overline{I^2_{n1}} = G^2\overline{I^2_{n0}} + 2e(GI)\Delta f = (G^2+G)2eI\Delta f$$
$$= G(G+1)\overline{I^2_{n0}}$$

$$\overline{I^2_{n2}} = G^2\overline{I^2_{n1}} + 2e(G^2I)\Delta f = \left(G^3(G+1)+G^2\right)2eI\Delta f$$
$$= G^2(G^2+G+1)\overline{I^2_{n0}}$$

$$\overline{I^2_{n3}} = G^2\overline{I^2_{n2}} + 2e(G^3I)\Delta f = \left[G^4(G^2+G+1)+G^3\right]2eI\Delta f$$
$$= G^3(G^3+G^2+G+1)\overline{I^2_{n0}}$$

$$\overline{I^2_{nn}} = G^n(G^n+G^{n-1}+G^{n-2}+ \ldots +G+1)2eI\Delta f$$
$$= \left[G^n \sum_{n=0}^{n} G^n\right] 2eI\Delta f$$

Figure E-4

$$\overline{I^2_{nn}} = 2eI\Delta f \cdot G^n \frac{(G^{n+}-1)}{G-1} \qquad \text{(E-6)}$$

$$I_0 = G^nI \qquad \text{(E-7)}$$

In the expression

$$\overline{I^2_{n1}} = G^2\overline{I^2_{n0}} + 2e(GI)\Delta f$$

the quantity $\left(G\sqrt{\overline{I^2_{n0}}}\right)^2$ is the mean square value of the fluctuation noise due to the incident current $G\sqrt{\overline{I^2_{n0}}}$. and The quantity $2e(GI)\Delta f$ is the mean-square value of the fluctuation noise about the average current GI due to the random emission from the first dynode.

From equation (E-6)

$$\overline{I_{nn}^2} = 2eI\Delta f G^n \frac{(G^{n+1}-1)}{G-1}$$

Since $G^{n+1} >> 1$, we can write the above as

$$\overline{I_{nn}^2} \simeq 2eI\Delta f \frac{G^{n+1}}{(G-1)} \qquad \text{(E-8)}$$

Thus, the mean-square value of the noise at the output of the p.m. tube is given by (E-8) and this noise fluctuates about $I_0 = G^n I$

PROBABILITY DENSITY FUNCTION OF THE NOISE AT THE OUTPUT OF THE P.M. TUBE

Recalling that the p.m. tube noise is shot-noise (Schwartz, 1959 and Davenport and Root, 1958), it can be expected that the total output current of the p.m. tube follows a normal probability density function. The total cathode current in the p.m. tube can be assumed to be the sum of a large number of independent and overlapping current pulses due to individual photons. Because of the random occurrence of these pulses, the total current fluctuates about a specific value, which is the effective average, over a very long period. The total current, ~~being~~ is the sum of a large number of independent random variables (current pulses), It can be expected to follow a normal density, in view of the central limit theorem (Papoulis, 1965, Ch. 8), under certain broad conditions. Experimental results totally support this conclusion.

Hence, the probability density function of the total current is given by,

$$f_{I_{Total}}(i_{Total}) = \frac{1}{\sqrt{2\pi}\,\sigma_{i_T}} \exp\left[-\frac{(i_T-I)^2}{2\sigma_{i_T}^2}\right] \qquad \text{(E-9)}$$

where I is the average current, σ_{i_T}, the standard deviation of the total current and I_T, a random variable.

Now the noise I_n (again a random variable) is given by

$$I_n = I_T - I \tag{E-10}$$

The conditional probability density function of the noise, assuming the signal, is given by,

$$f_{I_n}(i_n|_{I=i}) = f_{I_T}(i_n+I)$$

$$f_{I_n}(i_n|_{I=i}) = \frac{1}{\sqrt{2\pi}\,\sigma_{i_T}} \exp\left[-\frac{i_n^2}{2\sigma_{i_T}^2}\right] \tag{E-11}$$

because $\sigma_{i_T} = \sigma_{i_n}$

or

$$f_{n'}(n'|_{X=x}) = \frac{1}{\sqrt{2\pi}\,\sigma_{N'}} \exp\left[-\frac{n'^2}{2\sigma_{N'}^2}\right] \tag{E-12}$$

where $\sigma_{N'}^2 = 2e\Delta f X$ with X corresponding to the variable operating current I. Thus, it may be observed that the variance of the noise is proportional to the operating current X.

Equation (E-12) gives the conditional probability density function of the noise at the output of the first stage of the p.m. tube, without considering secondary emission from the first dynode. It is a simple matter to deduce that, because the system is linear (Papoulis, 1965, Ch. 12), the conditional probability density function of the noise at the output of the p.m. tube is also normal with zero mean, however, the variance given by equation (E-8) where $\overline{I_{nn}^2}$ is the variance of the noise.

Thus, the output of the p.m. tube can be written as

$$Y = G^n X + N$$

where N is normal with the variance given by ε_N

It may be worthwhile to mention that an increase in the gain of the first dynode (for example, $G_1 = 2G_2 = 2G_3 = \ldots 2G_n = 2G$) over those of the rest can be shown to result in a small improvement of the peak-to-peak signal to r.m.s. noise current.

So far, only the noise due to the fluctuations in the number of incident photons, or equivalently, in the intensity of the incident light has been considered. However, there are other factors which contribute noise. Figure (E-5) (Amos and Wang, 1969) shows a "model" of the p.m. tube including the other components:

2. It is inevitable that extraneous and undesirable light from the background of the p.m. tube is incident on the photocathode. This, then, contributes to another noise component. Again, the noise due to background intensity fluctuations obeys the shot-noise (Schwartz, 1959 and Davenport and Root, 1958), the mean-square value given by

$$\overline{I_{nb}^2} = 2e\Delta f I_b \frac{G^{2n+1}}{G-1} \qquad \text{(E-14)}$$

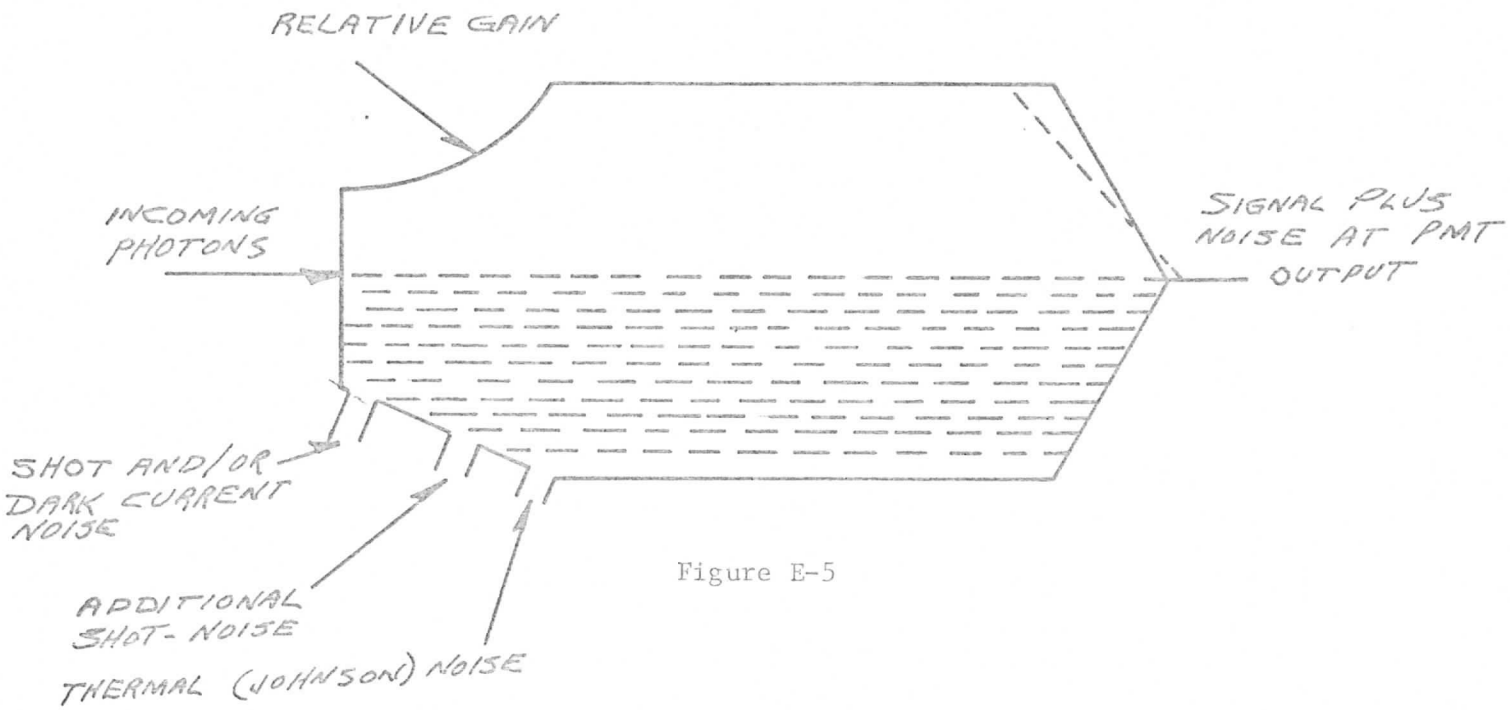

Figure E-5

A SHOT-NOISE DUE TO SIGNAL CURRENT = $\alpha(2e\Delta f I)^{1/2}$

SHOT NOISE DUE TO BACKROUND = $B(2e\Delta f I_B)^{1/2}$

SHOT NOISE DUE TO DARK CURRENT = $\alpha(2e\Delta f I_D)^{1/2}$

B SHOT NOISE DUE TO AMPLIFICATION = $\gamma(2e\Delta f I_n)^{1/2}$

C JOHNSON OR THERMAL NOISE DUE THERMAL AGITATION = $\delta\left(\frac{4kT\Delta f}{R_{eq}}\right)^{1/2}$

$$\alpha = \frac{G^{2n+1}}{G-1}$$

where I_b is the "average background" photocurrent about which the noise fluctuates. Because of the origin of this noise, this is very difficult to account for and so will be omitted.

2) Dark current (Amos and Wang, 1969): Another noise component in a p.m. tube is due to what is known as the "dark current". When a p.m. tube is operated in complete darkness, electrons are still emitted from the photocathode due to agencies other than incident light. The resulting "dark current" is amplified by the multiplier system and sets a limit to the lowest intensity of light that can be detected directly. With most photocathodes, thermionic emission appears to be responsible for the largest component of the dark current. At ambient temperatures, the thermal dark current I_t obeys Richardson's law approximately as

$$I_t = 1.20 \times 10^2 T^2 \exp\left[\frac{-1.16\times10^4}{T}\,\phi_t\right] \text{amp. cm}^{-2} \qquad \text{(E-15)}$$

where T is the absolute temperature in K and ϕ_t is the thermal work function for the cathode material. It is clear from Equation (E-15) that cooling the photocathode will have the effect of reducing the thermal component of the dark current. For all normal cathodes except the $AgOC_s$(s-1) type, it is found that the thermal component of the dark current may be virtually eliminated by cooling to -40°C. and no significant improvement is obtained by cooling to lower temperatures, below this. But the photocathode of the S.M.S. p.m. tube is not cooled to such low temperatures.

Again the mean-square value of the short-noise due to dark current (principally thermionic emission current) is given by

$$\overline{I_{nd}^2} \simeq 2e\Delta f I_t \cdot \frac{G^{2n+1}}{G-1} \qquad \text{(E-16)}$$

The final model for the p.m. tube is shown below.

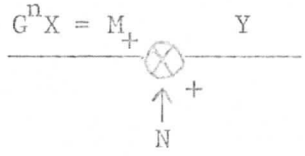

$$f_N\left(n \Big/ _{M=m}\right) = \frac{1}{\sqrt{2\pi\sigma_n^2}} \exp\left[-\frac{n^2}{2\sigma_n^2}\right]$$

$$\sigma_n^2 = 2e\Delta f \frac{G^{2n+1}}{G-1} x$$

$$\sigma_n^2 = 2e\Delta f \frac{G^{n+1}}{G-1} M$$

Figure E-6

Finally, the term "pulse height distribution" (Bay and Prapp, 1964) used in connection with p.m. tubes needs some explanation. In a multiplier phototube, each photoelectron undergoes cascade amplification within the tube and arrives at the anode as a pulse of many (say 10^{16}) electrons. If all the photoelectrons were multiplied equally, they would contribute to the signal current equally. In actual practice, however, the amount of multiplication is very different from one photoelectron to another, so that the stream of pulses at the anode includes a very broad range of amplitudes. Some contribute ~~as much as~~ ten times as much as the ~~to the photo current as~~ do others. Since the pulses are not of equal size, it is evident that the SNR of a multiplier phototube will be lower when used in combination with an ordinary current measuring system which introduces measurement noise, than when used in a system that counts only the pulses with equal weight regardless of their sizes. This is the fundamental difference between pulse counting techniques and current measuring techniques.

APPENDIX F

Optimum Quantizer

We develop the necessary conditions for the parameters of a quantizer to be optimum on the basis of overall mean-square error. It is not clear what criterion was used in the design of the present SMS quantizer. The performance of the present quantizer is equivalent to optimally quantizing the noise from the photomultiplier tube, which is only statistically dependent on the VISSR data. Our results, while not complete through the actual numerical solution of the equations, indicate that the design is not as simple as the reasoning which produced the present quantizer would suggest. An adjunct of the development of the necessary equations is that the quantizer parameters are sensitive to the statistical distribution of the input data.

A simple block diagram of the S.M.S. system (one visible channel) is shown below:

Figure F-1

The optical signal at the input to the PMT is converted to electrical signal by the PMT at its output. During this process, a noise is also added to the signal. The principal component of this noise is due to the signal itself, and for a given signal, it has a normal conditional probability density function, with a zero mean and a variance proportional to the signal itself. It is now assumed that any other noise generated after the PMT output up to the input to the quantizer is very small compared to the noise due to the signal, and so will be omitted in the following analysis. So, for the purpose of designing an optimum quantizer such that the mean-square error between the output of the quantizer and the signal is minimum, the following model is assumed.

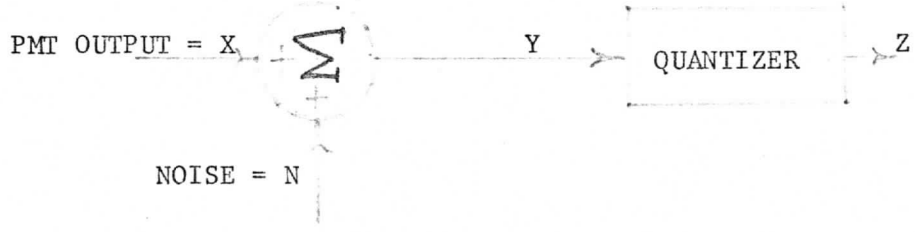

Figure F-2

The PMT output signal is equal to the PMT input signal multiplied by the PMT total gain.

As mentioned before, the criterion or performance index, which is minimized while choosing the quantizer levels, is the mean-square error between Z and X, and is defined by:

$$\overline{\varepsilon^2} \triangleq E\left[(Z-X)^2\right] = E\left\{E\left((Z-X)^2 \mid N=n\right)\right\} \qquad \text{(F-1)}$$

The following notations are adopted throughout this appendix:

1) Capital letters indicate random variables.

2) Small letters indicate the variables assumed by the random variables.

3) $f_X(x)$ represents the probability density function of X.

4) $f_N(n|X=x)$ represents the conditional probability density function of N, given X=x.

5) E( ) denotes the expected value of a random variable.

6) $f_{XN}(x,n)$ denotes the joint probability density function of X and N.

If we denote the quantizer thresholds by the set of real numbers, $\{y_i\}_{i=1}^{k+1}$, and the corresponding output levels by the set $\{z_i\}_{i=1}^{k}$, we may proceed to develop the necessary equations for these quantities to yield a minimum mean-square error.

$$E\left\{(Z-X)^2|N=n\right\} = \int_{x=0}^{b} (z-x)^2 f_X(x|N=n)\,dx \qquad \text{(F-2)}$$

$$= \sum_{i=1}^{k} \int_{x_i}^{x_{i+1}} (z_i-x)^2 f_X(x|N=n)\,dx$$

$$= \sum_{i=1}^{k} \int_{y_i-n}^{y_{i+1}-n} (z_i-x)^2 f_X(x|N=n)\,dx$$

The above equations imply that, for a fixed noise n, there is a one-to-one mapping between the x_i's, and the y_i's, and so the z_i's. Otherwise, for a given X=x, there is no unique Y=y because of the addition of noise.

The overall mean-square error is given by:

$$\overline{\varepsilon^2} = \int_{n=-\infty}^{\infty} \left\{ \sum_{i=1}^{k} \int_{y_i-n}^{y_{i+1}-n} (z_i-x)^2 f_{XN}(x,n)\,dx \right\} dn \qquad \text{(F-3)}$$

To minimize the mean-square error, a necessary set of conditions are is

$$\frac{\partial(\overline{\varepsilon^2})}{\partial y_j} = 0 \qquad \text{(F-4)}$$

and

$$\frac{\partial(\overline{\varepsilon^2})}{\partial z_j} = 0 \quad \text{for } j = 1, 2, 3, \ldots, k \tag{F-4}$$

The first set of these equations yields:

$$\int_{n=-\infty}^{\infty} \left[(y_j - n - z_{j-1})^2 - (y_j - n - z_j)^2 \right] f_{XN}(y_j - n, n)\, dn = 0 \tag{F-5}$$

$j = 2, 3, \ldots k$

(For $j=1$, $y_1 = 0$ because x_1 is assumed to be zero ~~and so also~~ as is the corresponding noise. Further, $f_{XN}(0,n) =$ Zero.)

Similarly, setting $\frac{\partial(\overline{\varepsilon^2})}{\partial z_j}$ equal to zero,

$$\frac{\partial(\overline{\varepsilon^2})}{\partial z_j} = \int_{n=-\infty}^{\infty} \left[\int_{y_j - n}^{y_{j+1} - n} (z_j - x)\, f_{XN}(x,n)\, dx \right] dn = 0 \tag{F-6}$$

$j = 1, 2, 3 \ldots k$

Up to this point, the treatment has been ~~very~~ general and without the assumption of any particular joint probability density $f_{XN}(x,n)$. To illustrate the procedure for obtaining the levels of an optimum quantizer, let it be assumed that X has a uniform distribution.

$$f_X(x) = \begin{cases} \frac{1}{b} & 0 < x \leq b \\ 0 & \text{elsewhere} \end{cases} \tag{F-7}$$

Equation (F-5) can be written as:

$$\int_{n=-\infty}^{\infty} \left[z_{j-1} + z_j - 2(y_j - n) \right] f_{XN}(y_j - n, n)\, dn = 0 \tag{F-8}$$

$j = 2, 3, \ldots k$

The "noise" due to the signal has a conditional probability density function (p·d·f). (See Appendix E.)

$$f_N(n|X=x) = \frac{1}{\sqrt{2\pi}\sqrt{\delta x}} \cdot \exp(-n^2|2\delta x)$$

where (F-9)

$$E[N|X=x] = 0; \quad \sigma^2_{N|X=x} = E[N^2|X=x] = \delta x,$$

δ is a known constant.

We can

As a check on the equation (F-8) we note that if it is assumed that the noise is very small, i.e., the fluctuations about any signal level are very small, then

$$y_j - n \simeq y_j .$$

In this case, the factor, $[z_{j-1} + z_j - 2(y_j-n)] \simeq (z_{j-1} + z_j - 2y_j)$ can be taken outside the integral over n as follows:

$$(z_{j-1} + z_j - 2y_j) \int_{\substack{\text{over a} \\ \text{small} \\ \text{range of n}}} f_{XN}(y_j,n)\, dn \simeq 0$$

yielding

$$y_j \simeq \frac{z_{j-1}+z_j}{2} \quad \text{in agreement with (Max, 1962).}$$

Equation (F-8) can be rewritten, using (F-9) and (F-7), as:

$$\int_{n=-\infty}^{\infty} [z_{j-1} + z_j - 2(y_j-n)] \left\{ \frac{1}{b} \frac{\exp[-n^2|2\delta(y_j-n)]}{\sqrt{2\pi\delta}\sqrt{y_j-n}} \right\} dn = 0 \qquad \text{(F-10)}$$

$$j = 2, 3, \ldots k$$

By using Bayes Rule (Papoulis, 1965) we have

$$f_{XN}(y_j-n,n) = f_X(y_j-n)\, f_N(n|X=y_j-n) \qquad \text{(F-11)}$$

Thus the random variable X takes values between 0 and b. And the argument of f_X (....) takes values between 0 and b, and in the expression, $x=y_j-n$, n

can only vary so that x is between 0 and b.

So: $n = y_j - b$ (corresponding to x = b)
negative maximum

(F-12)

$n = y_j$ (corresponding to x = 0)
positive maximum

Substituting these results in equation (F-10) and performing a change of variables, we have that part of a set of necessary conditions is given by:

$$\int_{m=0}^{b} (z_{j-1} + z_j - 2m) \exp\left(-\frac{m}{2\delta} - \frac{y_j^2}{2\delta m}\right) \frac{dm}{\sqrt{m}} = 0 \qquad \text{(F-13)}$$

$j = 2, 3, \ldots k.$

After some straightforward but tedious manipulations which involve the use of standard integral tables, we finally arrive at one set of necessary equations.

$$z_{j-1} + z_j = \delta \left\{ \frac{2}{\sqrt{\pi}} \frac{\exp\left(-\frac{(y_j - b)^2}{2\delta b}\right)}{\operatorname{erfc}\left(\frac{y_j - b}{\sqrt{\delta b}}\right)} \left[\frac{y_j - b}{\sqrt{2\delta b}}\right] + 2 + \frac{2y_j}{\delta} \right\} \qquad \text{(F-14)}$$

$j = 2, 3, \ldots k$

Here where the complimentary error function x is defined by:

$$\operatorname{erfc}(x) = \frac{1}{2} - \int_0^x \frac{1}{\sqrt{2\pi}} \exp\left(\frac{-\alpha^2}{2}\right) d\alpha$$

Now the second set of equations become, from equation (F-6):

$$\frac{\partial(\overline{\varepsilon^2})}{\partial z_j} = \int_{n=-\infty}^{\infty} \left[\int_{y_j - n}^{y_{j+1} - n} (z_j - x) \exp\left(-n^2 / 2\delta x\right) \frac{dx}{\sqrt{x}} \right] dn = 0 \qquad \text{(F-15)}$$

$j = 1, 2, \ldots k$

This may be rewritten as

$$\int_{n=-\infty}^{+\infty} (I'' - z_j I') \, dn = 0 \qquad j = 1, 2, \ldots k \tag{F-16}$$

where

$$I' = \int_{y_j - n}^{y_{j+1} - n} \exp\left\{\frac{-n^2}{2\delta x}\right\} \frac{dx}{\sqrt{x}} \tag{F-17}$$

$$I'' = \int_{y_j - n}^{y_{j+1} - n} \sqrt{x} \exp\left\{\frac{-n^2}{2\delta x}\right\} dx \tag{F-18}$$

Since I' and I" involve "error" functions with arguments as function of n, the above integral can be evaluated only by doing a numerical double integration, with the limits of the inner integral, a function of n. To avoid this difficulty and to arrive at an analytical expression relating the z_j's, y_j's and the y_{j+1}'s, the following approximations are made over the interval $[y_j - n, y_{j+1} - n]$.

For low levels of x, the function $\exp\left(\frac{-n^2}{2\delta x}\right)$ varies or increases somewhat faster than it does at higher levels. At higher levels, it varies ~~very~~ slowly, as it approaches 1 asymptotically.

The function $\frac{1}{\sqrt{x}}$ decreases faster at low levels (quite fast for very small values of x) than it does at higher levels. At higher levels, it varies slowly, as it asymptotically approaches zero.

Hence, over the range $(y_j - n, y_{j+1} - n)$, the function $\exp\left(-\frac{n^2}{2\delta x}\right)$ increases, $\frac{1}{\sqrt{x}}$ decreases, and ~~so~~ the product $\frac{1}{\sqrt{x}} \exp\left(\frac{-n^2}{2\delta x}\right)$ is smoothed by these changes. ~~Further,~~ only at very low levels are their variations significant.

Next, we consider the product $\sqrt{x} \exp\left(-\frac{n^2}{2\delta x}\right)$. Both $\sqrt{x}$ and $\exp\left(-\frac{n^2}{2\delta x}\right)$ ~~are~~ increasing over the indicated range. $\sqrt{x}$ increases faster than $\exp\left(-\frac{n^2}{2\delta x}\right)$. But $\sqrt{x}$ itself increases ~~only~~ slowly over the whole range of x ~~and~~.

so its variation over an interval $\left[y_j-n,\ y_{j+1}-n\right]$ will be relatively small. So the product $\sqrt{x}\exp\left(-\frac{n^2}{2\delta x}\right)$ can be expected to vary only slightly over any range $\left[y_j-n,\ y_{j+1}-n\right]$.

Hence, for both the functions, $\sqrt{x}\exp(-n^2/2\delta x)$ and $\frac{1}{\sqrt{x}}\exp(-n^2/2\delta x)$, we can approximate in the integral with

$$x \simeq \frac{y_j-n + y_{j+1}-n}{2} \qquad \text{(mean value)} \qquad \text{(F-19)}$$

Hence,

$$\frac{\partial(\overline{\varepsilon}_j^2)}{\partial Z_j} \simeq \int_{n=-\infty}^{\infty}\left[\frac{\left(y_{j+1}+y_j-2n\right)}{2} - z_j\right]\frac{1}{b\sqrt{2\pi\delta}}\ \exp\frac{\left[\frac{-n^2}{2\delta\left(\frac{y_j+y_{j+1}-2n}{2}\right)}\right]}{\sqrt{\frac{y_j+y_{j+1}-2n}{2}}}\left(y_{j+1}-y_j\right)dn$$

$$= 0 \qquad \text{(F-20)}$$

$$j = 1, 2, 3, \ldots k$$

Using the fact that the thresholds are distinct and performing extensive manipulations, equation (F-20) can be reduced to:

$$\exp\left\{-\frac{\left(\frac{y_j+y_{j+1}}{2}-b\right)^2}{2\delta b}\ \frac{\left(\frac{y_j+y_{j+1}}{2}-b\right)}{\sqrt{2\delta b}}\right\} + (1 + 2\sqrt{cd}\ \sqrt{\pi}\ \operatorname{erfc}\left\{\frac{\frac{y_j+y_{j+1}}{2}-b}{\sqrt{\delta b}}\right\}$$

$$\simeq \sqrt{c^3}\frac{Z_j}{\sqrt{c}}\ 2\sqrt{\pi}\ \operatorname{erfc}\left\{\frac{\frac{y_j+y_{j+1}}{2}-b}{\sqrt{\delta b}}\right\} \qquad \text{(F-21)}$$

where $c = \frac{1}{2\delta}$ and $d = \left(\frac{y_j+y_{j+1}}{2}\right)^2\Big|2\delta$

Finally solving for the output levels of the quantizer

$$Z_j \simeq \delta\left\{\frac{\frac{1}{\sqrt{\pi}}\exp\left[-\frac{\left(\frac{y_j+y_{j+1}}{2}-b\right)^2}{2\delta b}\right]\ \frac{\left(\frac{y_j+y_{j+1}}{2}-b\right)}{\sqrt{2\delta b}}}{\operatorname{erfc}\left\{\frac{\frac{y_j+y_{j+1}}{2}-b}{\sqrt{\delta b}}\right\}} + 1 + \frac{y_j+y_{j+1}}{2\delta}\right\} \qquad \text{(F-22)}$$

$$j = 1, 2, \ldots k$$

This set of equations, coupled with those in equations (F-14), represents the necessary conditions for selecting the threshold levels $\{y_j\}$ and the output levels $\{z_j\}$.

We will briefly outline a numerical technique for solving for the unknown levels. Assume that $y_1=0$. Then one item in equations (F-22) relates z_1 and y_2, and likewise, one of the equations (F-14) relates z_1, z_2, and y_2.

So if we can pick some z_1, we can generate y_2 from (F-22), and using this y_2, we can find z_2 from (F-14). Thus, we can, step by step, find all the y_i's and the z_i's.

One procedure will be to pick z_1 first, generate all the z_i's and y_i's, and then calculate the mean-square error. Then the value of z_1 may be changed and again the corresponding m·s· error can be found out. If this is greater than the previous one, then another z_1 on the other side of the original z_1 may be tried and the m·s· error can be computed again. This iterative procedure is repeated till we get a set of y_i's and z_i's corresponding to the minimum mean-square error.

However, to use this approach, we must compute the mean-square error. This is given by:

$$\overline{\varepsilon^2} = \int_{n=-\infty}^{n=\infty} \left[\sum_{j=1}^{k} \int_{y_j-n}^{y_{j+1}-n} (x-z_j)^2 \frac{1}{b\sqrt{2\pi\delta}} \exp\left(\frac{-n^2}{2\delta x}\right) \frac{dx}{\sqrt{x}} \right] dn \qquad \text{(F-23)}$$

Employing the same approximations which lead to equation (F-19), we may arrive at the following complicated expression for $\overline{\varepsilon^2}$.

$$\overline{\varepsilon^2} \simeq \sum_{j=1}^{k}\left(y_{j+1}-y_j\right)\left[Z_j^2\exp(-2\sqrt{cd})\operatorname{erfc}\left(\frac{\frac{y_j+y_{j+1}}{2}-b}{\sqrt{\delta b}}\right)\cdot\frac{2\sqrt{\pi}}{\sqrt{c}}\right.$$

$$-2z_j\frac{\exp(-2\sqrt{cd})}{\sqrt{c^3}}\cdot\left\{\exp\left[-\left(\frac{\frac{y_j+y_{j+1}}{2}-b}{2\delta b}\right)^2\right]\left[\frac{\frac{y_j+y_{j+1}}{2}-b}{\sqrt{2\delta b}}\right]\right.$$

$$\left.+(1+2\sqrt{cd})\sqrt{\pi}\operatorname{erfc}\frac{\left(\frac{y_j+y_{j+1}}{2}-b\right)}{\sqrt{\delta b}}\right\}$$

$$+\frac{\exp(-2\sqrt{cd})}{\sqrt{c^5}}\left\{\exp\left[-\left(\frac{\frac{y_j+y_{j+1}}{2}-b}{2\delta b}\right)^2\right]\cdot\left[\left(\frac{\frac{y_j+y_{j+1}}{2}-b}{2\delta b}\right)^2\right]^{3/2}\right.$$

$$+3\exp\left[-\left(\frac{\frac{y_j+y_{j+1}}{2}-b}{2\delta b}\right)^2\right]\left(\frac{\frac{y_j+y_{j+1}}{2}-b}{2\delta b}\right)\cdot\left[\frac{1}{2}+\left(\frac{y_j+y_{j+1}}{2}\cdot\frac{1}{2\delta}\right)\right]$$

$$+\sqrt{\pi}\operatorname{erfc}\left[\frac{\left(\frac{y_j+y_{j+1}}{2}-b\right)}{\sqrt{\delta b}}\right]\left[\frac{3}{2}+3\left(\frac{y_j+y_{j+1}}{2}\cdot\frac{1}{2\delta}\right)\right.$$

$$\left.\left.+2\cdot\left(\frac{\frac{y_j+y_{j+1}}{2}}{4\delta^2}\right)^2\right\}\right] \qquad \text{(F-24)}$$

where for each j, $2\sqrt{cd}=\dfrac{y_j+y_{j+1}}{2\delta}$.

The procedure described previously can be used to get the quantizer levels corresponding to the minimum mean-square error.

Similarly, other probability density functions, such as Rayleigh, normal, can be assumed for $f_X(x)$ and the quantizer levels are again obtained by using the above procedure. It may be difficult to evaluate equation (F-3) and (F-5). In such cases, numerical integration may be employed. Also, the sensitivity of the quantizer levels to different probability density functions may be studied. The merit of this procedure lies in the fact that a chosen performance index (mean-square error) is minimized while obtaining the quantizer levels and thresholds.

APPENDIX G

AUTOCORRELATION PLOTS

The autocorrelation function is the inverse Fourier transform of the power spectral density. It is useful in some data analysis using second-order statistics and is included for reference here. Essentially what was done ~~is to take~~ we took the inverse Fourier transform of the power spectra presented in Chapter 2. For convenience, the plots are normalized so that: $R(0) = 1$.

FIGURE G.1. PLOTS OF THE NORMALIZED

AUTOCORRELATION OF SELECTED PORTIONS OF APOLLO VI PHOTOGRAPHS

Apollo AS6-2-877
Lines: 200-204
Elements: 10-521

AVERAGE AUTOCORRELATION
GRAPH PLOT NO. 03

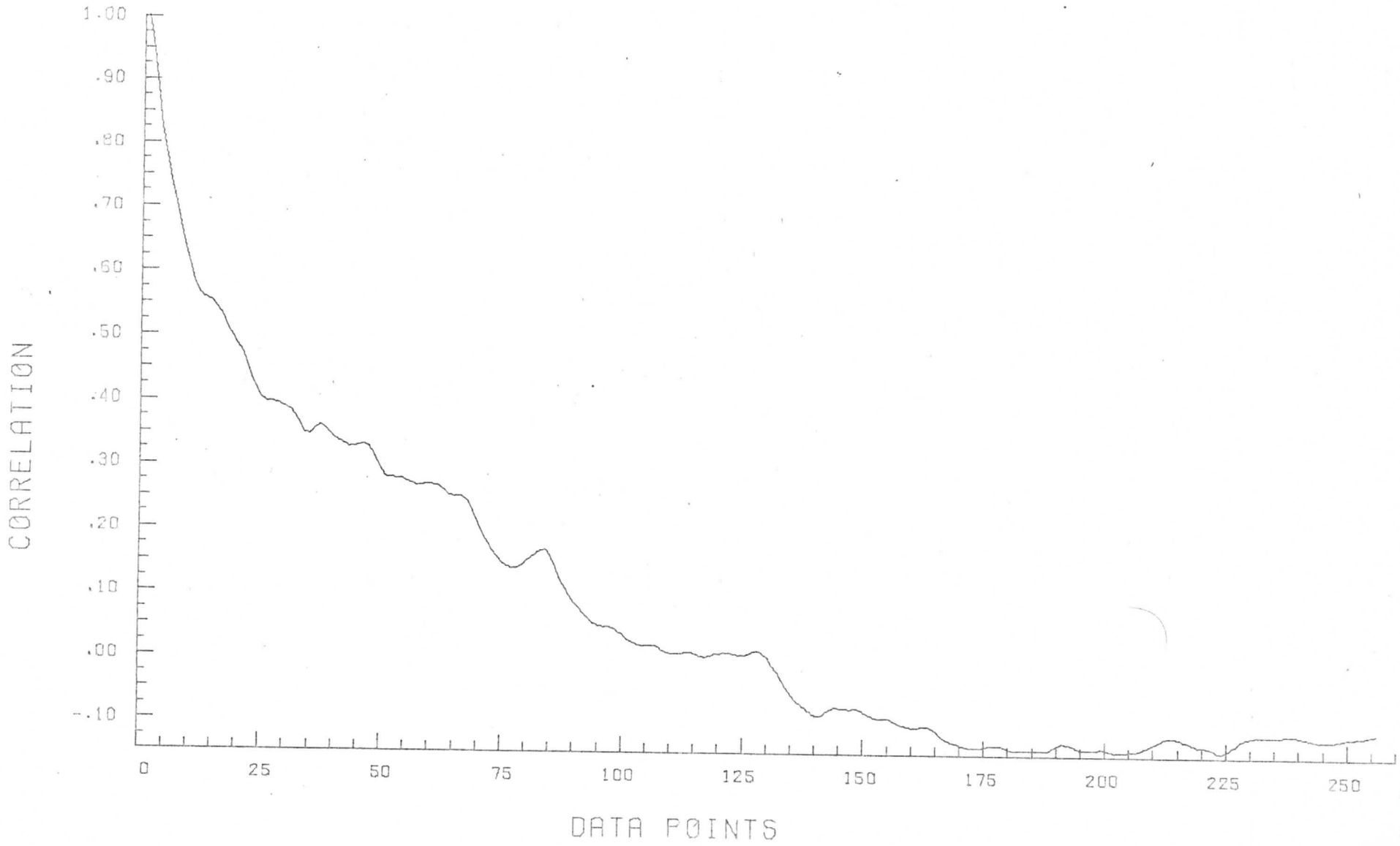

Apollo AS6-2-877
Lines: 200-204
Elements: 510-1021

AVERAGE AUTOCORRELATION
GRAPH PLOT NO. 06

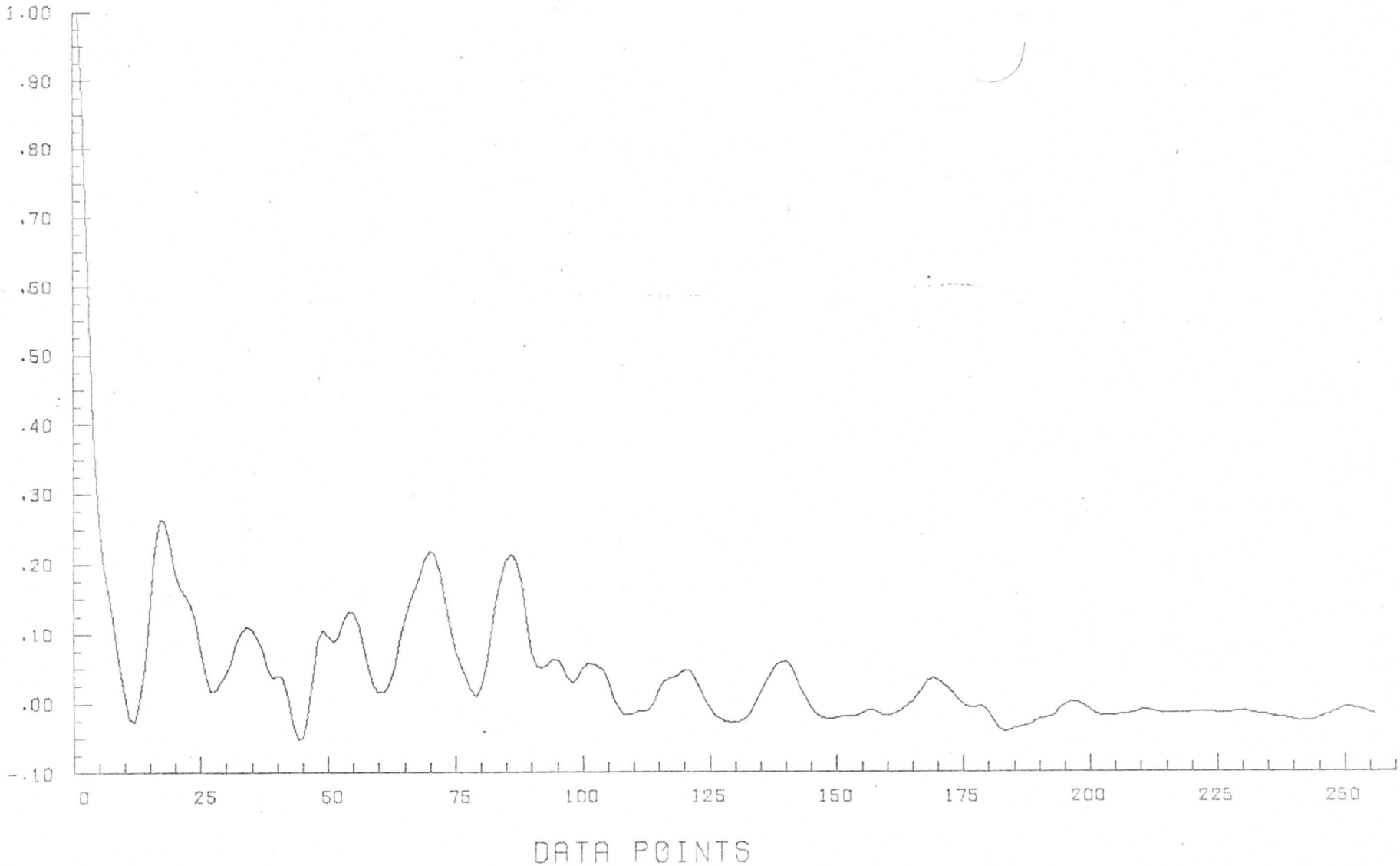

Apollo AS6-2-877
Lines: 850-854
Elements: 510-1021

AVERAGE AUTOCORRELATION
GRAPH PLOT NO. 09

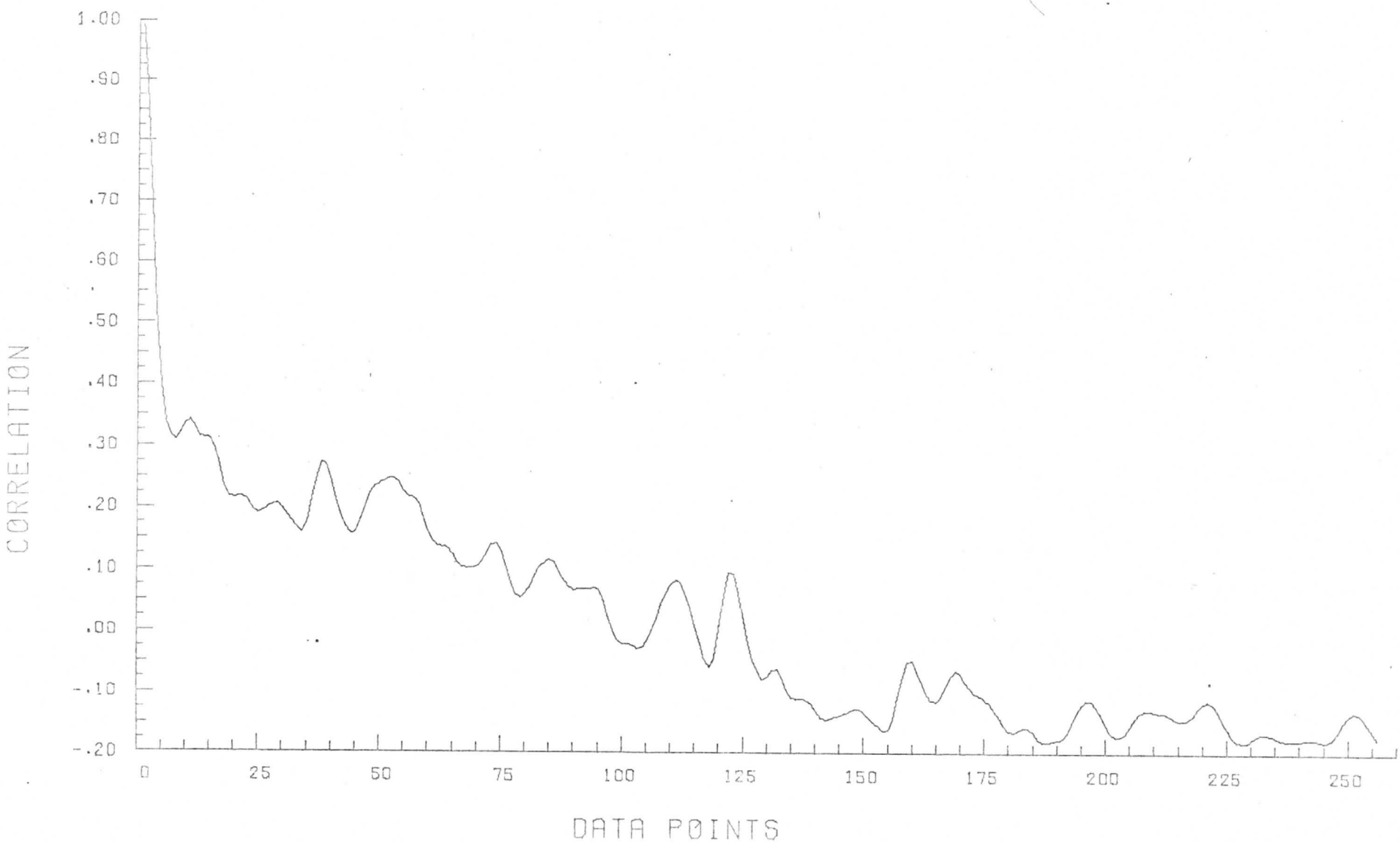

Apollo AS6-2-934
Lines: 100-104
Elements: 510-1021

AVERAGE AUTOCORRELATION
GRAPH PLOT NO. 12

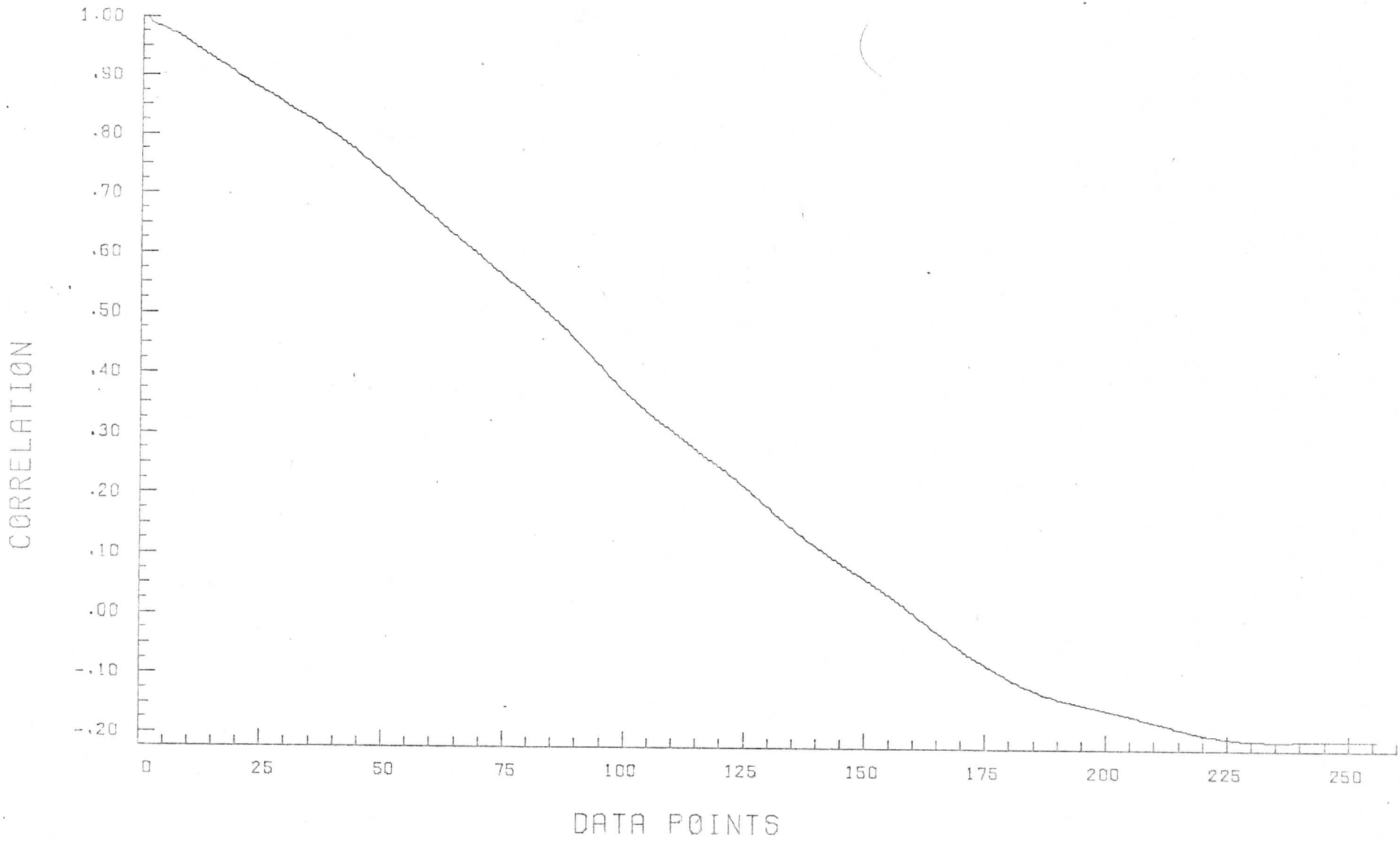

Apollo AS6-2-934
Lines: 250-254
Elements: 510-1021

AVERAGE AUTOCORRELATION
GRAPH PLOT NO. 15

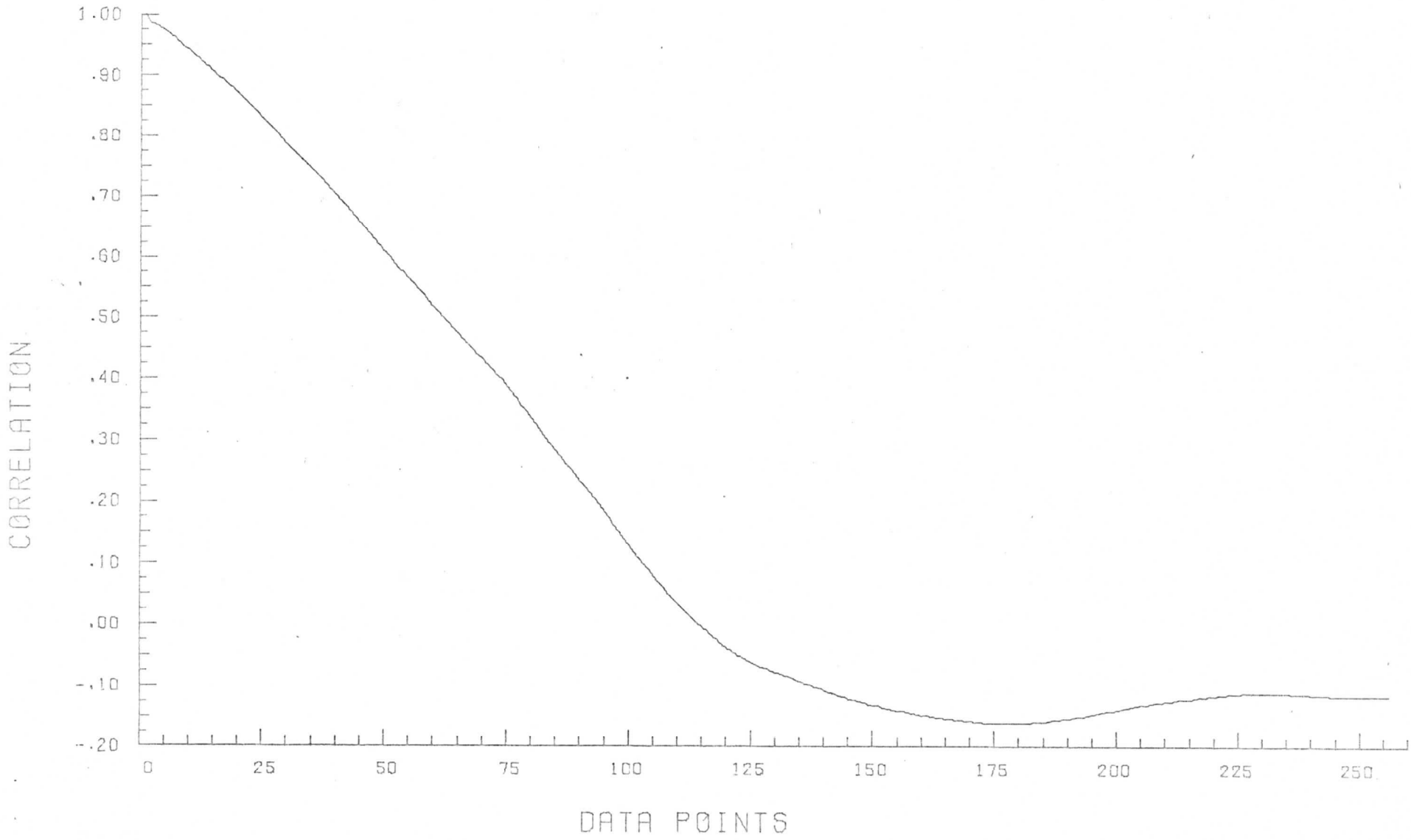

Apollo AS6-2-948
Lines: 800-804
Elements: 10-521

AVERAGE AUTOCORRELATION
GRAPH PLOT NO. 18

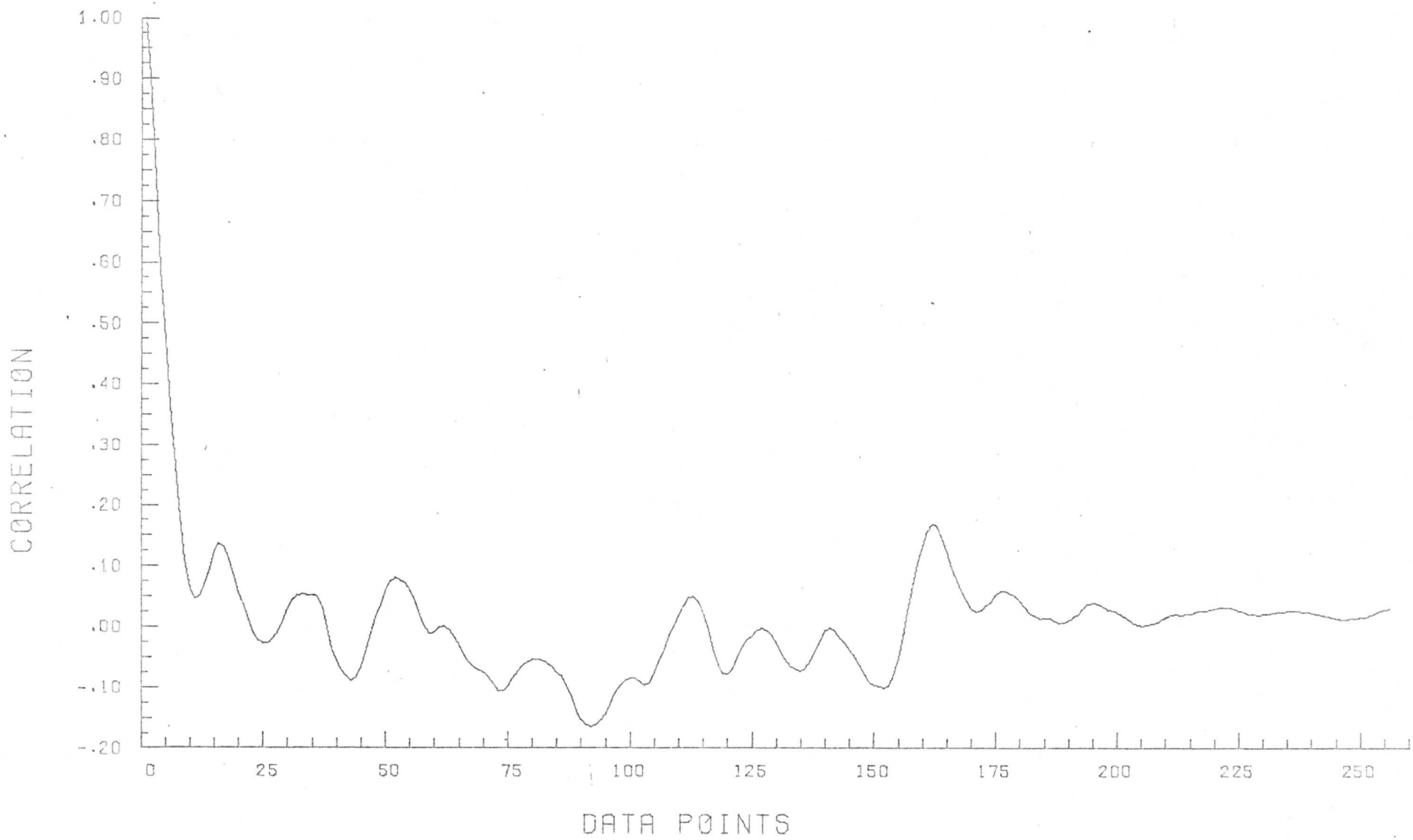

Apollo AS6-2-1064
Lines: 130-134
Elements: 510-1021

AVERAGE AUTOCORRELATION
GRAPH PLOT NO. 21

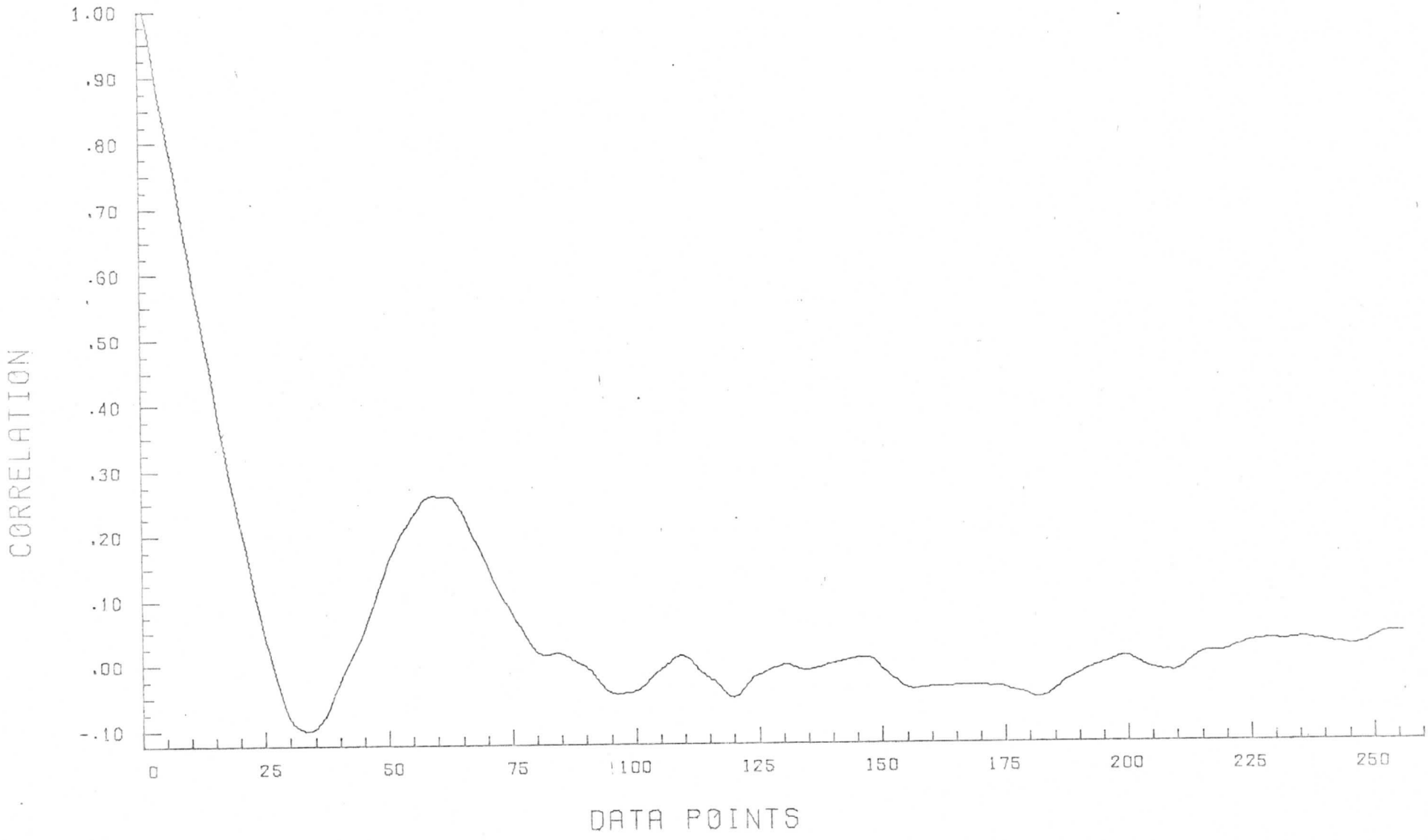

Apollo AS6-2-1429
Lines: 250-254
Elements: 510-1021

AVERAGE AUTOCORRELATION
GRAPH PLOT NO. 24

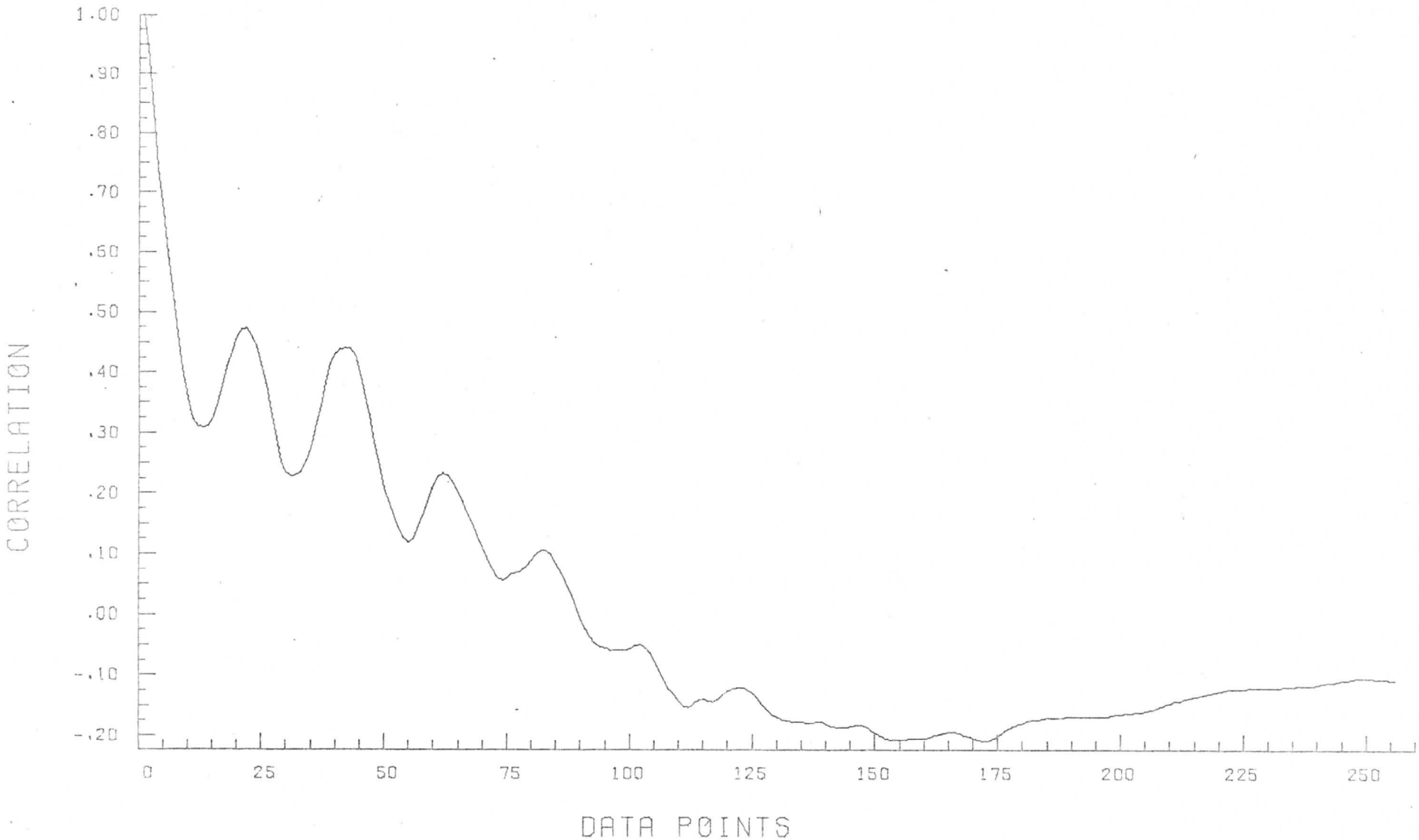

Apollo AS6-2-1429
Lines: 700-704
Elements: 510-1021

AVERAGE AUTOCORRELATION
GRAPH PLOT NO. 27

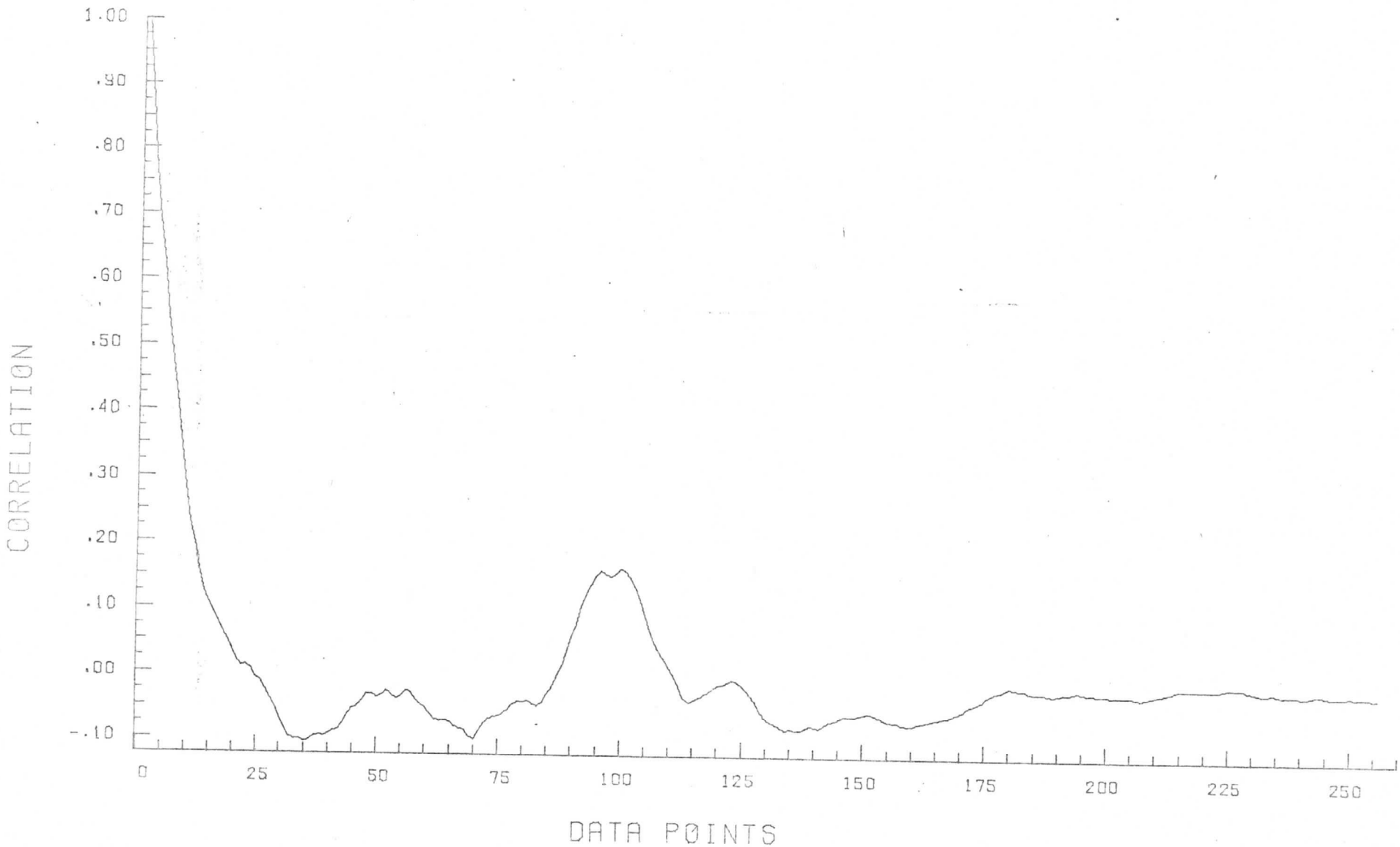

Apollo AS6-2-1430
Lines: 500-504
Elements: 260-771

AVERAGE AUTOCORRELATION
GRAPH PLOT NO. 30

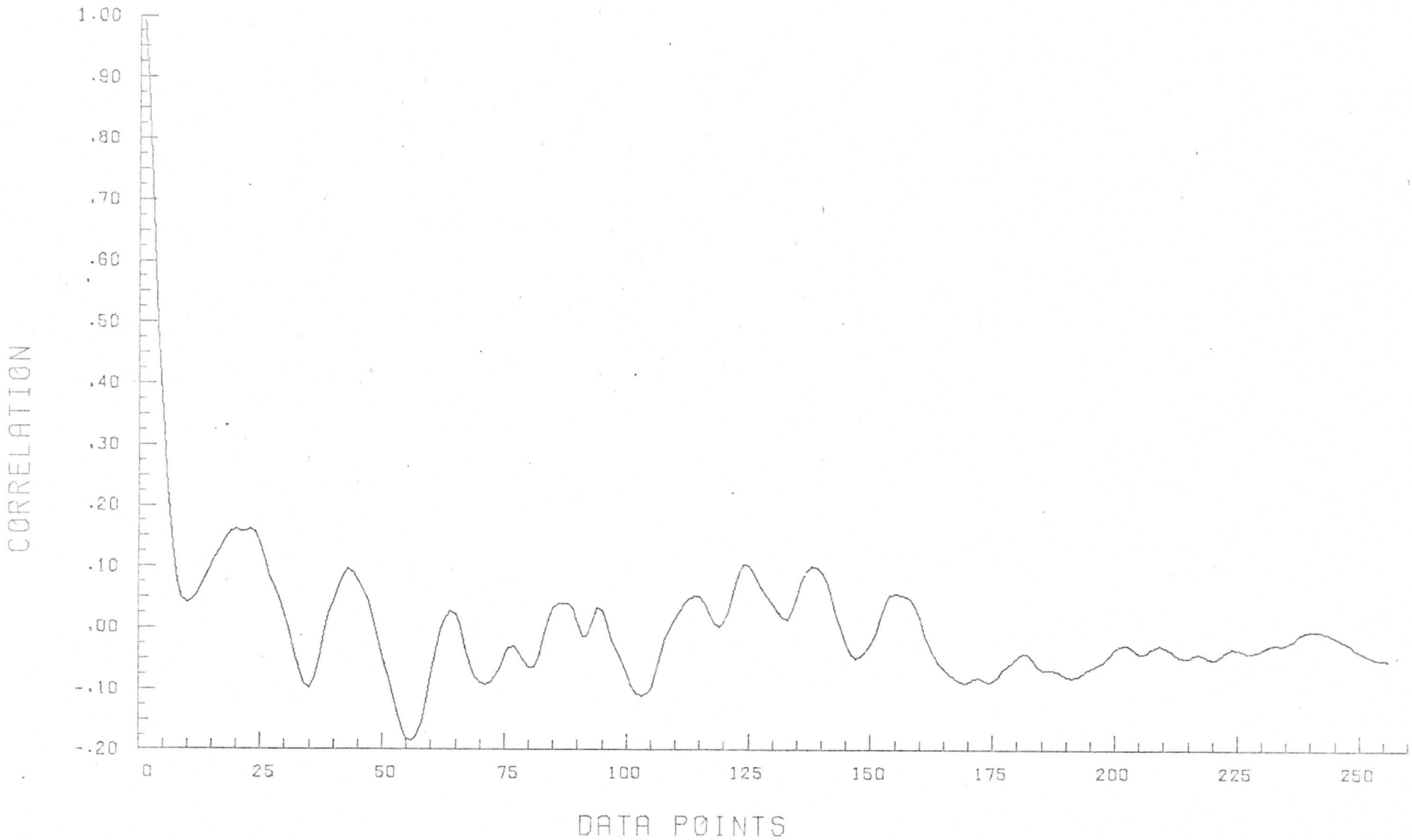

Apollo AS6-2-1467
Lines: 800-804
Elements: 10-521

AVERAGE AUTOCORRELATION
GRAPH PLOT NO. 33

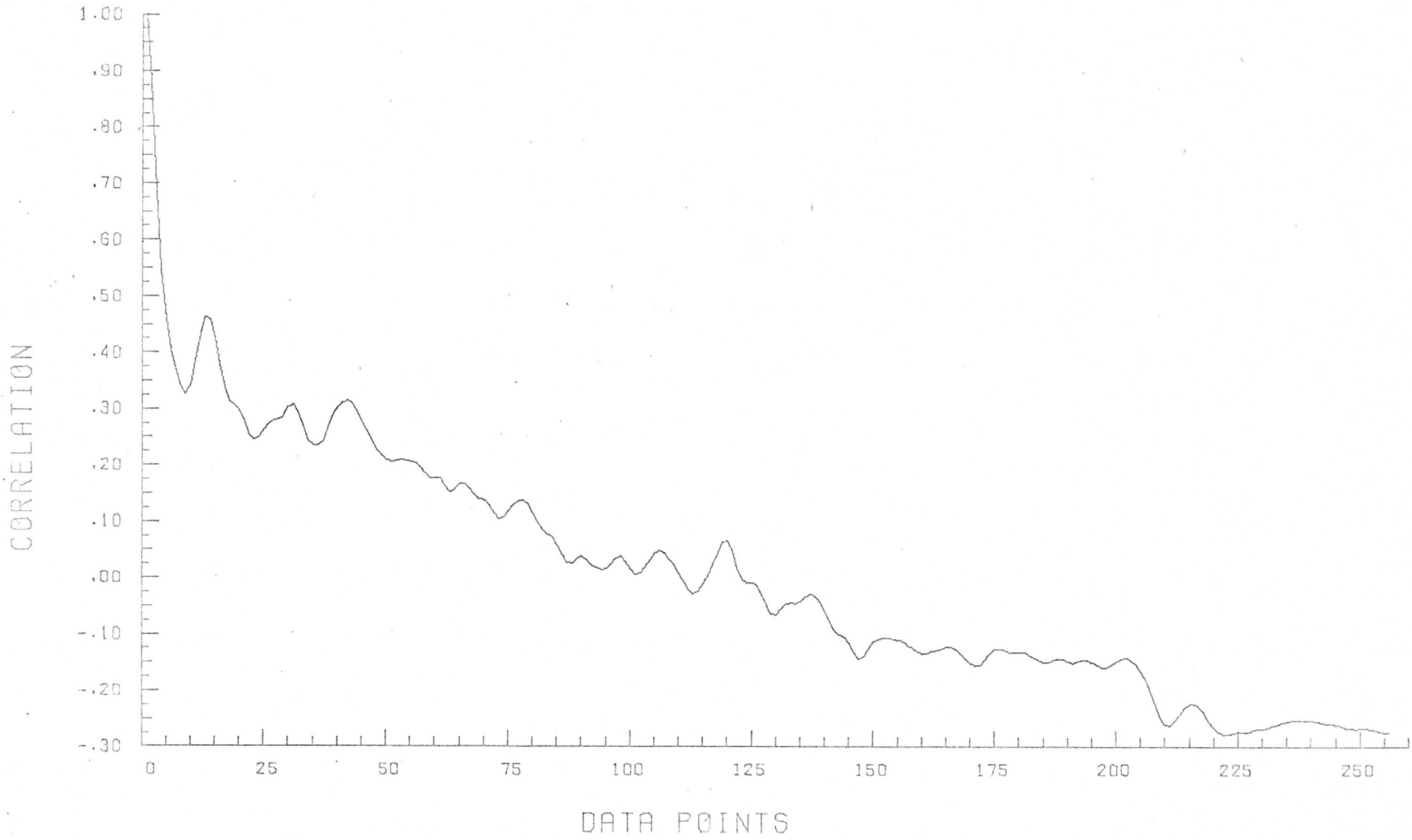

Apollo AS6-2-1468
Lines: 650-654
Elements: 510-1021

AVERAGE AUTOCORRELATION
GRAPH PLOT NO. 36

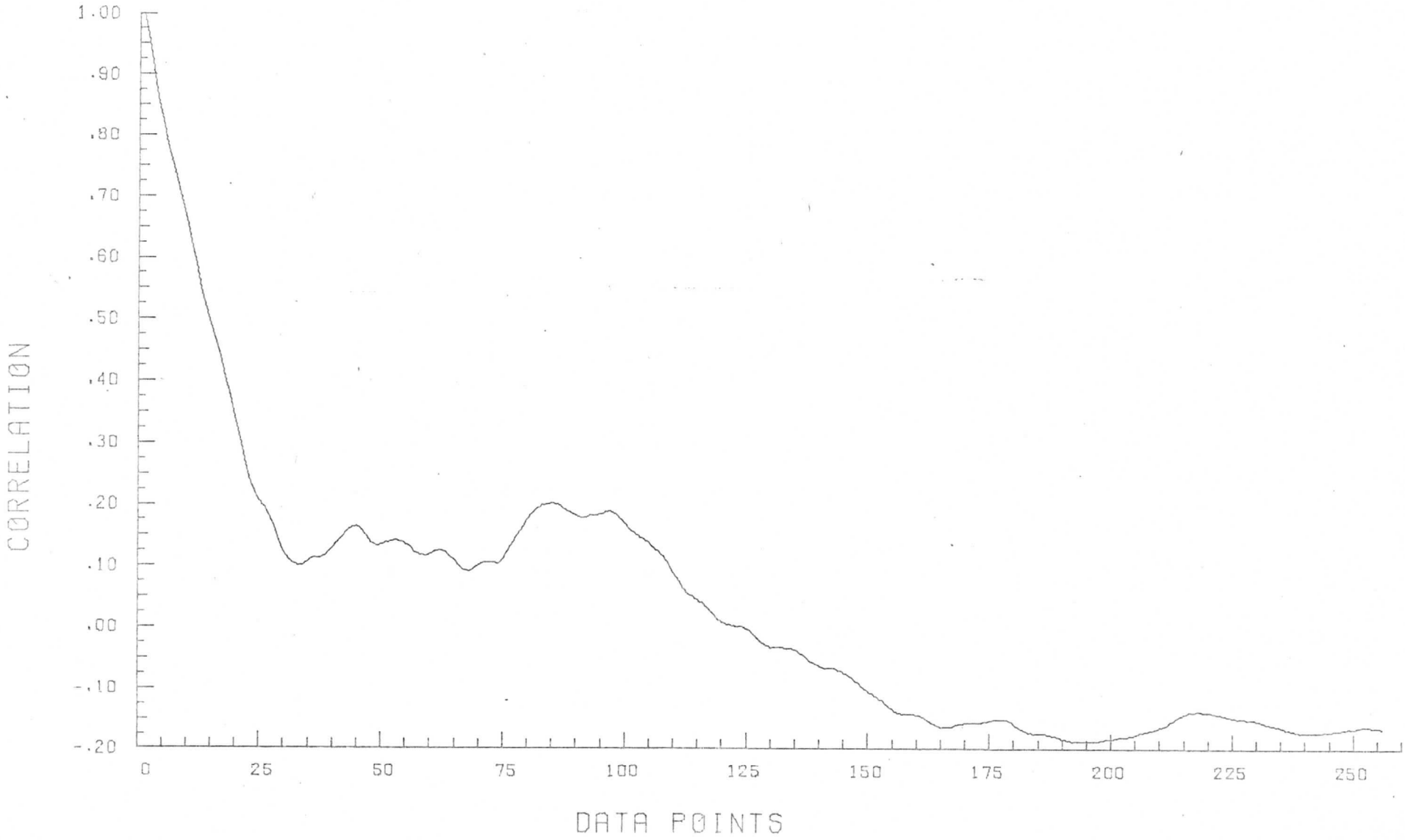

Apollo AS6-2-1468
Lines: 850-854
Elements: 10-521

AVERAGE AUTOCORRELATION
GRAPH PLOT NO. 39

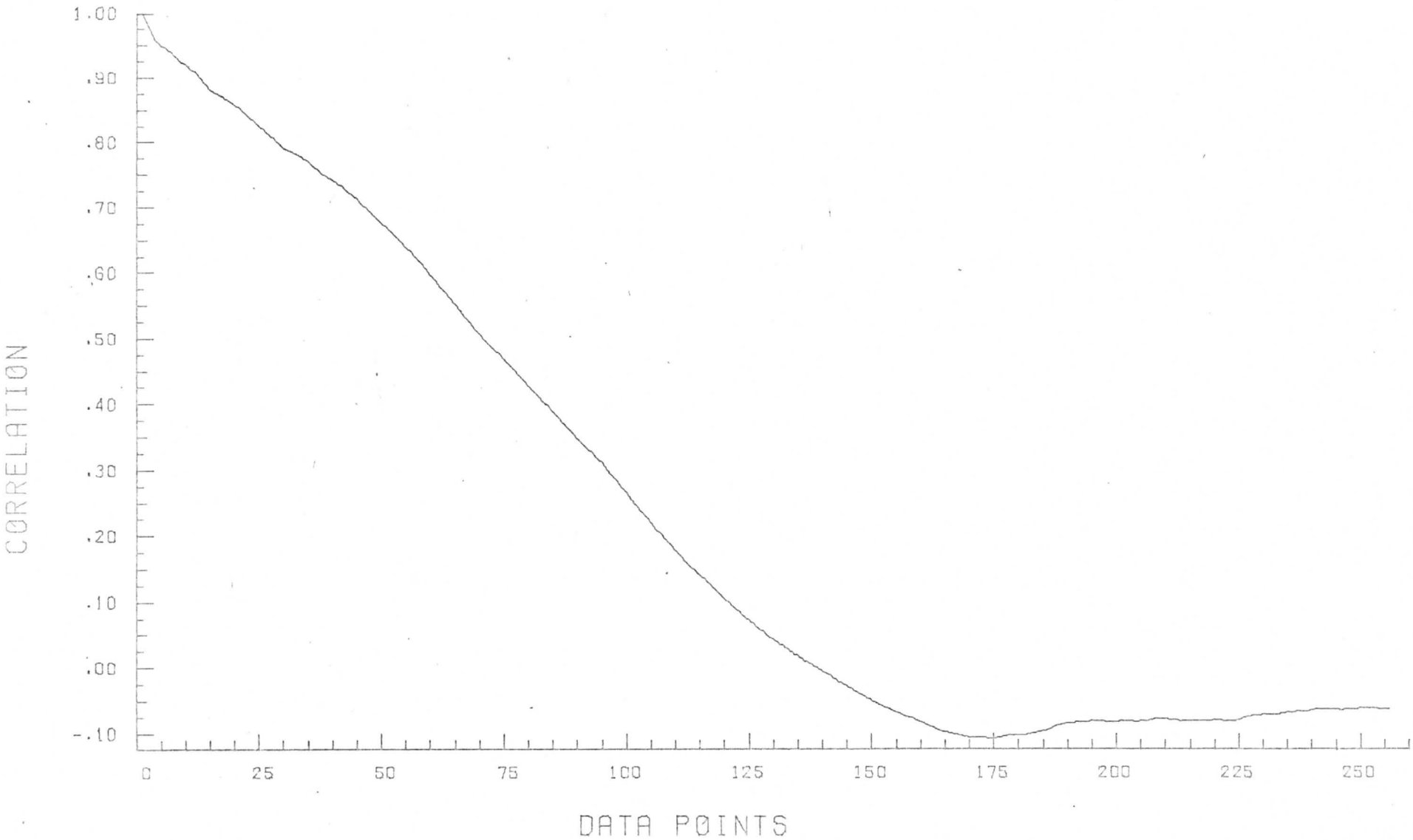

Apollo AS6-2-1469
Lines: 100-104
Elements: 510-1021

AVERAGE AUTOCORRELATION
GRAPH PLOT NO. 42

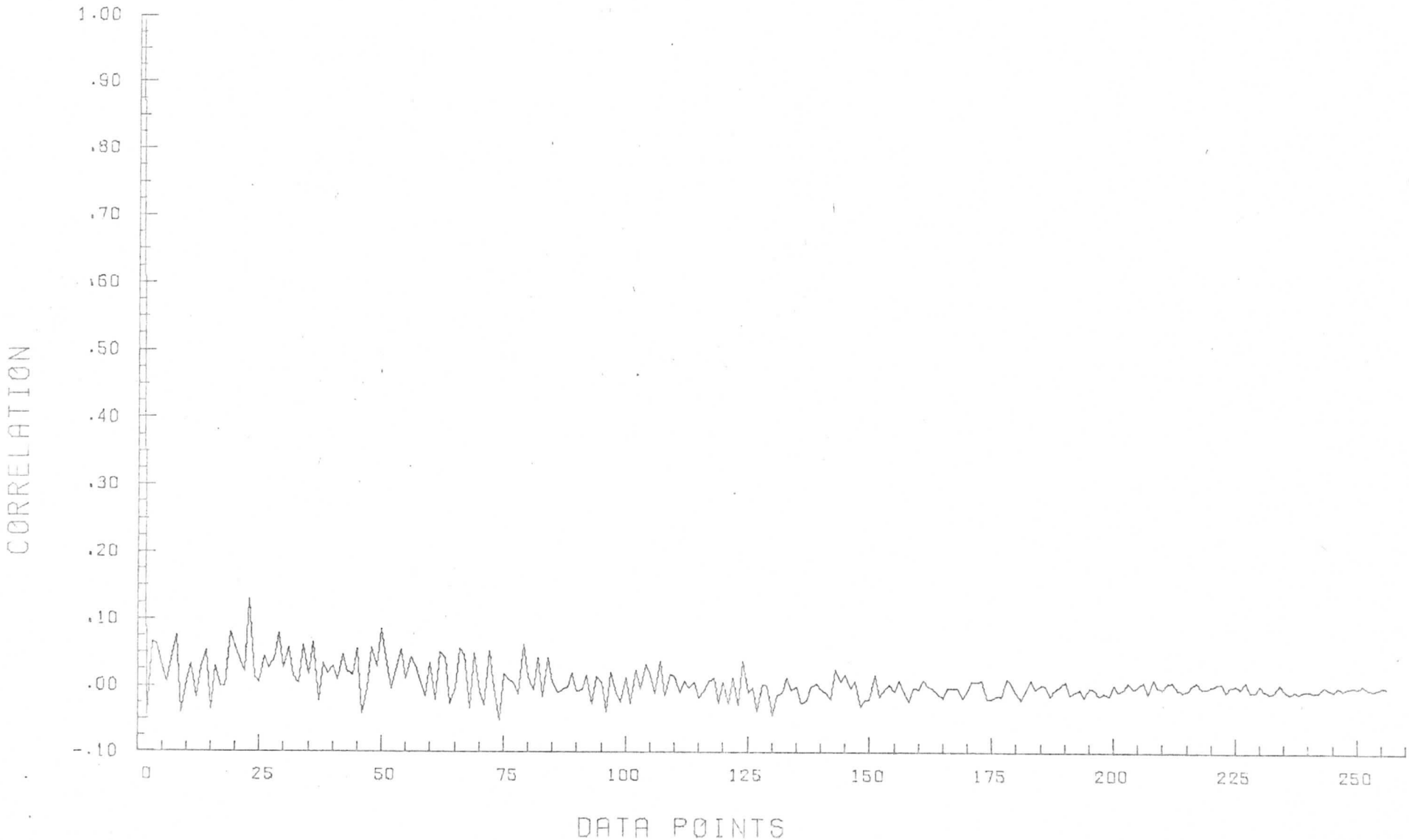

Apollo AS6-2-1469
Lines: 760-764
Elements: 10-521

AVERAGE AUTOCORRELATION
GRAPH PLOT NO. 45

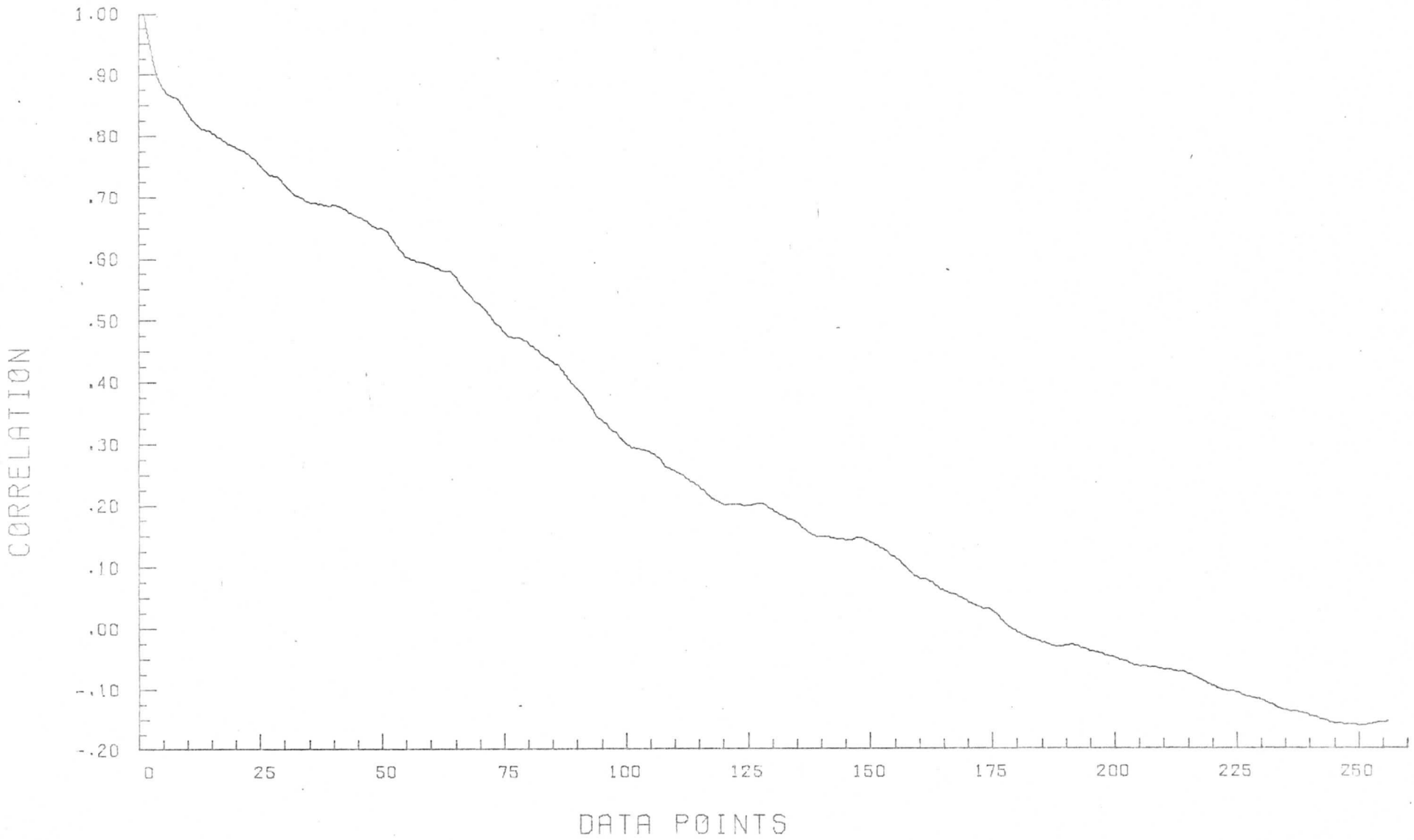

Apollo AS6-2-1469
Lines: 760-764
Elements: 510-1021

AVERAGE AUTOCORRELATION
GRAPH PLOT NO. 48

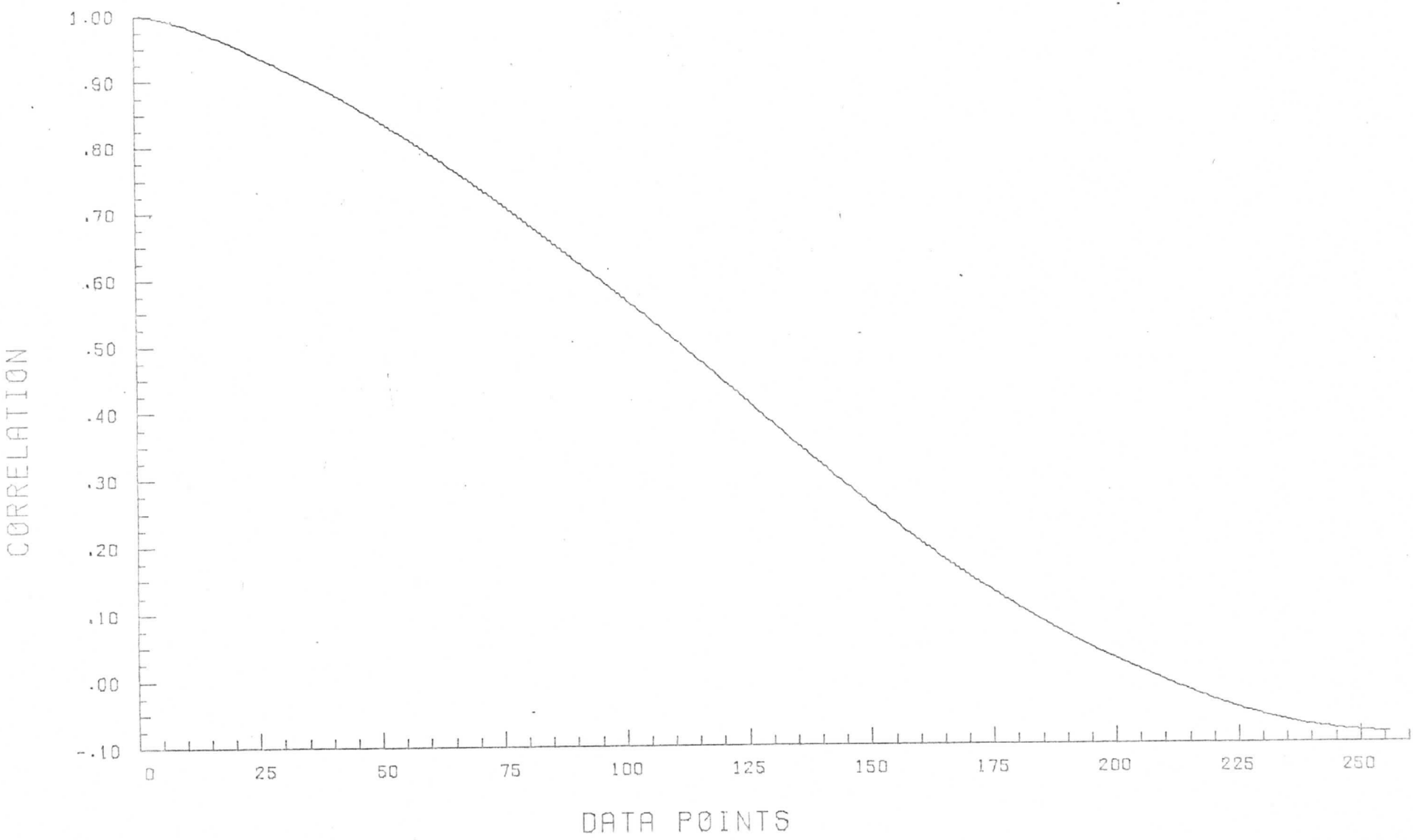

Apollo AS6-2-1484 (horiz.)
Lines: 350-354
Elements: 510-1021

AVERAGE AUTOCORRELATION
GRAPH PLOT NO. 51

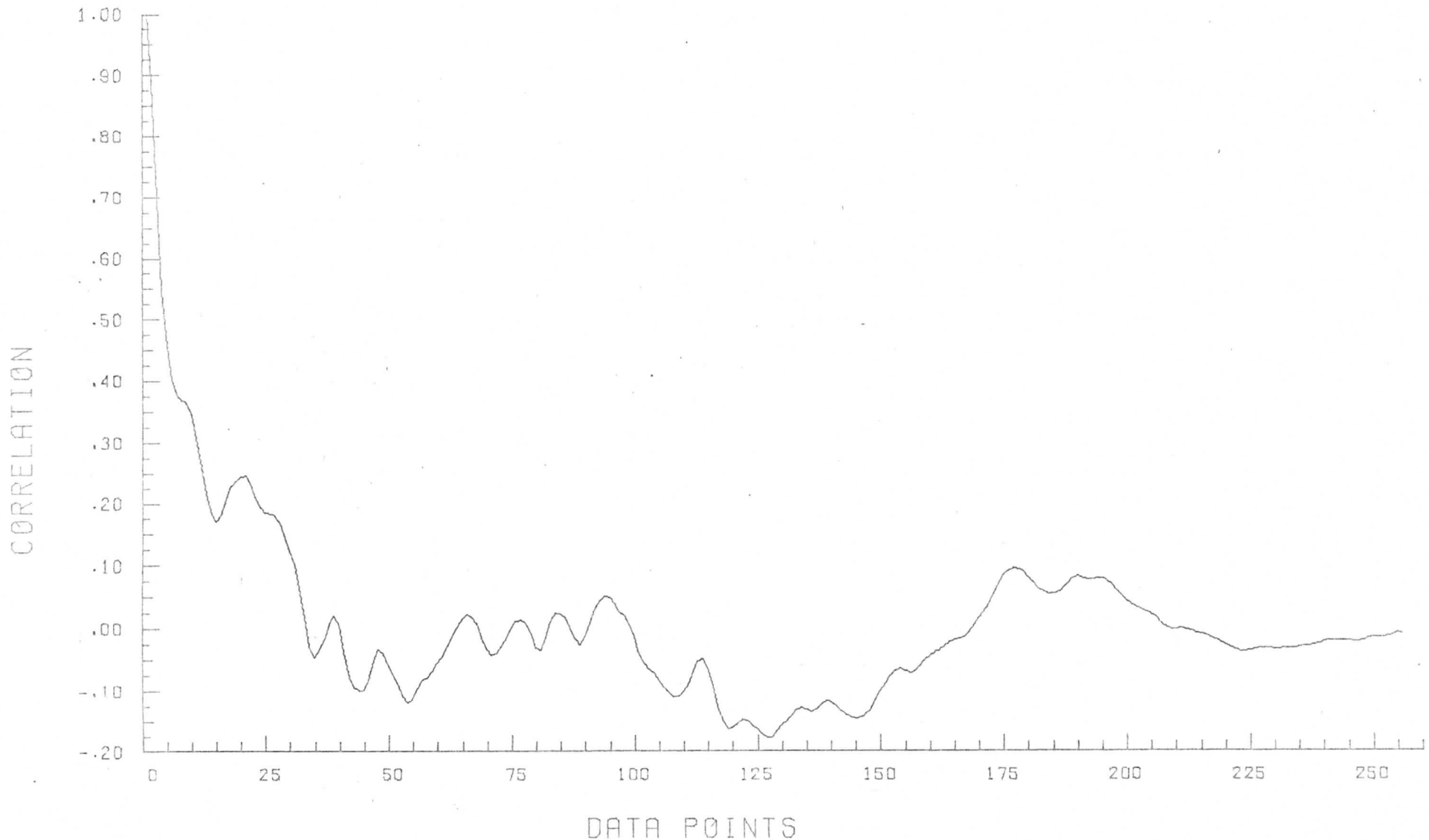

Apollo AS6-2-1484 (horiz.)
Lines: 350-354
Elements: 260-771

AVERAGE AUTOCORRELATION
GRAPH PLOT NO. 54

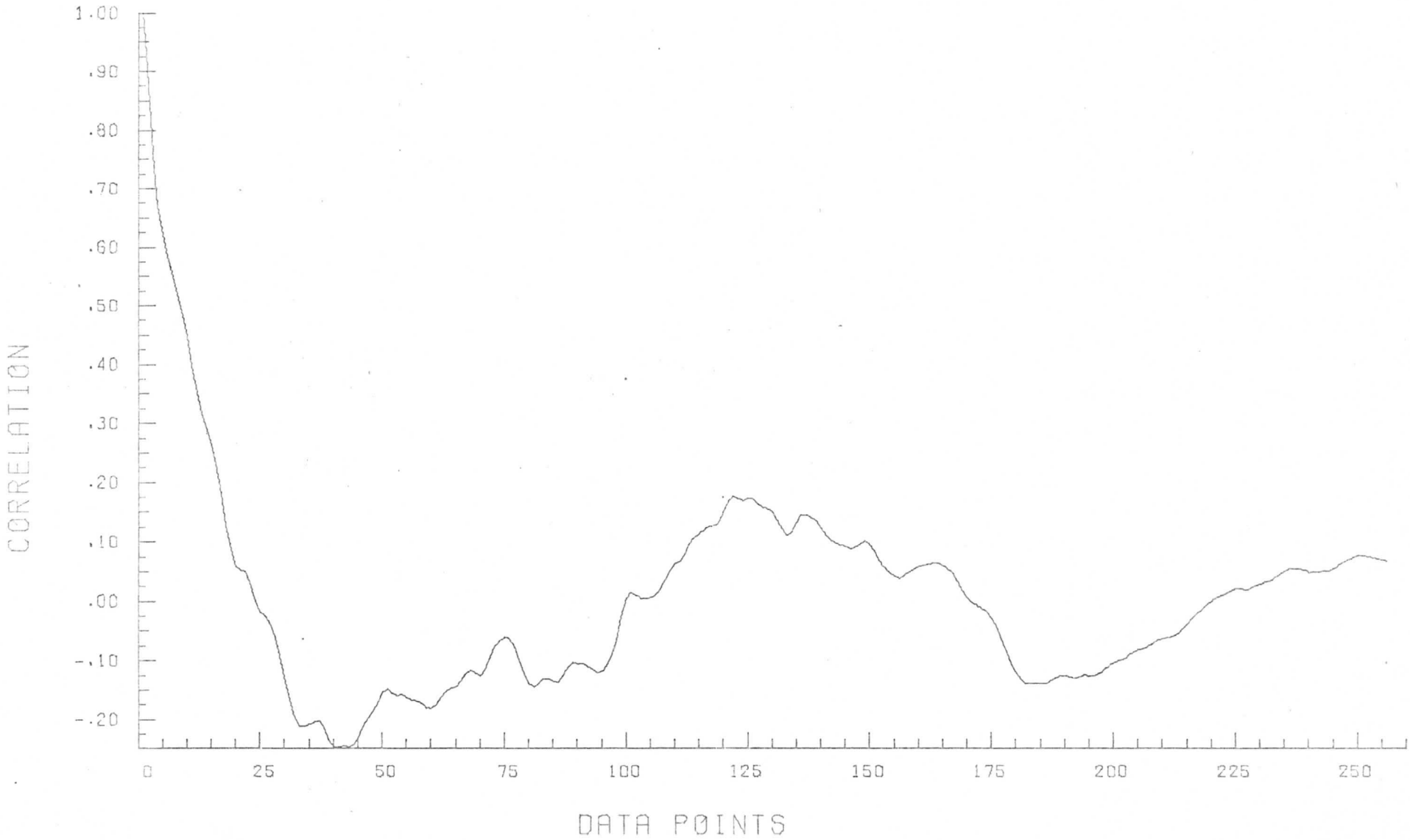

Apollo AS6-2-1484 (vert.)
Lines: 100-104
Elements: 260-771

AVERAGE AUTOCORRELATION
GRAPH PLOT NO. 57

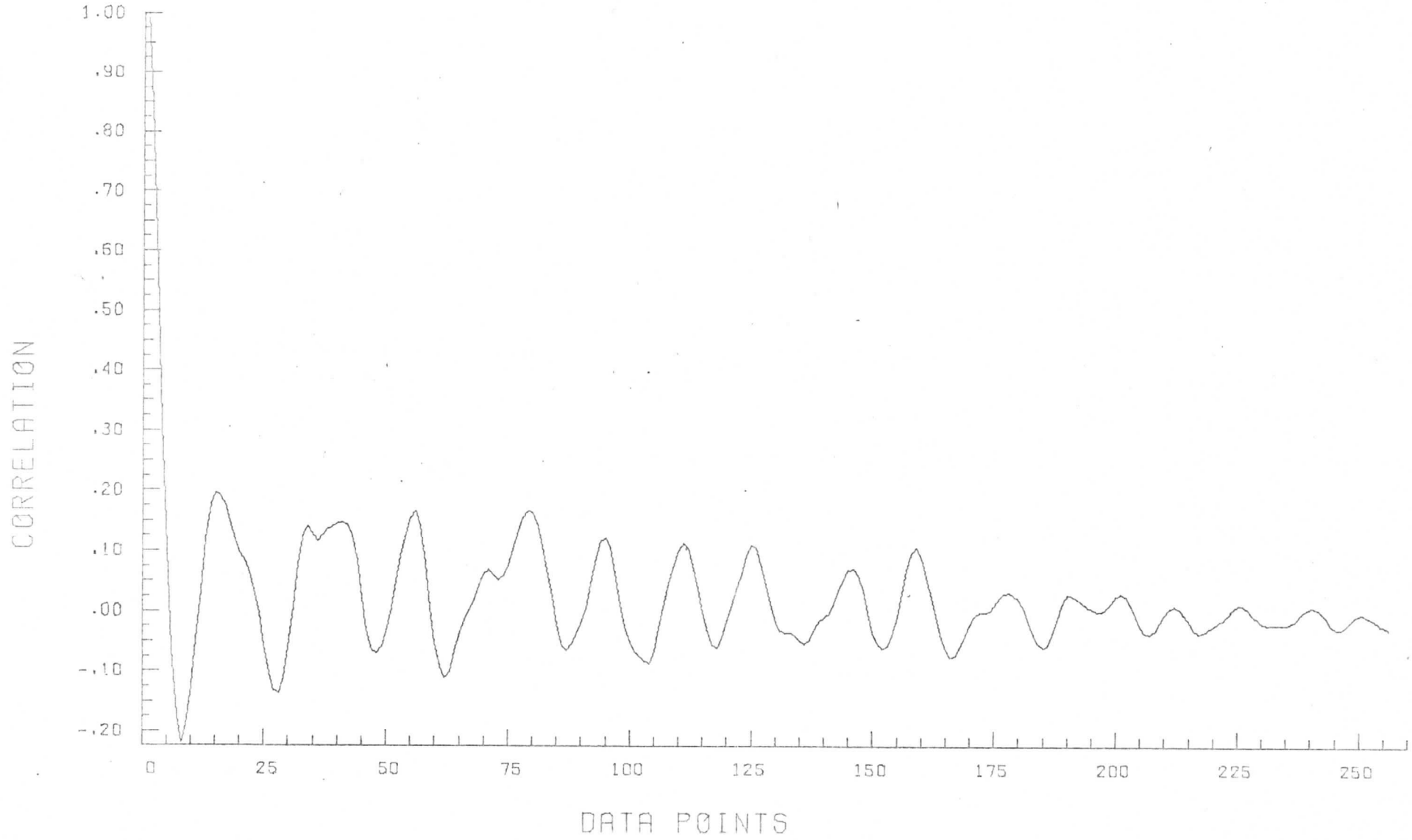

Delete Appendix H

APPENDIX H

UNSMOOTH POWER SPECTRAL PLOTS

The plots shown were generated using a 512-point FFT routine in the UNIVAC 1108 with a rectangular data window and no data smoothing. The average value was also removed.

The computer-generated plots follow the same order: (1) the (logarithimic) power spectral plot of the first sample line; (2) the autocorrelation function of the first sample line; (3) the (logarithimic) power spectral plot of the fifth sample line; (4) the log of the average power spectrum of five consecutive lines; (5) the average autocorreclation function of five consecutive lines. Averaging over five lines decreases the spectral randomness in the measurement and is essentially averaging over a scan of 5 x .079 = 0.395 n.mi. in width.

FIGURE H.1. UNSMOOTHED POWER SPECTRAL

PLOTS OF APOLLO VI PHOTOGRAPHS

Apollo 56-2-877, (rect.)
Locator: Tape 17, File 1
Records: 860 - 864 Date: 2/1/73
Elements: 510 - 1021
Plot: Log Power Spectrum, First Line

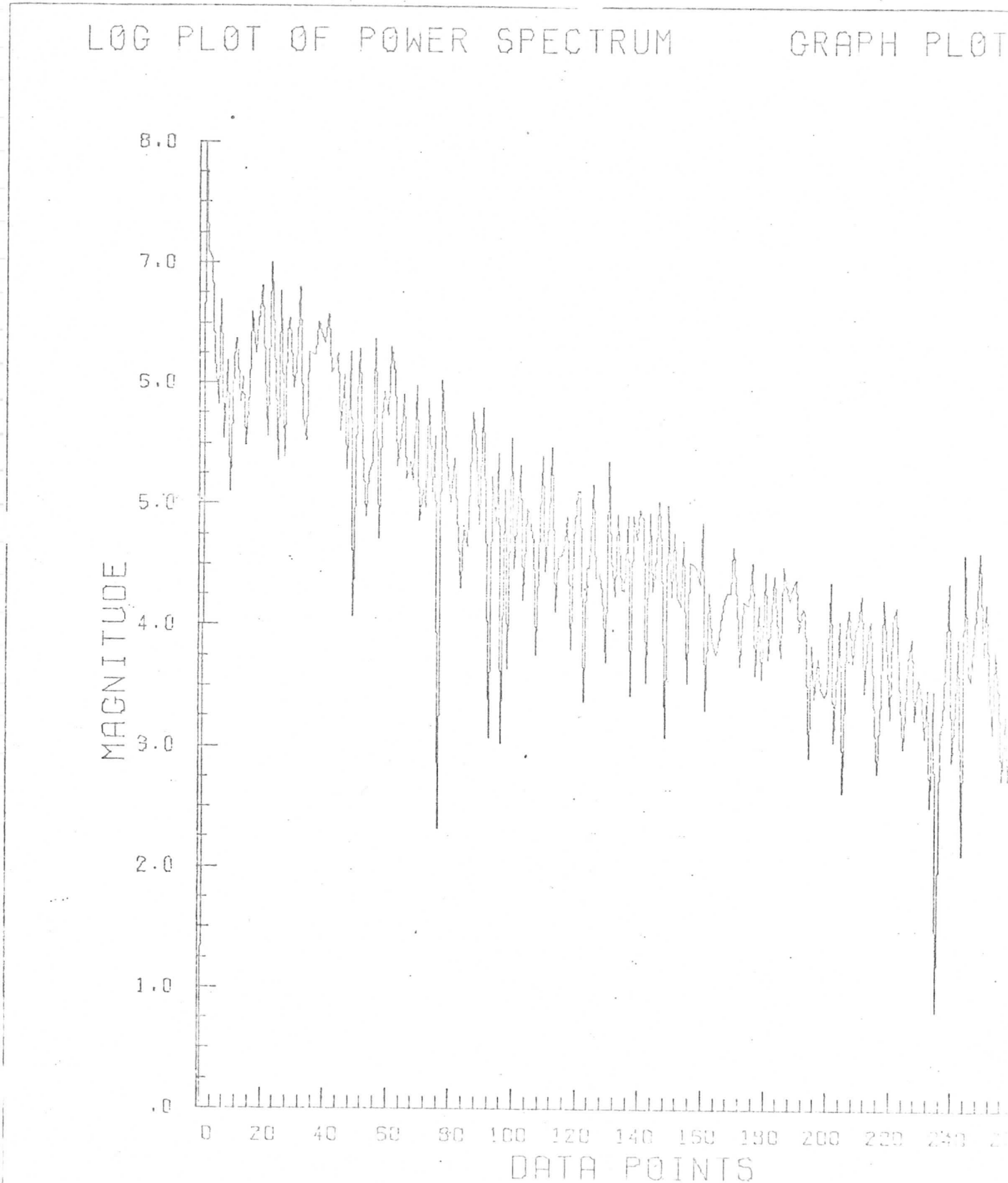

Apollo 56-2-877, (rect.)
Locator: Tape 17, File 1
Records: 860 - 864 Date: 2/1/73
Elements: 510 - 1021
Plot: Autocorrelation, First Line

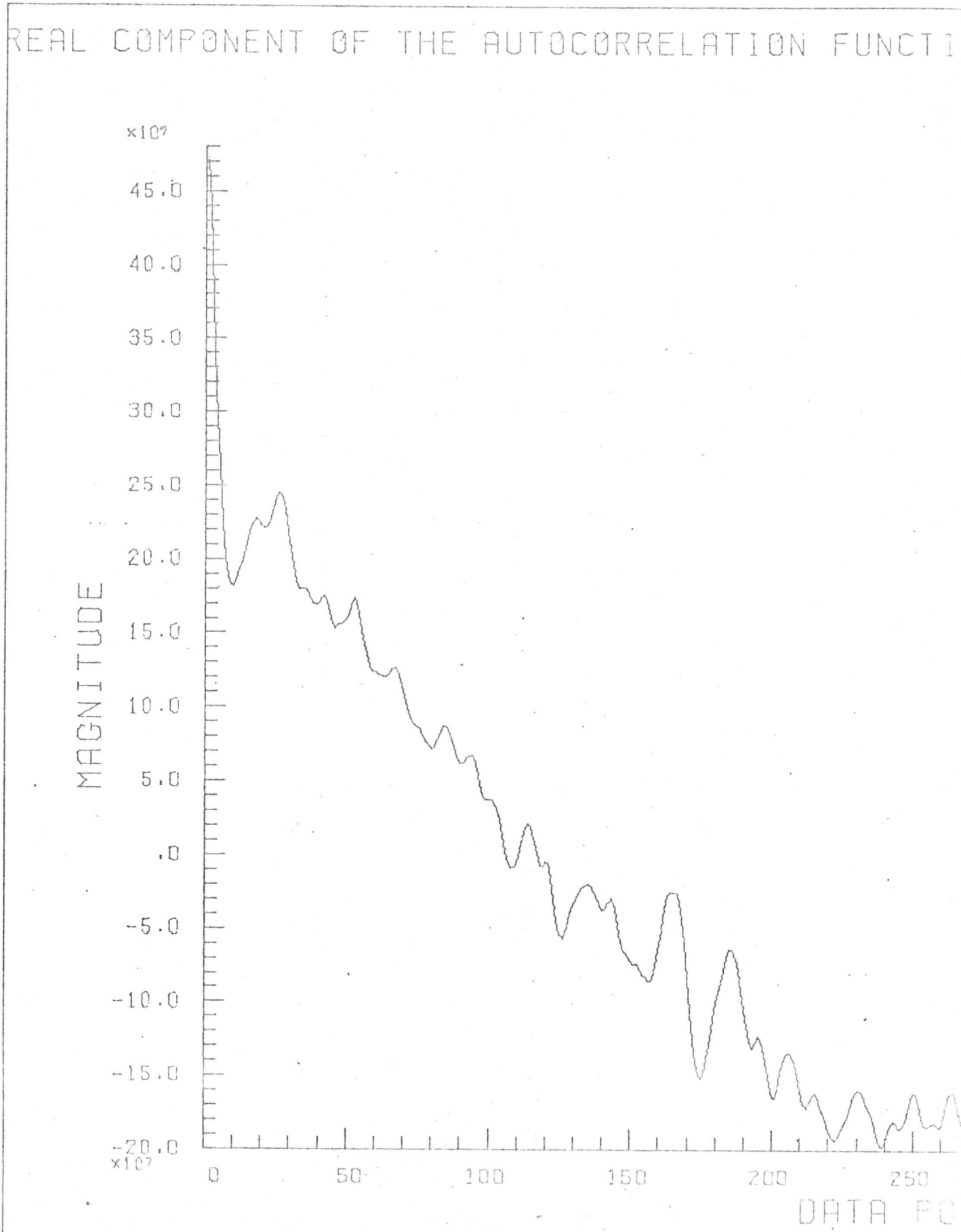

Apollo 56-2-877, (rect.)
Locator: Tape 17, File 1
Records 860 - 864 Date: 2/1/73
Elements: 510 - 1021
Plot: Log Power Spectrum, Fifth Line

H-5

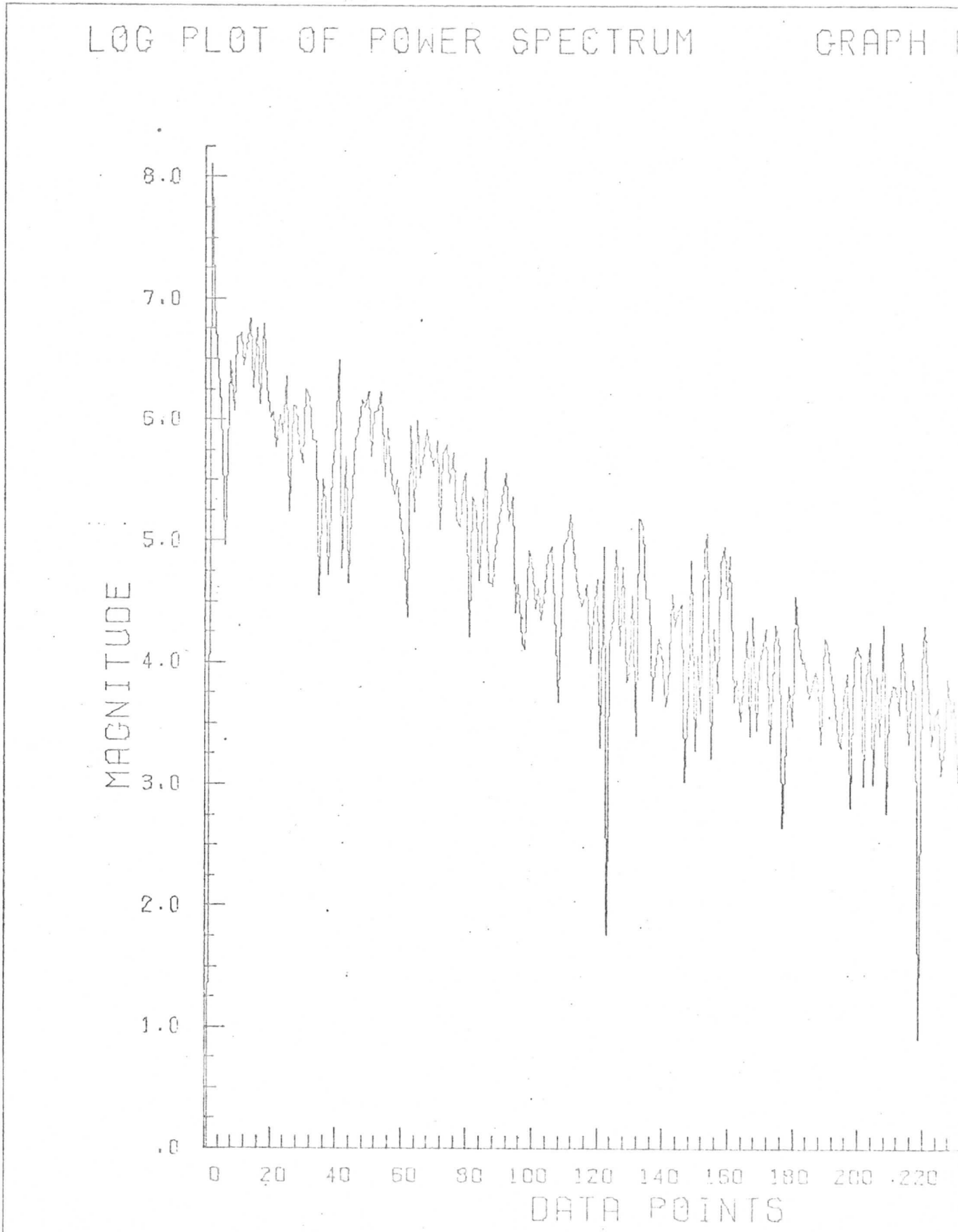

Apollo 56-2-877, (rect.)
Locator: Tape 17, File 1
Records: 860 - 864 Date: 2/1/73
Elements: 510 - 1021
Plot: Log Avg. Power Spectrum

H-6

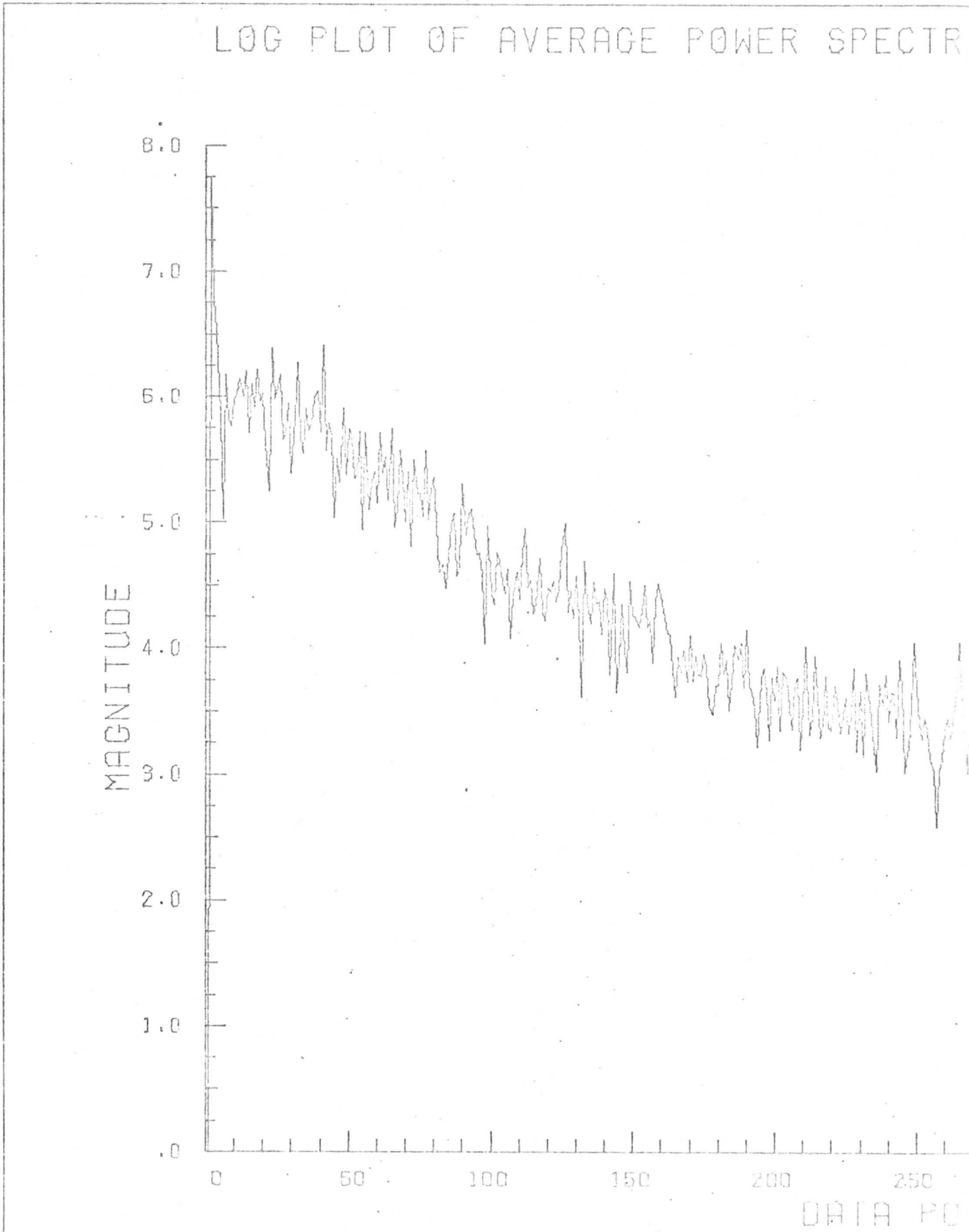

Apollo 56-2-877, (rect.)
Locator: Tape 17, File 1
Records: 860 - 864 Date: 2/1/73
Elements: 510 - 1021
Plot: Avg. Autocorrelation

H-7

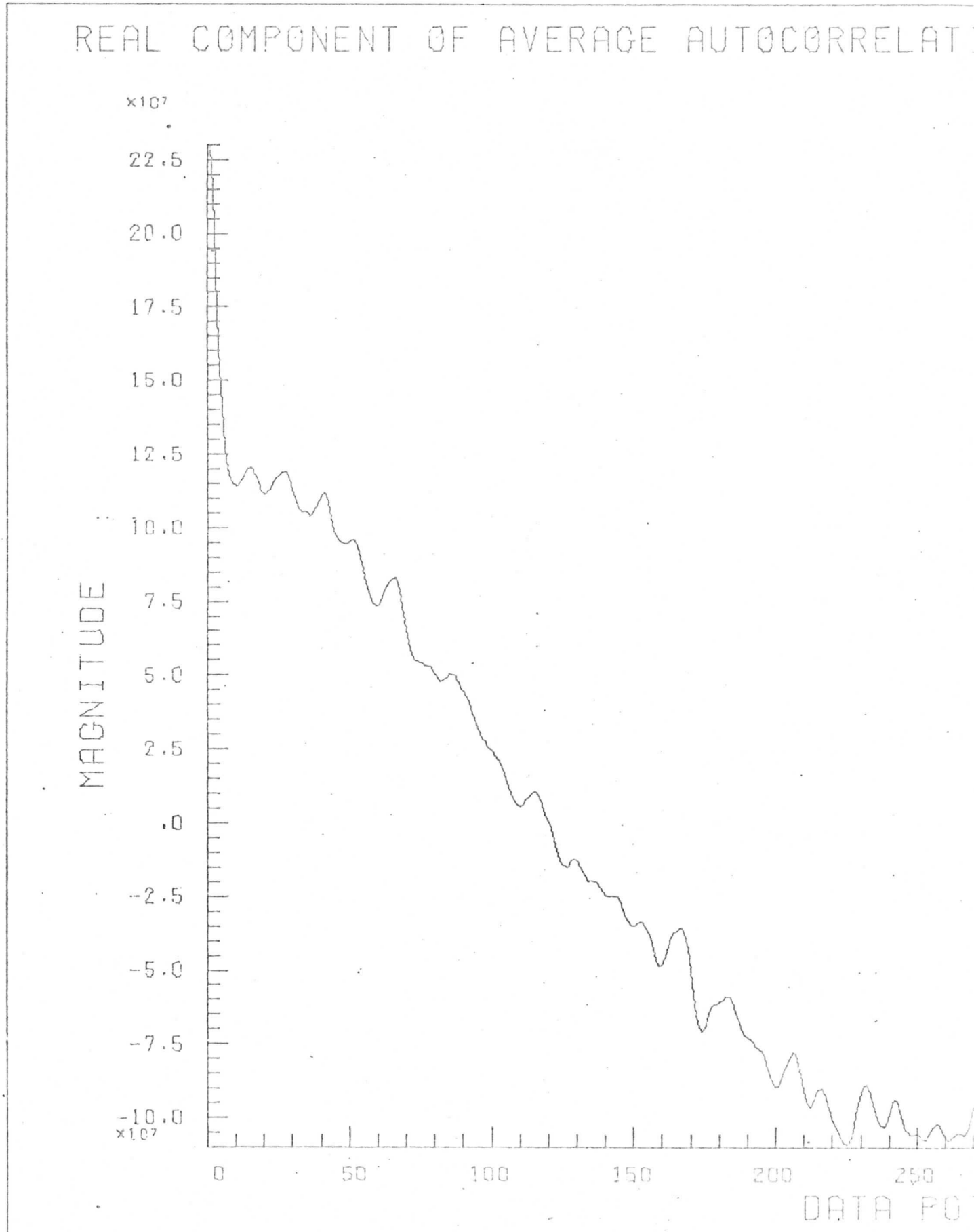

Apollo 56-2-934, (rect.)
Locator: Tape 17, File 2
Records: 100 - 104 Date: 2/1/73
Elements: 510 - 1021
Plot: Log Power Spectrum, First Line

H-8